INAUGURAL – DISSERTATION

zur

Erlangung der Doktorwürde

der

Naturwissenschaftlich-Mathematischen

Gesamtfakultät

der

Ruprecht-Karls-Universität

Heidelberg

vorgelegt von

Diplom-Geologe René Wilhelm Grobe

aus Weinheim

Tag der mündlichen Prüfung: 28. Februar 2011

Long-term landscape evolution, cooling and exhumation history of Variscan rocks in the western Cantabrian Mountains (NW Spain)

Gutachter: apl. Prof. Dr. Ulrich A. Glasmacher
Prof. Dr. Cornelia Spiegel

"A man with a watch knows what time it is. A man with two watches is never sure."

Segal's Law

"As complexity increases, precise statements lose meaning,
and meaningful statements lose precision."

L.A. Zadeh

Acknowledgement – Danksagung

My very special thanks go to my supervisor apl. Prof. Dr. Ulrich A. Glasmacher, who sparked my interest in thermochronology and made my PhD project possible. Of course, I particularly like to thank also my second supervisor Dr. Joaquina Alvarez-Marrón from Barcelona who helped me tireless and unfailing during field work as well as during the creation of this work in endless e-mail correspondence over continents (as Iberia is a microcontinent). My sincere thanks also go to Prof. Dr. Cornelia Spiegel, who agreed to write an expertise for the present PhD thesis. I also owe thanks to Prof. Dr. Jean Braun, who supported the thermokinematic modelling part of this study not only by providing his computer code PECUBE, but also by giving me feedback and guidance during the modelling process. I am also grateful to Dr. Finlay Stuart and Dr. Luigia Di Nicola for supporting me while doing the apatite (U-Th-Sm)/He analyses in Glasgow. Also, I am especially grateful to Prof. Dr. Rosana Menendéz-Duarte and Prof. Dr. Susana Fernández-Menendéz for supporting me during the field work in Asturias. I would also like to thank Dr. Dennis Brown and Prof. Dr. Andrés Pérez-Estaún for their comments and feedback on the manuscripts. Furthermore, I want to thank the whole staff of the 'Research Group Thermochronology and Archaeometry' at the University of Heidelberg, namely Margit Brückner and all of the student assitants who where involved in my project. Also, I want to thank Jens Baumgärtner, my roommate and fellow in misery during the final weekends before finishing our theses. Of course, I would like to particularly thank my friend and roommate Manuel Sehrt for the long and profound discussions concerning thermochronological and other questions of meaning, which I will sadly miss for sure.

Mein besonderer Dank gilt vor allem meinen Eltern und meiner Schwester Denise für ihre bedingungslose Unterstützung, welche die Entstehung dieser Arbeit erst ermöglicht hat. Nicht zuletzt möchte ich auch meinen Verwandten und Freunden für die uneingeschränkte Unterstützung jeglicher Art danken. Mein größter Dank gilt meiner Freundin Rike, welche mich während dieser Arbeit durch alle Höhen und Tiefen begleitet hat, und mich immer motiviert hat wenn es schwierig wurde.

Danke!

Funding

Of course, I also owe thanks to the LGF committee (Landesgraduiertenförderung des Landes Baden-Württemberg) for their confidence in me and the current project by granting a 3-year PhD scholarship. I particularly thank the Spanish Ministry of Education and Science for funding the project through the National Plan of Research, projects BTE2002-00330 and CGL2007-60230/BTE. The study was included in the framework of Consolider-Ingenio 2010, No. CSD2006-00041 (TOPO-IBERIA Project).

Abstract

The present study introduces the first comprehensive regional research of apatite-fission track (AFT) and apatite (U-Th-Sm)/He (AHe) thermochronology including state-of-the-art 3D thermokinematic modelling of long-term landscape evolution in the western termination of the Cantabrian Mountains (NW Spain). The study sets out to analyse and interpret thermochronological data to constrain the pattern and history of cooling and exhumation in the NW Iberian Massif. This allows to better resolve the potential coupling of tectonic and climatic events and their impact on long-term landscape evolution. In terms of tectonic evolution the Cantabrian Mountains are a well-studied area, providing a well-suited domain to examine the impact of tectonic events on the topography. The mountains reach elevations of more than 2,600 m along the northern coast of Spain and are composed of a Variscan crustal section uplifted in the course of Cenozoic shortening along the northern Iberian Plate. Since the end of the Variscan orogeny in Late Palaeozoic, the Iberian Massif was affected by two major tectonic episodes, (1) Mesozoic rifting that lead to continental break-up by 115 Ma and opening of the Atlantic and Bay of Biscay to the West and North, and (2) limited convergence along the Bay of Biscay margin from Middle Eocene times onwards. The study constrains the pattern and history of exhumation within the Paleozoic bedrock and Variscan intrusions over the past c. 250 Ma. Thirty-five AFT samples reveal ages from 246.7 (26.9) to 68.1 (5.0) Ma, with mean track lengths between 10.4 (1.2) and 12.6 (1.8) µm. Six AHe samples range in age from 70.6 (5.2) to 114.4 (14.2) Ma. Time-temperature path modelling of the data indicates that continuous cooling at different rates took place during the main tectonic events that affected the area. A rapid cooling event that ended by Late Jurassic corresponds to topographic decay during unroofing of the Variscan orogen and the break-up of Pangea, and is responsible for the largest amount of exhumation at a rate of c. 0.3 km/Ma. Samples in Galicia cooled contemporaneously with rifting in the North Atlantic and Bay of Biscay during Late Jurassic to Early Cretaceous at exhumation rates of c. 0.25 km/Ma. By about 80 to 100 Ma most samples cooled below 60 °C, indicating that regional denudation has not exceeded c. 1.7 km since then, for geothermal gradients ≥ 27 ºC/km and a surface temperature of 15 °C. An extensive, low relief area in Central Galicia underwent very slow exhumation (0.02 km/Ma) since post-rift stage (80 to 100 Ma), and is interpreted as the remains of a pre-Eocene paleolandscape. Surface uplift of a ridge next to the northern coastline since late Middle Eocene caused minor exhumation during activation of the North Iberian margin. This ridge that reaches heights up to 1,000 m seems to be associated to reactivation of an inherited 60 to 80 Ma old escarpment. An average exhumation rate between 0.02 to 0.07 km/Ma reflects latest denudation as the new mountainous relief developed since incipient subduction along the northern Iberian Margin by 46 Ma due to shortening associated with convergence along the northern Iberian Plate. Reasonable estimates on the initial maximum mean elevation of the area after the end of the Variscan orogeny are determined between 2,400 and 3,400 m by 3D thermokinematic modelling. The strong coincidence between timing of major tectonic events and changes in topography and exhumation rates suggest that the major controlling factor of landscape evolution in this area is tectonic forcing while climatic effects have probably only a second order impact.

Zusammenfassung

Die vorliegende Studie stellt die erste umfassende regionale Forschungsarbeit im Bereich der Apatit-Spaltspur (AFT)- und Apatit-(U-Th-Sm)/He (AHe)-Thermochronologie des Kantabrischen Gebirges (NW Spanien) dar. Neben AFT und AHe werden in der Studie modernste thermokinematische 3D Simulationen der langzeitlichen Landschaftsentwicklung herangezogen. Ziel der Arbeit ist die Analyse und Interpretation thermochronologischer Daten, um das Muster und die Abkühlungs- und Exhumierungsgeschichte im nordwestlichen Iberischen Massiv nachzuzeichnen. Dies wiederum dient der besseren Auflösung einer potentiellen Kopplung von tektonischen und klimatischen Prozessen und deren Auswirkungen auf die langzeitliche Landschaftsentwicklung. Im Hinblick auf die tektonische Entwicklung stellt das Kantabrische Gebirge ein außerordentlich gut erforschtes Orogen dar, und ist somit geeignet, den Einfluss von tektonischen Ereignissen auf die Landschaftsoberfläche zu untersuchen. Der Gebirgszug entlang der Nordküste von Spanien erreicht Höhen von über 2600 m und besteht aus einem Krustensegment, welches im Zuge Känozoischer Deformation entlang der Nordiberischen Platte angehoben wurde. Seit dem Ende der variszischen Gebirgsbildung im Spätpaläozoikum wurde das Iberische Massiv zwei großen tektonischen Episoden unterzogen: (1) Riftbildung im Mesozoikum, die um 115 Ma zum kontinentalen Abbruch und zur Öffnung des Atlantiks und des Golfs von Biskaya im Westen und Norden führte, (2) begrenzte Konvergenz entlang des Grabenrands des Golfs von Biskaya ab dem mittleren Eozän. Die vorliegende Studie grenzt die Abkühlgeschichte und daraus resultierende Exhumierung des Paläozoischen Grundgebirges und Variszischer Intrusionen während der vergangenen ca. 250 Ma ein. Fünfunddreißig AFT Proben zeigen Abkühlater im Bereich von 246,7 (26,9) und 68,1 (5,0) Ma, mit durchschnittlichen Spaltspurlängen zwischen 10,4 (1,2) und 12,6 (1,8) µm. Sechs AHe Proben werden zwischen 70,6 (5,2) und 114,4 (14,2) Ma datiert. Modellierung von Zeit-Temperatur-Pfaden weisen auf ein kontinuierliches Abkühlen mit unterschiedlichen Raten hin. Dieses fand während der großen, das Gebiet beeinflussenden tektonischen Ereignisse statt. Ein schnelles Abkühlungsereignis, welches im Spätjura endete, korreliert mit der Absenkung der Geländeoberfläche während der Abtragung des variszischen Gebirges und dem Auseinanderbrechen von Pangäa und ist verantwortlich für die größte Exhumierung mit einer Rate von ca. 0,3 km/Ma. Proben in Galizien kühlten gleichzeitig mit der Riftbildung im Nordantlantik und im Golf von Biskaya im Zeitraum Spätjura bis Frühkreide ab. Sie weisen Exhumierungsraten von ca. 0,25 km/Ma auf. Zwischen 80 bis 100 Ma sind die meisten Proben unter 60 °C abgekühlt, was darauf hinweist, dass der großflächige Abtrag seit dieser Zeit nicht mehr als 1,7 km betrug, unter Annahme eines geothermischen Gradienten von ≥ 27 ºC/km und einer Oberflächentemperatur von 15 °C. Das ausgedehnte Gebiet Zentralgaliziens mit seinem niedrigen Relief wurde nach der post-Riftbildungsphase (80 bis 100 Ma) einer sehr langsame Exhumierung (0,02 km/Ma) unterzogen und wird als Überbleibsel einer prä-Eozänen paläo-Geländeoberfläche interpretiert. Durch die Heraushebung eines Geländerückens nahe der Nordküste Spaniens, während der Aktivierung des Nordiberischen Kontinentalrands, kam es ab dem späten Mitteleozän zu geringfügiger Exhumierung. Dieser Rücken erreicht Höhen von bis zu 1.000 m und scheint mit der Reaktivierung einer ererbten 60 bis 80 Ma alten Steilstufe verbunden zu sein. Durchschnittliche Exhumierungsraten zwischen 0,02 und 0,07 km/Ma spiegeln die jüngste Abtragung während der Bildung des rezenten Reliefs wider. Diese Reliefentwicklung geht auf die beginnende Subduktion entlang des nordiberischen Kontinentalrands vor 46 Ma zurück, verbunden mit der daraus resultierenden Stauchung aufgrund der Konvergenz entlang der nordiberischen Platte. Vertretbare Abschätzungen anhand thermokinematischer 3D-Simulation der durchschnittlichen ursprünglichen Maximalhöhe des Gebirges nach der variszischen Gebirgsbildung bewegen sich zwischen 2.400 und 3.400 m. Die auffällige Übereinstimmung zwischen dem zeitlichen Auftreten der großen tektonischen Ereignisse und Änderungen der Geländeoberfläche sowie der Exhumierungsraten weisen auf tektonische Ursachen als maßgeblichen Faktor der Landschaftsentwicklung im Untersuchungsgebiet hin. Klimatische Effekte indessen spielen vermutlich nur eine nachgeordnete Rolle.

Keywords: low-temperature thermochronology; long-term landscape evolution; Cantabrian Mountains; northwestern Spain; cooling and exhumation history; apatite fission-track analysis; (U-Th-Sm)/He analysis; 3D integrated thermokinematic modelling; HeFTy©; PECUBE

Table of contents

1 Introduction

The landscape of an area in general and – due to their mere extend – mountain ranges in particular, are one major factor controlling basic surficial processes (e.g. climate, ecology, hydrology) of the Earth's system. Nevertheless, orogens themselves are no static features representing fixed geographic boundary conditions but evolve dynamically over space and time within geological timescales (Reiners and Shuster, 2009). This evolution is supposed to be controlled in turn mainly by the complex coupling between solid earth (e.g. tectonic) and surficial processes (e.g. erosion).

The comprehension of this interaction is crucial to improve the development of more precise climate and erosion models and to elucidate their impact on the evolution of biosphere (e.g. for the evaluation of appropriate long-term storage and disposal sites for CO_2 or nuclear waste, amongst others). Therefore, the understanding of the effect of coupling between tectonic and erosion on mountain ranges and long-term landscape evolution is a matter of intense research efforts (e.g. Bishop, 2007; Reiners, 2007; Reiners and Ehlers, 2005; Whipple *et al.*, 1999; Beaumont, 1999; Kooi and Beaumont, 1996).

One of the best established and most sensitive techniques for investigating these coupling processes are low-temperature thermochronology (LTT) methods like apatite fission-track (AFT) and apatite (U-Th-Sm)/He (AHe) thermochronology. The thermally controlled retention of radiogenic products in thermochronometers like AFT and AHe occurs not at a well-defined temperature but over a certain temperature range, referred to as 'partial annealing zone' (PAZ) or 'partial retention zone' (PRZ), respectively. The PAZ of the AFT system is settled between the 110 °C and 60 °C isotherms (Green *et al.*, 1986; Crowley *et al.*, 1991; Carlson *et al.*, 1999), while laboratory studies of He diffusion (Farley, 2000) and empirical calibrations (Wolf *et al.*, 1996; Wolf *et al.*, 1998) demonstrate that the PRZ of the AHe chronometer lies approximately between the 70 °C and 40 °C isotherms. These temperature isotherms are perturbed by the evolving topography as well as by the rate of rock uplift and exhumation (Fig. 1.1). This perturbation decreases exponentially with depth (Braun, 2002b). Hence, especially LTT provides effective tools to draw conclusions on the feedback between rock uplift, erosion and the resulting exhumation and denudation processes, respectively.

LTT techniques have been applied successfully to unravel rates of exhumation in a variety of tectonic scenarios, such as active orogens (Reiners and Ehlers, 2005; Reiners and Brandon, 2006; Bishop, 2007), rift environments and passive margins (Gunnell *et al.*, 2009) as well as post-orogenic topographic decay in areas of tectonic quiescence (Reiners *et al.*, 2003), among others. However, the rates of exhumation of upper crustal rocks and, therefore, the behaviour of the tectonic-erosion system are not well documented in natural examples of early stages of rock uplift along juvenile coastal orogens.

The Cantabrian Mountains (Fig. 1.2) represent such a young and evolving coastal orogen. It trends E-W, parallel to the northern coast of Spain for more than 300 km, and locally reaches elevations of more than 2,600 m. Along this mountain range, rocks previously deformed and metamorphosed during the Variscan orogeny have been uplifted due to minor shortening and limited convergence

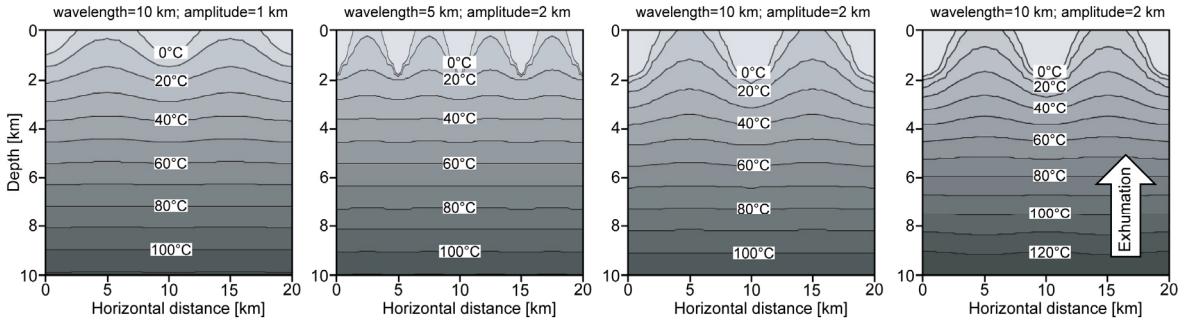

Fig. 1.1: Sketch illustrating the influence of wavelength and amplitude of topography as well as rock exhumation on the perturbation of the temperature isotherms in the upper crust (redrafted after Braun *et al.*, 2006).

between Eurasia and Iberia in the Cenozoic (Boillot *et al.*, 1979; Alonso *et al.*, 1996; Pulgar *et al.*, 1996; Alvarez-Marrón *et al.*, 1997). Although the geology and tectonic evolution of this area is well known, the variation in timing, rate and amount of exhumation of the Paleozoic rocks presently exposed at the surface is largely unconstrained, not least because the area lacks any Mesozoic sedimentary deposits. The cooling history of these rocks has possibly been influenced by several tectonothermal scenarios, including post-orogenic topographic decay of the Variscan edifice, far-field effects of rifting and seafloor spreading due to the opening of the Atlantic and Bay of Biscay ocean basins, and a subsequent surface uplift caused by shortening during convergence along an incipient active margin.

The present study sets out to better resolve the long-term landscape evolution together with the thermal and structural evolution in the western termination of the Cantabrian Mountains and, therewith, provide insights on the behaviour of the coupled tectonic-erosional system. The current research combines common thermochronological interpretation tools like AFT and AHe cooling age distributions at the surface, age-elevation-relationship plots and single sample cooling path modelling with HeFTy© (Ketcham, 2005; Ketcham *et al.*, 2007a; b; Ketcham *et al.*, 2009), together with state-of-the art numerical modelling of integrated multi-sample 3D simulation using the software code PECUBE (Braun, 2003a).

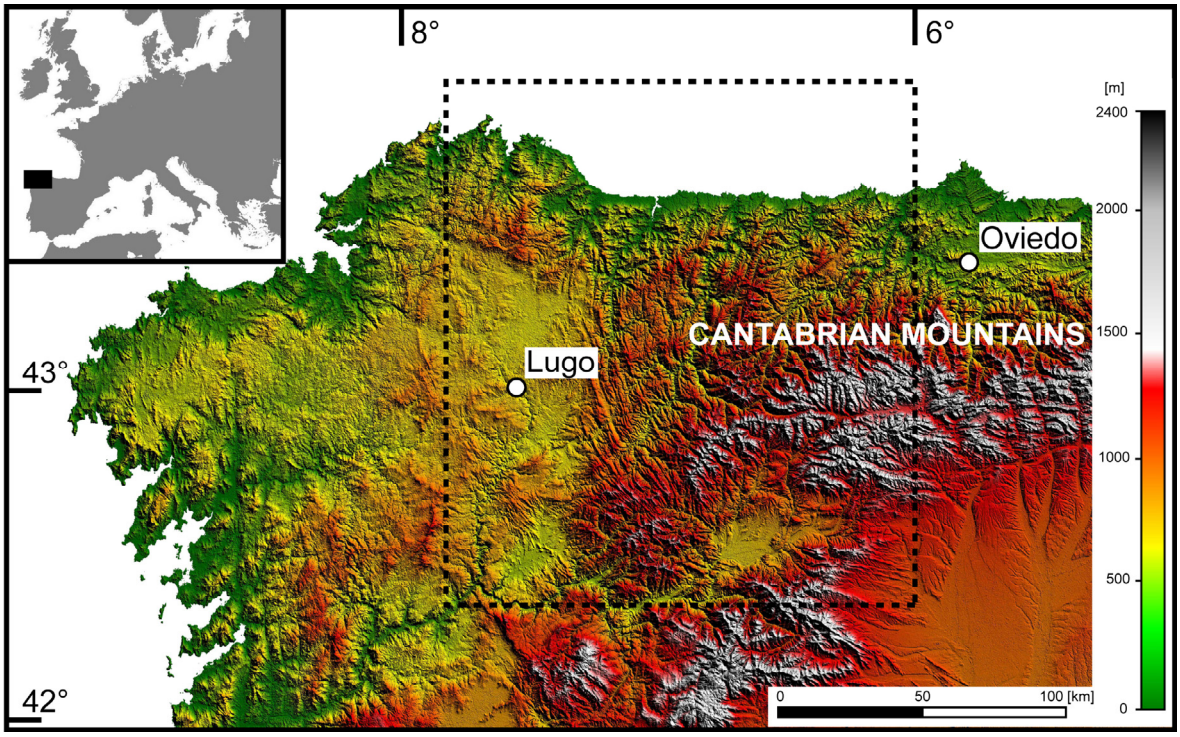

Fig. 1.2: Overview of the study area (black rectangle) at the western termination of the Cantabrian Mountains in NW Spain. Digital elevation model (DEM) derived from ASTER GDEM (ASTER GDEM is a product of METI and NASA).

2 Geological background

2.1 Study area

Galicia is situated at the western termination of the Cantabrian Mountains that form a juvenile evolving mountain range at an incipient active margin. The Cantabrian Mountains represent the westernmost prolongation of the Pyrenees at the northern coast of Spain (Fig. 2.1) and are part of the NW Iberian Variscan belt which comprises the westernmost exposures of the European Variscan orogeny.

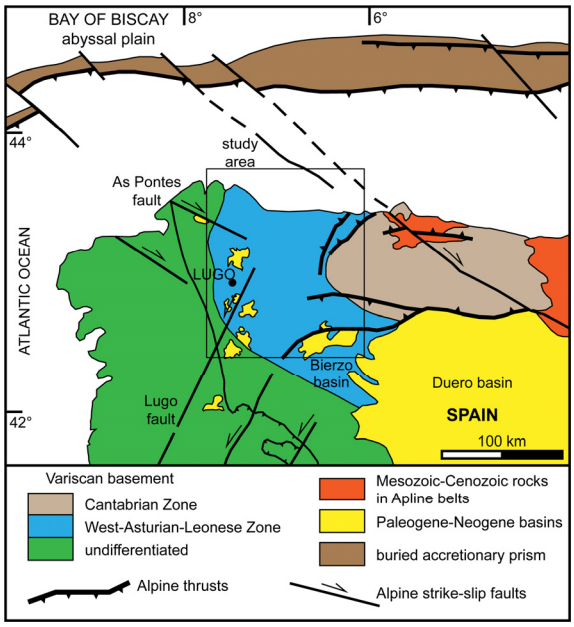

Fig. 2.1: Geological overview map of the study area (black rectangle; cp. Fig. 2.3) within the West-Asturian-Leonese Zone (redrafted from Boillot and Malod, 1988).

The area represents the transition zone (West-Asturian-Leonese Zone) between the foreland areas (Cantabrian Zone) to the east and the hinterland (Central Iberian Zone) to the west. The West-Asturian-Leonese Zone (WALZ) is bound to the east by the Narcea antiform and the Allande thrust. The western boundary to the Central Iberian Zone (CIZ) is marked by the Mondoñedo antiform and the Viveiro suture. The Narcea antiform marks the transition to dominantly younger rocks within the Cantabrian Zone that underwent deformation at shallower crustal levels in the foreland areas of the Variscan orogen. In the Mondoñedo antiform at the western side of the WALZ, rocks that were affected by deformation at deeper crustal level conditions crop out (Pérez-Estaún *et al.*, 1988; 1991).

2.2 Tectonic evolution

The tectonic evolution of the Northern Iberian Peninsula includes three major events: (1) the Variscan orogeny that ended by Late Paleozoic times, (2) the rifting during Pangea break-up in Permian-Triassic times with subsequent opening of the Atlantic Ocean and Bay of Biscay in the Mesozoic marked by chron M0 (118 Ma; Verhoef and Srivastava, 1989) and the Aptian-Albian break-up unconformity in the Cantabrian platform (c.115 Ma; Montadert *et al.*, 1979; García-Mondejar *et al.*, 2005), and 3) limited convergence between Iberia and Eurasia since Middle Eocene times.

The Paleozoic and older rocks of the Iberian Massif in NW Spain provide an unusually well preserved record of the thermal and structural events that contributed to the final assembly of the supercontinent Pangea that formed during the Variscan collision in the Carboniferous and Early Permian (Martínez-Catalán *et al.*, 2007). The following Pangea break-up initiated during Late Permian-Triassic times and lead to the individualization of a separated continental microplate known as the Iberian Massif (Ziegler, 1989). Evidences of extensional tectonics are found outside of the study area to the east. Formation of minor fault bounded continental basins and related alkaline volcanism occur near Oviedo (Martínez-García *et al.*, 2004) and further to the west in the Basque-Cantabrian basin (Espina *et al.*, 2004).

Subsequent widespread rifting events that lead to the opening of the Atlantic Ocean to the west and oblique separation of Iberia from Eurasia to open the Bay of Biscay ocean to the north occurred during Late Jurassic-Early Cretaceous (Le Pichon *et al.*, 1971; Srivastava *et al.*, 1990) (Fig. 2.2a). Seafloor spreading was active in the Bay of Biscay since the Early Cretaceous and lasted until the Late Cretaceous (Srivastava *et al.*, 1990) (Fig. 2.2b). The Variscan structures preserved in the Cantabrian Mountains were overprinted and uplifted during the Cenozoic convergence between Iberia and Eurasia. Magnetic anomalies in the North

Atlantic and Bay of Biscay indicate that limited convergence along the North Iberian Margin started at 49 Ma and went on until 20 Ma (Srivastava *et al.*, 1990) (Fig. 2.2c).

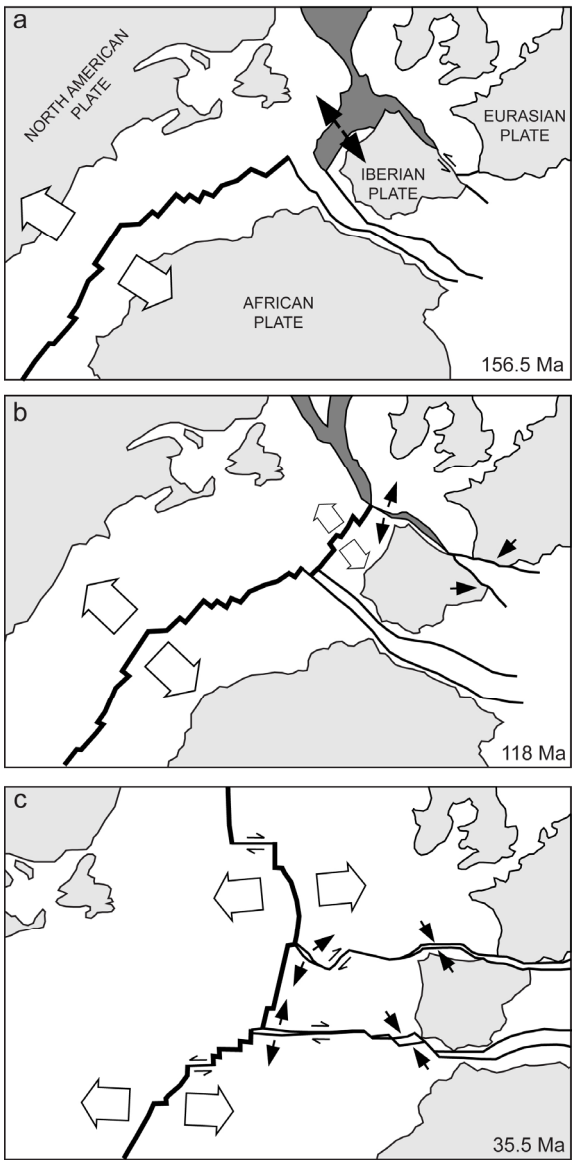

Fig. 2.2: Three time stages with North American and Iberian Plate motions relative to a fixed Eurasian Plate (redrafted from Srivastava *et al.*, 1990): (a) shaded areas north and west of Iberia are areas undergoing stretching after 156.5 Ma, (b) indicates seafloor spreading starting by 118 Ma, and (c) oblique convergence along the northern margin of Spain by 35.5 Ma.

A N-S crustal-scale section at about 5º W longitude shows a northward imbrication of the Iberian crust beneath the Cantabrian Mountains reaching current crustal thickness of more than 50 km (Pulgar *et al.*, 1996; Fernández-Viejo *et al.*, 2000; Pedreira *et al.*, 2003) and limited southward subduction of the Bay of Biscay oceanic crust along the continental margin (Sibuet and Le Pichon, 1971; Boillot *et al.*, 1979; Grimaud *et al.*, 1982). This early subduction caused the formation of an accretionary prism at the foot of the continental slope, that was active in the western part of the margin from Lutetian to Burdigalian times (Alvarez-Marrón *et al.*, 1997). By Middle Eocene times continental sediments started to accumulate in the Duero foreland basin. This marks the shortening and onset of surface uplift in the Cantabrian Mountains (Gallastegui, 2000). In the study area, minor N-S shortening occurred with formation of south-directed thrusts that cut the Paleogene to Neogene continental sediments of the Bierzo basin (Andeweg, 2002) (Fig. 2.3). Small continental basins developed in the west associated to WNW-ESE transpressional faults that accommodated minor N-S shortening (Santanach, 1994). The largest of these faults is the As Pontes fault (Fig. 2.1 and 2.3) that cuts through sediments ranging in age from 28 to 22 Ma within the As Pontes basin (Huerta *et al.*, 1996).

Convergence along the northern margin of Iberia slowed significantly since the Early Miocene (20 Ma) (Rosenbaum *et al.*, 2002), although younger brittle faulting has been documented on land (Cabral, 1989; Andeweg, 2002; Rodríguez-García *et al.*, 2006; Alvarez-Marrón *et al.*, 2008). The area and surrounding continental margins continue to be weakly seismically active today (López-Fernández *et al.*, 2004; Díaz *et al.*, 2008).

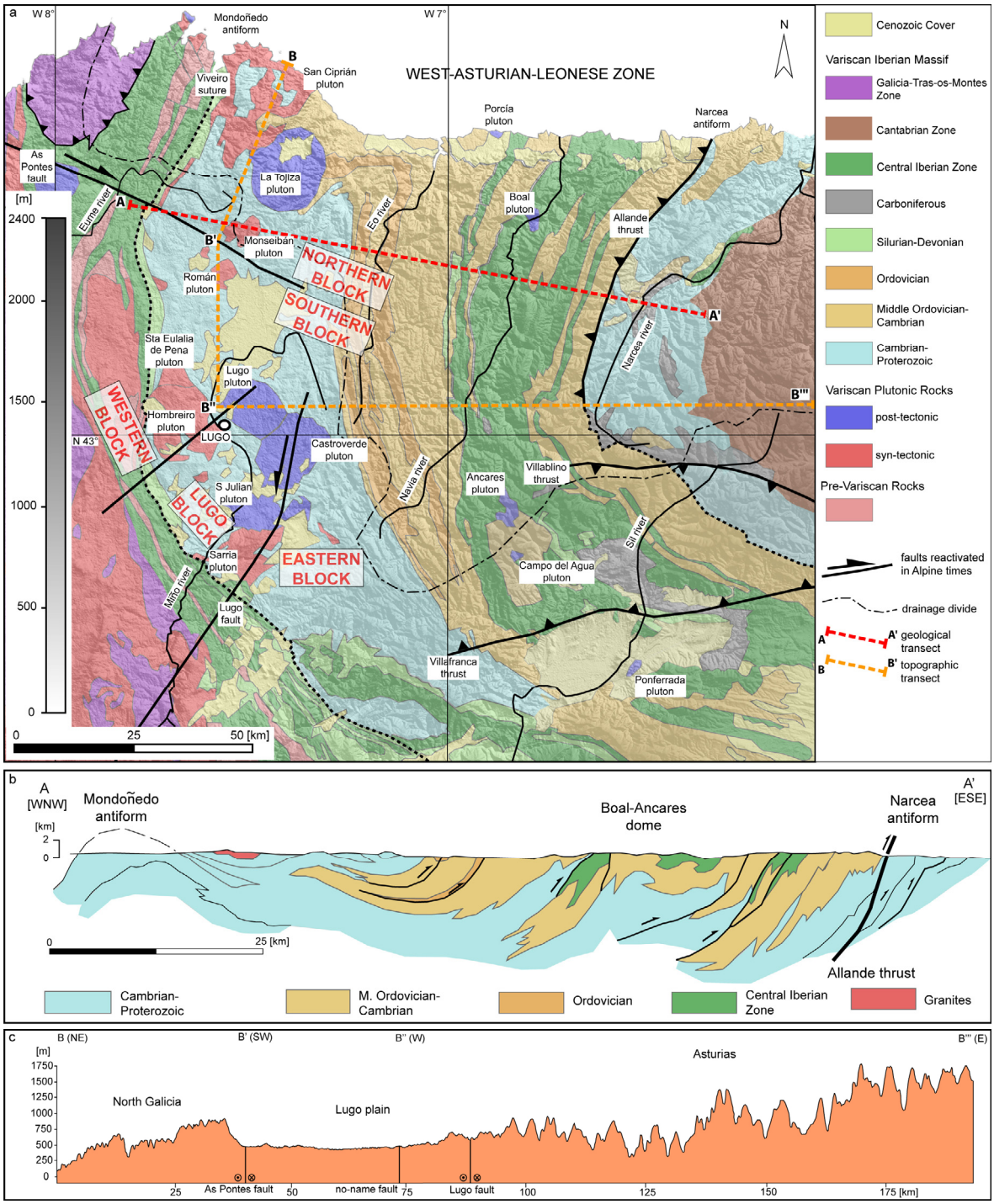

Fig. 2.3: (a) Geological map of the study area with digital elevation model (ASTER GDEM). Thin black lines mark rivers; thick black lines faults reactivated in Alpine times; narrow dashed line represents boundary of WALZ; wide dashed line represents the drainage divide; names of faults, plutons and rivers are given in white boxes; red dashed line is geological transect (A-A'); orange dashed line is transect highlighting topographic features (B-B'-B''-B'''). (b) Geological transect. (c) Topographic transect.

2.3 Regional geology

2.3.1 Structural features

The main post-Variscan structures in the WALZ are the western prolongation of the Cenozoic thrusts at the deformation front of the Cantabrian Mountains and two main strike-slip fault systems in the west (Fig. 2.1 and 2.3). The thrusts in the study area are represented by the Allande, Villablino and Villafranca thrust. They are responsible for the surface uplift of the Cantabrian Mountains and coeval with the evolution of the Bierzo basin. The latter is filled with up to 700 m of terrigenous continental deposits dated near the base as latest Early Oligocene (Freudenthal *et al.*, 2010). The two strike-slip fault systems in Galicia are represented by right-lateral WNW trending faults in the northern part of Galicia and left-lateral NE trending faults in northern and central Galicia. The As Pontes fault that extends for more than 50 km is the largest fault of the northern strike-slip system related to the opening of the Atlantic and the relative motion of the European and African plates (Mauffret *et al.*, 1978; Boillot and Malod, 1988). This fault underwent up to 1 km horizontal right-lateral slip and a maximum of 455 m vertical displacement during formation of the As Pontes basin (Santanach *et al.*, 2005). The As Pontes basin was filled by up to 300 m of continental deposits, mainly siliciclastic assemblages, interfingered with significant brown coal seams and minor carbonate deposits. Sedimentation in the As Pontes basin lasted at least until 22.5 Ma (Huerta *et al.*, 1996). The main tectonic movement of thrusts, normal faults and NW-SE dextral strike-slip fault systems began in the Stampian (33.9 (0.1) to 28.4 (0.1) Ma) and stopped in the upper Aquitanian-Burdigalian (~20 Ma). The end of the movement of the onshore and offshore strike-slip fault systems in NW Iberia coincides with the end of the seafloor spreading at the NW Iberian Plate boundary. A significant south-facing topographic escarpment that reaches locally more than 300 m is associated to the As Pontes fault. In contrast, the strike-slip fault system in central and southern Galicia (e.g. Lugo fault) shows no significant topographic variations. The faults, however, trend parallel to the left-lateral strike-slip fault systems that stem from the deformation front of the Cantabrian Mountains. These faults extend for hundreds of km southward into Portugal and are linked to the Lisbon basin (Fig. 2.1). Holocene activity has been reported for faults of this set in Portugal (Cabral, 1989). Patches of a few hundred meters thick, Neogene continental deposits covering unconformably the Iberian Massif rocks are common in Galicia (Barrón and Santos, 1998).

2.3.2 Lithologies

Along their western flank, within the study area, the Cantabrian Mountains comprise the NW Iberian relative autochthon and consist of deformed Neoproterozoic and Lower Cambrian metasedimentary rocks (Fig. 2.4). These include 11,000 m of Cambrian-Ordovician siliciclastic rocks (Fig. 2.5) belonging to the margin of Gondwana (based on faunistic and stratigraphic correlation: Paris and Robardet, 1977; Blaise and Bouyx, 1980; Martínez-Catalán, 1990), which collided with Laurussia during the Varsican orogeny (Pérez-Estaún *et al.*, 1990; Pérez-Estaún *et al.*, 1991; Martínez-Catalán *et al.*; 2007).

Fig. 2.4: Fine grained yellowish meta-sandstone of Neoproterozoic to Lower Cambrian metasedimentary units (# JU-21).

Fig. 2.5: Nearly vertical dipping alternating quartzite-slate layers from the Cambrian siliciclastic units. Picture taken at sample location ESP-12.

Fig. 2.6: Handspecimen of post-Variscan calcalkaline granite in the Castroverde pluton (# JU-22).

Fig. 2.7: Outcrop of syn-Variscan leucogranite in Román pluton (# JU-38).

During two main episodes relative to the Variscan deformation the area was intruded by abundant granitic magma. Syn- to post-Variscan granitoids (Fig. 2.6 and 2.7) are widespread in the western part of the WALZ (Fig. 2.3). These range in age from 286 (2) to 323 (+9/-5) Ma obtained from U-Pb geochronology (Fernández-Suárez *et al.*, 2000b), whereas some of these plutons have been dated between 274.1 (0.7) and 298.2 (0.6) Ma ($^{40}Ar/^{39}Ar$; Rb/Sr). In the central part in Porcía, Boal, Ancares, Campo del Agua and Ponferrada along the Boal-Ancares dome, small granitic bodies crop out (Fig. 2.3). Several of these have been dated by U-Pb geochronology between 289 (3) and 295 (3) Ma (Fernández-Suárez *et al.*, 2000b). The published ages of the plutons within the WALZ and the technique used for dating are summarized in Table 2.1.

Table 2.1.
Published geochronological data of several granitoids and rocks from the WALZ.

Pluton Name (Sample Name)	Lithology	Age (error) [Ma]	Dating Method	Reference
Vivero pluton (VGI-20)	synk. calc-alkaline	323 (+9/-5)	U-Pb (zircon-monazite)	Fernández-Suárez et al., 2000b
Vivero pluton (VGI-20)	synk. calc-alkaline	323 (n.a.)	Pb-Pb (monazite)	Fernández-Suárez et al., 2000b
Vivero pluton (VGI-20)	synk. calc-alkaline	295 (2)	U-Pb (monazite)	Fernández-Suárez et al., 2000b
San Ciprián pluton (VIV-7)	synk. leucogranite	286 (2)	U-Pb (monazite)	Fernández-Suárez et al., 2000b
San Ciprián pluton (VIV-7)	synk. leucogranite	318 (n.a.)	Pb-Pb (zircon)	Fernández-Suárez et al., 2000b
San Ciprián pluton (WALZ-4)	synk. leucogranite	274.1 (0.7)	$^{40}Ar/^{39}Ar$ (muscovite)	Dallmeyer et al., 1997
La Tojiza pluton (TOJ-5)	postk. calc-alkaline	295 (2)	U-Pb (zircon-monazite)	Fernández-Suárez et al., 2000b
La Tojiza pluton (WALZ-6)	postk. calc-alkaline	283.8 (0.7)	$^{40}Ar/^{39}Ar$ (muscovite)	Dallmeyer et al., 1997
Castroverde pluton	postk. calc-alkaline	287 (n.a.)	Rb-Sr (whole rock)	Cocherie, 1978
Sarria pluton (SA-4)	synk. leucogranite	313 (2)	U-Pb (monazite)	Fernández-Suárez et al., 2000b
Sarria pluton (WALZ-1)	synk. leucogranite	282.2 (0.8)	$^{40}Ar/^{39}Ar$ (muscovite)	Dallmeyer et al., 1997
Shist from Mondoñedo Nappe (WALZ-2)	Precambrian shist	298.2 (0.6)	$^{40}Ar/^{39}Ar$ (muscovite)	Dallmeyer et al., 1997
Porcía pluton (Porj-9)	postk. calc-alkaline	295 (3)	U-Pb (zircon)	Fernández-Suárez et al., 2000b
Boal pluton (DJ-29)	postk. calc-alkaline	292 (3)	U-Pb (zircon-monazite)	Fernández-Suárez et al., 2000b
Ancares pluton (DJ-277)	postk. calc-alkaline	289 (3)	U-Pb (zircon-monazite)	Fernández-Suárez et al., 2000b

synk.: syn-kinematic, postk.: post-kinematic, n.a.: not available.

2.3.3 Geomorphology

The topographic edifice that makes up the Cantabrian Mountains has an average elevation of 1,800 m, with the highest elevation reaching more than 2,600 m in the Picos de Europa area, east of Oviedo. The current study area covers a region of about 150 by 100 km in the western termination of the Cantabrian Mountains where the overall elevation is lower, ranging from c. 450 m to 1,900 m (Fig. 2.3). Changes in wavelength and amplitude of elevation occur across the area. For example, there is long wavelength (tens of km) and moderate amplitude relief (a few hundred meters) in large areas to the west (Galicia), whereas to the east, a shorter wavelength (a few km) and higher amplitude (more than 1,000 m) pattern is dominant.

The relief pattern in Central Galicia is characterised by an extensive, relatively flat area around the city of Lugo (Fig. 2.8a) that averages between 450 to 500 m elevation above sea level and higher (up to 1,000 m), more rugged topography to the north (Fig. 2.8b). The abrupt transition is bound by the As Pontes fault, reaching elevations of more than 1,000 m in its northern block.

In Asturias (Fig. 2.8c), the highest elevations are along the drainage divide at 50 to 100 km from the coastline. To the north of the divide, there are areas with moderate amplitudes, such as the Oscos plateau region with elevated surfaces of low relief at 700-800 m and shallow incised rivers. In contrast, areas of higher amplitude to the east are associated to the Alpine Allande thrust. This fault reactivates a N-S trending Variscan structure with associated topography in excess of 1,200 m (Alvarez-Marrón *et al.*, 2003). South of the drainage divide, elevations decrease down to an area with subdued topography in the Bierzo basin with average elevations of 600 m.

Superimposed on this relief pattern, the drainage system includes rivers that flow north into the Bay of Biscay and rivers that flow southwest into the Atlantic, separated by a divide with a complex trace (Fig. 2.3). Southwest draining rivers belong to the Miño river basin of Galicia and form a broad basin with widely spaced tributaries shallowly incised into the flat lands of Lugo. In contrast, the Sil river that flows through the Bierzo basin, forms the largest tributary basin that is deeply incised into the higher topographic areas in the east. The north draining rivers are commonly short bedrock courses, closely spaced and deeply incising into the bedrock.

The largest rivers that drain highest topographic areas are the Eo, Navia and Narcea river (cp. Fig. 2.9). The alternating nearly vertical dipping quartzite and slate layers with a dominant N-S structural trend in the bedrock impose an important control on the morphology of these river basins (e.g. Fig. 2.5, 2.8a and 2.9).

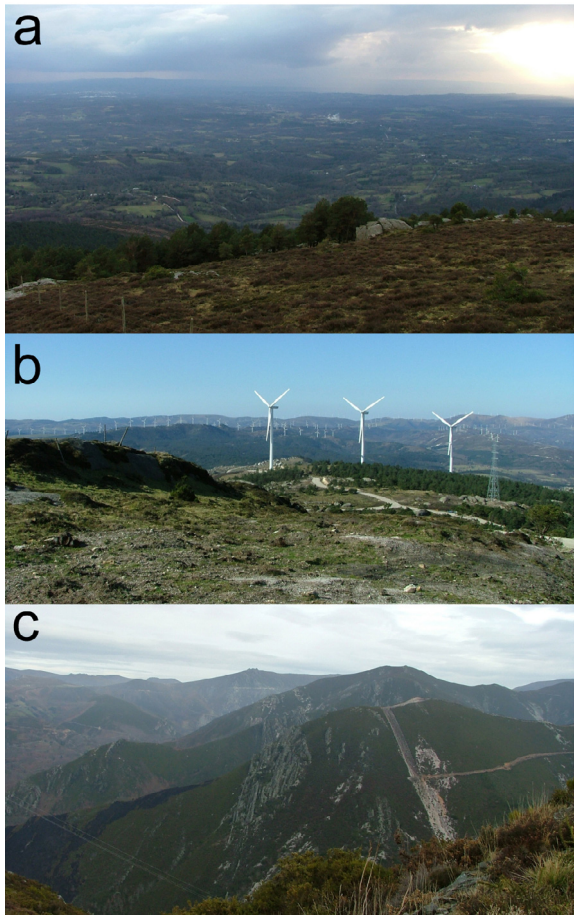

Fig. 2.8: (a) View from the Pico de Monseibán (at 915 m) into the flat topography area around Lugo. The picture is taken close to the escarpment near the As Pontes fault. View is in southward direction. (b) View at the top of La Tojiza peak (at 835 m) showing the rugged topography in North Galicia with extensive distribution of wind turbines. (c) Typical rough topography of Asturias showing a nearly vertical dipping N-S striking quartzite layer. The alternating quartzite-sandstone-slate layers impose an important control on the N-S incision of rivers in Asturias (c.p. Fig. 2.9). Picture taken near sample ESP-18 in central Asturias.

Fig. 2.9: Deeply incised Navia river. Picture taken c. 15 km east of sample ESP-12.

3 Methods and techniques

3.1 Low-temperature thermochronology

Thermochronologic methods, such as fission-track (FT) and (U-Th-Sm)/He analysis, are based on (1) radiometric dating as well as (2) the knowledge about the thermal sensitivity of the observed chronometric system. Radiometric dating uses the nuclear decay of certain radiogenic mother isotopes and therewith involved production of measurable decay products (such as daughter isotopes or radiation damages) described by the general decay equation:

$$N_d = N_{d0} + N_p\left(e^{\lambda t} - 1\right) \qquad (1)$$

This enables to determine the age the observed radiometric system is thermodynamically closed at, by the general age equation:

$$t = \frac{1}{\lambda}\ln\left(1 + \frac{N_d}{N_p}\right) \qquad (2)$$

In contrast to other chronometers, thermochronometers reveal a thermally controlled retention of the decay products. This thermal sensitivity of thermochronometers, and thereof revealed ages provide information about the cooling history of the rocks, rather than only the crystallization ages of its minerals (see e.g. Reiners and Brandon, 2006). Thus, thermochronomentric dating refers to cooling ages, rather than crystallization ages.

3.1.1 Low-temperature thermochronology and landscape evolution

The landscape of an area is no static feature but can be understood as the geomorphic expression of the dynamical feedback between erosion and tectonics (Fig. 3.1). Recently, many efforts have been carried out to determine the rate at which the landscape can respond to external changes (i.e. tectonic; climate changes) (Willett *et al.*, 1993; Montgomery, 2001; Whipple *et al.*, 1999).

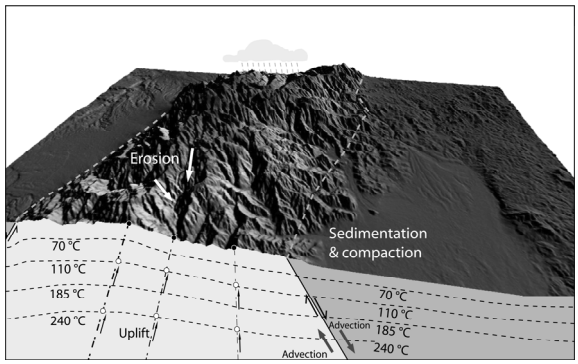

Fig. 3.1: Dynamic feedback between erosion and tectonics. (modified after Bauer *et al.*, 2010; and Ehlers and Farley, 2003)

Near-surface isotherms are deflected by the overlying (evolving) topography (e.g. Braun, 2002a). The intensity of this perturbation and its depth of penetration are controlled by the wavelength and amplitude of the topography as well as by the rock exhumation rate. While the influence of temporally steady-state topography on the deflection of the isotherms is relatively well understood (Stüwe *et al.*, 1994, Mankeltow and Grasemann, 1997), Braun (2002a) has shown the potential effects of a temporally varying, evolving topography on the perturbation of isotherms and yet the impact on thermochronological age-elevation profiles (Fig. 3.2).

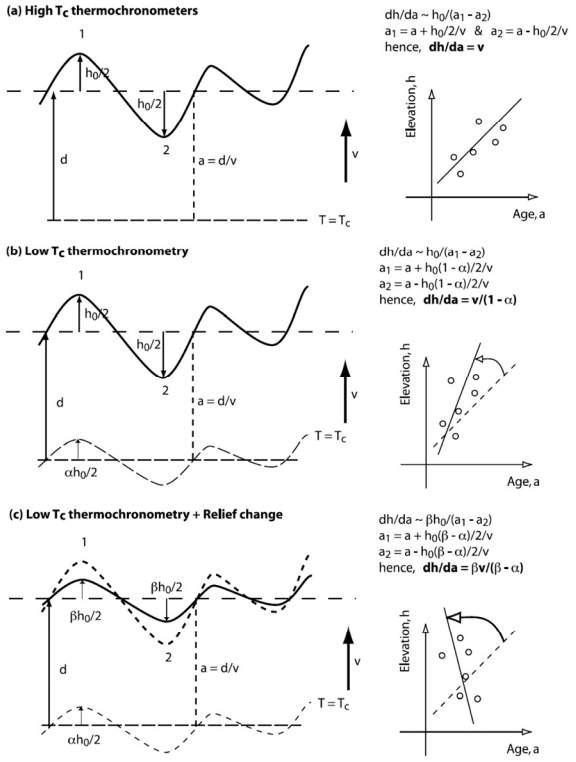

Fig. 3.2: Three scenarios in which the exhumation rate can be estimated from the slope of an age-elevation relationship (AER). (a) High-T thermochronometers: the slope is equal to the exhumation rate. (b) Low-T thermochronometers: the slope overestimates the exhumation rate. (c) A decrease in relief leads to a further overestimate of the exhumation rate of the AER. A large decrease in relief can even lead to a negative slope. (from Braun, 2002b).

3.1.2 Apatite fission-track (AFT) thermochronology – principles

The basic concept of apatite fission-track (AFT) thermochronology is the spontaneous fission of ^{238}U during which the heavy fragments of this fission leave chemically corrodible linear defects (fission-tracks) in the apatite crystal (Fig. 3.3) (Wagner, 1972). In terms of radiometric dating, the uranium content of the mineral represents the mother isotope, while the fission-tracks stand for the daughter isotope. The fission-tracks are metastable and the rate the tracks anneal is a function of time and temperature (Fig. 3.4). Fission-tracks fully anneal at temperatures above c. 110 °C/10 Ma and the chronometer is reset. Below 110 °C/10 Ma the system begins to accumulate daughter products, i.e. it is thermodynamically closed. The particular isotherm is referred to as the closure temperature (T_c) of the system (Dodson, 1973; 1979). On the other hand, the annealing is virtually zero not until temperatures below c. 60 °C/10 Ma. Therefore, AFT thermochronology is sensitive to the temperature range between c. 110-60 °C/10 Ma, called the partial annealing zone (PAZ) (Gleadow and Fitzgerald, 1987). Though, Spiegel *et al.* (2007) also reported track shortening ranging between 4 and 11% during long-term exposure (~15-120 Ma) to temperatures below the temperature range of the PAZ. In the case of the present study, assuming a geothermal gradient of 27 °C/km (Fernández *et al.*, 1998) and a surface temperature of 15 °C, AFT thermochronology reflects the thermal history of rocks being exhumed through 3.5 to 1.7 km depth.

Concerning AFT analysis the information on the thermal history of apatite is, therefore, stored in two archives: (1) the etch pit areal density of tracks giving the cooling age and (2) the length distribution of horizontal confined fission-tracks recording the cooling path (e.g. Wagner and Van den haute, 1992; Lisker *et al.*, 2009 and literature cited therein).

However, the time and temperature sensitive annealing of fission-tracks is also governed by two other important effects (1) the chemical composition of the apatite and (2) the crystallographic orientation of the spontaneous tracks.

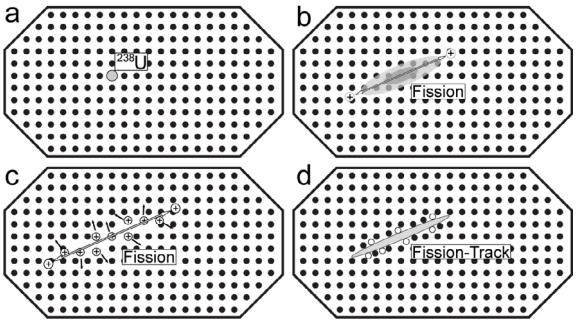

Fig. 3.3: Sketch of fission-track formation according to the 'ion explosion model' after Fleischer *et al.* (1975). (a) Trace amounts of ^{238}U are present in the crystal lattice. (b) Spontaneous fission of ^{238}U produces two highly charged heavy fragments that repel each other. (c) Ionisation of the lattice atoms by the moving charged particles. (d) Ionised lattice atoms repel each other forming the fission-track (redrafted after Juez-Larré, 2003).

The annealing speed of fission-tracks at a given temperature is slower in apatite grains with high chlorine content than in fluorine rich apatite grains (Gleadow and Duddy, 1981; Green *et al.*, 1985; 1986; Burtner *et al.*, 1994; O'Sullivan and Parrish, 1995; Carlson, 1990; Crowley *et al.*, 1991; Crowley, 1993; Carlson *et al.*, 1999; Donelick *et al.*, 1999; Ketcham *et al.*, 1999; Barbarand *et al.*, 2003a; b). Donelick (1993; 1995) first described the linear relation between the etch pit size parallel to the c-axis ($D_{par}^{®}$) and the fluorine and chlorine content of the apatite. Further research by Barbarand *et al.* (2003a; b) confirmed this relation. $D_{par}^{®}$ can be used in the thermokinematic modelling software HeFTy© (Ketcham, 2005; Ketcham *et al.*, 2007a; b; Ketcham *et al.*, 2009) as a kinetic parameter.

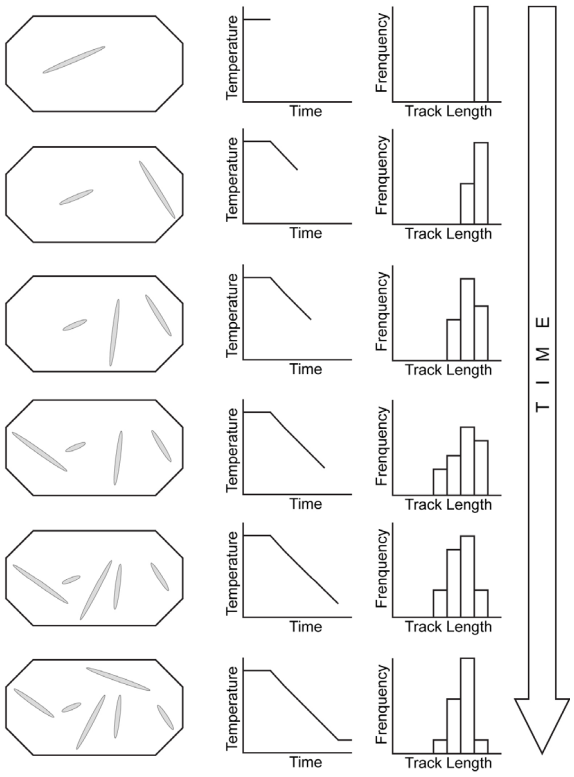

Fig. 3.4: Sketch of time-temperature dependent annealing of fission-tracks and its influence on track length distribution.

The annealing of spontaneous fission-tracks, furthermore, is influenced by their crystallographic orientation (e.g. Green and Durrani 1977). Tracks orthogonal to the c-axis anneal more rapid than tracks parallel to the c-axis (Green, 1988). This anisotropy increases with annealing (Green, 1981; Laslett *et al.*, 1984; Donelick *et al.*, 1990; 1999; Galbraith *et al.*, 1990; Donelick, 1991). Donelick *et al.* (1990; 1999) and Donelick (1991) further extended the database on crystallographic effects of annealing in apatite and integrated the results in the recent annealing model of Ketcham *et al.* (1999; 2007a; b) and Ketcham (2003). The confined fission-track lengths measured in this study were corrected for their crystallographic orientation by applying the computer code HeFTy© to the data set.

3.1.3 Apatite (U-Th-Sm)/He (AHe) thermochronology – principles

Apatite (U-Th-Sm)/He (AHe) thermochronology is based on the accumulation of ^{4}He during α-decay of ^{238}U, ^{235}U, ^{232}Th, their daughter products, and ^{147}Sm in the apatite grain until the closure temperature is reached. Radiogenic ^{4}He diffuses out of the mineral as a function of time, temperature and the helium (He) diffusivity of the mineral. The closure temperature (T_c) of mineral grains is dependent on: activation energy (E_a), a geometric factor for the crystal form (A), thermal diffusivity (D_0), the length of the average diffusion pathway from the interior to the surface of the grain (a) and the cooling rate at closure temperature (dT/dt) (Dodson, 1973). In general, the apatite T_c is in the range of 70 °C for a simple monotonic cooling rate of 1 °C/Ma and a subgrain domain size ≥ 60 µm (Farley *et al.*, 1996; Farley, 2000; Stöckli *et al.*, 2000; Wolf *et al.*, 1996; 1998). At a temperature of less than c. 40 °C/1 Ma (Wolf *et al.*, 1996) the total ^{4}He is retained in the mineral. Therefore, the AHe system is sensitive to the temperature space between c. 40-70 °C/1 Ma, in literature referred to as the partial retention zone (PRZ) (Wolf *et al.*, 1998).

There are various complicating factors in AHe thermochronology which may contribute to false cooling ages and, therefore, also to considerable intra-sample single grain age variation. These factors can be α-ejection or implantation (e.g. from surrounding host U–Th rich sedimentary components) (Farley, 2000; Spiegel *et al.*, 2009), radiation damage (Shuster *et al.*, 2006) due to variation in effective Uranium concentration, U-/Th-rich (micro-) inclusions, fluid inclusions, variation in grain

size (Reiners and Farley, 2001), zonation and cooling rate, among others (cp. Reiners and Ehlers, 2005). In some cases these complicating factors can be avoided by accurate selection of appropriate grains (idiompophic, inclusion- and crack-free grains with accurate grain size). In other cases (for α-ejection, implantation, radiation damage) a correction procedure can be applied. However, some 'complicating' factors leading to intra-sample age variation may also contribute to better constrain the thermal history (age-grain size-relationship) of the sample (Reiners and Farley, 2001).

The α-ejection correction is based on the fact, that α-particles are emitted with high kinetic energy during decay of U, Th and Sm, and travel significant distances before coming to rest, which in turn poses a complication for the He dating method, as α-particles may be ejected out of the crystal being dated or injected into the crystal from decay occurring in surrounding grains. Therefore, a correction has to be applied for the loss/gain of radiogenic He generated within an outer rim of the mineral grain by the α-stopping distances (apatite: 25µm) (Wolf *et al.*, 1996, Farley *et al.*, 1996, Farley, 2000).

To avoid false α-ejection correction in cases of low U-Th-apatites Spiegel *et al.* (2009) recommend to check the possibility of He implantation and suggest a correction procedure by mechanically abrading the outer part of grains applicable for complications caused by implantation as well as for α-ejection.

While the α-ejection correction is applied more routinely, the recently introduced correction for radiation damage is still in progress (Shuster *et al.*, 2006; Shuster and Farley, 2009; Flowers *et al.*, 2006; Flowers *et al.*, 2009). Shuster *et al.* (2006) noted that ^{4}He diffusion in apatite is impeded by radiation-induced damage to the crystal structure. Their ^{4}He production-diffusion model predicts that the effective ^{4}He closure temperature of apatite will vary with cooling rate and effective uranium concentration (eU), and may differ from the commonly assumed T_c of ~70 °C/1 Ma by up to ±15 °C (Shuster *et al.*, 2006; Shuster and Farley, 2009). To account for the accumulation of crystal defects due to the radioactive decay the eU factor (eU = [U] + 0.235 [Th], concentrations in weight %) was introduced (Shuster *et al.*, 2006). This factor characterizes the dependency of ^{4}He-diffusion on the amount of accumulated crystal defects created by the movements of the fission products and the alpha-recoil nucleus in the crystal lattice.

Because most complicating factors cause AHe ages that are 'too old', Fitzgerald *et al.* (2006), propose to determine a weighted mean age and suggest that the most representative age for the sample lies between the minimum AHe age and the weighted mean age. The approach is most reliable in cases were the full age variability of the sample is covered, and they propose to determine 20-25 single grain ages to robustly constrain the full age variability.

3.2 Sampling strategy

The landscape of the study area is characterized by a complex topography with a distribution of elevations that varies significantly in N-S and E-W directions. For this reason, in a first field campaign samples were taken following as closely as possible one N-S and one E-W topographic section covering the entire study area. In a second field campaign focus was lain on the Galicia area. Samples were taken following two transects crossing the major structural features, the As Pontes and the Lugo fault, respectively. Samples were taken from elevations between 0 and 1,256 m above sea level and from a number of lithologies, including low to high-grade siliciclastic metasediments ranging from Neoproterozoic to Lower Paleozoic age and granites of Carboniferous to Permian age.

3.3 Sample processing and preparation

Heavy mineral concentrates (i.e. Apatites and Zircons) necessary for fission-track and (U-Th-Sm)/He analysis were obtained following standard processing techniques as proposed e.g. by Grist and Ravenhurst (1992a; b) or Stöckli (2005) and described below.

3.3.1 Rock crushing and heavy mineral separation

Rock samples between 3-5 kg each were washed to avoid any contamination and crushed with the rock splitter (Fig. 3.5). A hand specimen was stored. Further chrushing to gravel size was done by a jaw crusher. Particles < 300 µm went directly to the shaking table (Wilfley table) to reduce sample amount by washing out the clay-sized fraction. Particles > 300 µm went to the roller mill (roll distance < 300 µm) to reduce grain size to < 300 µm. A subsequent sieving procedure separated the fraction still > 300 µm. This fraction went back to a further cycle through the roller mill. This procedure was repeated until less than 15 % of sample amount was still > 300 µm. This fraction then was stored. The rest was processed by the shaking table (see above). The subsequent sieving through 63 µm assured that no particles smaller than 63 µm were further processed. At the end of the crushing procedure a sample fraction with grain sizes between 63 and 300 µm was obtained.

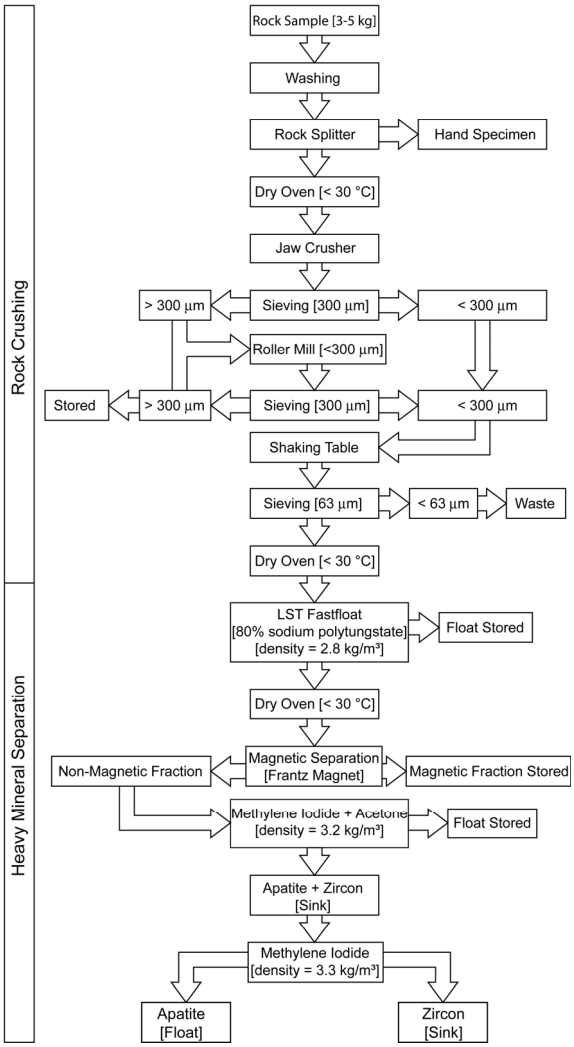

Fig. 3.5: Flow chart summarizing the processes of rock crushing and heavy mineral separation to obtain apatite and zircon aliquots.

Heavy mineral separation was carried out to obtain concentrates of apatite and zircons. This was achieved in four steps: (1) heavy liquid separation by LST Fastfloat (80 % sodium polytungstate) with a density of 2.8 kg/m^3 in a heavy liquid centrifuge. (2) Subsequent magnetic separation with a Frantz magnetic separator. (3) The non-magnetic fraction was further processed by a solution of methylene iodide and acetone with a density of 3.2 kg/m^3 and (4) of pure methylene iodide with a density of 3.3 kg/m^3 in a centrifuge.

3.3.2 AFT sample preparation

Apatite grains for AFT analysis were embedded in epoxy resin (Fig. 3.6). These epoxy resin grain mounts were cut, grinded and polished to reveal the internal mineral surface. The actual fission-tracks are too small for observation under the optical microscope. To make fission-tracks visible an etching procedure has to be applied. Sobel and Seward (2010) examined the influence of etching conditions on D_{par}®. They pointed out the importance of controlled etching conditions for further use of D_{par}® as a kinetic parameter in thermal models like HeFTy©. Apatites were etched in 5.5 M HNO_3 for 20 (1) s at 21 (1) °C. As external detector U-free micas are attached in close contact with the polished sample mount and packed into an aluminium tube in the presence of three glass neutron dosimeter (CN5) of known uranium content at top, middle and bottom of the sample batch (aluminium tube) as well as two Durango apatite samples as internal age standards. Samples were irradiated at the research reactor FRM II, Munich, with an aspired neutron flux of 1 x 10^{16} thermal neutrons/cm^2. After irradiation detection mica (external detector) is etched in 48 % HF for 20 (1) min at 20 (1) °C. To avoid false (incomplete) lengths measurements due to water release into the horizontal confined tracks

as a result of irradiation, sample mounts have been cleaned with 99.9 % ethanol in ultrasonic bath and dried for 10 min at 90 °C. Finally grain mount and detection mica are attached side by side to a glass slide for further processing under the optical microscope.

3.3.3 AHe sample preparation

Apatite concentrates revealed from heavy mineral separation were screened for apatite crystals appropriate for AHe dating. AHe analytical work needs well defined apatite crystals with a minimum size of 60 µm in diameter that should be free of any mineral or fluid inclusions and free of cracks, therefore, accurate sample selection and preparation is crucial. For each sample selected for dating, at least two grains were processed, whenever the quality of the apatite grains allowed, up to five grains were analyzed. The apatite concentrate, therefore, was searched through under the binocular to select appropriate apatite crystals by hand picking, using fine tweezers. Before being packed into U-free Pt-foil tubes the shape dimensions of the grains were measured (Mitchell and Reiners, 2003).

3.4 Data acquisition

3.4.1 AFT data acquisition

Area densities (tracks/cm^2) of spontaneous and induced tracks, distribution of horizontal confined track lengths and c-axis oriented etch pit diameters (D_{par}®; Donelick 1993; 1995) were determined at the Heidelberg FT-1 system (Fig. 3.6). The Heidelberg FT-1 system consists of an Olympus® 'BX50' optical microscope with an Autoscan® 'AS3000i' 3-axis microscope stage, a high-resolution Peltier-cooled color CCD camera 'ColorView III' (5 megapixel) of Olympus® and a high performing Windows® based computer system with two high resolution flat screens. To increase the precision of stage movement each axis is equipped with the external laser scale sensor 'BL 55 RE' of Sony®. These sensors guarantee a deviation of less than 500 nm along 4-5 cm of movement. The entire setup is operated through the Autoscan® software Trakscan®. Applying the largest possible resolution, each pixel is equivalent to less than 250 nm in size. Area densities were counted by using a 50x dry objective. Horizontal confined track lengths and etch pit size were measured by a 100x dry objective using the Autoscan® computer code 'EasyLength®'.

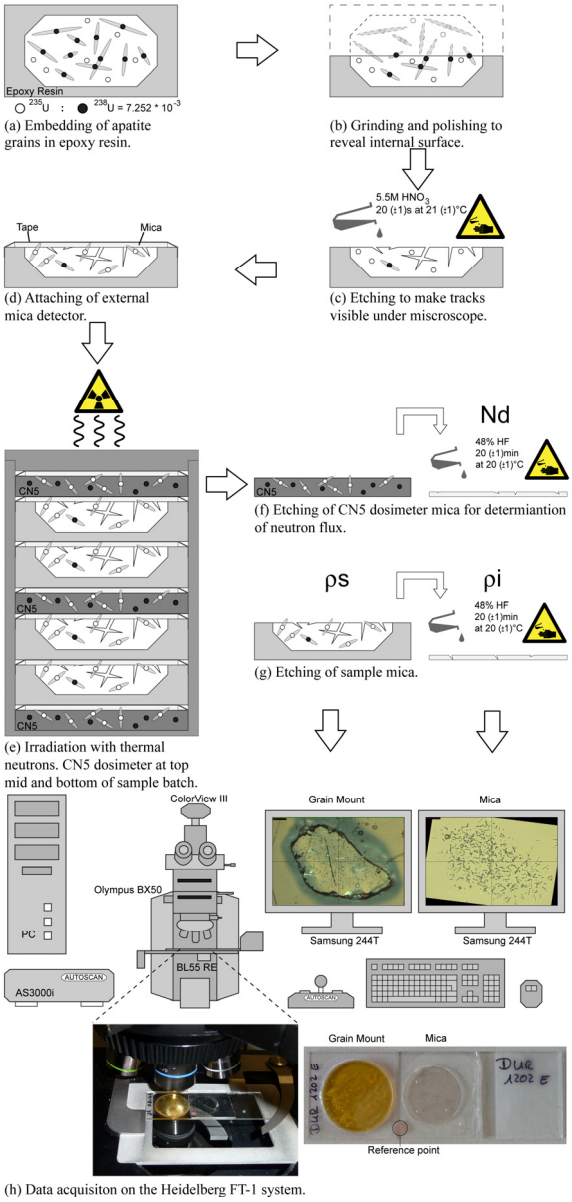

Fig. 3.6: Sketch of laboratory procedure to conduct single grain age determination at the Heidelberg FT-1 system (redrafted after Juez-Larré, 2003).

AFT ages were calculated applying the external detector method (Fleischer *et al.*, 1965a) in combination with the ζ-method described by Hurford and Green (1982; 1983). The ζ-values of 356.21 (11.24), 337.91 (10.31), 341.41 (15.48) and 340.59 (14.68) were obtained by counting several Durango apatite

age standards. All ages, 1σ errors, and radial plots were determined by using the computer code 'Trackkey' (Dunkl, 2002). The results are reported after the recommendation of Hurford (1990), with AFT ages reported as central ages (Galbraith and Laslett, 1993).

3.4.2 AHe data acquisition

The AHe analytical work was performed at the Isotope Geosciences Unit, SUERC, Scottish Enterprise and Technology Park, East Kilbride, UK, following the procedures in Foeken *et al.* (2006). U, Th and Sm extraction and analysis followed the procedures of Dobson *et al.* (2005). Technically the analytical procedure to determine the AHe ages involves the following steps: i) Measurement of He content: He degassing of single apatite crystals was performed using a diode laser (Foeken *et al.*, 2006), followed by purification and quantification by noble gas spectrometry done with a Hiden quadrupole mass spectrometer (QMS); ii) Measurement of U-Th-Sm content of the degassed crystals: Apatites are removed from vacuum system and dissolved within HNO_3 to analyze U, Th and Sm on an ICP-MS. All quantities were measured on a single crystal, to eliminate uncertainties that arise from grain to grain heterogeneities (Farley and Stöckli, 2002; Ehlers and Farley 2003).

Raw ages were calculated following Meesters and Dunai (2005). An α-ejection correction has been applied to the raw ages using HeFTy©, based on the recommendations of Ketcham *et al.* (2009). All models of diffusion kinetics are based on a spherical diffusion domain. In nearly spherical grains, the radius of the modelled sphere approximately corresponds to the average radius. In contrast, for more elongate grains, Meesters and Dunai (2002) recommend that the radius should correspond to a sphere with the same surface-to-volume ratio (S/V) as the actual mineral grain. Therefore, the equivalent sphere radius for each grain was calculated (Ketcham, 2009):

$$radius_{Eq.Sphere} = \frac{3}{(S/V)} \qquad (3)$$

on which the further α-ejection correction is based.

3.5 Rock uplift, surface uplift, rock exhumation

To avoid misconception while describing rock movements, the recommendations of England and Molnar (1990) were followed (see also Ring *et al.*, 1999a; Lisker *et al.*, 2009) defining the terms rock uplift, surface uplift and rock exhumation. Rock uplift and surface uplift describe the displacement of rocks or the Earth's surface, respectively, with respect to the geoid (or another frame of reference), while rock exhumation specifies the movement of rocks with respect to the Earth's surface.

The relationship of the three displacements is given by the equation:

surface uplift = rock uplift – rock exhumation (4)

The rate of rock exhumation equals the rate of denudation, i.e. the rate of removal of overburden by tectonic or erosional processes from a region or point. While exhumation describes the unroofing of a point, denudation applies to an area (Ahnert, 2003; Summerfield and Brown, 1998). As described later PECUBE is able to model the parameters rock uplift and surface uplift and, therewith, the exhumation.

3.6 Thermal modelling

In his work on 'General Model Theory' Stachowiak (1973) pointed out that a model is characterized by three fundamental attributes. These are: (1) a model is an imitation of a real process, (2) it is simplified and (3) pragmatic. In other words, a model is an imitation of a real process or an extract of reality obtained through generalization and simplification in order to solve a certain question of a certain relevant part of reality.

For numerical models this means that an image of reality is defined by boundary conditions described by physical equations and parameterized according to the initial question. Results are displayed for given boundary conditions and model parameters, i.e. for a given geological scenario. These results can be compared with real observed data to verify the

plausibility of the model. So far this is called the 'forward approach' of modelling. In a further step the results of the comparison of observed data with the predicted data from modelling can be ranked by calculating consistencies (misfits) and are then used to re-define model parameters. Such an 'inverse approach' can be used to iteratively improve model parameters in order to reduce the difference between modelled and observed data. Finally, we have to consider that all models are wrong, but can be useful to sharpen the initial question (cf. Box and Draper, 1987). Therefore, in modelling certain questions arise: (1) how good is the model, (2) how well does the model fit the observations and (3) is the model too complex (i.e. does it overinterpret the data). If these questions are taken into account and answered properly numerical models are a powerful tool to specify the interpretation of data.

3.6.1 Time-temprature path modelling

Determination of the low-temperature thermal history can be achieved by a modelling procedure that considers known annealing kinetics of fission-tracks in apatite, as well as He-diffusion behaviour of apatite and combines it with the real fission-track data set (single grain ages, confined fission-track lengths distribution, fluorine and chlorine content with D_{par}® as a proxy), as well as with the determined (U-Th-Sm)/He age (if available) and the time-temperature coordinates obtained from the known geological evolution of the area. Therefore, the modelling process tests the geological evolution against the thermochronological data set to determine a best fit t-T evolution by using HeFTy© (v1.7 beta 2). The primary goal of the program is to define envelopes in t-T space that contain all paths passing baseline statistical criteria and being conformed to the user-entered geological constraints. A good fit corresponds to a merit value of 0.5 or higher (goodness of fit [G.O.F] ≥ 50%). An acceptable fit corresponds to a merit value of 0.05 or higher (G.O.F ≥ 5%), indicating that the model has not failed the null hypothesis test that forms the basis of the applied statistics (Ketcham, 2009; Ketcham *et al.*, 2009).

In a first step, the data was modelled in a forward approach, considering information from geological evolution of the study area and determined AHe ages where available. The resulting t-T path provides one solution for a possible cooling history of the area. Based on the best forward model, the inverse modelling was initiated. Along the t-T path several constraint boxes can be set, acting as starting fields for the inverse model. In a Monte Carlo approach the computer code attempts to find out of 10,000 up to 1,000,000 single t-T paths, those ones that best approximate the measured data. It is evident that the more degrees of freedom are existent (i. e. the more parameters are modelled; e. g. AFT ages, AFT lengths, AHe ages, AHe diffusion, etc.) the more model runs are needed to find the best possible solution. Performed sensitivity tests revealed that for a simple AFT modelling 10,000 model runs are sufficient to find the best solution. However, if AHe data is added, the modelling procedure needs more runs to achieve that. Usually a number of 1,000,000 model runs is sufficient to find the best possible solution. For each sample which also yields AHe data as many single grain ages as possible were tested to model together with the AFT data. Therefore, each He-diffusion model available in HeFTy© (Wolf *et al.*, 1996; Farley, 2000; Shuster *et al.*, 2006; Flowers *et al.*, 2009) was tested and the amount of modelled single grain AHe ages consecutively reduced until considerable good fits were achieved.

The first constraint box was always chosen at a temperature around 160 °C with the younger age limit such that the AFT age of the sample is included in the box. The upper age limit was set at about 50-70 Ma older (based on outcomes from age-elevation relationship plots). In this way, the modelling algorithm tests a wide range of cooling paths at which the samples have entered the PAZ. First the samples with the most horizontal confined tracks available (i.e. the most reliable samples for modelling) were modelled and further constraint boxes were introduced to increase the amount of good fits. In the next step samples of the same blocks were modelled with equal

constraint boxes to test similar cooling histories for samples of each block.

3.6.2 3D integrated thermokinematic modelling

Joint modelling of multiple samples is the intention of integrated 3D thermokinematic modelling to better exploit their spatial relationship and common thermal history information. Compared to HeFTy© models additional parameters (e.g. surface evolution, rock uplift rate etc.) are taken into account to get closer to a realistic geological scenario. As shown e.g. by Braun and Van der Beek (2004), Herman *et al.* (2007; 2009), Valla *et al.* (2010) and van der Beek *et al.* (2010), an integrated 3D thermokinematic model is essential for getting a better idea of the coupling between tectonic and climate forcing (interaction between solid Earth and overlying atmosphere) and, therefore, the long-term landscape evolution. Recent developments in computer technologies allow to provide large computing power routinely and, therefore, to perform state-of-the-art numerical modelling of sophisticated integrated 3D models closer to reality. Braun (2003a) provided such a 3D thermokinematic model with the software code PECUBE.

In order to predict thermal histories and thermochronological ages at the Earth's surface from a given thermal and structural scenario the transient heat transport equation has to be solved in three dimensions, including conductive and convective terms as well as the effect of an evolving surface topography and changing rock uplift rates on the temperature field in the underlying crust. Three-dimensional heat transfer in the crust is governed by the following equation (Carslaw and Jaeger, 1959):

$$\rho_c c\left(\frac{\partial T}{\partial t}+\dot{R}\frac{\partial T}{\partial z}\right)=\left[\kappa\frac{\partial^2 T}{\partial x^2}+\kappa\frac{\partial^2 T}{\partial y^2}+\kappa\frac{\partial^2 T}{\partial z^2}\right]+\rho_c H \quad (5)$$

Where T is temperature, t is time, x, y and z are spatial coordinates, ($\dot{R}$) is the vertical rock uplift rate (i.e. the velocity of rocks with respect to the fixed base at z = -L) (cp. Chapter 3.5), κ is the thermal diffusivity, H is the rate of radiogenic heat production per unit mass, ρ_c is crustal density, and c is heat capacity.

This equation has to be solved for a given initial temperature distribution:

$$T_0 = T_0(x, y, z, t = 0) \quad (6)$$

and a set of boundary conditions:

$$T(x, y, z = -L, t) = T_L \quad (7)$$

$$T(x, y, z = S(x, y, t), t) = T_{MSL} + \beta S \quad (8)$$

$$\frac{\partial T}{\partial n} = 0 \text{ along the side boundaries} \quad (9)$$

where $S(x,y,t)$ is the assumed, time-varying surface topography. T_L is the assumed temperature at the base of the model (e.g. Moho or the base of the lithosphere), T_{MSL} is the assumed temperature at mean sea level, and β is the atmospheric lapse rate (i.e. the rate of change of temperature with elevation in the atmosphere), n is the outward normal to the side boundaries.

3.6.2.1 PECUBE

The software code PECUBE (Fig. 3.7a) developed by Braun (2003a) is a 3D thermokinematic model based on a finite element method (FEM) code solving the transient heat transport equation in three dimensions. It has been designed to accurately predict the effect of a finite-amplitude, time-varying surface topography on the underlying structure. From the solution of the transient heat transport equation it determines the thermal history of rock particles that will end up at the surface of the model at the end of the computations. From the thermal histories (*t-T* paths) it computes AFT ages, using the annealing models of Laslett *et al.* (1987) and Crowley *et al.* (1991), as well as AHe ages using a finite difference scheme to solve the time-dependent, thermally activated solid-state diffusion equation for helium in apatite (Wolf *et al.*, 1998) for all points at the surface of the model. It enables, therefore, predictions of thermal histories and thermochronological ages from input rock uplift rates and relief

development histories (i.e. long-term landscape evolution). PECUBE is combined with an inversion method (Fig. 3.7b) based on the Neighbourhood Algorithm (NA) of Sambridge *et al.* (1999a; b). This allows to 'invert' the forward approach to search through a predefined parameter space for an optimal set of parameter values that result in age predictions that best agree with the observed ages (within uncertainties). The agreement of predicted and observed ages is calculated by a misfit function, which is defined as the L^2-norm of the weighted difference between the observation vector (O) and the prediction vector (P):

$$\text{misfit} = \frac{1}{n}\sqrt{\sum_{i}^{n}\left(\frac{O_i - P_i}{\Delta O_i}\right)^2} \qquad (10)$$

where n is the number of measured ages and ΔO_i are the observational errors. Misfit values of ≤ 1 imply that the observed ages could be reproduced within uncertainty. The higher the misfit value the worse is the replication of observed data.

To perform this inversion the NA method navigates through parameter space to find, in an optimum manner, the minimum of the misfit function, i.e. the best agreement of predicted and observed ages, by using the natural neighbour interpolation and Voronoi diagram concepts.

3.6.2.2 Model set up and parameterization

In the models all parameters except for the rock uplift rate and the surface uplift rate (defined by the amplification factor of the topography) and, therewith, the resulting exhumation rate, are spatially uniform and constant through time over the whole model (i.e. the boundary conditions of the model). The surface uplift rate can vary through time, controlled by the time steps, but is spatially uniform, whereas the rock uplift rate can vary through space and time controlled by the fault movement. It is, therefore, differentiated between parameters that are: (1) uniform through space and constant through time, (2) uniform through space and variable through time and (3) variable through space and time. Furthermore, it is differentiated between 'fixed' parameters (representing the boundary conditions of the model) and the 'free' parameters which are inverted for.

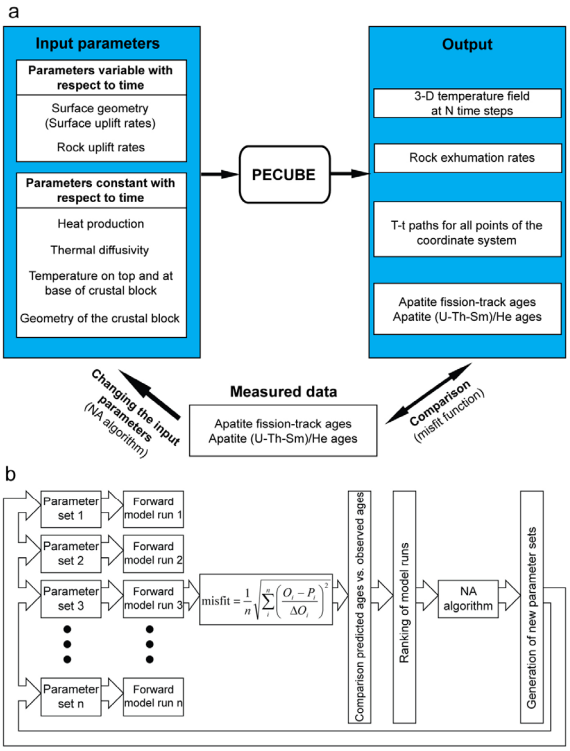

Fig. 3.7: Schematic flow chart describing (a) the general operating mode of PECUBE (modified after Braun, 2003a; b) and (b) the operating mode of the inverse approach of PECUBE (modified after Braun, 2003a).

3.6.2.3 Boundary conditions – 'fixed' parameters

The model spatial resolution (Fig. 3.8) depends on the wavelength of the topography that will affect the isotherm corresponding to the closure temperature of the thermochronological system(s) being used. This wavelength is thus given by the following relationship (Braun, 2002a):

$$\omega_c = \frac{T_c}{G_0} \qquad (11)$$

where T_c is the closure temperature of the thermochronometer used and G_0 is the local geothermal gradient. In the current case the 'critical wavelength' for the AFT thermochronometer is equal to 4 km for a closure temperature of 110 (10) °C (Gleadow and Duddy, 1981) and a geothermal gradient of

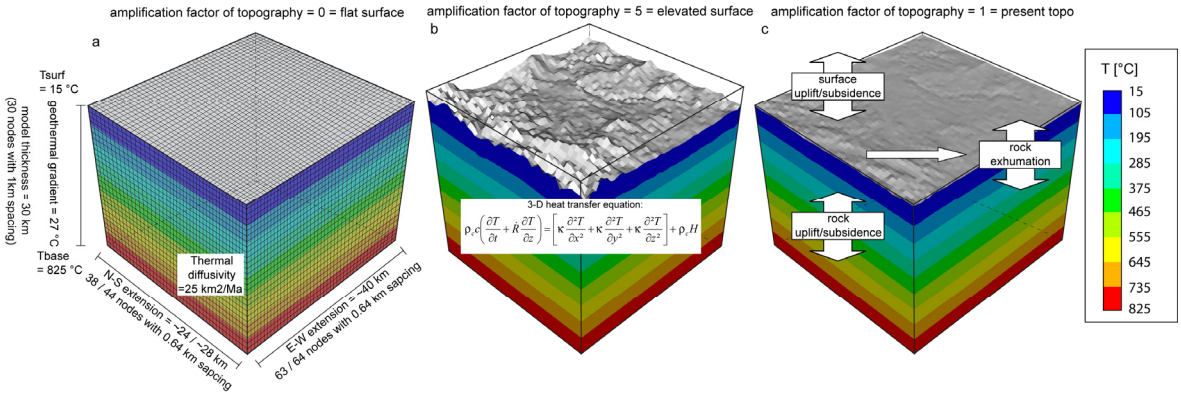

Fig. 3.8: (a) Modelled crustal block with boundary conditions, FEM discretization (model resolution); (b) basic 3D heat transfer equation to be solved, (c) the relationship between rock uplift, surface uplift (amplification factor of topography) and rock exhumation (cp. Chapter 3.5).

27 °C (Fernández *et al.*, 1998). Accordingly, the 'critical wavelength' for the AHe thermochronometer is equal to 2.6 km for a T_c of 70 (5) °C (Farley *et al.*, 1996; Farley, 2000; Stöckli *et al.*, 2000; Wolf *et al.*, 1996; 1998). Therefore, the initial horizontal spacing between the nodes (i.e. the horizontal resolution of the model) was originally set to 480 m. However, a test run to determine the sensitivity of the model revealed that a decreased resolution of 640 m yielded indistinguishable results at much lower computing costs.

Two key areas have been selected for modelling (Fig. 3.9) and were modelled separately: (1) North Galicia area, (2) Central Galicia area. The intention was to model across the major structural features to catch the difference in timing and rate of exhumation of different fault blocks. The modelled area in North Galicia has been defined as a rectangle with about 40 x 24 km edge length in E-W and N-S extension, respectively, with 63 x 38 nodes. In Central Galicia an area of about 40 x 28 km has been defined with 64 x 44 nodes. The gridding between each node is 0.008 arc degrees. As discussed above this corresponds to a spacing of 640 m between the nodes. The model (crustal) thickness has been set to 30 km with a resolution of 1 km, i.e. 30 nodes in z-direction. The temperature at the surface has been set to 15 °C while the temperature at the base of the model is specified to 825 °C. This gives an initial geothermal gradient of 27 °C/km. Thermal diffusivity has been set to 25 km^2/Ma, a value most likely for rocks of the Earth's crust.

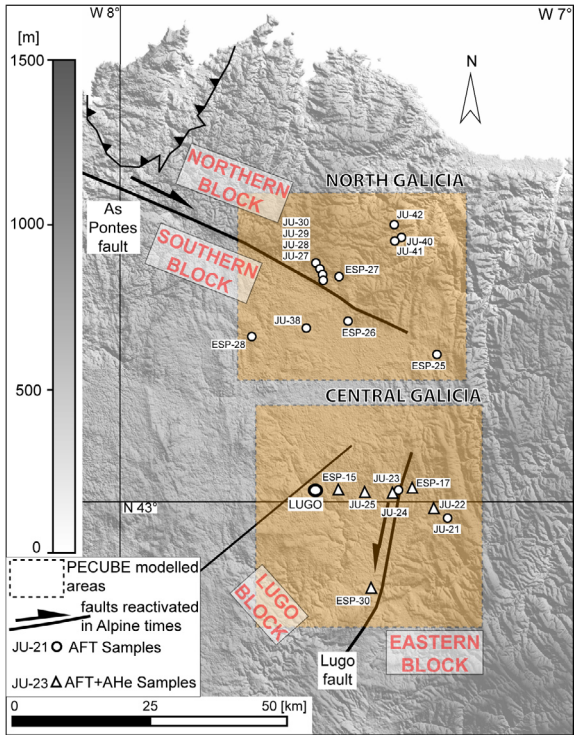

Fig. 3.9: Map visualizing the two areas modelled with PECUBE, as well as the different blocks separated by major faults and locations of modelled samples.

3.6.2.4 Thermochronological data

A total of 12 observed AFT cooling ages in the North Galicia area as well as 8 AFT and 6 AHe cooling ages (Fig. 3.9) in the Central Galicia area have been integrated in the 3D thermokinematic models for comparison with predicted cooling ages.

3.6.2.5 Fault geometry

In the North Galicia area a NW-SE striking fault, representing the As Pontes fault, has been

defined, dividing the crustal block in the Northern and the Southern block. In Central Galicia a NW-SE striking fault representing the Lugo fault has been defined, dividing the area in the Lugo and the Eastern block. The vertical dipping of the faults is unknown, therefore, the dipping of the faults is set to 90°. This enables to model vertical rock movements at each side of the fault and neglect lateral mass movements.

3.6.2.6 Time steps

Subsequently, the time steps to characterize the tectonomorphic scenario have to be defined (Tab. 3.1). The starting point (Ma in the past) of each model has been set to 290 Ma, marking the end of the Variscan orogeny (Pérez-Estaún *et al.*, 1990; 1991; Martínez-Catalán *et al.*; 2007). The ending point is set at present. Intermediate time steps describe (assumed) important breaks in the tectonothermal evolution, i.e. a change in rock uplift rate or relief evolution (surface uplift rate), according to geological constraints. They are set to: 165 Ma which coincides with the onset of active rifting in the continental margin (Le Pichon *et al.*, 1971; Srivastava *et al.*, 1990); 115 Ma marks the starting of the post-rift phase in the continental margin (García-Mondejar *et al.*, 2005; Verhoef and Srivastava, 1989; Montadert *et al.*, 1979). The time step at 85 Ma was chosen to better resolve the post-rift phase that culminated with a low relief surface whose remains are preserved in Central Galicia today. Only in the North Galicia area an additional time step at 35 Ma was set to simulate a flat surface until 35 Ma and the onset of activity along the As Pontes fault through Late Paleogene times (Huerta *et al.*, 1996; Santanach *et. al.*, 2005).

3.6.2.7 Inverse modelling – 'free' parameters

As the major task of the 3D modelling is to determine the timing and quantify the rate of exhumation governed by the evolving

Table 3.1.

PECUBE Model parameterization and parameter space.

	Evolving Topography							**Surface Uplift**		**Rock uplift**		**Rock exhumation**	
Time steps	present mean elevation	amplification factor of topography		resulting mean elevation		Time segment		surface uplift rate		rock uplift rate		rock exhumation rate	
[Ma]	[m]			[m]		[Ma]		[km/Ma]		[km/Ma]		[km/Ma]	
		min	max	min	max	from	to	min	max	min	max	min	max
North Galicia													
290	510	3	8	1530	4080						*Northern block*		
165	510	2	3	1020	1530	290	165	-0.004	-0.024	0	0.3	0.024	0.304
115	510	1	2	510	1020	165	115	-0.010	-0.020	0	0.3	0.020	0.310
85	510	0	0	0	0	115	85	-0.017	-0.034	0	0.3	0.034	0.317
35	510	0	0	0	0	85	35	0.000	0.000	0	0.3	0.000	0.300
0	510	1	1	510	510	35	0	0.015	0.015	0	0.3	-0.015	0.285
											Southern block		
										0	0.3	0.024	0.304
										0	0.3	0.020	0.310
										0	0.3	0.034	0.317
										0	0.3	0.000	0.300
										0	0.3	-0.015	0.285
Central Galicia													
290	540	5	8	2700	4320						*Lugo block*		
165	540	3	5	1620	2700	290	165	-0.009	-0.022	0	0.3	0.022	0.309
115	540	2	3	1080	1620	165	115	-0.011	-0.032	0	0.3	0.032	0.311
85	540	1	2	540	1080	115	85	-0.018	-0.036	0	0.3	0.036	0.318
0	540	1	1	540	540	85	0	0.000	-0.006	0	0.3	0.006	0.300
											Eastern block		
										0	0.3	0.022	0.309
										0	0.3	0.032	0.311
										0	0.3	0.036	0.318
										0	0.3	0.006	0.300

Greyish colour marks time steps during which the block movement is coupled.

topography and the rock uplift, these two parameters (surface uplift and rock uplift) have been inverted for. The parameter space of the inversions as well as the resulting ranges for exhumation rates are summarized in Table 3.1.

3.6.2.8 Landscape evolution (surface uplift rate)

At each time step an amplification factor of the topography is imposed to change the amplitude of the topography, i.e. to model changes in surface relief. It has to be considered that the topography only varies in amplitude but not in shape. This necessary simplification is likely to be correct during the post-orogenic phase of a mountain belt, where the potential for stream capture and reorganization of the fluvial network is assumed to be small and, therefore, valleys and interfluves are regarded as static features (Braun and Robert, 2005). In the Central Galicia area the intention was to simulate a continuous decay in relief since the end of Variscan orogeny until present. A similar continuous decay in relief was simulated for the North Galicia area with the exception that the decay occurred faster and ended already at 85 Ma with a flat surface. From 35 Ma this flat relief was intended to grow to present elevation as a result of Alpine fault activity (Boillot *et al.*, 1979; Alonso *et al.*, 1996; Pulgar *et al.*, 1996; Alvarez-Marrón *et al.*, 1997).

3.6.2.9 North Galicia

The maximum height of a mountain range is controlled and, therefore, limited by several factors (i.e. climate, glaciation, isostatic effects) (Thomson *et al.*, 2010, Whipple and Meade, 2004; Montgomery and Brandon, 2002; Dahlen and Suppe, 1988). Thus, in North Galicia the range for the initial mean elevation was set between 4,080-1,530 m (Tab. 3.1) as a reasonable range for the maximum mean elevation of the Variscan orogen topography. Subsequently a nearly linear decrease of topography with an elevation range between 1,530-1,020 m at 165 Ma and 1,020-510 m at 115 Ma to a flat surface at 85 Ma was simulated. The flat surface was simulated to last until 35 Ma, when the increase of surface relief to mean present elevation was initiated. The flat surface at time steps 85 and 35 Ma refers to constraints of Huerta *et al.* (1996) and Santanach *et al.* (2005) taking the evolution of the As Pontes basin into account. These dated continental deposits in the basin are cut by the As Pontes fault between 30-22 Ma.

3.6.2.10 Central Galicia

The rock uplift rate during the first interval was coupled and decoupled not until the second time step. This means, the fault activity was allowed to start not until 165 Ma.

3.6.2.11 Output

The output after the entire computation processes consists of the complete 3D temperature field at any pre-defined time step, as well as the exhumation rates and the temperature experienced through time by rocks that reached the surface at the end of the computations. These t-T paths are then used to predict AFT and AHe cooling ages which are compared to the observed ages (Fig. 3.7).

4 Results

4.1 Apatite fission-track (AFT) ages

In total 35 AFT cooling ages have been determined covering the entire study area (Fig. 4.1; Tab. 4.1). The ages cover a wide range from 68.1 (5.0) to 246.7 (26.9) Ma (Fig. 4.1; Tab. 4.1). All ages are younger than the corresponding sedimentation, metamorphic or intrusive age of the sampled rocks. All single grain age distributions fulfilled the χ^2-test, indicating that all single grain ages are consistent with a common true value (Galbraith, 1981). The χ^2 test is passed when χ^2 > 5 %. Because of the very different nature of the topography and considering the major structural features the data were grouped into three areas: (1) the Asturias area, (2) the North Galicia area and (3) the Central Galicia area.

4.1.1 Asturias area

In the Asturias area, 12 samples yielded AFTages that range from 96.2 (9.4) and 246.7 (26.9) Ma with all ages being younger than the protolith age. However, there is an apparent relationship between fission-track age and protolith age, with the oldest Neoproterozoic rocks yielding older average fission-track ages than younger rocks. Three samples from Neoproterozoic rocks within the Narcea antiform yielded ages of 202.2 (9.9) Ma (# ESP-35), 246.2 (26.9) Ma (# ESP-18) and 202.8 (25.2) Ma (# ESP-13), with no apparent relationship between age and elevation (Fig. 4.2). One sample (# ESP-33) from the Neoproterozoic rocks of the Narcea antiform yielded an age of 134.0 (9.3) Ma. Furthermore, two samples (# ESP-25, 31) from Proterozoic to Lower Cambrian rocks within the Mondoñedo antiform yielded ages between 142.6 (7.6) and 215.7 (21.3) Ma. Carboniferous and Permian syn- and post-kinematic granites yielded ages

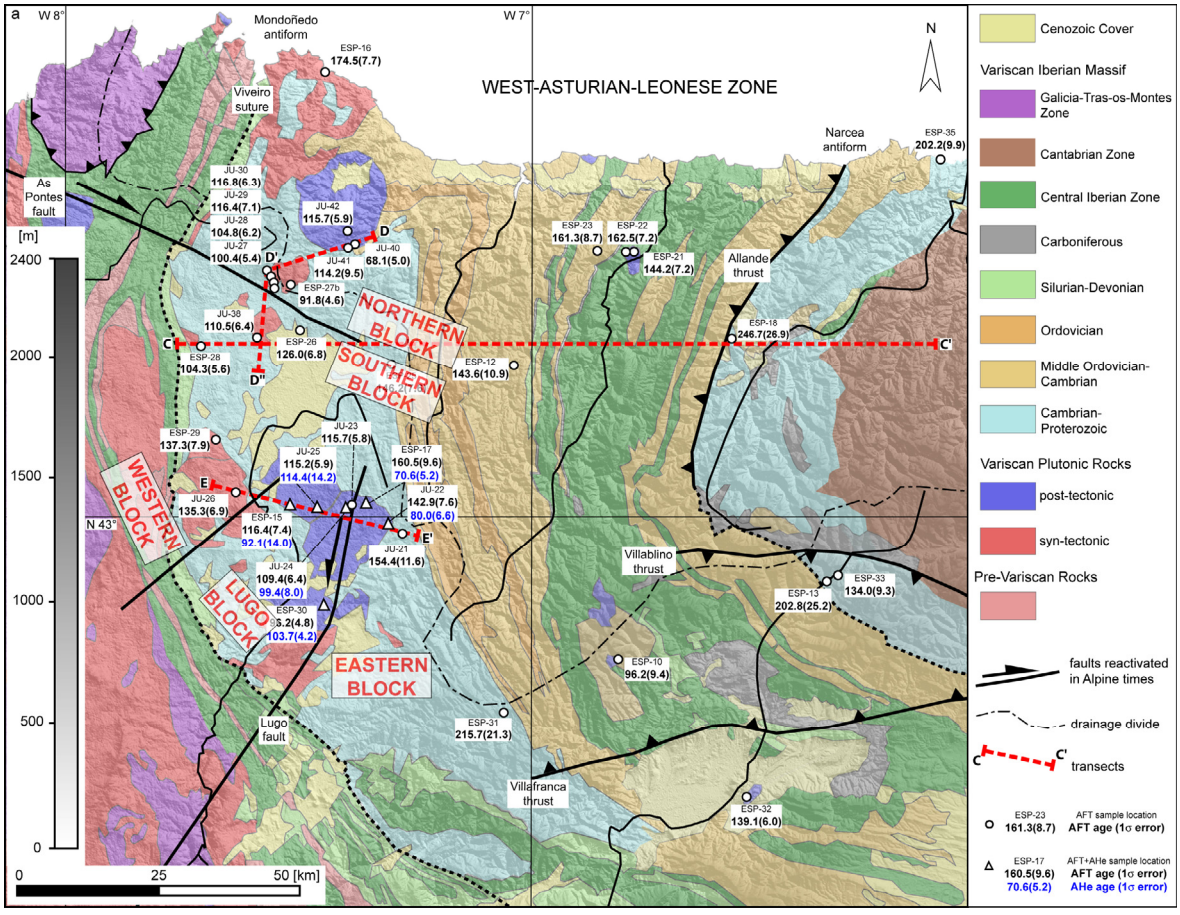

Fig. 4.1: Geological map of the study area with sample locations and AFT central ages as well as the youngest AHe age (were available). Positions of three topographic transects discussed in Chapter 5 are also displayed.

Table 4.1.
Apatite fission-track results.

Sample	Elev. [m a.s.l.]	N Latitude	W Longitude	Lith.	Pluton	Form. age [Ma]	U (std) [µg/g]	n	Sp. Tracks ρ_s [10^5 tr/cm^2]	Sp. Tracks N_s	Ind. Tracks ρ_i [10^5 tr/cm^2]	Ind. Tracks N_i	$P(\chi^2)$ [%]	Central age [Ma]	Error ± 1σ [Ma]
Asturias															
ESP-10	1256	42°46'26"	6°49'14"	gr	C. del Agua	pok-va	11.9 (10.3)	18	4.8	160	13.0	436	99.3	96.2	9.4
ESP-12	787	43°14'20"	7°03'15"	msd	-	CO	18.2 (12.7)	28	11.9	327	21.6	595	99.9	143.6	10.9
ESP-13	910	43°01'23"	6°14'52"	msd	-	PC	7.3 (4.1)	21	6.1	124	7.8	159	100.0	202.8	25.2
ESP-18*	590	43°16'35"	6°36'10"	mgrd	-	P	12.5 (2.2)	7	13.6	192	12.5	177	75.9	246.7	26.9
ESP-21*	547	43°26'23"	6°48'47"	gr	Boal	pok-va	42.6 (16.9)	20	27.7	1119	43.6	1763	98.9	144.2	7.2
ESP-22*	659	43°26'35"	6°49'05"	gr	Boal	pok-va	50.0 (19.0)	20	35.7	1872	49.7	2607	94.7	162.5	7.2
ESP-23*	399	43°26'24"	6°52'46"	sd	-	CO	30.2 (16.6)	18	17.8	900	24.9	1259	76.1	161.3	8.7
ESP-25*	524	43°14'23"	7°17'58"	msd	-	LC	20.2 (12.9)	39	13.0	1010	20.0	1554	81.0	146.2	7.6
ESP-31*	1099	42°43'30"	7°01'06"	msd	-	PC	11.1 (5.8)	20	11.4	229	11.5	230	91.2	215.7	21.3
ESP-32*	668	42°33'30"	6°33' 23"	gr	Ponferrada	pok-va	37.9 (5.3)	24	26.0	2041	40.6	3187	92.6	139.1	6.0
ESP-33*	935	42°54'12"	6°22'00"	msd	-	P	19.6 (10.4)	21	11.7	421	19.0	681	94.6	134.0	9.3
ESP-35*	10	43°33'53"	6°08'48"	msd	-	P	10.8 (6.5)	30	10.6	1724	11.3	1846	56.1	202.2	9.9
North Galicia															
ESP-16	0	43°41'50"	7°26'25"	gr	San Ciprián	synk-va	12.6 (5.0)	30	6.9	510	14.1	1039	99.1	116.4	7.4
ESP-26*	443	43°17'33"	7°29'41"	msd	-	PC	22.0 (15.6)	39	10.7	1206	19.2	2163	13.3	126.0	6.8
ESP-27a*	639	43°21'58"	7°30'55"	fr-gr	Monseibán	synk-va	40.6 (10.1)	20	15.1	1067	43.1	3047	71.4	78.1	3.7
ESP-27b*	645	43°22'00"	7°30'58"	gr	Monseibán	synk-va	31.7 (9.2)	20	14.0	1470	34.3	3593	45.0	91.8	4.6
ESP-28*	544	43°16'05"	7°42'30"	fo-gr	-	PC	17.0 (6.6)	21	8.7	910	18.4	1927	21.1	104.3	5.6
JU-27**	606	43°21'51"	7°33'48"	gr	Monseibán	synk-va	29.9 (13.4)	21	14.3	2362	32.2	5312	26.5	100.4	5.4
JU-28**	697	43°22'29"	7°33'54"	gr	Monseibán	synk-va	34.3 (9.3)	23	17.3	1364	37.3	2938	13.1	104.8	6.2
JU-29**	800	43°22'51"	7°34'04"	gr	Monseibán	synk-va	18.8 (6.8)	25	10.6	976	20.4	1885	86.1	116.4	7.1
JU-30**	915	43°23'19"	7°34'26"	gr	Monseibán	synk-va	24.7 (7.4)	23	13.4	2077	25.6	3986	41.2	116.8	6.3
JU-38**	425	43°17'02"	7°36'00"	gr	Román	synk-va	24.2 (11.6)	20	11.5	1631	25.6	3618	13.1	110.5	6.4
JU-40**	350	43°25'57"	7°23'08"	gr	La Tojiza	pok-va	6.4 (3.4)	17	2.1	399	7.6	1426	79.4	68.1	5.0
JU-41**	526	43°25'39"	7°24'18"	gr	La Tojiza	pok-va	18.5 (14.4)	5	8.0	305	17.0	642	81.1	114.2	9.5
JU-42**	835	43°27'09"	7°24'18"	gr	La Tojiza	pok-va	21.5 (6.9)	25	11.8	3630	24.3	7501	46.8	115.7	5.9
Central Galicia															
ESP-15	470	43°01'03"	7°30'56"	gr	Lugo	pok-va	12.6 (5.0)	30	6.9	510	14.1	1039	99.1	116.4	7.4
ESP-17	507	43°01'11"	7°21'12"	gr	Castroverde	pok-va	6.2 (2.7)	25	4.5	675	6.7	1014	100.0	160.5	9.6
ESP-29*	447	43°07'14"	7°40'33"	gr	Sta. Eulalia	synk-va	25.4 (14.0)	20	14.8	715	23.7	1146	49.3	137.3	7.9
ESP-30*	382	42°53'43"	6°23'03"	gr	S. Julian	pok-va	28.5 (11.7)	20	12.7	955	29.0	2178	82.6	96.2	4.8
JU-21***	618	42°58'37"	7°17'23"	sl	-	LC	11.9 (8.0)	14	9.3	444	14.5	688	99.2	154.4	11.6
JU-22***	558	42°59'22"	7°19'10"	gr	Castroverde	pok-va	11.6 (4.2)	33	8.2	1823	13.8	3061	99.8	142.9	7.6
JU-23***	534	43°01'18"	7°23'31"	gr	Castroverde	pok-va	17.1 (8.2)	34	9.6	2649	19.9	5516	97.9	115.7	5.8
JU-24**	487	43°00'52"	7°24'21"	gr	Castroverde	pok-va	15.6 (4.2)	30	8.1	1298	16.8	2687	23.6	109.4	6.4
JU-25***	495	43°01'00"	7°28'09"	mgrd	Lugo	pok-va	16.1 (4.5)	34	9.5	2084	19.9	4368	95.9	115.2	5.9
JU-26***	410	43°02'36"	7°38'47"	gr	Hombreiro	synk-va	44.5 (19.6)	17	29.9	3065	53.3	5458	17.5	135.3	6.9

Geodetic reference system of coordinates: WGS 84, Lith.: lithology, U: Uranium concentration, std: standard deviation, n: number of apatite grains, ρs: density of spontaneous tracks, Ns: number of spontaneous tracks, ρi: density of induced tracks, Ni: number of induced tracks, $P(\chi^2)$: probability that single grain ages are consistent and belong to the same population. Test is passed if $P(\chi^2) > 5\%$ (Galbraith, 1981), Nd = 10474 tracks counted on CN5 dosimeter glass. Ages are calculated using a ζ-value of 337.91 (10.31). Samples marked with "*": Nd = 13802, ζ-value of 356.21 (11.24), "**": Nd = 15555, ζ-value of 341.41 (15.48), "***": Nd = 15386, ζ-value of 340.59 (14.68). fo-gr: foliated granite, fr-gr: fractured granite, gr: granite, mgrd: meta-granodiorite, msd. meta-sandstone, sl: slate, synk-va: syn-kinematic Variscan, pok-va: post-kinematic Variscan, P: Proterozoic, PC: Proterozoic-Cambrian, CO: Cambrian-Ordivician, LC: Lower-Cambrian.

between 96.2 (9.4) and 162.5 (7.2) Ma. The youngest age of 96.2 (9.4) Ma was obtained from a granite sample taken at 1,256 m (# ESP-10), the highest elevation of all samples. Three samples from small post-Variscan granitic bodies along the central Boal-Ancares dome (# ESP-21, 22, 32) yielded an average age of 149 Ma (σ_{std} = 12 Ma), somewhat older than similar rocks in the Galicia area. One sample (# ESP-23) from within the sediments near granite samples ESP-21 and 22 yielded an age of 161.3 (8.7) Ma, similar to the samples from the granitic rocks. A sample within the Oscos plateau area (# ESP-12) at 780 m elevation yielded an age of 143.4 (10.9) Ma that could be correlated with samples from the Lugo plain.

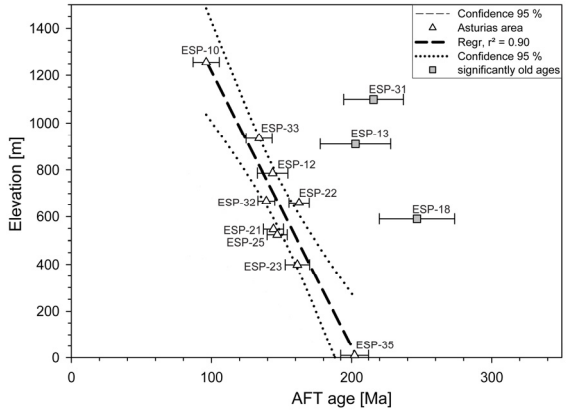

Fig. 4.2: Age elevation-relationship plot (AER) of samples from the Asturias area. AFT ages reported with 1σ error.

The age-elevation relationship (AER) plot for the Asturias area samples shows a rather large degree of scatter (Fig. 4.2). However, if the three significantly old ages (# ESP-13, 18, 31) which also show significantly high errors obtained from the Neoproterozoic rocks are not taken into account, a well defined negative slope can be observed. According to Braun (2002b) this negative slope is indicative for a general decay in relief.

4.1.2 North Galicia area

In North Galicia, 13 samples record AFT central ages that range from 68.1 (5.0) to 126.0 (6.8) Ma. Three samples (# JU-40, 41, 42) in the La Tojiza pluton, yielded AFT ages that range between 68.1 (5.0) to 115.7 (5.9) Ma. Sample JU-40 with an age of 68.1 (5.0) Ma at 350 m elevation is also the youngest AFT age determined so far in Galicia. The four samples taken in the Monseibán pluton (# JU-27, 28, 29, 30) along the near vertical transect coinciding with the As Pontes fault escarpment yielded AFT ages that range from 100.4 (5.4) to 116.8 (6.3) Ma. Two additional samples (# ESP-27a, b) were taken in the same pluton with ages of 78.1 (3.7) and 91.8 (4.6) Ma, respectively. At the northern coast one sample (# ESP-16) from the San Ciprián pluton revealed an age of 116.4 (7.4) Ma. Three samples (# ESP-26, 28, JU-38) taken south of the As Pontes fault yielded AFT ages between 104.3 (5.6) and 126.0 (6.8) Ma. The age-elevation relationship (AER) plot of all samples from North Galicia is presented in Figure 4.3. Samples north of the As Pontes fault indicate a positive trend in AER with a break in slope at c. 115 Ma. Samples ESP-27a from a fractured granite and JU-41 that had only 5 datable grains are considered outside of the trend. Sample ESP-16 from the coast is too far away to be included in the trend. The exhumation rates derived from regression lines are ~0.25 km/Ma for the fast exhumation at 115 Ma and ~0.01 km/Ma after this event.

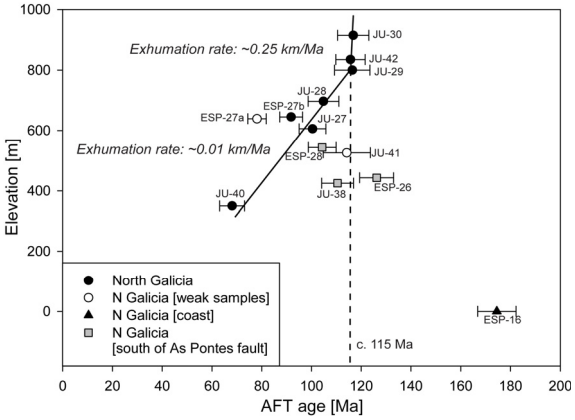

Fig. 4.3: Age elevation-relationship plot (AER) of samples from North Galicia. Regression line through selected samples from the north of the As Pontes fault (Northern block) with calculated exhumation rates. Dashed line marks break in slope at ~115 Ma. AFT ages reported with 1σ error.

South of the As Pontes fault data is too scarce to reveal a significant trend.

4.1.3 Central Galicia area

In Central Galicia, 10 samples record AFT central ages that range from 96.2 (4.8) to 160.5 (9.6) Ma. Samples were taken at elevations between 382 and 618 m. Except for the Lower Cambrian slate of sample JU-21 all samples are granitic-granodioritic rocks from syn- to post-tectonic Variscan plutons.

In Central Galicia the Lugo fault separates the Eastern block from the Lugo block and a no-named fault separates the Lugo block from the Western block (Fig. 4.1). Both faults are trending NNE-SSW. A sharp change in AFT age occurs across the Lugo fault. Samples to the east of the fault (# JU-21, JU-22 and ESP-17) with ages ranging from 160.5 (9.6) to 142.9 (7.6) Ma are much older than samples to the west. The samples to the west (# JU-23, 24, 25 and ESP-15, 30), range in age between 96.2 (4.8) and 116.4 (7.4) Ma. This difference is observed also between samples taken across the fault, in the same pluton and at similar elevations. This difference is interpreted to indicate movement along the fault at ~116 Ma. The westernmost samples (# JU-26, ESP-29) bear AFT cooling ages of 135.3 (6.9) and 137.3 (7.9) Ma, respectively. This is significantly older than the samples from the Lugo block west of the Lugo fault mentioned above. The difference is interpretd as caused by faulting at ~116 Ma. This time of fault activity is similar to that of the Lugo fault, and several faults with the same trend as the Lugo fault are mapped in the area between samples ESP-15 and JU-26 (González-Lodeiro *et al.*, 1982). These results indicate that the NNE-SSW trending set of faults within the low relief areas of Lugo were active during the main episode of rifting in the Early Cretaceous thus causing significant variation in AFT age (in the order of several tens of Ma) across them.

The resulting AER plot (Fig. 4.4) provides a similar trend for samples from the Lugo block as of those from North Galicia north of the As Pontes fault. The AER shows fast exhumation at a rate ~0.25 km/Ma with a significant break in slope at c. 115 Ma and a subsequent moderate exhumation at a rate of ~0.01 km/Ma.

The trend of the samples from the Eastern and Western block is not significant due to scarce data.

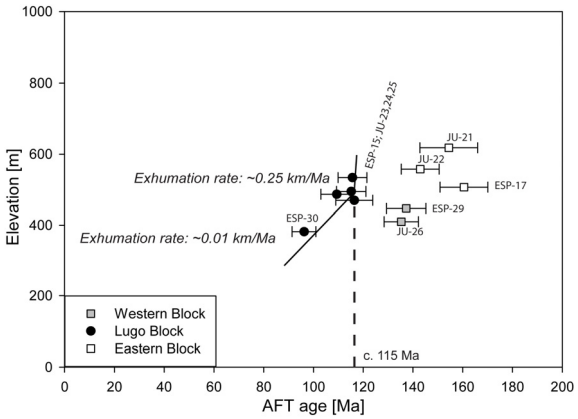

Fig. 4.4: Age elevation-relationship plot (AER) of samples from Central Galicia. Regression line through selected samples with calculated exhumation rates. Dashed line marks break in slope at ~115 Ma.AFT ages reported with 1σ error.

4.1.4 Etch pit size and track length distribution

A total of 7,675 single D_{par}® values were determined for all apatite grains used in this study (Tab. 4.2). The mean D_{par}® values determined for each sample show a very narrow range between 1.2 (0.1) to 1.8 (0.1) µm. Indicating a very homogenous chemical composition with respect to the fluorine chlorine content of the apatites. The skewness of all single D_{par}® values determined for each sample lies between -0.70 and 5.80. With exception of samples JU-24, 28, 42 and ESP-23 all samples exhibit a positive skewness. The skewness is a measure of symmetry of the distribution; positive skewness indicates a tailing towards larger values while negative skewness indicates a tailing towards smaller values. The largest etch pit size of 2.9 (0.1) µm was measured in sample ESP-35. This sample shows also the largest spread in etch pit size between 0.9 (0.1) and 2.9 (0.1) µm. No positive correlation between single grain ages and D_{par}® values has been detected.

A total of 2,459 lengths of horizontal confined spontaneous fission-tracks were measured (Tab. 4.2). The obtained mean track lengths range from 10.4 (1.2) to 12.6 (1.8) µm. Excep for samples JU-24 and ESP-10, 21, 22, 23 all samples show a negative skewness between -0.05 and -1.67 indicating a tailing towards shorter track lengths. The skewness is not very significant, indicating a simple cooling history. There is no relation between track lengths distribution and elevation or AFT ages. The measured confined track lengths were corrected for their orientation to the crystallographic c-axis by applying the computer code HeFTy© to the data set. The mean c-axis projected lengths changed to a distribution between 12.4 (1.1) and 14.1 (1.1) µm. With the exception of samples JU-21, 23 and ESP-22, 25 all samples show a negative skewness between -0.15 and -2.59. Again there is no correlation between track lengths and AFT ages or elevation.

4.2 (U-Th-Sm)/He (AHe) ages in Central Galicia

Apatite (U-Th-Sm)/He (AHe) ages in Central Galicia were determined from 6 samples with 2-5 single grain ages for each sample. Five samples (# ESP-17, 15, JU-22, 24, 25) lie on a more or less linear transect across the Lugo fault and were taken in the Castroverde and Lugo pluton, respectively. One sample (ESP-30) was taken in the San Julian pluton in the south. Raw AHe ages (Tab. 4.3) range from 42.6 (3.2) to 118.8 (6.3) Ma. α-ejection correction after Ketcham *et al.* (2009) was applied to all grains giving ages between 70.6 (5.2) and 171.8 (16.5) Ma (Tab. 4.3, Fig. 4.1).

According to the recommendations of Fitzgerald *et al.* (2006) weighted mean ages were calculated and 'most represantitve ages' were determined. As the results do not differ significantly from the youngest AHe ages, the youngest α-ejection corrected AHe was used for further interpretation.

Sample ESP-15 shows good intra-aliquot age replication within 10% error. In Sample ESP-17 the two youngest AHe ages replicate within 10% error, while in samples JU-22 and 24 the two youngest AHe ages reproduce within 15% error. The poor intra-aliquot age replication in other samples may be due to undetected mineral or fluid inclusions or related to slow cooling

through the PRZ (Fitzgerald *et al.*, 2006). All

Table 4.2.
Detailed apatite fission-track length data.

Sample	n CT	M.-l. [µm]	Stdev [µm]	CT skew factor	Lc [µm]	Stdev [µm]	Lc skew factor	n D_{par}	D_{par} [µm]	Stdev [µm]	D_{par} skew factor
Asturias											
ESP-10	13	11.2	2.6	0.13	n.a.	n.a.	n.a.	n.a.	n.a.	n.a.	n.a.
ESP-12	15	11.4	1.9	-1.51	n.a.	n.a.	n.a.	n.a.	n.a.	n.a.	n.a.
ESP-13	11	12.4	1.2	-1.09	n.a.	n.a.	n.a.	n.a.	n.a.	n.a.	n.a.
ESP-18	24	12.0	1.4	-0.88	13.6	0.9	-0.51	105	1.6	0.3	0.65
ESP-21	34	10.4	1.2	0.70	12.4	1.1	-0.11	146	1.5	0.2	0.91
ESP-22	69	12.0	1.4	0.39	13.7	0.9	0.08	100	1.4	0.1	0.34
ESP-23	50	12.1	1.2	0.22	13.6	0.9	-0.32	186	1.6	0.2	-0.18
ESP-25	81	12.0	1.5	-0.05	13.6	1.0	0.35	465	1.4	0.2	0.15
ESP-31	19	11.7	2.6	-1.67	13.7	1.2	-0.54	146	1.4	0.2	0.32
ESP-32	122	10.4	1.8	-0.11	12.8	1.0	-0.05	226	1.5	0.1	0.36
ESP-33	60	11.7	1.8	-1.12	13.5	1.1	-0.66	262	1.4	0.2	0.42
ESP-35	49	12.1	1.5	-0.19	13.6	1.2	-0.47	237	1.6	0.3	1.15
North Galicia											
ESP-16	131	12.4	1.3	-0.43	13.9	0.9	-0.53	191	1.8	0.2	0.78
ESP-26	94	11.8	1.6	-0.56	13.5	1.1	-0.97	392	1.4	0.2	1.16
ESP-27a	117	11.8	1.4	-0.59	12.9	1.3	-0.72	299	1.4	0.1	0.17
ESP-27b	121	12.3	1.6	-0.34	13.8	1.1	-0.61	331	1.4	0.1	0.18
ESP-28	43	10.6	1.7	-0.91	12.8	1.3	-0.73	225	1.5	0.2	0.05
JU-27	180	11.8	1.9	-1.14	13.6	1.2	-1.11	346	1.3	0.1	1.40
JU-28	90	11.0	1.7	-0.35	13.2	1.1	-0.15	260	1.3	0.1	-0.30
JU-29	84	11.6	1.9	-1.36	13.4	1.3	-1.59	305	1.3	0.1	4.30
JU-30	58	12.2	1.7	-1.54	13.7	1.3	-2.59	175	1.3	0.1	0.60
JU-38	100	12.4	1.5	-0.44	14.0	1.0	-0.30	294	1.4	0.1	5.80
JU-40	n.a.	n.a.	n.a.	n.a.	n.a.	n.a.	n.a.	84	1.4	0.1	0.30
JU-41	n.a	n.a.	n.a.	n.a.	n.a.	n.a.	n.a.	25	1.4	0.1	0.00
JU-42	147	12.6	1.8	-1.14	14.1	1.1	-0.98	135	1.5	0.1	-0.40
Central Galicia											
ESP-15	95	12.4	1.2	-0.37	13.9	0.9	-0.63	366	1.5	0.2	0.41
ESP-17	88	12.4	1.3	-0.86	13.9	1.0	-1.03	261	1.8	0.2	0.26
ESP-29	57	11.3	1.6	-0.08	12.9	1.4	-1.03	225	1.5	0.2	0.05
ESP-30	75	12.1	1.9	-0.93	13.6	1.4	-1.16	229	1.3	0.1	0.35
JU-21	36	11.4	2.0	-1.56	13.3	1.2	0.24	150	1.6	0.1	1.50
JU-22	106	11.4	1.9	-0.30	13.2	1.3	-0.64	396	1.5	0.1	0.49
JU-23	60	10.7	2.6	-0.17	13.0	1.5	0.19	362	1.4	0.1	4.87
JU-24	52	11.6	1.5	0.07	13.3	1.2	-0.25	269	1.2	0.1	-0.70
JU-25	69	11.4	2.0	-0.57	13.2	1.4	-0.46	382	1.3	0.1	0.60
JU-26	109	11.6	2.2	-0.41	13.2	1.6	-0.79	100	1.5	0.1	0.80

n CT: number of confined tracks measured, M.-l.: mean track length, std: standard deviation, skew.: skewness of distribution relative to the mean value (measure of asymmetry of the distribution), Lc: mean track length after c-axis correction, n Dpar: number of etch pit diameters measured, Dpar: mean eatch pit diameter.

age distribution (Reiners and Farley, 2001) AHe single grain ages of sample ESP-30 are older than its AFT age (Fig. 4.5) indicating that the full age variability has not been covered and the measured ages are too old, i.e. not enough grains were analysed to find the true AHe age. From the remaining samples at least one AHe single grain age was younger than the AFT age.

There is a different trend in AHe ages compared to AFT ages in the samples at each flank of the Lugo fault. Samples ESP-17 and JU-22 to the east of the fault show a large gap between the youngest AHe ages (70.6 (5.2) and 80.0 (6.6) Ma) and the AFT ages (160.5 (9.6) and 142.9 (7.6) Ma). In contrast, samples west of the Lugo fault (# ESP-15, 30, JU-24, 25) bear similar AHe and AFT ages with a narrow age range between 92.1 (14.0) and 116.4 (7.4) Ma.

Except for sample JU-22 (east of the Lugo fault) there is no clear correlation between equivalent grain radius (grain size) and AHe (Fig. 4.6). Two of the samples (# ESP-17, JU-22) seem to show a positive correlation between single grain AHe age and effective Uranium concentration (eU = U + 0.235Th; e.g. Shuster *et al.*, 2006), whereas the other samples show no clear correlation between eU and AHe (Fig. 4.7). In both cases a positive correlation is indicative for a long residence time in the PRZ.

Table 4.3.
Apatite (U-Th-Sm)/He data

Sample	m	Eq. SV Sphere Radius	F_t	U	U Error	Th	Th Error	Sm	$_4$He	$_4$He Error	TAE	Th/U	eU	Raw age	Error	Corr. Age	Error
	[µg]	[µm]		[µg/g]	[%]	[µg/g]	[%]	[µg/g]	[nmol/g]	[%]	[%]		[µg/g]	[Ma]	± 1σ [Ma]	[Ma]	± 1σ [Ma]
ESP-15a	3.0	49.57	0.70	5.6	6.6	9.9	6.2	b.d.l.	2.90	1.3	9.1	1.8	7.9	67.43	6.14	95.6	8.7
b	4.0	57.56	0.74	12.9	4.0	18.0	3.7	b.d.l.	6.92	1.3	5.6	1.4	17.1	74.04	4.15	99.0	5.6
c	2.7	51.63	0.71	9.0	4.6	13.3	5.1	b.d.l.	4.85	1.3	7.0	1.5	12.1	73.45	5.11	102.2	7.1
d	3.0	51.92	0.71	6.2	5.9	11.1	6.0	b.d.l.	3.45	1.3	8.5	1.8	8.8	71.97	6.12	100.2	8.5
e	0.9	34.85	0.57	7.9	6.4	4.5	13.7	b.d.l.	2.69	1.3	15.2	0.6	9.0	55.02	8.35	***92.1***	***14.0***
															Mean	**97.8**	**4.0**
															Wt mean	**99.0**	**3.5**
															most represantative age	**95.6**	**8.7**
ESP-17a	1.3	35.65	0.58	15.4	4.4	11.5	5.8	b.d.l.	4.21	1.3	7.4	0.7	18.1	42.61	3.16	***70.6***	***5.2***
b	0.6	29.69	0.50	18.3	7.7	26.1	10.0	b.d.l.	8.24	1.3	12.7	1.4	24.4	61.94	7.86	118.6	15.0
c	0.8	32.94	0.54	14.4	7.8	24.0	9.4	b.d.l.	7.57	1.3	12.3	1.7	20.0	69.22	8.50	122.6	15.1
d	1.1	36.56	0.59	14.3	5.4	20.5	7.4	b.d.l.	6.37	1.3	9.2	1.4	19.1	61.05	5.62	100.6	9.3
e	2.0	43.54	0.66	10.3	4.6	19.2	4.3	b.d.l.	4.27	1.3	6.5	1.9	14.8	53.07	3.43	79.8	5.2
															Mean	**98.4**	**23.0**
															Wt mean	**82.6**	**3.3**
															most represantative age	**76.6**	**4.2**
ESP-30a	1.3	45.00	0.67	31.6	2.9	6.6	5.4	b.d.l.	17.88	1.3	6.2	0.2	33.2	98.35	6.12	142.5	8.9
b	0.6	43.75	0.66	37.4	3.1	78.1	2.3	b.d.l.	21.00	1.3	4.1	2.1	55.7	69.00	2.80	***103.7***	***4.2***
c	0.8	45.00	0.67	40.3	3.4	11.5	8.9	b.d.l.	27.99	1.3	9.6	0.3	43.0	118.55	11.38	171.8	16.5
d	1.1	71.21	0.79	22.2	3.0	6.4	4.2	b.d.l.	15.43	1.3	5.3	0.3	23.7	118.80	6.31	148.0	7.9
															Mean	**141.5**	**28.2**
															Wt mean	**120.0**	**3.4**
															most represantative age	**111.8**	**3.8**
JU-22b	5.6	59.34	0.75	18.0	3.6	23.9	2.9	b.d.l.	14.30	1.3	4.8	1.3	23.6	110.52	5.28	146.1	5.7
c	1.8	43.98	0.66	14.6	5.7	14.8	5.7	b.d.l.	5.31	1.3	8.2	1.0	18.0	53.94	4.42	***80.0***	***6.6***
d	2.2	46.67	0.68	15.3	3.6	20.4	3.2	b.d.l.	7.13	1.3	5.0	1.3	20.1	65.08	3.24	94.3	4.7
e	1.0	35.69	0.58	16.9	5.4	29.6	6.3	b.d.l.	9.06	1.3	8.3	1.8	23.9	69.47	5.80	116.6	9.7
f	2.4	47.21	0.68	16.3	3.9	22.1	4.2	b.d.l.	11.82	1.3	5.8	1.4	21.5	100.38	5.84	144.6	8.4
															Mean	**116.3**	**29.5**
															Wt mean	**112.2**	**2.8**
															most represantative age	**96.1**	**4.7**
JU-24d	2.8	49.09	0.69	12.4	5.2	16.9	5.9	b.d.l.	6.26	1.3	8.0	1.4	16.3	70.11	5.61	***99.4***	***8.0***
g	1.4	37.70	0.60	20.8	4.9	26.8	7.0	b.d.l.	10.11	1.3	8.7	1.3	27.1	68.29	5.91	110.2	9.5
															Mean	**104.8**	**7.6**
															Wt mean	**103.9**	**6.1**
															most represantative age	**101.6**	**7.1**
JU-25a	1.1	36.56	0.59	10.6	6.6	13.9	9.1	b.d.l.	6.58	1.3	11.3	1.3	13.9	86.73	9.81	142.4	16.1
b	0.6	30.00	0.50	13.1	7.6	3.4	9.7	b.d.l.	4.71	1.3	12.4	0.3	13.9	61.91	7.68	***114.4***	***14.2***
e	0.7	31.03	0.52	18.4	2.8	14.7	3.6	b.d.l.	9.00	1.3	4.7	0.8	21.8	75.43	3.57	137.5	6.5
															Mean	**131.4**	**15.0**
															Wt mean	**134.6**	**5.6**
															most represantative age	**124.5**	**9.9**

Av. Radius: average radius of crystal; Eq. Sphere Radius: equivalent sphere radius of crystal; F_t: alpha recoil correction factor after Farley *et al.* (1996); U: Uranium concentration; Th: Thorium concentration; Sm: Samarium concentration; ^{4}He: ^{4}He concentration; TAE: total analytical error; eU: effective Uranium concentration; Corr. Age: corrected age; b.d.l.: below detection limit; Wt Mean: weighted mean age; youngest AHe age is highlighted in bold italics.

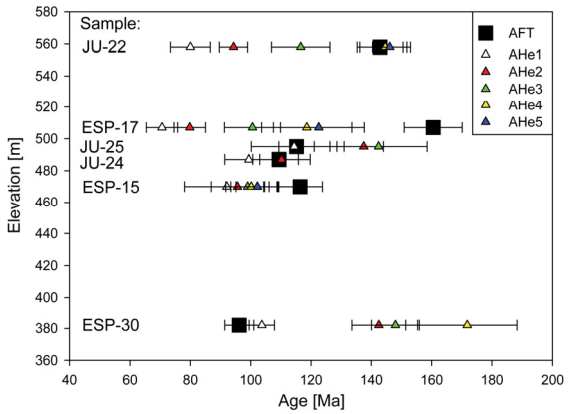

Fig. 4.5: AFT and AHe ages plotted versus elevation. Different colors of triangles represent the AHe single grain ages of each sample from young (white) to old (blue).

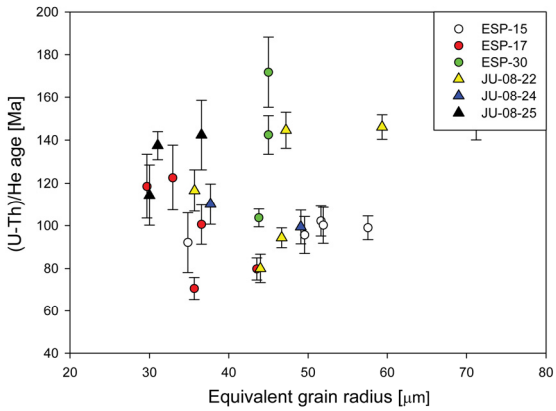

Fig. 4.6: AHe single grain ages (with 1σ error) plotted versus equvivalent grain radius.

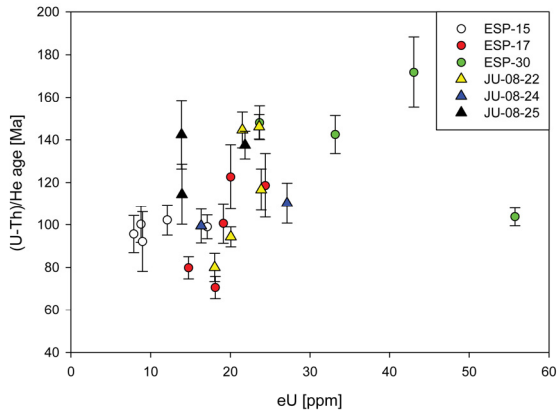

Fig. 4.7: AHe single grain ages (1σ error) plotted versus effective Uranium content (eU= U+0.235Th).

4.3 Thermal modelling

4.3.1 Time-temperature path modelling

In total 23 samples revealed more than 50 measured horizontal confined fission-tracks to perform single time-temperature (t-T) path modelling. Out of those, it was possible to perform AFT+AHe based HeFTy© modelling in three samples (# ESP-17, 15 and JU-22), being the rest AFT based HeFTy© models. In the following section, exhumation rates from t-T path derived cooling rates are calculated by assuming a constant geothermal gradient of 27 ºC/km. This value corresponds to the geothermal gradient determined from the present day heat flow density of 65 (5) mWm^{-2} in the area (Fernández *et al.*, 1998).

4.3.1.1 Asturias area

Four samples in the Asturias area revealed enough tracks to model t-T paths. Three of them (# ESP-22, 25, 32) show a three-segmented cooling history (Fig. 4.8) with an incipient fast cooling between 230 and 170 Ma with exhumation rates around 0.3 km/Ma (Tab. 4.4). The subsequent plateau phase of almost no cooling lasted until ~30 Ma. Since then an increased cooling with calculated exhumation rates of ~0.04 km/Ma is observed. The cooling history of another sample in the block between the Villablino and Villafranca thrust is significantly different. It shows a two-phased cooling that begins between 180 and 140 Ma with a fast exhumation rate of 0.278 km/Ma. The proximate slower cooling occurred at an exhumation rate of 0.12 km/Ma.

4.3.1.2 North Galicia area

Cooling patterns of the 10 t-T paths modelled from samples of the North Galicia area were arranged in three groups according to the sample location, i.e. (1) one sample at the coast, (2) samples from north of the As Pontes fault and (3) samples from south of the As Pontes fault (Fig. 4.9). Sample ESP-16 at the coast shows a similar three-phased cooling path as described from the Asturias area. However,

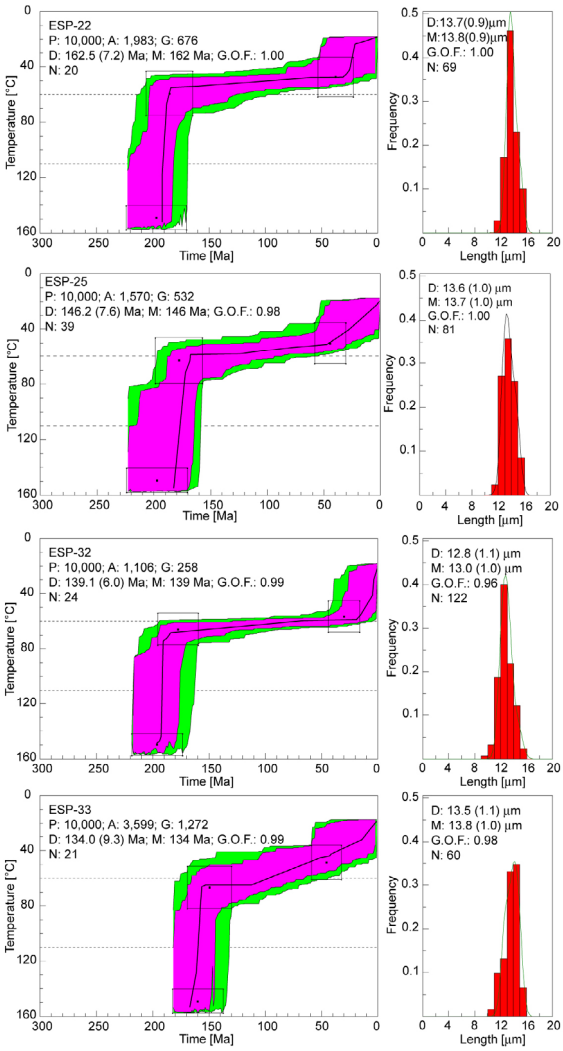

Fig. 4.8: Results of the numerical modelling of samples from Asturias. Modelling is done using the computer code 'HeFTy©' (Ketcham, 2005; Ketcham *et al.*, 2007a; b; Ketcham *et al.*, 2009). Displayed are the t-T paths (left) and the c-axis corrected confined fission-track length (cC-FT-L) distribution (right) overlain by a calculated probability density function (best fit). The results in the t-T curve show three different reliability levels (green envelope: acceptable fit = all t-T paths with a goodness of fit (G.O.F.) of > 0.05 (5%), pink envelope: good fit = all t-T paths with a G.O.F. of > 0.5 (50%), black line: best fit. P: number of tested inverse models, A: acceptable fit models, G: good fit models, D: determined AFT age (1σ error) and cC-FT-L, M: modelled AFT age and cC-FT-L, G.O.F.: goodness of fit of best fit model, N: number of single grains and measured confined fission-track lengths.

the intial exhumation rate is with 0.16 km/Ma slightly slower (Tab. 4.4). In turn, the plateau phase between 190 and 30 Ma shows a faster exhumation rate of 0.008 km/Ma. Since 30 Ma an increased exhumation rate of ~0.04 km/Ma is observed.

Modelled t-T paths from samples north of the As Pontes fault are in very good agreement (Fig. 4.9). The paths show a relatively fast cooling below temperatures of 80 °C between ~150 and 100 Ma with a mean exhumation rate of ~0.25 km/Ma (Tab. 4.4). The subsequent slower cooling after ~100 Ma yielded a reduction in exhumation rates to 0.01-0.02 km/Ma. However, two paths (# JU-28, 29) reveal a slightly different 3-phased cooling history with an increased exhumation rate of ~0.07 km/Ma around 20 Ma.

Samples from south of the As Pontes fault (# ESP-26, JU-38) show a similar cooling pattern like samples from north of the fault.

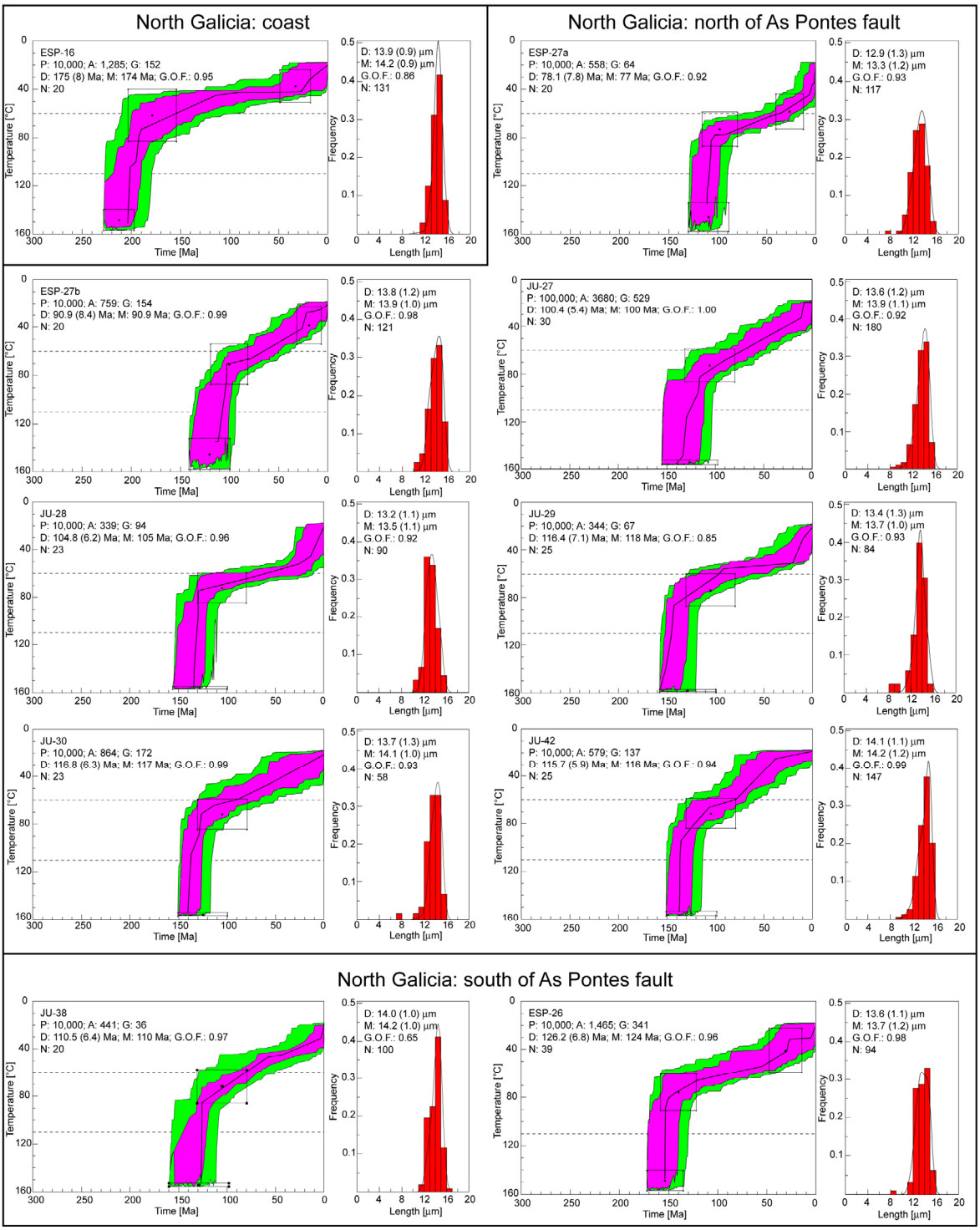

Fig. 4.9: Results of the numerical modelling of samples from North Galicia (for futher details see Fig. 4.8).

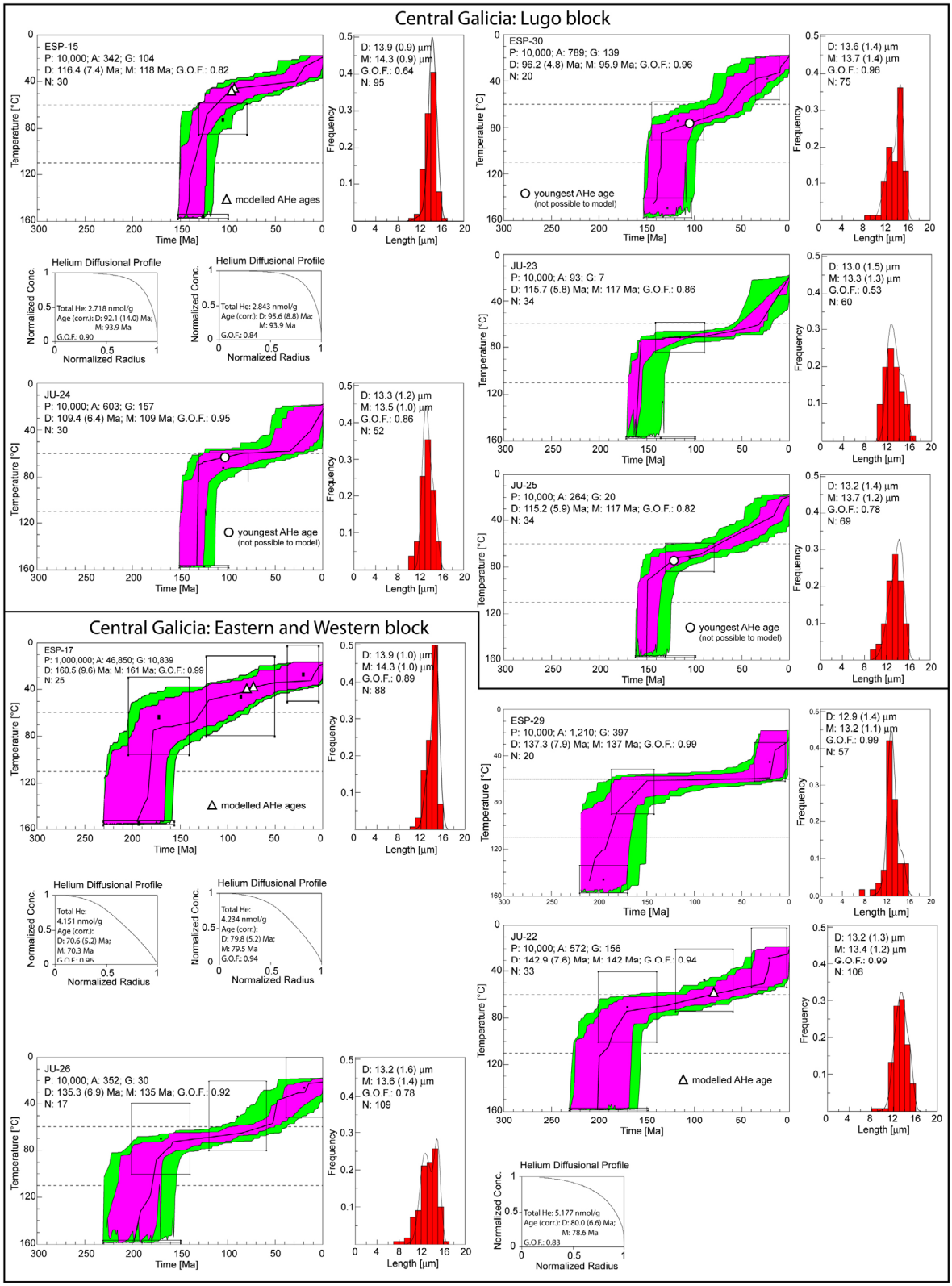

Fig. 4.10: Results of the numerical modelling of samples from Central Galicia (for futher details see Fig. 4.8). Where available Helium diffuision profiles are displayed.

4.3.1.3 Central Galicia area

The t-T paths of samples from Central Galicia display a larger dispersion in cooling history (Fig. 4.10). However, if grouped into the three different blocks a similar trend as seen in the AER plots can be observed. Samples from the Lugo block cooled below temperatures

of 80 °C between 160 and 130 Ma with an average exhumation rate of about 0.25 km/Ma (Tab. 4.4). The subsequent decrease in exhumation rate to ~0.02 km/Ma after 130 Ma can also be monitored. Time-temperature paths from the Eastern and Western block show a significantly different cooling history. Samples cooled below ~80 °C already at times between 210 and 180 Ma at an average rate of 0.25 km/Ma. After 180 Ma the average exhumation rate decreased to 0.01 km/Ma. As observed in North Galicia, the current samples (# JU-22, 23, 24, 26) also tend to show a 3-phased cooling history with an increase of exhumation rates to ~0.04-0.05 km/Ma between 30 and 40 Ma.

Table 4.4. (1)

Cooling and exhumation rates derived from modelled t-T paths.

Sample	Elevation [m a.s.l.]	t-t segment [Ma]		T-T segment [°C]		Cooling rate [°C/Ma]	Geothermal gradient [°C/km]	Exhumation rate [km/Ma]
Asturias								
ESP-22	659	192	184	140	55	10.63	27	0.394
		184	30	55	48	0.05	27	0.002
		30	0	48	15	1.10	27	0.041
ESP-25	524	180	168	140	58	6.83	27	0.253
		168	50	58	50	0.07	27	0.003
		50	0	50	15	0.70	27	0.026
ESP-32	668	192	183	140	68	8.00	27	0.296
		183	20	68	58	0.06	27	0.002
		20	0	58	15	2.15	27	0.080
ESP-33	935	165	155	140	65	7.50	27	0.278
		155	0	65	15	0.32	27	0.012
Mean Asturias								
3-segmented paths		188	178	140	62	8.12	27	0.301
		178	33	62	53	0.06	27	0.002
		33	0	53	15	1.14	27	0.042
North Galicia coast								
ESP-16	0	205	190	140	75	4.33	27	0.160
		190	28	75	42	0.20	27	0.008
		28	0	42	15	0.96	27	0.036
North Galicia north of As Pontes fault								
ESP-27a	639	110	102	140	78	7.75	27	0.287
		102	0	78	15	0.62	27	0.023
ESP-27b	645	112	102	140	70	7.00	27	0.259
		102	0	70	15	0.54	27	0.020
JU-27	606	135	115	140	80	3.00	27	0.111
		115	0	80	15	0.57	27	0.021
JU-28	697	135	130	140	75	13.00	27	0.481
		130	15	75	45	0.26	27	0.010
		15	0	45	15	2.00	27	0.074
JU-29	800	150	140	140	85	5.50	27	0.204
		140	20	85	50	0.29	27	0.011
		20	0	50	15	1.75	27	0.065
JU-30	915	140	125	140	70	4.67	27	0.173
		125	0	70	15	0.44	27	0.016
JU-42	835	150	140	140	90	5.00	27	0.185
		140	0	90	15	0.54	27	0.020
Mean North Galicia north of As Pontes fault								
2-segmented paths		129	117	140	78	4.95	27	0.183
		117	0	78	15	0.54	27	0.020
3-segmented paths		143	135	140	80	8.00	27	0.296
		135	18	80	48	0.28	27	0.010
		18	0	48	15	1.86	27	0.069

continuation next page

Table 4.4 (2) (continuation)

Cooling and exhumation rates derived from modelled t-T paths.

Sample	Elevation [m a.s.l.]	t-t segment [Ma]		T-T segment [°C]		Cooling rate [°C/Ma]	Geothermal gradient [°C/km]	Exhumation rate [km/Ma]
North Galicia south of As Pontes fault								
ESP-26	443	155	150	140	80	12.00	27	0.444
		150	0	80	15	0.43	27	0.016
JU-38	425	130	125	140	85	11.00	27	0.407
		125	0	85	15	0.56	27	0.021
Mean North Galicia south of As Pontes fault								
2-segmented paths		143	138	140	83	11.50	27	0.426
		138	0	83	15	0.49	27	0.018
Central Galicia Lugo block								
ESP-15	470	140	120	140	60	4.00	27	0.148
		120	0	60	15	0.38	27	0.014
ESP-30	507	140	135	140	85	11.00	27	0.407
		135	0	85	15	0.52	27	0.019
JU-23	534	160	155	140	75	13.00	27	0.481
		155	30	75	60	0.12	27	0.004
		30	0	60	15	1.50	27	0.056
JU-24	487	135	130	140	70	14.00	27	0.519
		130	35	70	60	0.11	27	0.004
		35	0	60	15	1.29	27	0.048
JU-25	495	150	140	140	85	5.50	27	0.204
		140	0	85	15	0.50	27	0.019
Mean Central Galicia Lugo block								
2-segmented paths Lugo block		143	132	140	77	5.43	27	0.201
		132	0	77	15	0.47	27	0.017
3-segmented paths Lugo block		148	143	140	73	13.50	27	0.500
		143	33	73	60	0.11	27	0.004
		33	0	60	15	1.38	27	0.051
Central Galicia Eastern and Western block								
ESP-17	507	190	180	140	75	6.50	27	0.241
		180	0	75	15	0.33	27	0.012
ESP-29	447	208	150	140	62	1.34	27	0.050
		150	20	62	58	0.03	27	0.001
		20	0	58	15	2.15	27	0.080
JU-22	558	200	170	140	75	2.17	27	0.080
		170	30	75	50	0.18	27	0.007
		30	0	50	15	1.17	27	0.043
JU-26	410	195	160	140	80	1.71	27	0.063
		160	50	80	60	0.18	27	0.007
		50	0	60	15	0.90	27	0.033
Mean Central Galicia Eastern and Western block								
3-segmented paths E and W block		201	160	140	72	1.65	27	0.061
		160	33	72	56	0.13	27	0.005
		33	0	56	15	1.23	27	0.046

Exhumation rates are calculated considering a geothermal gradient of 27 °C (Fernández et al., 1998).

4.3.2 3D integrated thermokinematic modelling

A total of 2,408 model runs was performed both for North Galicia and Central Galicia to find a best fit model in the final modelling step. Figure 4.11 shows the results of all models by plotting the two parameters which have been inverted for, i.e. the amplification factor of topography and the rock uplift rate, at each time interval against each other. The different time intervals between the time steps (290-165 Ma; 165-115 Ma; 115-85(35) Ma; 85(35)-0 Ma) are marked by different greyscales to discriminate against each other. The 35 Ma time step in the North Galicia model is set in brackets as the topographic evolution is decoupled from the fault movement. While the surface was set to be flat already between 85-35 Ma the fault movement started not until 35 Ma. The grey fields of each time interval also illustrate the parameter space (range) of the inverted parameters. Each point of the plots represents one model run at the accordant time interval (i.e. 2,048 points for 2,048 models at each interval). The color of the points visualizes the resulting misfit.

4.3.2.1 North Galicia – inverse models

For the Northern and Southern block in North Galicia the inverse models reveal a large range of misfit values between c. 41.1 and 0.5 (Fig. 4.11a, b). The large range indicates that the chosen parameter space was wide enough to give enough freedom not forcing the model in

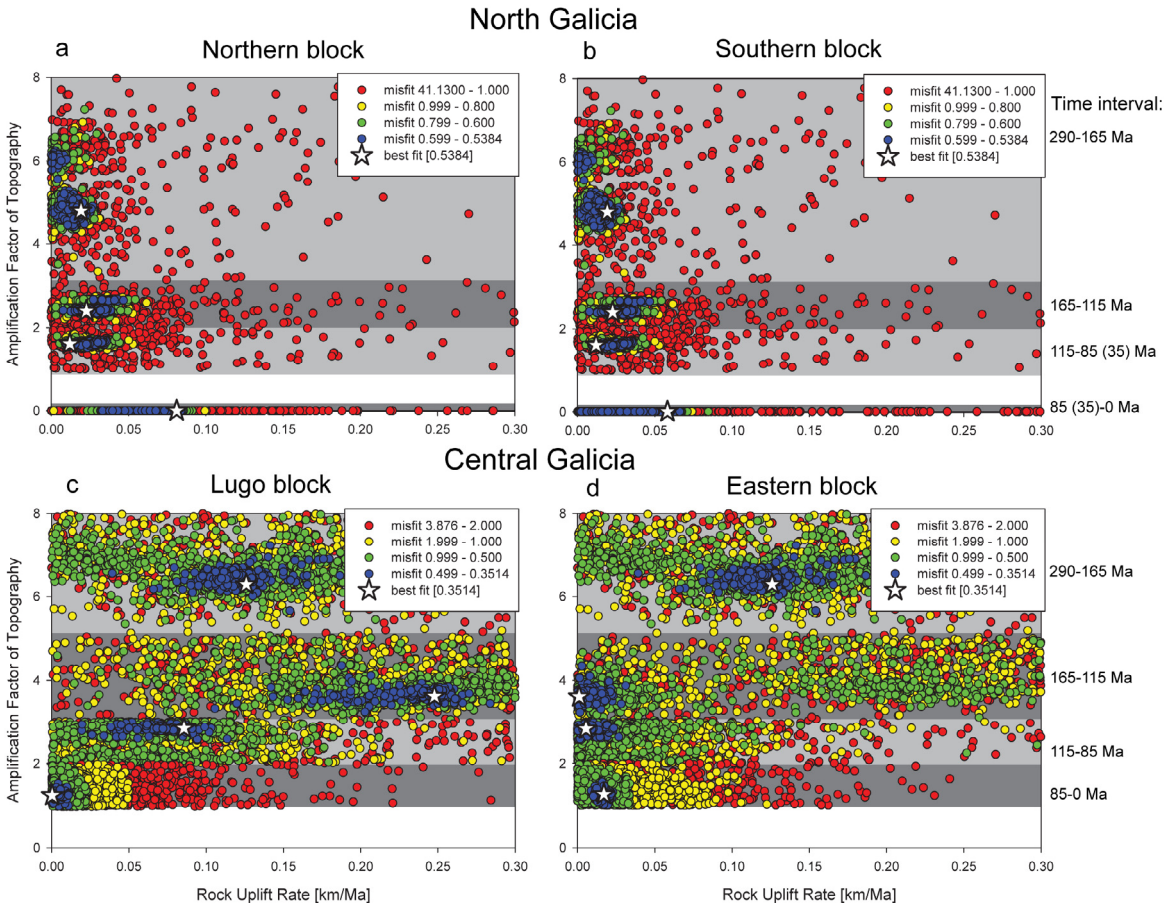

Fig. 4.11: Scatter plots showing summary of all 2,408 model runs from each modelled block. Each plot is subdivided into the accordant modelled time intervals marked by different greyish colors. Each point represents one model run at the accordant time step, while the shape and the colors of the points indicate the level of misfit (star: best fit; decreasing misfit in the order blue (low misfit), green, yellow, red (high misfit)). (a) and (b) Northern and Southern block of the North Galicia area with the time intervals 290-165 Ma; 165-115 Ma; 115-85(35) Ma; 85(35) Ma-present. (c) and (d) Lugo and Eastern block of the Central Galicia area with the time intervals 290-165 Ma; 165-115 Ma; 115-85 Ma; 85 Ma-present.

advance to a good fit. In contrast, the good fits cluster in narrow areas, indicating that the model calculations migrated fast towards the lowest misfits.

In the first three time intervals from 290 to 35 Ma, the rock uplift rates of the two blocks were coupled, therefore, the plots show the same results in this time span. From 290-165 Ma the plot shows two clusters very close to each other. The amplification factor of the topography ranges from ~6 to 4.5 (i.e. ~3,060-2,300 m)while the rock uplift rate plots between 0 and 0.025 km/Ma with a trend towards larger rock uplift rates at lower amplification of topography. During the second interval from 165-115 Ma the topography decays as predefined by the model to factors between 2.3 and 2.6 (i.e. ~1,170-1,330 m) while the rock uplift rate varies between 0.01 and 0.05 km/Ma. This time there is no correlation between rock uplift and topography as the topography is very stable around 2.5 (i.e. ~1,280 m). During the next interval the topography again is sharply determined at ~1.6 (i.e. ~820 m)while the range for the rock uplift rate decreases slightly from 0.01-0.04 km/Ma with a trend towards lower values (see best fit). At the last time steps the topography was predefined as flat surface from 85-35 Ma (indicated by the flat line at 0 m elevation in Fig. 4.11a, b). Also the fault has been activated allowing each block a different movement. The rock uplift rate from 35 Ma to present in the Northern block increases significantly in comparison to the preceding interval. It now ranges from 0.025 to 0.090 km/Ma. In the Southern block the change is more undifferentiated. The best fit model also points to an increase in rock uplift rate but with a total range between 0 to 0.070 km/Ma.

4.3.2.2 North Galicia – exhumation rates (best fit model)

The results from thermokinematic modelling for the best fit model are given in Table 4.5 and Figure 4.12a. Northern and Southern block movement was coupled until 35 Ma. Therefore, between 290-35 Ma N and S block yielded similar rates. Referring to equation (4) values for surface uplift and rock uplift rates resulted in exhumation rates for both blocks of 0.029 km/Ma between 290-165 Ma, 0.031 km/Ma between 165-115 Ma and 0.040 km/Ma between 115-35 Ma (Tab. 4.5). From 35 Ma until present fault movement was active and the blocks have been decoupled. The exhumation rate of the Northern block was determined to 0.066 km/Ma between 35 Ma until present, while the exhumation rate in the Southern block was 0.043 km/Ma during the same time span.

The modelled AFT ages are in good agreement with the correspondent ages observed at each side of the fault (Fig. 4.13a, b, c).

4.3.2.3 Central Galicia – inverse models

Again 2,408 model runs have been performed in order to find a combination of surface subsidence rate and rock uplift rate that best reproduces the observed ages. The results are given in Figure 4.11c (Lugo block) and 4.11d (Eastern block). In comparison to the previous model in North Galicia, here a much larger spread of low misfits can be observed as well as a much smaller range in misfit values from ~3.88 to 0.35. This can be indicative for two things either 1) the model is not well constrained by the data or 2) the parameter space has been defined more narrow with respect to the possible solutions (therefore, the difference in appearance of the plots of each area is a problem of scale, or in other words: for the Galicia area there is a wider range of reasonable rock uplift rates to reproduce the observed data). As the very low misfit values do not support the first assumption the second explanation is more preferable. During the first time interval from 290 to 165 Ma the Lugo and the Eastern block were coupled allowing no fault movement. The models with the lowest misfit cluster around an amplification factor of topography between 6.9 and 6.0 (i.e. ~3,730-3,240 m) and rock uplift rates between 0.08 and 0.14 km/Ma. From 165 Ma onward both blocks have been decoupled allowing different rock uplift rates at each side of the fault. In the western flank of the fault in the Lugo block the rock uplift rate increase significantly to a large range of values between 0.15 and 0.27 km/Ma. However, most of the low misfit models as well as the best fit cluster between 0.23 and 0.26 km/Ma. On the contrary for the Eastern block the models suggest a considerable decrease in rock uplift rates ranging from 0 to 0.03 km/Ma. The amplification factor of the topography plots

Table 4.5.

PECUBE Model results from best fit model.

Evolving Topography						Surface Uplift	Rock uplift	Rock exhumation	*HeFTy*
Time steps [Ma]	present mean elevation [m]	amplification factor of topography	resulting mean elevation [m]	Time segment [Ma] from	to	surface uplift rate [km/Ma]	rock uplift rate [km/Ma]	rock exhumation rate [km/Ma]	rock exhumation rate [km/Ma]
North Galicia									
290	510	4.79	2441					*Northern block*	
165	510	2.41	1229	290	165	-0.010	0.019	0.029	n.a.
115	510	1.63	830	165	115	-0.008	0.023	0.031	0.111
85	510	0.00	0	115	85	-0.028	0.012	0.040	0.029
35	510	0.00	0	85	35	0.000	0.012	0.012	0.014
0	510	1.00	510	35	0	0.015	0.081	0.066	0.029
								Southern block	
							0.019	0.029	n.a.
							0.023	0.031	0.090
							0.012	0.040	0.010
							0.012	0.012	0.011
							0.058	0.043	0.031
Central Galicia									
290	540	6.29	3397					*Lugo block*	
165	540	3.61	1951	290	165	-0.012	0.126	0.138	n.a.
115	540	2.83	1528	165	115	-0.008	0.248	0.256	0.121
85	540	1.26	680	115	85	-0.028	0.085	0.113	0.016
0	540	1.00	540	85	0	-0.002	0	0.002	0.018
								Eastern block	
							0.126	0.138	0.094
							0.001	0.009	0.012
							0.005	0.033	0.007
							0.017	0.019	0.012

Greyish colour marks time steps during which the block movement is coupled.

between 4 and 3 (i.e. ~2,160-1,620 m). While the rock uplift rates in the Eastern block during the subsequent time step from 115 to 85 Ma show no change suggesting still relative quiescence with respect to rock uplift rates the rates in the Lugo block decrease slightly to a range from 0.04 to 0.10 km/Ma and are, therefore, still notably higher than in the Eastern block. Models with the lowest misfit suggest an amplification factor of topography between 3.0 and 2.5 (i.e. ~1,620-1,350 m) at this time step. During the last time step from 85 Ma to present the rock uplift rates of each block again adapt ranging from 0 to 0.02 km/Ma. However, in contrast to the previous time steps now the rates in the Eastern block seem to be slightly higher. The amplification factor of topography settles around 1.3 (i.e. ~700 m).

4.3.2.4 Central Galicia – exhumation rates (best fit model)

The results from thermokinematic modelling for the best fit model are given in Table 4.5 and Figure 4.12b. The values for surface uplift and rock uplift rates resulted in exhumation rates for the Eastern block of 0.138 km/Ma between 290-165 Ma, 0.009 km/Ma between 165-115 Ma, 0.033 km/Ma between 115-85 Ma and 0.019 km/Ma from 85 Ma until present. The exhumation rates of the Lugo block were determined to 0.138 km/Ma between 290-165 Ma (same like in the Eastern block because of coupling), an acceleration of exhumation rate to 0.256 km/Ma between 165-115 Ma, 0.113 km/Ma between 115-85 Ma and very slow exhumation at a rate of 0.002 km/Ma from 85 Ma until present.

The modelled AFT and AHe ages are in good agreement with the correspondent ages observed at each side of the fault (Fig. 4.13d, e, f, g).

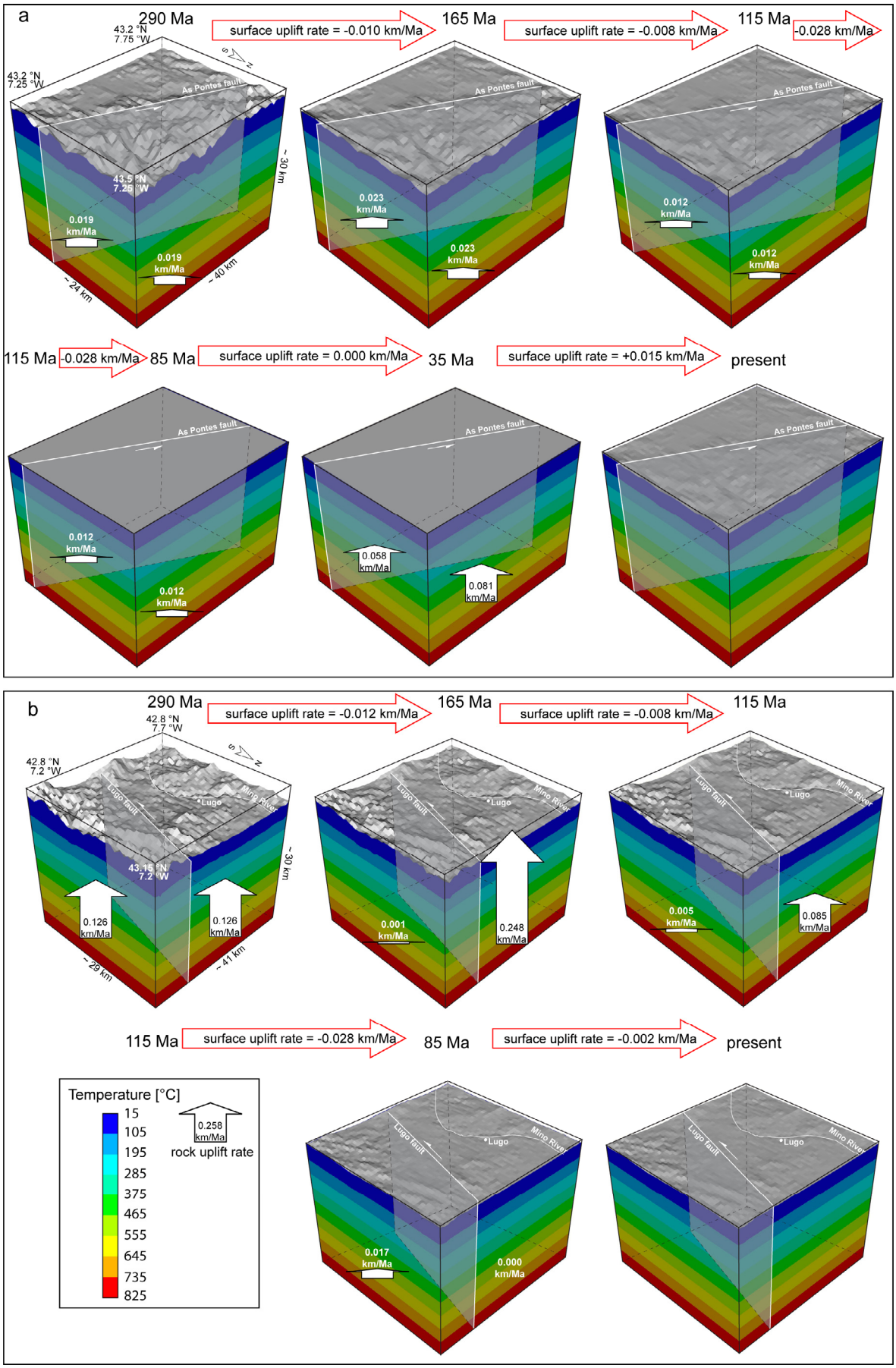

Fig. 4.12: 3D visualizations of the best fit model from (a) North Galicia and (b) Central Galicia. Each cube represents a time step showing the amplification factor of topography, rock uplift rate of each block from this time step to the next, the surface uplift/subsidence rates as well as the underlying temperature field.

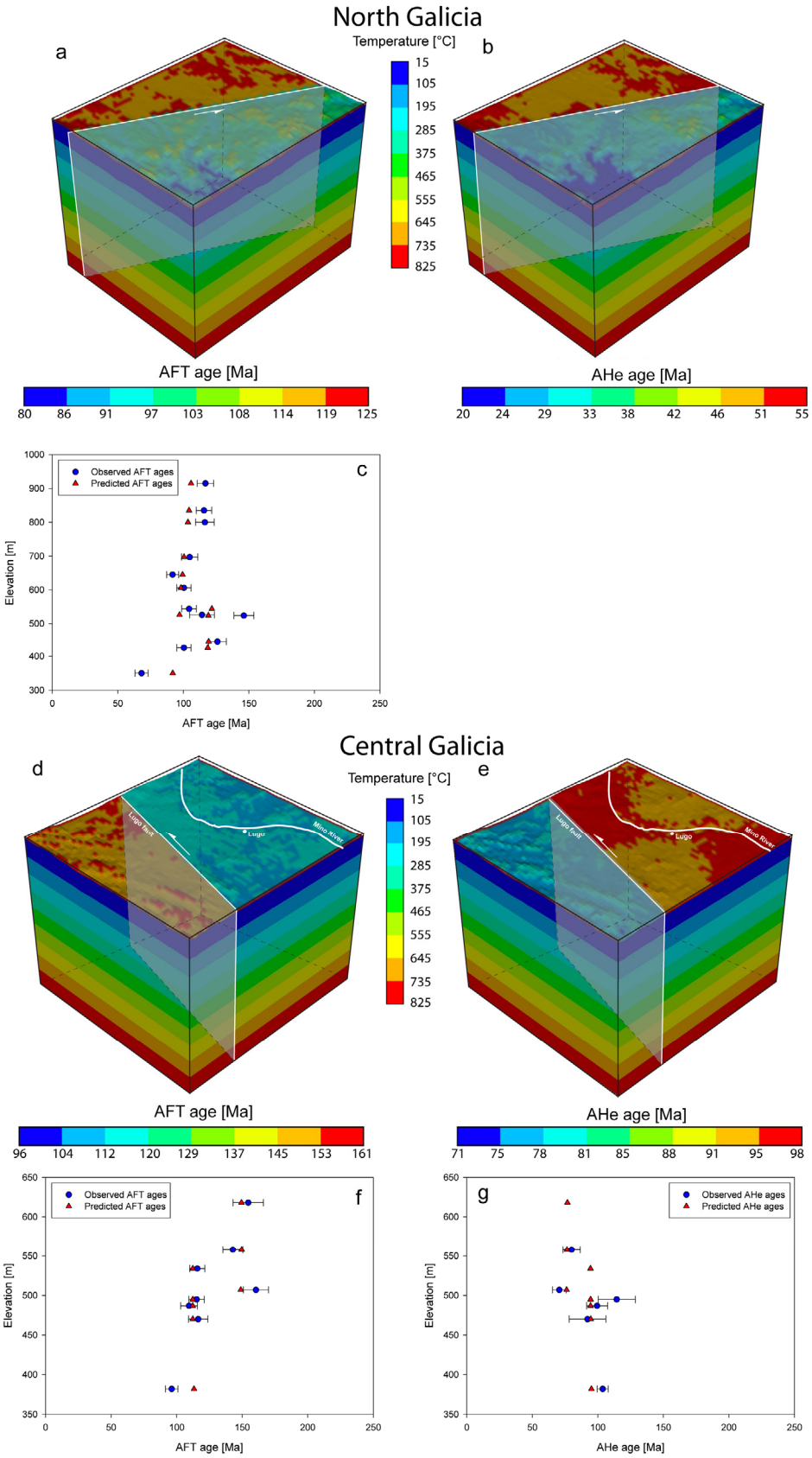

Fig. 4.13: Predicted cooling age distribution at surface from each best fit model as well as AER plots comparing observed and predicted cooling ages. (a) AFT North Galicia, (b) AHe North Galicia, (c) AER-AFT North Galicia, (d) AFT Central Galicia, (e) AHe Central Galicia, (f) AER-AFT Central Galicia, (g) AER-AHe Central Galicia AFT and AHe ages reported with 1σ error).

5 Discussion

The AFT and AHe age distribution considering all samples analysed in the study area ranges from Middle Triassic to Late Cretaceous. There are no evidences in the track length distributions of the samples to suggest multiphase heating histories. Track length distributions show clearly defined peaks with only minor skewness. For these reasons thermal overprinting as a cause of the variation in AFT ages and cooling histories is discarded. Modelled time-temperature histories based on AFT track length distribution (and AHe data where available) further suggest spatially heterogeneous, continuous cooling and exhumation at varied rates since the end of the Variscan orogeny by Late Paleozoic times (Fig. 5.1).

5.1 Asturias area

The age distribution and corresponding t-T paths in the Asturias transect (C-C') (Fig. 5.2) indicate that the rocks cooled below 60 °C through events older than 100 Ma and that samples in the west cooled later than samples in the east, regardless of elevation. This E-W distribution of cooling ages may correlate with the final distribution of rocks within the Variscan section (Fig. 4.1). The upper crustal, cooler rocks that underwent shallower deformation conditions are to the east and the deeper, hotter crustal rocks that underwent high-grade metamorphism are to the west (Martínez-Catalán *et al.*, 1990). Furthermore, when combined in three groups (Lugo plain-, Oscos plateau- and Allande- group; Fig. 5.2) the age distribution seems to pick a signal that correlates with preservation at different elevations of low relief surfaces in Lugo, Oscos and Allande (Alvarez-Marrón *et al.*, 2003).

5.1.1 Interpretation of cooling paths and exhumation history

The detailed cooling and exhumation history of the rocks in the western Cantabrian Mountains is illustrated in Figure 5.1 by comparing the modelled t-T paths and major tectonic events.

An initial, rapid episode of cooling which lasted from the Triassic to the Late Jurassic occurred predominately before initiation of widespread Mesozoic rifting that led to the opening of the Atlantic and the Bay of Biscay oceans (Le Pichon *et al.*, 1971; Srivastava *et al.*, 1990). The modelled t-T paths indicate a rapid cooling to temperatures below 70 °C (Fig. 5.1). The amount of exhumation that took place during this earliest episode of cooling was larger than 2.5 km, with rates of ~0.3 km/Ma. A plausible explanation for this earliest cooling may be, that it is related to erosional exhumation during post Variscan unroofing, that was initiated subsequently to cooling at shallow depths of post orogenic granitoid intrusions by Early Permian times (Fernández-Suárez *et al.*, 2000).

A similar unroofing process has been proposed for the cooling of the Appalachians in Pennsylvania during Late Permian to Early Jurassic (Blackmer *et al.*, 1994). They were part of the orogenic belt that amalgamated Pangea during Carboniferous and Early Permian times (Ziegler, 1989). Also, similar exhumation rates have been obtained for the cooling during topographic decay of the Dabie Shan orogen in China (Reiners *et al.*, 2003).

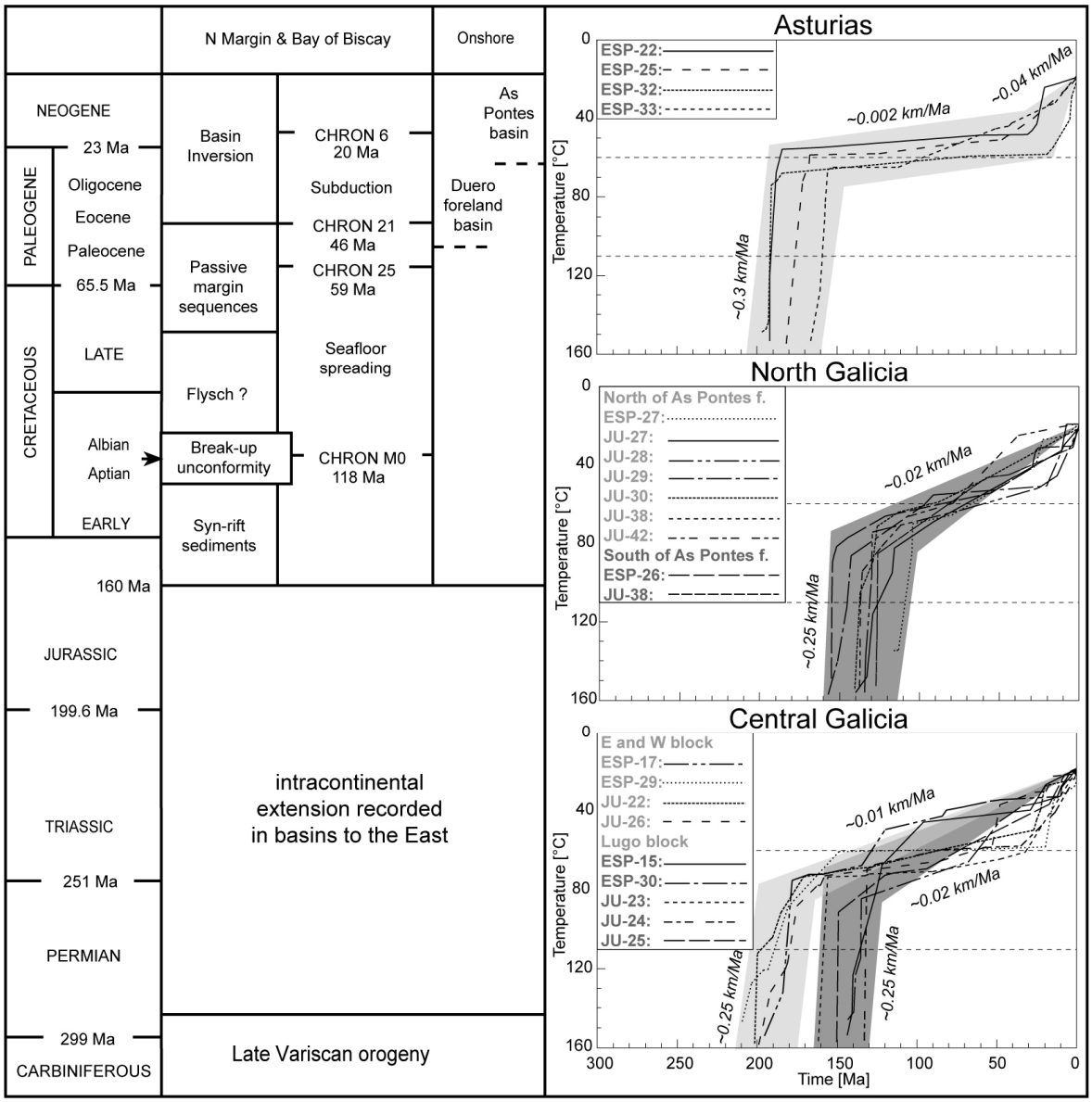

Fig. 5.1: Cooling histories combined with tectonic events (cp. text for references on event ages; time-scales of Haq and van Eysinga (1998)) Cooling histories are grouped in (1) Asturias; (2) North Galicia; (3) Central Galicia. Grey envelopes highlight the common cooling history with calculated average exhumation rates (Tab. 4.4) for different segments.

No records are found in the thermochronological data of Asturias that indicate possible effects associated to thermal expansion during the Permo-Triassic Pangea continental break-up. However, during this intracontinental rifting episode, the Oviedo and Basque-Cantabrian basins developed to the east of the study area (Martínez-García *et al.*, 2004; Espina *et al.*, 2004). These basins contain shallow marine Early Jurassic carbonates, explained as a widespread transgression during post-rifting thermal relaxation that is present across large parts of Europe (Quesada *et al.*, 2005). There is no evidence in the study area to suggest that any marine incursion took place during Early Mesozoic times. Instead, it seems to have been an exposed continental landmass, as previously suggested by Ziegler and Roure (1999), further indicating that erosion during topographic decay may have been the dominant process for the exhumation of rocks in the western Cantabrian Mountains before the Late Jurassic.

A lack of significant variations of topography in the region since Late Cretaceous and before formation of the present topography may correspond to a time of quiescence during the post-rift stage. In this situation, planation

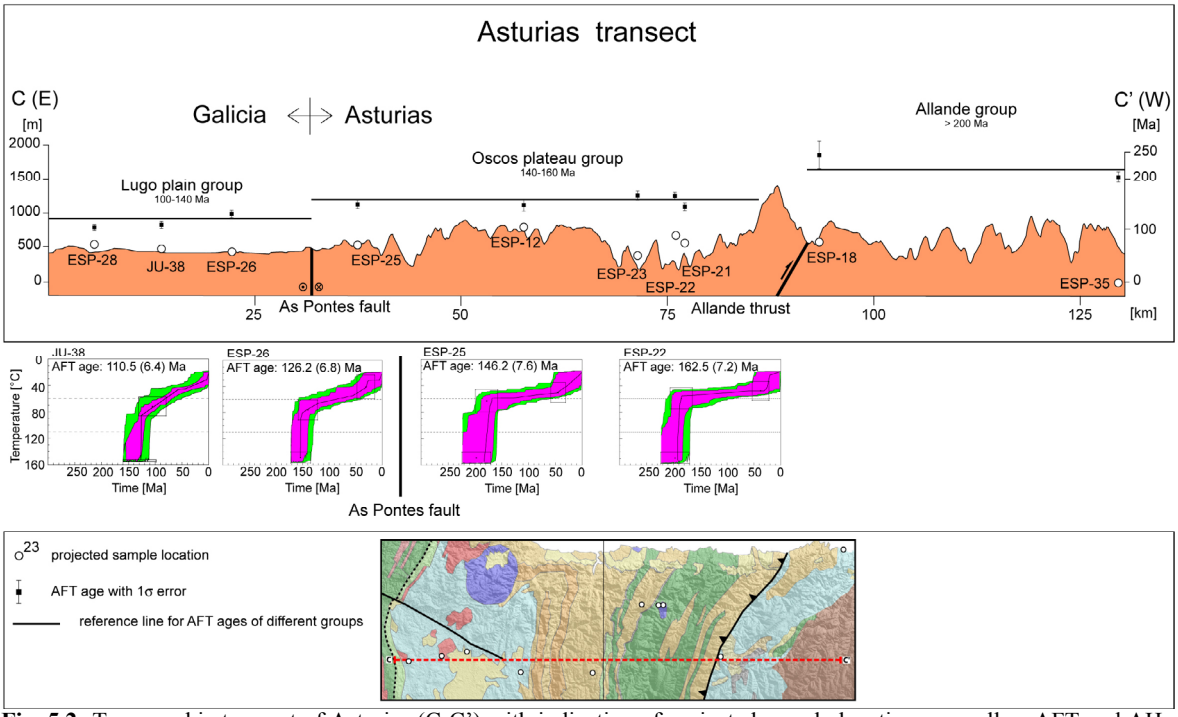

Fig. 5.2: Topographic transect of Asturias (C-C') with indication of projected sample locations as well as AFT and AHe ages. Modelled t-T paths are plotted below transect.

may occur at the surface if the denudational system reached a state of sufficiently low energy due to stabilization of base levels (Gunnell *et al.*, 2009). This process may explain the development of a peneplain across the region since Late Cretaceous times. The lowlands around Lugo and the elevated surfaces of low relief found in Oscos are suggested to be the remains of this peneplain. This inherited paleolandscape appears now dissected by faulting and fluvial incision due to Cenozoic tectonism (Alvarez-Marrón *et al.*, 2003). Extensive planation surfaces and common weathering mantles developed by Late Cretaceous times across Variscan terrains in central Europe (Migón and Lidmar-Bergstroem, 2001; Thiry *et al.*, 2006).

5.2 Galicia area

5.2.1 Interpretation of cooling paths and exhumation history

The thermochronological data in Galicia indicate that cooling through shallow crustal levels started by Late Triassic times (Fig. 5.1). A few samples from across the low relief areas of Central Galicia record exhumation rates between ~0.25 and ~0.05 km/Ma from ~200 to ~160 Ma. Thus, indicating exhumation across inland areas of the Iberian Massif occurred possibly due to incremental erosion/unroofing of material in the southern shoulder of the Triassic intracontinental rift. However, the main episode of cooling below 80 °C that caused exhumation of most samples through shallow crustal levels in Galicia occurred between ~160 to ~120 Ma (Fig. 5.1). This exhumation was coeval with the Atlantic and Bay of Biscay widespread rifting episode that generated the continental margins to the North and West of Galicia from Late Jurassic to Early Cretaceous times (Le Pichon *et al.*, 1971; Srivastava *et al.*, 1990). The largest average exhumation rates of ~0.5 km/Ma during this event are registered across the North Galicia transect (Fig. 5.3, transect (D-D'-D'')), indicating largest erosion/unroofing of uplifted material near the rift shoulder.

Fast cooling during Late Jurassic – Early Cretaceous was also detected in Variscan basement granites from the SW England coast and interpreted as rift-related surface uplift (Chen *et al.*, 1996). Paleogeographical reconstructions represent this area of SW

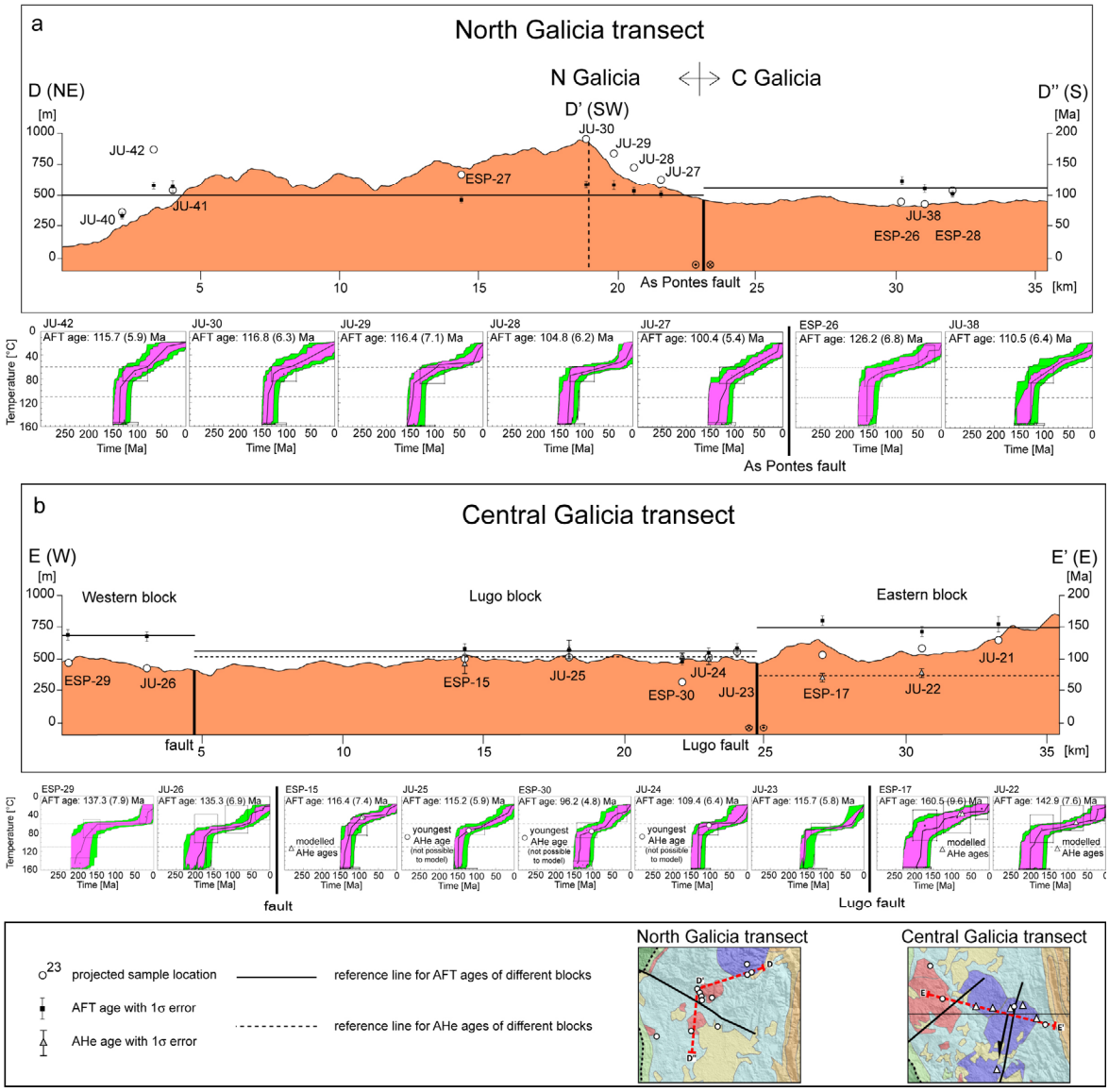

Fig. 5.3: Topographic transects of (a) North Galicia (D-D'-D'') and (b) Central Galicia (E-E') with indication of projected sample locations as well as AFT and AHe ages. Modelled t-T paths are plotted below transects.

England as the North Galicia conjugate flank of the Bay of Biscay rift (Ziegler, 1989).

In comparison to the fast exhumation across the North Galicia transect, the more inland areas of the Central Galicia transect register similar exhumation rates of ~0.1-0.5 km/Ma during the same period (Tab. 4.4). In this central area of Galicia, however, the AFT age distribution with differential exhumation between fault blocks indicates activity at ~116 Ma along the NNE-SSW trending system of post-Variscan faults. The activity of these fault systems during the main Mesozoic rifting episode is plausible considering that the Lugo fault connects southwards with bounding faults of the Lusitanian basin that contains significant thickness of Early Cretaceous sediments (Rasmussen *et al.*, 1998; Alves *et al.*, 2003).

Data from seafloor magnetic anomalies established the continental break-up and initiation of seafloor spreading at chron M0 that corresponds to 118 Ma (Verhoef and Srivastava, 1989). This correlates with the initiation of the Mesozoic post-rift stage and initiation of the passive evolution of the continental margin that is marked by the Aptian-Albian break-up unconformity in the Cantabrian platform (c. 115-110 Ma; Montadert *et al.*, 1979; García-Mondejar *et al.*, 2005).

In the North Galicia area reduced exhumation rates of ~0.02 km/Ma are calculated for the time span between 110 to

60 Ma, during the Early Cretaceous to Early Paleocene period of post-rift evolution of the northern continental margin. This interpretation also coincides with values of 0.01 km/Ma between ~115 and ~70 Ma indicated by the AER in the higher topographic areas of North Galicia. However, the t-T path models indicate a significant reduction of exhumation rate since ~120 Ma, reaching exhumation rates of less than 0.02 km/Ma since that time. These low rates are indicative of stable thermal conditions in the upper crust from the Late Cretaceous to the Eocene across the NW Iberian Massif. A weak indication of a possible short episode of fast cooling at around 115 Ma across the transect in North Galicia would be indicative of a rapid and short-lived thermal contraction of the continental crust at the onset of the post-rift stage.

In the southern Australian passive margin such a process of fast cooling during continental break-up is explained as due to escarpment retreat (Persano *et al.*, 2002). This interpretation would also be plausible in the case of North Galicia, considering this northern region is closest to the coastline.

5.2.2 Implications from 3D thermokinematic modelling

5.2.1.1 North Galicia

In North Galicia, a scenario with constant decrease in topography since Variscan orogeny from 290 to 85 Ma was simulated. From 85 to 35 Ma a flat surface according to geological constraints was pre-determined. Subsequently, the surface uplift from 0 elevation (flat surface) at 35 Ma to present elevation until recent times was simulated. The best fit model suggested a mean elevation of the area of ~2,400 m after Variscan orogeny and a subsequent decay of relief to ~1,200 m at 165 Ma, 830 m at 115 Ma and 0 m at 85 Ma. This corresponds to surface subsidence rates in orders of magnitude between ~0.01 to ~0.03 km/Ma. The surface uplift from 0 m at 35 Ma to 510 m present mean elevation corresponds to a rate of 0.015 km/Ma. The exhumation rates of the Northern and Southern block were coupled until 35 Ma to prevent onset of fault activity before 35 Ma. For the Northern block the exhumation rates are in an order of 0.03 to 0.04 km/Ma from 290 to 85 Ma. This is in good agreement with HeFTy© derived exhumation rates for the Northern block (Tab. 4.5) which derived exhumation rates of 0.111 km/Ma from 165-115 Ma and 0.029 km/Ma from 115-85 Ma for a fixed geothermal gradient of 27 °C/km and a surface temperature of 15 °C. In the Southern block HeFTy© derived exhumation rates were slightly slower with 0.090 km/Ma from 165-115 Ma and 0.010 km/Ma from 115-85 Ma. Also in both modelling approaches, HeFTy© and PECUBE, a subsequent decrease in exhumation rate to 0.012 km/Ma (PECUBE; both blocks) compared with 0.014 km/Ma (Northern block) and 0.011 km/Ma (Southern block) can be monitored. The important observation is the significant increase during the last time step during which both blocks were decoupled in the models to allow fault activity. The increase led to exhumation rates of 0.066 km/Ma (PECUBE; Northern block) and 0.043 km/Ma (PECUBE; Southern block) compared to 0.029 and 0.031 km/Ma, respectively (HeFTy©). Both approaches, therefore, record a significant increase in exhumation rates around 35 Ma, which is also in good agreement with the incipient Alpine convergence in this area. However, comparing the exhumation rates derived from the two models and evaluating the results, different model features which complicate the direct comparison have to be considered. HeFTy© calculates cooling rates by taking the cooling age as well as the track lengths distribution of a sample into account. This cooling rate is then translated into an exhumation rate by assuming a fixed geothermal gradient. HeFTy© models, therefore, do not account for changes in surface elevation or rock uplift rate nor do they integrate several samples into one single model. At high exhumation rates the relationship between cooling rate and exhumation rate becomes highly non-linear. Due to the large convection of heat the geothermal gradient becomes exponential resulting in compressed isotherms towards the surface. In this case of high exhumation rates the cooling age of a sample is twice influenced by (1) a shorter travel time to the surface due to the increased travel speed as well as (2) a shorter travel distance from the closure isotherm to the

surface due to the compressed isotherms. As both modelling approaches can be considered as in good accordance an overall slow exhumation rate can be deduced for the area. This would result in a weak influence of the exhumation rate on the geothermal gradient and in turn minimize the difference to model approaches with a fixed geothermal gradient.

5.2.1.2 Central Galicia

In Central Galicia a scenario with constant decay in relief from 290 Ma until present was simulated. Fault movement of the Lugo fault was allowed to be active between 165 Ma until present. The best fit model suggests an elevation of topography of ~3,400 m at 290 Ma and subsequent decay to ~2,000 m at 165 Ma, ~1,500 m at 115 Ma and 680 m at 85 Ma unless recent mean elevation with 540 m is reached. The resulting rate of surface subsidence ranges from 0.012 km/Ma over 0.008 km/Ma, 0.028 km/Ma to 0.002 km/Ma during the last time step. Comparing the exhumation rates with the HeFTy© derived exhumation rates the picture is not as concordant like in North Galicia. The PECUBE derived exhumation rates in the Lugo block show fast rates with 0.138 km/Ma between 290-165 Ma, even an increase to 0.256 km/Ma between 165-115 Ma, subsequent decrease to 0.113 km/Ma between 115-85 Ma and very slow exhumation with 0.002 km/Ma between 85 Ma until present. In the first time step the exhumation rate in the Eastern block is coupled to that of the Lugo block and, therefore, equals 0.138 km/Ma. During the next time interval between 165-115 Ma the exhumation rate in the Eastern block decreases dramatically to 0.009 km/Ma. While in the subsequent interval between 115-85 Ma it increases to 0.033 km/Ma. In the last time interval between 85 Ma to present the exhumation rate again decreases moderately to 0.019 km/Ma. These values differ significantly from those derived from HeFTy© modelled cooling paths. As stated above, this is reasonable because the difference can be explained by the more complex cooling history in Central Galicia, which has in turn a much larger effect on the complicating factors that impede to compare the two approaches. In fact, the overall picture that the 3D thermokinematic model draws is a fast exhumation of the Lugo block between 165-85 Ma and very slow exhumation thereafter while in the Eastern block the fastest exhumation occurred between 290-165 Ma with subsequent quiescence and a moderate reactivation between 115-85 Ma. This is in good agreement with the thermal history based on AFT, AHe and HeFTy© modelling results discussed above.

5.3 Implications on landscape evolution

It is evident from the available thermochronological data that rocks in the NW Iberian Massif where exhumed through the upper kilometres of the crust in relation to processes older than the initiation of convergence along the North Iberian Margin by Middle Eocene times (Srivastava *et al.*, 1990; Alvarez-Marrón *et al.*, 1997; Gallastegui, 2000).

These AFT ages from the Cantabrian Mountains are in contrast with the younger ages reported for Variscan rocks in other ranges of Iberia that underwent compression during Cenozoic. For example, AFT data from Variscan rocks in the central Pyrenees yielded Eocene-Oligocene exhumation ages (Fitzgerald *et al.*, 1999) and in the Iberian Central System thermochronological ages ranging from the Middle Eocene to recent were obtained (De Bruijne and Andriessen, 2002). These younger cooling ages are in agreement with exhumation related to Alpine compression in the Pyrenees and in the Betics, respectively.

The N-S compression that raised the Cantabrian Mountains is associated to convergence along the northern Iberian Margin. The North Atlantic and Bay of Biscay magnetic anomalies indicate that limited southward subduction along this margin started at 49 Ma (chron 21) and went on until 20 Ma (chron 6) (Srivastava *et al.*, 1990; Roest and Srivastava, 1991). Shortening and surface uplift along the Cantabrian Mountains occurred since Middle Eocene when erosion started to provide sediments to the Duero foreland basin to the south (Alonso *et al.*, 1996; Gallastegui, 2000). However, the amount of N-S shortening that accumulated until Neogene has been small, only 25 km along a section near 4º W longitude

(Espina *et al.*, 1996) and was progressively smaller westwards towards the study area (Santanach, 1994; Alvarez-Marrón et al, 1997). The reduced shortening is correlative with the relatively small amounts of sediments accumulated within the Paleogene to Neogene Bierzo basin to the south of the drainage divide (Andeweg, 2002) and within the Oligocene to Early Miocene As Pontes basin in Galicia (Huerta *et al.*, 1996).

In the low relief areas of Central Galicia slow exhumation rates persisted since ~120 Ma. The AHe data indicate that less than 1.5 km of overburden has been eroded since then at slow average denudation rates of 0.02 km/Ma across Central Galicia.

The low exhumation rates that persisted in Central Galicia have not been significantly modified during the Oligocene active faulting that caused surface uplift along the higher topographic areas in North Galicia. The modelling suggests that most samples in North Galicia cooled below 60 °C since 80 Ma ago (Fig. 5.1). Vertical movement along the As Pontes fault of a maximum of 455 m vertical displacement has been calculated during formation of the As Pontes basin from 30 to 22 Ma (Huerta *et al.*, 1996; Santanach *et al.*, 2005).

The thermochronological data indicates that this faulting episode did not modify sufficiently the previously established thermal structure possibly due to minor exhumation during that time. This preservation of the thermal structure in the upper crust during Lutetian to Burdigalian times also indicates that the upper crust remained unaffected by any significant thermal effects in relation to incipient subduction and development of the small accretionary prism at the foot of the North Iberian Margin (Alvarez-Marrón *et al.*, 1997).

The fact that AFT ages determined from the western Cantabrian Mountains are older than Cenozoic, indicates that the surface uplift process responsible for the present mountainous topography was associated with insufficient exhumation to reset the AFT clock.

The correlation of AFT ages along the E-W profile with preservation of low relief surfaces in Lugo, Oscos and Allande suggests that those surfaces correspond to relicts of a pre-Alpine paleotopography, and that denudation since then has been insufficient to be registered by the AFT method.

Considering all data, the recent rough topography in North Galicia and Asturias must have formed since the middle Eocene with average estimated exhumation rates between c. 0.02 to 0.07 km/Ma, since 40-50 Ma. The surface uplift responsible for formation of the incipient mountainous topography seems to have been associated to possibly less than 1.7 km of denudation.

6 Conclusions

The 250 Ma cooling history of rocks exposed in the western Cantabrian Mountains reveals that the main exhumation process and fast cooling occurred during unroofing of the Variscan orogenic topography and Pangea break-up. Throughout the Triassic up to the Late Jurassic rocks in Asturias reached upper crustal levels with exhumation rates of about 0.3 km/Ma.

In Galicia, the effects of active rifting and subsequent thermal relaxation during the Mesozoic may explain the geographical pattern of cooling ages across the outcropping Iberian Massif. The data and the modelling indicate that Galicia underwent various rates of continuous cooling in post-Variscan times, with the largest exhumation of ~0.5 km/Ma coeval with the period of Late Jurassic to Early Cretaceous Atlantic and Bay of Biscay rifting activity. The rocks in Asturias underwent very little, slow cooling and exhumation during the same rifting episode, with very slow exhumation rates of 0.002 km/Ma since the Upper Jurassic that lasted for more than 100 Ma.

The post-Variscan faults in the interior areas of Central Galicia were active and caused differential exhumation across fault blocks during the Early Cretaceous. The results indicate that there has been no significant exhumation or sedimentary burial across the area since 115-80 Ma. The Cenozoic convergence associated to limited southward subduction along the North Iberian Margin that caused activation of faults and surface uplift in North Galicia generated minor effects in the previously attained thermal structure of the upper crust. Since Eocene to present, all samples including Asturias and Galicia, cooled below 60 °C indicating about 1.7 km of denudation during surface and rock uplift of the Cantabrian Mountains. In the low relief areas of Lugo the total amount of exhumation since 80 Ma ago can be estimated to 1.5 km at an averaged rate of ~0.02 km/Ma. These low topographic areas of Lugo are considered remains of a low relief paleotopography predating the Alpine tectonism along the North Iberian Plate.

AFT central ages measured in Variscan basement rocks across the western termination of the Cantabrian Mountains are older than the end of the Mesozoic, indicating that Cenozoic surface uplift associated to minor Alpine compression during convergence along the North Iberian Margin caused insufficient exhumation to reset the pre-established AFT thermal distribution in the upper crust.

Results from 3D thermokinematic modelling of North and Central Galicia provide good agreement with the available thermochronological data by modelling an evolution of continuous surface decay and subsequent surface uplift, respectively, in North Galicia.

The lack of profound and detailed data of paleoclimate impedes a final conclusion whether the changes in surface evolution and rock uplift rates are climatically or tectonically controlled. The strong coincidence between timing of major tectonic events, derived changes in topography and rock uplift rates, however, strongly suggest that the major driving factor of landscape evolution in this area is tectonic forcing rather than changes in climate. The comparatively good agreement between 3D thermokinematic modelling and single sample t-T path modelling despite their different approaches can be related to the overall slow exhumation rates in the area which results in a weak influence of the exhumation rate on the geothermal gradient.

References

Ahnert, F., 2003. Einführung in die Geomorphologie. UTB/Ulmer, Stuttgart, 440 p.

Alonso, J.L., Pulgar, J.A., García-Ramos, J.C., Barba, P., 1996. Tertiary basins and Alpine tectonics in the Cantabrian Mountains (NW Spain), In: Friend, P.F., Dabrio, C.J. (Eds.), Tertiary Basins of Spain: The Stratigraphic Record of Crustal Kinematics, 214-227, Cambridge Univ. Press, New York.

Alvarez-Marrón, J., Rubio, E., Torne, M., 1997. Alpine age subduction structures in the North Iberian Margin. Journal of Geophysical Research 102, 22495–22511.

Alvarez-Marrón, J., Menéndez, R., Marquínez, J., 2003. Intramontane landscape evolution in the initial stages of coastal mountain growth (Cantabrian Mountains, Spain). Geophysical Research Abstracts 5, #3650. European Geophysical Society 2003.

Alvarez-Marrón, J., Hetzel, R., Niedermann, S., Menéndez, R., Marquínez, J., 2008. Origin, structure and exposure history of a wave-cut platform more than 1 Ma in age at the coast of northern Spain: a multiple cosmogenic nuclide approach. Geomorphology 93, 316-334.

Alves, T.M., Gawthorpe, R.L., Hunt, D.W., Monteiro, J.H., 2003. Post-Jurassic tectono-sedimentary evolution of the Northern Lusitanian Basin (Western Iberian Margin). Basin Research 15, 227-249.

Andeweg, B., 2002. Cenozoic tectonic evolution of the Iberian Peninsula causes and effects of changing stress fields. Ph.D. Thesis, Vrije Universiteit Amsterdam, ISBN 90-9015593-7. Netherlands Research School of Sedimentary Geology, publication no. 20020101.

Barbarand, J., Carter, A., Wood, I., Hurford, T., 2003a. Compositional and structural control of fission-track annealing in apatite. Chemical Geology 198, 107-137.

Barbarand, J., Hurford, T., Carter, A., 2003b. Variation in apatite fission-track length measurement: implications for thermal history modelling. Chemical Geology 198, 77-106.

Barrón, E., Santos, L., 1998.Critical paleobotanical synthesis of Galicia Tertiary Basins (Spain). Cuadernos de Paleontología 49, 41-53.

Bauer, F.U., Glasmacher, U.A., Malikwisha, M., Mambo, V.S., Mutete B.V., 2010. The Eastern Congo – a beauty spot, rediscovered from a geological point of view. Geology Today, Vol. 26, No. 2, March–April 2010.

Beaumont, C., Kooi, H. and Willett, S., 1999. Coupled tectonic-surface process models with applications to rifted margins and collisional orogens. In: Summerfield, M.A. (ed.), Geomorphology and Global Tectonics: John Wiley and Sons Ltd., 29-55.

Bishop, P., 2007. Long-term landscape evolution: linking tectonics and surface processes. Earth Surface Processes and Landforms 32, 329-365.

Blackmer, G.C., Omar, G.I., Gold, D.P., 1994. Post-Alleghanian unroofing history of the Appalachian Basin, Pennsylvania, from apatite fission track analysis and thermal models. Tectonics 13 (5), 1259-1276.

Boillot, G., Malod, J., 1988. The north and north-west Spanish continental margin: a review, Rev. Soc. Geol. Esp. 1 (3–4), 295–316.

Boillot, G., Auxietre, J.-L., Dunand, J.-P., Dupeuble, P.-A., Mauffret, A., 1979. The northwestern Iberian margin: a Cretaceous passive margin deformed during Eocene. In: Talwani, M., Hay, W., Ryan, W.B.F. (Eds.), Deep Drilling Results in the Atlantic Ocean: Continental Margins and Paleoenvironment: Am. Geophys. Union, Maurice Ewing Ser., 3, 138-153.

Box, G. E. P., Draper, N. R., (1987), Empirical Model Building and Response Surfaces, John Wiley & Sons, New York, NY.

Braun, J., 2002a. Estimating exhumation rate and relief evolution by spectral analysis of age-elevation datasets. Terra Nova 14, 210-214.

Braun, J., 2002b. Quantifying the effect of recent relief changes on age-elevation relationships. EPSL 200, 331-343.

Braun, J., 2003a. Pecube: a new finite-element code to solve the 3D heat transport equation including the effects of a time-varying, finite-amplitude surface topography. Computers & Geosciences 29, 787-794.

Braun, J., van der Beek, P., 2004. Evolution of passive margin escarpments: What can we learn from low-temperature thermochronology? Journal of Geophysical Research 109, F04009, doi:10.29/2004JF000147.

Braun, J., Robert, X., 2005. Constraints on the rate of post-orogenic erosional decay from low-temperature thermochronological data: application to the Dabie Shan, China. Earth Surf. Process. Landforms 30, 1203-1225.

Burtner, R.L., Nigrini, A., Donelick, R. A., 1994. Thermochronology of Lower Cretaceaous source rocks in the Idaho-Wyoming Thrust Belt. AAPG Bull. 78: 1613-1636.

Cabral, J., 1989. An example of intraplate neotectonic activity, Vilarica basin, northeast Portugal. Tectonics 8 (2), 285-303.

Carlson, W. D., 1990. Mechanisms and kinetics of apatite fission-track annealing. Am. Mineral. 75, 1120-1139.

Carlson, W. D., Donelick, R. A., Ketcham, R. A., 1999. Variability of apatite fission-track annealing kinetics: I. Experimental results. Am. Mineral. 84, 1213-1223.

Carslaw, H.S., Jaeger, C.J., 1959. Conduction of Heat in Solids, 3rd Edition. Clarendon Press, Oxford, 510pp.

Cocherie, A., 1978. Géochemie des terres rares dans le granitoides. Tesis Doctoral, Univ. Rennes. 207 p.

Chen, Y., Zentilli, M.A., Clark, A.H., Farrar, E., Grist, A.M., Willis-Richards, J., 1996. Geochronological evidence for post-Variscan cooling and uplift of the Carnmenellis granite, SW England. Journal of the Geological Society 153, 191-195.

Crowley, K.D., 1993. Mechanisms and kinetics of apatite fission-track annealing – Discussion. Am. Min. 78, 210-212.

Crowley, K.D., Cameron, M., Schaffer, L.R., 1991. Experimental studies of annealing of etched fission tracks in fluorapatite. Geochim. Cosmochim Acta 55, 1449-1465.

Dahlen FA, Suppe J. 1988. Mechanics, growth, and erosion of mountain belts. In: Clark, S.P.J., Burchfiel, B.C., Suppe, J., (Eds.), Processes in Continental Lithospheric Deformation, pp. 161–78. Denver, CO: Geol. Soc. Am.

De Bruijne, C.H., Andriessen, P.A.M., 2002. Far field effects of Alpine plate tectonism in the Iberian microplate recorded by fault-related denudation in the Spanish central system. Tectonophysics 349, 161–184.

Díaz, J., Gallart J., Gaspà O., Ruiz M., Córdoba D., 2008. Seismicity analysis at the Prestige oil-tanker wreck area (Galicia Margin, NW of Iberia), Marine Geology 249, 150-165.

Dobson, K.J., Olive, V., Persano, C., Stuart, F.M, 2005. A new procedure for the routine zircon (U-Th)/He age measurement. Geophys. Res. Abstr. 7, EGU05-A-06696.

Dodson, M.H., 1973. Closure temperature in cooling geochronological and petrological systems. Contrib. Mineral. Petrol. 40, 259-74.

Dodson, M.H., 1979. Theory of cooling ages. In: Jager, E., Hunziker, J.C., (Eds.), Lectures in Isotope Geology, pp. 194–202. Berlin: Springer-Verlag.

Donelick, R.A., 1991. Crystallographic orientation dependence of mean etchable fission-track length in apatite: An empirical model and experimental observations. Am. Mineral. 76, 83-91.

Donelick, R.A., 1993. A method of fission track analysis utilizing bulk chemical etching of apatite. U.S. Patent #5,267,274.

Donelick, R.A., 1995. A method of fission track analysis utilizing bulk chemical etching of apatite. Australia Patent #658,800.

Donelick, R.A., Roden, M.K., Mooers, J.D., Carpenter, B.S., Miller, D.S., 1990. Etchable length reduction of induced fission tracks in apatite at room temperature, c. 23 °C. crystallographic orientation effects and "initial" mean lengths. Nucl. Tracks. Radiat. Meas. 17, 261-265.

Donelick, R.A., Ketcham, R.A., Carlson, W.D., 1999. Variability of apatite fission-track annealing kinetics: II. Crystallographic orientation effects. Am. Min. 84, 1224-1234.

Dunkl, I., 2002. Trackkey: a Windows program for calculation and graphical presentation of fission track data. Computer & Geosciences 28, 3-12.

Ehlers, T.A., Farley, K.A., 2003. Apatite (U-Th)/He thermochronometry: methods and applications to problems in tectonic and surface processes. Earth and Planetary Science Letters 206, pp.1–14.

England, P., Molnar, P., 1990. Surface uplift, uplift of rocks, and exhumation of rocks. Geology 18, 1173-1177.

Espina, R.G., Alonso, J.L., Pulgar, J.A., 1996. Growth and propagation of buckle folds determined from syntectonic sediments (the Ubierna Fold Belt, Cantabrian Mountains, N Spain), Journal of Structural Geology 18 (4), 431–441.

Espina, R.G., Alonso, J.L., Pulgar, J.A, 2004. Extensión Triásica en la Cuenca Vasco-Cantábrica. In: Vera, J.A. (Ed.), Geología de España, 338-339, SGE-IGME, Madrid.

Farley, K.A., 2000. Helium diffusion from apatite: general behaviour as illustrated by Durango fluorapatite. J. Geophys. Res., 105, 2903–2914.

Farley, K.A:, Stöckli, D.F., 2002. (U-Th)/He Dating of Phosphates: Apatite, Monazite, and Xenotime. Reviews of Mineralogy and Geochemisty 48, 559-577, doi:10.2138/rmg.2002.48.15.

Farley, K.A., Wolf, R.A., Silver, L.T., 1996. The effects of long alpha-stopping distances on (U-Th)/He ages. Geochimica et Cosmochimica Acta 60 (21), 4223-4229.

Fernández, M., Marzán, I., Correia, A., Ramalho, E., 1998. Heat flow, heat production, and lithospheric thermal regime in the Iberian Peninsula. Tectonophysic 291, 29-53.

Fernández-Suárez, J. Dunning, G.R., Jenner, G.A., Gutiérrez-Alfonso, 2000. Variscan collisional magmatism and deformation in NW Iberia: Constraints from U-Pb geochronology of granitoids. Journal of the Geological Society 157 (3), 565-576.

Fernández-Viejo, G., Gallart, J., Pulgar, J.A., Cordoba, D., Danobeitia, J.J., 2000. Seismic signature of Variscan and Alpine tectonics in NW Iberia: Crustal structure of the Cantabrian Mountains and Duero basin. Journal of Geophysical Research B: Solid Earth 105 (2) ,3001-3018.

Fitzgerald, P.G., Munoz, J.A., Coney, P.J., Baldwin, S.L., 1999. Asymmetric exhumation across the Pyrenean orogen: Implications for the tectonic evolution of a collisional orogen. Earth and Planetary Science Letters. 173 (3), 157-170.

Fitzgerald, P.G., Baldwin, S.L., Webb, L.E. and O'Sullivan, P.P., 2006. Interpretation of (U-Th) /He single grain ages from slowly cooled crustal terranes: a case study from the transantarctic Mountains of southern Victoria Land. Chem. Geol., 225, 91–120.

Fleischer, R.L., Price, P.B., Walker, R.M., 1965a. Tracks of charged particels in solids. Science 149, 383-93.

Fleischer, R.L., Price, P.B.,Walker, R.M., 1975. Nuclear Tracks in Solids. Principles and Applications. University of California Press, Berkeley, CA.

Flowers, R. M., Bowring, S. A., and Williams, M. L., 2006, Timescales and significance of high-pressure, high-temperature metamorphism and mafic dike anatexis, Snowbird tectonic zone, Canada: Contributions to Mineralogy and Petrology 151(5), 558-581.

Flowers, R.M., Ketcham, R.A., Shuster, D.L., Farley, K.A., 2009. Apatite (U–Th)/He thermochronometry using a radiation damage accumulation and annealing

modelGeochimica et Cosmochimica Acta 73, 2347–2365.

Foeken, J.P.T., Stuart, F.M., Dobson, K.J., Persano, C., Vilbert, D., 2006. A diode laser system for heating minerals for (U-Th)/He chronometry. Geochemistry, Geophysics, Geosystems 7 (4), Q04015, doi:10.1029/2005GC001190.

Freudenthal, M., Martín-Suarez, E., Carballo, N., Rodriguez-Fernández, L.R., Martín-González, F., 2010. Rodents from the Lower Oligocence of the Bierzo Basin (Leon, Spain). Neues Jahrbuch für Geologie und Paläontologie-Abhandlungen 257 (3), 317-340.

Galbraith, R.F., 1981. On statistical models for fission track counts. Mathematical Geology, 13, 471-478.

Galbraith, R.F., Laslett, G.M., 1993. Statistical models for mixed fission track ages. Nucl. Tracks Radiat. Meas. 21 (4), 459-470.

Galbraith, R.F., Laslett, G.M., Green, P.F., Duddy, I.R., 1990. Apatite fission track analysis: geological thermal history analysis based on a three-dimensional random process of linear radiation damage. Philos. Trans. R. Soc. Lond., A 332, 419-438.

Gallastegui, J., 2000. Estructura Cortical de la Cordillera y Margen Continental Cantábricos: Perfiles ESCIN-N. Trabajos Geol.Univ. Oviedo, 22, 9-234.

García-Mondejar, J., Lopez-Horgue, M.A., Aranburu, A., Fernández-Mendiola, P.A., 2005. Pulsating subsidence during a rift episode: Stratigraphic and tectonic consequences (Aptian-Albian, northern Spain). Terra Nova 17 (6), 517-525.

Gleadow, A.J.W., Duddy, I.R., 1981. A natural long term track annealing experiment for apatite. Nucl. Tracks 5, 169-174.

Gleadow, A.J.W., Fitzgerald, P.G. 1987. Uplift history and structure of the Transantarctic Mountains: new evidence from fission track dating of basement apatites in the Dry Valleys area, southern Victoria Land. Earth and Planetary Science Letters, 82, 1–14.

González-Lodeiro, F., Hernández-Urroz, J., Klein, E., Martínez-Catalán, J.R., Pablo-Maciá, J.G., 1982. Mapa Geológico de España, (Escala 1:200000) Hoja de Lugo. Instituto Geológico y Minero de España, Servicio de publicaciones del Ministerio de Industria.

Green, P.F., 1981. "Track-in track" length measurements in annealed apatites. Nucl. Tracks 5, 121-128.

Green, P.F., 1988. The relationship between track shortening and fission track age reduction in apatite: combined influences of inherent instabitlity, annealing anisotropy, length bias and systems calibration. EPSL 89, 335-352.

Green, P.F., Durrani, S.A., 1977. Annealing studies of tracks in crystals. Nucl. Track. Det. 1, 33-39.

Green, P.F., Duddy, I.R., Gleadow, A.J.W., Tingate, P.R., Laslett, G.M., 1985. Fission track annealing: track length measurements and the form of the Arrhenius plot. Nucl. Tracks 10: 323-328.

Green, P.F., Duddy, I.R., Gleadow, A.J.W., Tingate, P.R., Laslett, G.M., 1986. Thermal annealing of fission tracks in apatite, 1. A quantitative description. Chem. Geol. 59, 237-253.

Grimaud, S., Boillot, G., Collete, B.J., Mauffret, A., Miles, P.R., Roberts, D.B., 1982. Western extension of the Iberian-European plate boundary during Early Cenozoic (Pyrenean) convergence: a new model, Marine Geology 45, 63-77.

Grist, A.M., Ravenhurst, C.E., 1992a. Mineral Separation Techniques used in Dalhousie University. In: Zentilli, M., Reynolds, P.H. (Eds.), Short Course on low temperature thermochronology, Min. Ass.Can. Short Course V 20, Appendix 2, 203-209.

Grist, A.M., Ravenhurst, C.E., 1992b. A Step-by-Step Laboratory guide to fission-track thermochronology at Dalhousie University. In: Zentilli, M., Reynolds, P.H. (Eds.), Short Course on low temperature thermochronology, Min. Ass.Can. Short Course V 20, Appendix 1, 190-201.

Gunnell, Y., Calvet, M., Brichau, S., Carter, A., Aguilar, J.-P., Zeyen, H., 2009. Low long-term erosion rates in high-ernergy mountain belts: Insights from thermo- and biochronology in the Eastern Pyrenees. Earth and Planetary Science Letters 278, 208-218.

Haq, B.U., van Eysinga, F.W.B., 1998. Geological Time Table, 5th ed. Elsevier, Amsterdam

Herman, F., Braun, J., Dunlap, W.J., 2007. Tectonomorphic scenarios in the Southern Alps of New Zealand. Journal of Geophysical Research 112. B04201, doi:10.1029/2004JB003472.

Herman, F., Cox, S.C., Kamp, P.J.J., 2009. Low-temperature thermochronology and thermokinematic modeling of deformation, exhumation, and development of topography in the central Southern Alps, New Zealand. Tectonics 28, TC5011, doi: 10.1029/2008TC002367

Huerta, A., Parés, J.M., Cabrera, L., Ferrús, B., Sáez, A., 1996. Datación magnetoestratigráfica de la cuenca terciaria de As Pontes (Galicia, NW España), Geogaceta 20, 1021-1024.

Hurford, A.J., 1990. Standardization of fission track dating calibration: recommendations by the Fission Track Working Group ofthe IUGS. Subcommission on Geochronology. Chemical Geology 80, 171-178.

Hurford, A.J., Green, P.F., 1982. A user's guide to fission-track dating calibration. Earth Planetary Science Letters 59: 343–354.

Hurford, A.J., Green P.F., 1983. The Zeta age calibration of fission-track dating. Isot. Geosci. 1: 285–317.

Juez-Larré, J., 2003. Post Late Paleozoic tectonothermal evolution of the northeastern margin of Iberia, assessed by fission-track and (U-T)/He analysis: a case history from the Catalan Coastal Ranges. Ph.D. thesis, Free University of Amsterdam. 200 pp.

Ketcham, R.A., 2003. Observations on the relationship between crystallographic orientation and biasing in apatite fission-track measurements. Am. Min. 88, 817-829.

Ketcham, R.A., 2005. Forward and inverse modeling of low-temperature thermochronometry data. Reviews in Mineralogy and Geochemistry, 58, 275-314.

Ketcham, R.A., 2009. HeFTy Version 1.6.7, Manual.

Ketcham, R.A., Donelick, R.A., Carlson, W.D., 1999. Variability of apatite fission-track annealing kinetics: III Extrapolation to geological time scales. Am. Min. 84, 1235-1255.

Ketcham, R.A., Carter, A., Donelick, R.A., Barbarand, J., Hurford, A.J., 2007a. Improved measurement of fission-track annealing in apatite using c-axis projection. Am. Min. 92, 789-798.

Ketcham, R.A., Carter, A., Donelick, R.A., Barbarand, J., Hurford, A.J., 2007b. Improved modelling of fission-track annealing in apatite. Am. Min. 92, 799-810.

Ketcham, R.A., Donelick, R.A., Balestrieri, M.L., Zattin, M., 2009. Reproducibility of apatite fission-track length data and thermal history reconstruction. Earth and Planetary Science Letters 284, 504-515.

Kooi, H., Beaumont, C., 1996. Large-scale geomorphology: classical concepts reconciled and integrated with contemporary ideas via a surface processes model. Journal of Geophysical Research 101, 3361–3386.

Laslett, G.M., Gleadow, A.J.W., Duddy, I.R., 1984. The relationship between fission track length and track density distributions. Nucl. Tracks 9, 29-38.

Laslett, G.M., Green, P.F., Duddy, I.R., Gleadow, A.J.W., 1987. Thermal annealing of fission tracks in apatite 2: A quantitative analysis. Chemical Geology 65, 1-13.

Le Pichon, X., Bonnin, J.C. Francheteau, J., Sibuet J.C., 1971. Une hypothese d'evolution tectonique du Golfe de Gascogne. In: Debysier, J., Le Pichon, X., Montadert, M. (Eds.), Histoire structurale du Golfe de Gascogne, VI.11.1-VI.11.44, Technip, Paris.

Lisker, F., Ventura, B., Glasmacher, U.A., 2009. Apatite thermochronology in modern geology. Geol. Soc. London Spec. Publ. 324, 1-23.

López-Fernández, C., Pulgar, J.A., Gallart, J., Glez-Cortina, J.M., Díaz, J., Ruiz, M., 2004. Sismicidad y tectónica en el área de Becerreá–Triacastela (Lugo, NO España). Geogaceta 36, 51–54.

Mancktelow, N.S., Grasemann, B., 1997. Time-dependent effects of heat advection and topography on cooling histories during erosion. Earth and Planetary Science Letters 270, 167–195.

Martínez-Catalán, J.R., Pérez-Estaún, A., Bastida, F., Pulgar, J.A., Marcos, A., 1990. West Asturian-Leonese Zone: Structure. In: Dallmeyer, R.D., Martínez-García, E. (Eds.), Pre-Mesozoic Geology of Iberia, 103–114, Springer-Verlag.

Martínez-Catalán, J.R., Arenas, R., Díaz-García, F., González-Cuadra, P., Gómez-Barreiro, J., Abati, J., Castiñeiras, P., Fernández-Suárez, J., Sánchez Martínez, S., Andonaegui, P., González Clavijo, E., Díez Montes, A., Rubio Pascual, F.J., and Valle Aguado, B., 2007. Space and time in the tectonic evolution of the northwestern Iberian Massif: Implications for the Variscan belt. Hatcher, R.D., Jr., Carlson, M.P., McBride, J.H., Martínez-Catalán, J.R. (Eds.), 4-D Framework of Continental Crust: Geological Society of America Memoir 200, 403–423.

Martínez-García, E., Antona, J.F., García-Sanchez, A., Quiroga de la Vega, J.L., 2004. Tectonics and metallogenic significance of sedimentary manganese deposits in the eastern Cantabrian Domain, Asturias, northwestern Spain. International Geology Review 46 (3), 273-288.

Mauffret, A., Boillot, G., Auxietre, J.L., Dunand, J.P., 1978. Evolution structurale de la marge continentale au Nord-Ouest de la péninsule ibérique. Bull. Soc. Géol. Fr. XX (4), 375–388.

Meesters, A.G.C.A., Dunai, T.J., 2002. Solving the production-diffusion equation for finite diffusion domains of various shapes: Part II. Application to cases with [alpha]-ejection and nonhomogeneous distribution of the source. Chemical Geology, 186, 347–363.

Meesters, A.G.C.A., Dunai, T.J., 2005. A noniterative solution of the (U-Th)/He equation. Geochemistry, Geophysics, Geosystems 6, Q04002.

Migón, P., Lidmar-Bergstroem, K., 2001. Weathering mantles and their significance for geomorphological evolution of central and northern Europe since the Mesozoic. Earth-Science Reviews 56, 285-324.

Mitchell, S.G., Reiners, P.W., 2003. Influence of wildfires on apatite and zircon (U-Th)/He ages. Geology 31:1025–1028

Montadert, L., Roberts, D.G., De Charpal, O., Guennoc, P., 1979. Rifting and subsidence of the northern continental margin of the Bay of Biscay. Initial reports of the Deep Sea Drilling Project, Leg 48, 1025-1060.

Montgomery, D.R., Balco, G., Willett, S.D., 2001. Climate, tectonics, and the morphology of the Andes, Geology 29, 579-582.

Montgomery, D.R, Brandon, M.T, 2002. Topographic controls on erosion rates in tectonically active mountain ranges. EPSL 201, 481-489.

O'Sullivan, P.B., Parrish, R.R., 1995. The importance of apatite composition and single-grain ages when interpreting fission track data from plutonic rocks: a case study from the Coast Ranges, British Columbia. EPSL 132, 213-224.

Pedreira D., Pulgar J.A., Gallart J., Díaz J., 2003. Seismic evidence of Alpine crustal thickening and wedging from the western Pyrenees to the Cantabrian Mountains (north Iberia). Journal of Geophysical Research B: Solid Earth, 108 (4), ETG 10-1 – ETG 10-21.

Pérez-Estaún, A., Bastida, F., Alonso, J.L., Marquínez, J., Aller, J., Alvarez-Marrón, J., Marcos, A., Pulgar, J.A., 1988. A thin-skinned tectonic model for an arcuate fold and thrust belt: Cantabrian Zone. Tectonics 7 (3), 517-537.

Pérez-Estaún, A., Bastida, F., Martínez-Catalán, J.R., Gutiérrez-Marco, J.C., Marcos, A., and Pulgar, J.A., 1990. West Asturian–Leonese Zone: stratigraphy. In: R.D. Dallmeyer and E. Martínez-García (Eds.), Pre-Mesozoic Geology of Iberia, 92-102, Springer-Verlag.

Pérez-Estaún, A., Martínez-Catalán, J.R., Bastida, F., 1991. Crustal thickening and deformation sequence in the footwall to the suture of the Variscan belt of northwest Spain. In: Pérez-Estaún A., Coward, M.P. (Eds.), Deformation and Plate Tectonics, Tectonophysics 191, 243-253.

Persano, C., Stuart, F.M., Bishop, P., Barfod, D.N., 2002. Apatite (U-Th)/He age constraints on the development of the Great Escarpment on the southeastern Australian passive margin. EPSL 200, 79-90.

Pulgar, J., Gallart, J., Fernández-Viejo, G., Pérez-Estaún, A., Alvarez-Marrón, J., and ESCIN Group, 1996. Seismic image of the Cantabrian Mountains uplift in the western extension of the Pyrenean Belt from integrated ESCIN reflection and refraction data. Tectonophysics 264, 1-20.

Quesada, S., Robles, S., Rosales, I., 2005. Depositional architecture and transgressive-regressive cycles within Liassic backstepping carbonate ramps in the Basque-Cantabrian basin, northern Spain. Journal of the Geological Society 162 (3), 531-548.

Rasmussen, E.S., Lomholt, S., Andersen, C., Vejbaek, O.V., 1998. Aspects of the structural evolution of the Lusitanian Basin in Portugal and the shelf and slope area offshore Portugal. Tectonophysics 3000, 199-225.

Reiners, P.W., 2007, Thermochronologic Approaches to Paleotopography, In: Kohn, M.J. (Ed.), Paleoaltimetry: Geochemical and Thermodynamic Approaches, Reviews in Mineralogy and Geochemistry 66, 243-267.

Reiners P.W., Brandon, M.T., 2006. Using Thermochronology to Understand Orogenic Erosion. Annu. Rev. Earth Planet. Sci. 34, 419–66.

Reiners, P.W., Ehlers, T.A. (Eds). 2005. Low-temperature thermochronology: techniques, interpretations, and applications. Reviews in Mineralogy and Geochemistry 58, v-ix, 1-622.

Reiners, P.W., Farley, K.A., 2001. Infuence of crystal size on apatite (U-Th)/He thermochronology: an example from the Bighorn Mountains, Wyoming. Earth and Planetary Science Letters 188, 413-420.

Reiners, P.W., Shuster, D.L., 2009. Thermochronology and landscape evolution. Phys Today 62(9): 31–36.

Reiners, P.W., Zhou, Z., Ehlers T. A., Xu, C., Brandon, M. T., Donelick, R. A., Nicolescu, S., 2003. Post-orogenic evolution of the Dabie Shan, eastern China, from (U-Th)/he and fission-track thermochronology. American Journal of Science 303, 489-518.

Ring, U., Brandon, M.T., Willett, S.D, Lister, G.S., 1999. Exhumation processes. In: Ring, U., Brandon, M.T., Lister, G.S., Willett, S.D. (Eds.), Exhumation Processes: Normal Faulting, Ductile Flow, and Erosion, Special Publications 154, 1-27, Geological Society London.

Rodríguez-Fernández, L.R., 2004. Mapa Geológico de España (Escala 1:200.000), In: Vera, J.A. (Ed.), Geología de España, SGE-IGME, Madrid

Rodríguez-García, A., Quintana, L., González-Menéndez, L., Suárez-Rodríguez, A., 2006. Neotectónica en el norte de Galicia: Fallas inversas de actividad cuarternica en la cuenca fluvial del alveolo de Alfoz, Lugo. Geogaceta 40, 23-26.

Roest, W.R., Srivastava, S.P., 1991. Kinematics of the plate boundaries between Eurasia, Iberia, and Africa in the North Atlantic from the Late Cretaceous to the present. Geology 19 (6), 613-616.

Rosenbaum, G., Lister, G.S., Duboz, C., 2002. Relative motions of Africa, Iberia and Europe during Alpine orogeny, Tectonophysics 359, 117-129.

Sambridge, M., 1999a. Geophysical inversion with a neighbourhood algorithm-I. Searching a parameter space. Geophys. J. Int. 138, 479-494.

Sambridge, M., 1999b. Geophysical inversion with a neighbourhood algorithm-II. Appraising the ensemble. Geophys. J. Int. 138, 727-746.

Santanach, P., 1994. The Tertiary basins of Galicia in the western termination of the Pyrenean reliefs. Cuadernos Laboratorio Xeoloxico de Laxe. 1957-71.

Santanach, P., Ferrús, B., Cabrera, L., Sáez, A., 2005. Origin of a restraining bend in an evolving strike-slip system: The Cenozoic As Pontes basin (NW Spain). Geologica Acta 3 (3), 225-239.

Shuster, D.L., Farley, K.A., 2009. The influence of artificial radiation damage and thermal annealing on helium diffusion kinetics in apatite. Geochimica et Cosmochimica Acta 73, 183–196.

Shuster, D.L., Flowers, R.M., Farley, K.A., 2006. The influence of natural radiation damage on helium diffusion kinetics in apatite. EPSL 249, 148-161.

Sibuet, J.C., Le Pichon, X., 1971. Structure gravimétrique du Golfe de Gascogne a partir des profils de sismique. In: Debysier, J., Le Pichon, X., Montadert, M. (Eds.), Histoire structurale du Golfe de Gascogne, VI.9.11–VI.9.18, Technip, Paris.

Sobel, E.R., Seward, D., 2010. Influence of etching conditions on apatite fission-track etch pit diameter. Chemical Geology 271, 59-69.

Spiegel, C., Kohn, B., Raza, A., Rainer, Th., Gleadow, A., 2007. The effect of long-term low-temperature exposure on fission track stability: a natural annealing experiment in the deep sea. Geochimica et Cosmochimica Acta 71, 4512-4537.

Spiegel, C., Kohn, B., Belton, D., Berner, Z., Gleadow, A., 2009. Apatite (U-Th-Sm)/He thermochronology of rapidly cooled samples: the effect of He implantation. Earth and Planetary Science Letters 285, 105-114.

Srivastava, S.P., Roest, W.R., Kovacs, L.C., Oakey, G., Lévesque, S., Verhoef, J., Macnab, R., 1990. Motion of Iberia since the Late Jurassic: Results from detailed aeromagnetic measurements in the Newfoundland Basin; Tectonophysics 184, Issues 3-4, 229-260.

Stachowiak, H., 1973. Allgemeine Modelltheorie. Spingerverlag, Wien.

Stöckli, D.F., 2005. Application of low-temperature thermochronometry to extensional tectonic settings. Reviews in Mineralogy and Geochemistry, 58, 411–448.

Stöckli, D.F., Farley, R.A., Dumitru, T.A., 2000. Calibration of the apatite (U-Th)/He thermochronometer on an exhumed fault block, White Mountains, California. Geology 28 (11), 983-986.

Stüwe, K.,White, L., Brown, R., 1994. The influence of eroding topography on steady-state isotherms. Application to fission track analysis. Earth and Planetary Science Letters, 124, 63–74.

Summerfield, M.A., Brown, R.W. (1998) Geomorphic factors in the interpretation of fission-track data. In Advances in Fission-Track Geochronology, 269-284.

Thiry, M., Quesnel, F., Yans, J., Wyns, R., Vergari, A., Theveniaut, H., Simon-Coincon, R., Ricordel, C., Moreau, M.-G., Giot, D., Dupuis, C., Bruxelles, L., Barbarand, J., Baele, J.-M., 2006. Continental France and Belgium during the early cretaceous: Paleoweatherings and paleolandforms. Journal of the Geological Society 163 (4), 723-736

Thomson, S.N., Brandon, M.T., Tomkin, J.H., Reiners, P.W., Vásquez, C., Wilson, N.J., 2010. Glaciation as a destructive and constructive control on mountain building. Nature 467, 313-317.

Valla, P.G., Herman, F., Van der Beek, P.A., Braun, J., 2010. Inversion of thermochronological age-elevation profiles to extract independent estimates of denudation and relief history – I: Theory and conceptual model. EPSL 295, 511-522.

Van der Beek, P.A., Valla, P.G., Herman, F., Braun, J., Persano, C., Dobson, K.J., Labrin, E., 2010. Inversion of thermochronological age-elevation profiles to extract independent estimates of denudation and relief history – II: Application to the French Western Alps. EPSL 296, 9-22.

Verhoef, J., Srivastava, S.P., 1989. Correlation of sedimentary basins across the North Atlantic as obtained from gravity and magnetic data, and its relation to the early evolution of the North Atlantic. In: Tankard, A.J., Balkwill, H.R. (Eds.), Extensional tectonics and stratigraphy of the North Atlantic margins, AAPG Memoir 46, 131-147.

Wagner, G.A., 1972. Spaltspurenalter von Mineralen und natürlichen Gläsern: eine Übersicht. Fortschr. Miner. 49, 114-145.

Wagner, G.A., van den Haute, P., 1992. Fission-Track Dating. In: Enke Verlag - Kluwer Academic Publishers, p. 285.

Whipple, K.X., Meade, B.J., 2004. Controls on the strength of coupling among climate, erosion, and deformation in two-sided, frictional orogenic wedges at steady state. Journal of Geophysical Research 109, 1-24.

Whipple, K.X., Kirby, E., Brocklehurst, S.H., 1999. Geomorphic limits to climate-induced increases in topographic relief. Nature 401, 39-43.

Willet, S., Beaumont, C., Fullsack, P., 1993. Mechanical model for the tectonics of doubly vergent compressional orogens. Geology 21 (4) 371-374.

Wolf, R.A., Farley, K.A., Silver, L.T., 1996. Helium diffusion and low-temperature thermochronometry of apatite. Geochimica et Cosmochimica Acta 60, 4231-4240.

Wolf, R.A., Farley, K.A., Kass, D.M., 1998. Modeling of the temperature sensitivity of the apatite (U–Th)/He thermochronometer. ChemicalGeology 148, 105–114.

Ziegler, P.A., 1989. Evlution of the North Atlantic-Overiview. In: Tankard, A.j., Balkwill, H.R. (Eds.), Extensional Tectonics and Stratigraphy of the North Atlantic Margins: AAPG Memoir 46, 11-130.

Ziegler, P.A., Roure, F., 1999. Petroleum systems of Alpine-Mediterranean foldbelts and basins. Geological Society Special Publication 156, 517-540.

Appendices

List of Publications submitted for this thesis

Publication 1 (Appendix A)

Low-temperature exhumation history of Variscan-age rocks in the western Cantabrian Mountains (NW Spain) recorded by apatite fission-track data.
René W. Grobe, Joaquina Alvarez-Marrón, Ulrich A. Glasmacher, Rosana Menéndez-Duarte
(2010)
Tectonophysics 489 (1-4), 76-90. doi:10.1016/j.tecto.2010.04.006

Status of Publication: **published in 'Tectonophysics'**

Own contributions:

- Data acquisition and analysis
- 2D thermal modelling
- Interpretation of thermal history (in collaboration with UAG and JAM)
- Preparation of tables and figures for publication
- Preparation of manuscript for publication (in collaboration with JAM, UAG and RMN)

Publication 2 (Appendix B)

Post-Paleozoic exhumation of the NW Iberian Massif and the remains of a pre-Alpine paleolandscape from apatite fission-track and (U-Th-Sm)/He data.
René W. Grobe, Joaquina Alvarez-Marrón, Ulrich A. Glasmacher, Finlay M. Stuart
(2010)
Manuscript #2010TC002852.

Status of Publication: **in review; submitted to 'Tectonics' (04th December, 2010)**

Own contributions:

- Sample collection (in collaboration with UAG and JAM)
- Sample processing and supervision of sample processing (AHe processing in collaboration with FMS)
- Data acquisition and analysis (AHe analysis in collaboration with FMS)
- 2D thermal modelling
- Interpretation of thermal history (in collaboration with UAG and JAM)
- Preparation of tables and figures for publication
- Preparation of manuscript for publication (in collaboration with JAM and UAG)

Publication 3 (Appendix C)

3D thermokinematic modelling of long-term landscape evolution of Variscan basement in Galicia, NW Spain.
René W. Grobe, Ulrich A. Glasmacher, Joaquina Alvarez-Marrón, Jean Braun, Francisco Cueto- Berciano
(2010)
Manuscript #IJES-S-10-00315.

Status of Publication: **in review; submitted to 'International Journal of Earth Sciences' (07th December, 2010)**

Own contributions:

- Set up of a computer cluster in Heidelberg to do the computations (in collaboration with FCB and JB)
- 3D thermokinematic modelling
- Interpretation of modelled history of long-term landscape and thermal evolution (in collaboration with UAG and JAM)
- Preparation of tables and figures for publication
- Preparation of manuscript for publication (in collaboration with UAG, JB and JAM)

Publication 4 (Appendix D)

Low-temperature exhumation history of Variscan-age rocks in the western Cantabrian Mountains (NW Spain) recorded by AFT-(U-Th-Sm)/He thermochronology and 2D-3D t-T path modelling. (Abstract)
René W. Grobe, Joaquina Alvarez-Marrón, Ulrich A. Glasmacher, Finlay M. Stuart
(2010)
12th International Thermochronology Conference, Glasgow 16-20 August, 2010

Status of Publication: **published**

Own contributions:

- Preparation of abstract for publication
- Oral presentation

Publication 5 (Appendix E)

Post-orogenic exhumation history of a Variscan mid-crustal basement in Galicia (NW Spain). (Abstract)
René W. Grobe, Joaquina Alvarez-Marrón, Ulrich A. Glasmacher, Finlay M. Stuart, Adolfo Castañeda-Zarauz
(2010)
Geophysical Research Abstracts Vol. 12, EGU2010-1214, EGU General Assembly 2010

Status of Publication: **published**

Own contributions:
- Preparation of abstract for publication
- Oral presentation

Publication 6 (Appendix F)

Low temperature exhumation history of Variscan-age rocks in the western Cantabrian Mountains (NW Spain) recorded by apatite fission-track data. (Abstract)
René W. Grobe, Joaquina Alvarez-Marrón, Ulrich A. Glasmacher, Rosana Menéndez-Duarte (2009)
5th TOPO-EUROPE Workshop, Villa Bosch, Klaus Tschira Foundation, Heidelberg, 15-17 October, 2009

Status of Publication: **published**

Own contributions:
- Preparation of abstract for publication
- Poster presentation

Publication 7 (Appendix G)

Early Mesozoic cooling from low temperature thermochronology in N Spain and N Africa. (Abstract)
René W. Grobe, Joaquina Alvarez-Marrón, Ulrich A. Glasmacher, Rosana Menéndez-Duarte (2009)
Geophysical Research Abstracts Vol. 11, EGU2009-944, EGU General Assembly 2009

Status of Publication: **published**

Own contributions:
- Preparation of abstract for publication
- Oral presentation

Publication 8 (Appendix H)

Low-temperature thermochronology, exhumation, and long-term landscape evolution in the western Cantabrian Mountains, NW Spain. (Abstract)
René W. Grobe, Joaquina Alvarez-Marrón, Ulrich A. Glasmacher, Rosana Menéndez-Duarte (2008)
Geophysical Research Abstracts Vol. 10, EGU2008-A-01435, EGU General Assembly 2008

Status of Publication: **published**

Own contributions:
- Preparation of abstract for publication
- Poster presentation

Confirmation of author's contribution

It is confirmed, that the contribution of René W. Grobe to the publications presented in this thesis and listed above is true, accurate and justified.

apl. Prof. Dr. Ulrich A. Glasmacher Dr. Joaquina Alvarez-Marrón

Contributions to other scientific projects

Publication 9 (Appendix I)

Evolution of the Albertine Rift in East Africa, evidence from the Western Rift shoulder (DRC). (Abstract)
Friederike U. Bauer, Ulrich. A. Glasmacher, René. W. Grobe, Matthias Starz, Meni Malikwisha, Vikandy S. Mambo, Bin V. Mutete
(2010)
12th International Thermochronology Conference, Glasgow 16-20 August, 2010

Status of Publication: **published**

Own contributions:

- Thermonkinematic modelling (in collaboration with FUB and MS)

Publication 10 (Appendix J)

Exhumation history of the eastern border of the Congo basin. (Abstract)
Friederike U. Bauer, Ulrich. A. Glasmacher, René. W. Grobe, Matthias Starz, Meni Malikwisha, Vikandy S. Mambo, Bin V. Mutete
(2010)
23rd Colloquium of African Geology, South Africa 8-14 January, 2011

Status of Publication: **accepted**

Own contributions:

- Sample collection (in collaboration with FUB, MS, VSM and BVM)
- Thermonkinematic modelling (in collaboration with FUB and MS)

Confirmation of author's contribution

It is confirmed, that the contribution of René W. Grobe to the publications presented in this thesis and listed above is true, accurate and justified.

apl. Prof. Dr. Ulrich A. Glasmacher Dr. Friederike U. Bauer

A. Publication 1

Low-temperature exhumation history of Variscan-age rocks in the western Cantabrian Mountains (NW Spain) recorded by apatite fission-track data.

René W. Grobe[1], Joaquina Alvarez-Marrón[2], Ulrich A. Glasmacher[1], Rosana Menéndez-Duarte[3]
(2010)

[1]Institute of Earth Sciences, University of Heidelberg, Germany

[2]Institute of Earth Sciences "Jaume Almera", CSIC, Barcelona, Spain

[3]Institue of Natural Resources (INDUROT), University of Oviedo, Spain

Tectonophysics 489 (1-4), 76-90. doi:10.1016/j.tecto.2010.04.006

Abstract

This paper presents the first regional study of apatite fission-track (AFT) thermochronology to be undertaken in the western termination of the Cantabrian Mountains (NW Spain). The mountains reach elevations of over 2600 m along the northern coast of Spain and are comprised of a Variscan crustal section uplifted due to Cenozoic shortening along the northern Iberian Plate. The study constrains the pattern and history of exhumation within the Paleozoic bedrock over the past c. 240 Ma. Twenty-one apatite fission-track samples range in age from 246.7 (26.9) Ma to 78.1 (3.7) Ma, with mean track lengths between 10.4 (1.8) µm and 12.4 (1.4) µm. Time-temperature path modelling of the data indicates that continuous cooling at different rates took place during the three main tectonic events that affected the area. A rapid cooling event that ended by the Late Jurassic corresponds to topographic decay during unroofing of the Variscan orogen and the break-up of Pangea, and is responsible for the largest amount of exhumation. Westernmost samples cooled coinciding with rifting in the North Atlantic and Bay of Biscay during the Late Jurassic to Early Cretaceous. By about 100-80 Ma most samples had reached, or passed through, the upper boundary of the apatite partial annealing zone, which indicate that regional denudation has not exceeded c. 1.7 km since then, for geothermal gradients ≥ 27 ºC/km and a surface temperature of 15 °C. Only three samples next to fault escarpments in the west cooled below 70 ºC since 80 Ma, reaching below 65 ºC before initiation of incipient subduction along the North Iberian Margin by 46 Ma. An average cooling rate of ≤ 1 ºC/Ma reflects latest denudation as the new mountainous relief developed since then due to shortening and incipient subduction associated with convergence along the northern Iberian Plate. The Cantabrian Mountains are one of the few natural examples of a coastal orogen in a juvenile stage of evolution.

1 Introduction

One of the best established and most sensitive techniques for reconstructing the cooling history of rocks that are being exhumed through the upper few km of the Earth's crust, over time scales of millions to hundreds of millions of years, is Apatite fission-track (AFT) thermochronology (Reiners and Ehlers, 2005). By modelling time-temperature (t-T) paths from AFT data and allowing certain assumptions, such as an estimation of the geothermal gradient over the period relevant to the sample's thermal history, the rates of cooling may be converted to denudation rates (Gunnell, 2000). In addition, when exhumation is driven by active tectonic processes, thermochronological studies provide estimates on the rates at which rocks are brought to the surface relative to the acting tectonic forcing (Reiners and Ehlers, 2005; Bishop, 2007). These estimates are valuable information for unravelling the behaviour of the coupled tectonic-erosion system (Allen, 2008), and in particular, for interpreting the overall movement of material through an orogenic system (Reiners and Brandon, 2006).

The AFT technique has been applied successfully to unravel rates of exhumation in a variety of tectonic scenarios, such as active orogens (Reiners and Ehlers, 2005; Reiners and Brandon, 2006; Bishop, 2007), rifting and passive margins (i.e. Gunnell *et al.*, 2009) and post-orogenic topographic decay in areas of tectonic quiescence (Reiners *et al.*, 2003), among others. However, the rates of exhumation of upper crustal rocks and, therefore, the behaviour of the tectonic-erosion system are not well documented in natural examples of early stages of rock uplift along juvenile coastal orogens. Here we present a case study of ca. 240 Ma cooling history of Paleozoic rocks uplifted along the Cantabrian Mountains, a young and evolving coastal orogen in northern Spain (Fig. 1).

The Cantabrian Mountains trend E-W, parallel to the north Spanish coast for more than 300 km, and locally reach elevations of more than 2600 m. Along this mountain range, rocks previously deformed and metamorphosed during the Variscan orogeny have been uplifted due to minor shortening and limited

convergence between Eurasia and Iberia in the Cenozoic (Boillot *et al.*, 1979; Alonso *et al.*, 1996; Pulgar *et al.*, 1996; Alvarez-Marrón *et al.*, 1997). Although the geology and tectonic evolution of this area is well known, the variation in timing, rate and amount of exhumation of the Paleozoic rocks presently exposed at the surface is largely unconstrained. The cooling history of these rocks has possibly been influenced by several tectonothermal scenarios, including post-orogenic topographic decay of the Variscan edifice, far-field effects of rifting and seafloor spreading due to the opening of the Atlantic and Bay of Biscay ocean basins, and a subsequent uplift caused by shortening during convergence along an incipient active margin.

Unravelling the exhumation history across the Cantabrian Mountains should provide constraints on the vertical component of material flow and on how cooling and exhumation may have varied through the several tectonic scenarios. In particular, we aim at discussing the incidence of exhumation during the latest uplift event associated with the minor shortening and convergence that took place along the North Iberian Plate in the Cenozoic. Data from natural examples of the initial stages of formation of a mountainous relief in a young and evolving coastal orogen are fundamental for improving our understanding of the rates at which cooling and exhumation of upper crustal rocks adapt to a new tectonic environment.

2 Geological background

2.1 Tectonic evolution

The tectonic evolution of the Northern Iberian Peninsula included three major events: (1) the Variscan orogeny that ended by Late Paleozoic times, (2) the rifting during Pangea break-up in Permian-Triassic times and subsequent opening of the Atlantic Ocean and Bay of Biscay in the Mesozoic and (3) limited convergence between Iberia and Eurasia since Middle Eocene times.

The Paleozoic and older rocks of the Iberian Massif in NW Spain provide an unusually well preserved record of the tectonothermal events that contributed to the final assembly of Pangea during the Carboniferous and Early Permian (Martínez-Catalán *et al.*, 2007). Evidences of extensional tectonics that began in Late Permian and Triassic times during the initiation of the break-up of Pangea are found outside our study area to the east. Formation of minor fault bounded continental basins and related alkaline volcanism occur near Oviedo (Martínez-García *et al.*, 2004) and in the Basque-Cantabrian basin (Espina *et al.*, 2004) (Fig. 1b). Widespread rifting during Late Jurassic-Early Cretaceous times by oblique separation of Iberia from Eurasia caused formation of the Atlantic and Bay of Biscay margins, located to the west and north of our study area (Le Pichon *et al.*, 1971; Srivastava *et al.*, 1990) (Fig. 2a). Subsequent seafloor spreading was active in the Bay of Biscay since the Early Cretaceous until the Late Cretaceous (Srivastava *et al.*, 1990) (Fig. 2b).

The Variscan-aged structure preserved in the Cantabrian Mountains was overprinted and uplifted during the Cenozoic convergence between Iberia and Eurasia. Magnetic anomalies in the North Atlantic and Bay of Biscay indicate that limited convergence along the North Iberian Margin started at 49 Ma and went on until 20 Ma (Srivastava *et al.*, 1990) (Fig. 2c). A N-S crustal-scale section at about 5º W longitude shows a northward imbrication of the Iberian crust beneath the Cantabrian Mountains reaching current crustal thickness of more than 50 km (Pulgar *et al.*, 1996; Fernández-Viejo *et al.*, 2000; Pedreira *et al.*, 2003) and limited southward subduction of the Bay of Biscay oceanic crust along the continental margin (Sibuet and Le Pichon, 1971; Boillot *et al.*, 1979; Grimaud *et al.*, 1982). This incipient subduction caused the formation of an accretionary prism at the foot of the continental slope, that was active in the western part of the margin from Lutetian to Burdigalian times (Alvarez-Marrón *et al.*, 1997). By Middle Eocene times continental facies sediments started to accumulate in the Duero foreland basin, thus marking the shortening and starting uplift in the Cantabrian Mountains. In the study area, the N-S shortening has been smaller with formation of south-directed thrusts that cut the Paleogene to Neogene age continental sediments of the Bierzo basin (Andeweg, 2002) (Fig. 3a). Small continental basins developed in the west

associated to WNW-ESE transpressional faults that accommodated minor N-S shortening (Santanach, 1994). The largest of this is the As Pontes fault (Fig. 1b and 3a) that cuts through sediments ranging in age from 28 Ma to 22 Ma within the As Pontes basin (Huerta *et al.*, 1996).

Convergence along the northern margin of Iberia slowed significantly since the Early Miocene (20 Ma) (Rosenbaum *et al.*, 2002), although younger brittle faulting has been documented on land (Cabral, 1989; Andeweg, 2002; Rodríguez-García *et al.*, 2006; Alvarez-Marrón *et al.*, 2008). The area and surrounding continental margins continue to be weakly seismically active today (López-Fernández *et al.*, 2004; Díaz *et al.*, 2008).

2.2 Regional geology

Along their western flank, within the current study area, the Cantabrian Mountains are comprised of deformed Early Paleozoic and Neoproterozoic metasedimentary rocks, including 11,000 m of Cambrian-Ordovician siliciclastic rocks belonging to the margin of Gondwana, which collided with Laurussia during the Variscan orogeny (Pérez-Estaún *et al.*, 1990; Pérez-Estaún *et al.*, 1991; Martínez-Catalán *et al.*; 2007). These rocks lie within the West Asturian-Leonese Zone (WALZ) of the Variscan section and underwent a great deal of strain with formation of folds (largely recumbent) and thrusts and associated cleavages and regional metamorphism (Fig. 3). Variscan-age metamorphic grade varies from very low in the east to high in the west (Martínez-Catalán *et al.*, 1990). The WALZ is bound to the east by the Narcea antiform that marks the transition to dominantly younger rocks within the Cantabrian Zone that underwent deformation at shallower crustal levels in the foreland areas of the Variscan orogen. In the Mondoñedo antiform at the western side of the WALZ, rocks that were affected by deformation at deeper crustal level conditions crop out (Pérez-Estaún *et al.*, 1988; 1991).

Syn- to post-Variscan granitoids are widespread in the western part of the WALZ (Fig. 3a). These range in age from 323 (5) Ma to 284 (8) Ma obtained from U-Pb geochronology (Fernández-Suárez *et al.*, 2000). In the central part, small granitic bodies crop out in Porcía, Boal, Ancares, Campo del Agua and Ponferrada along the Boal-Ancares dome (Fig. 3a and b). Several of these have been dated by U-Pb geochronology between 295 (3) Ma and 284 (8) Ma (Fernández-Suárez *et al.*, 2000).

The trend of Variscan structures changes from mainly N-S to mainly E-W from the northern to the southern slope of the Cantabrian Mountains. Although, the overall Variscan structural grain in the study area is dominantly N-S (Fig. 1 b).

3 Geomorphology of the study area

The topographic edifice that makes up the Cantabrian Mountains has an average elevation of 1800 m, with the highest elevation reaching more than 2600 m in the Picos de Europa area, east of Oviedo. The current study area covers the region of about 150 by 100 km in the western termination of the mountains where the overall elevation is lower, ranging from c. 450 m to 1900 m (Fig. 4). Changes in wavelength and amplitude of elevation occur across the area. For example, there is long wavelength (tens of km) and moderate amplitude relief (a few hundred meters) in large areas to the west (Galicia), whereas to the east, a shorter wavelength (a few km), higher amplitude (over 1000 m) pattern is dominant (Fig. 4b, profile A-A').

The relief pattern in Galicia is characterised by an extensive, relatively flat area around the city of Lugo that averages between 450 and 500 m elevation above sea level and higher, more rugged topography to the north (Fig. 4b, profile B-B'). The abrupt transition north of Lugo is bounded by the As Pontes fault, reaching elevations of over 1000 m in its northern block. In Asturias, the highest elevations are along the drainage divide at 50 to 100 km from the coastline. To the north of the divide, there are areas with moderate amplitudes, such as the Oscos plateau region with elevated surfaces of low relief at 700-800 m and shallowly incised rivers (Fig. 4b, profile A-A'). In contrast, areas of higher amplitude to the east are associated to the Alpine-aged Allande thrust. This fault

reactivates a N-S trending Variscan structure and has associated topography in excess of 1200 m (Alvarez-Marrón *et al.*, 2003). South of the drainage divide, elevations decrease until the area with subdued topography in the Bierzo basin with average elevations of 600 m (Fig. 4b, profile C-C').

Superimposed on this relief pattern, the drainage system includes rivers that flow north into the Bay of Biscay and rivers that flow southwest into the Atlantic separated by a divide with a complex trace (Fig. 4). Southwest draining rivers belong to the Miño river basin that in the area of Galicia forms a broad basin with widely spaced tributaries shallowly incised into the flat lands of Lugo. In contrast, the Sil river that flows through the Bierzo basin, forms the largest tributary basin that is deeply incised into the higher topographic areas in the east. The north draining rivers are commonly short bedrock courses, closely spaced and deeply incised into the bedrock. The largest basins that drain highest topographic areas are the Eo, Navia and Narcea (Fig. 4a and b, profile A-A' and C-C'). The alternating quartzites and slates with a dominant N-S structural trend in the bedrock impose an important control on the morphology of these river basins.

4 Methodology

4.1 Sampling strategy

The landscape of the study area is characterized by a complex topography with a distribution of elevations that varies significantly in N-S and E-W directions. For this reason, samples were taken following as closely as possible two N-S and one E-W topographic sections, (Fig. 4a and b). Samples were taken from elevations between 0 and 1256 m above sea level and from a number of lithologies, including low to high-grade siliciclastic metasediments ranging from Neoproterozoic to Lower Paleozoic age and granites of Carboniferous to Permian age. Twenty-one samples with a sufficient amount of apatite to perform fission-track thermochronology were obtained.

4.2 Apatite fission-track thermochronology

The basic concept of AFT dating is the spontaneous fission of ^{238}U during which the heavy fragments of this fission leave chemically etchable linear defects (fission-tracks) in the apatites (Wagner, 1972). The fission-tracks are metastable in relation to time and temperature. While fission-tracks fully anneal at temperatures above c. 110 °C/10 Ma and the chronometer is reset, the annealing is virtually zero at temperatures below c. 60 °C. Therefore, AFT thermochronology is sensitive to the temperature space between c. 110 and 60 °C, called the partial annealing zone (PAZ). Given a geothermal gradient of 27 °C/km and a surface temperature of 15 °C, AFT thermochronology reflects the thermal history of rocks between 1.7 and 3.5 km depth. The information on the thermal history of apatite is stored in two archives: (1) the etch pit areal density of tracks at an artificially polished internal surface of the apatites giving the cooling age and (2) the length distribution of horizontal confined tracks recording the cooling path (e.g. Wagner and van den Haute 1992; Lisker *et al.* 2009 and literature cited therein).

In general, the annealing of spontaneous fission-tracks is governed by temperature and the time the apatite grains have been kept at a certain temperature. However, the temperature sensitive annealing of fission-tracks in apatite is also constraint by two important effects 1) the chemical composition of the apatite and 2) the crystallographic orientation of the spontaneous tracks.

1) The annealing of fission-tracks at a given temperature is slower in apatite grains with high chlorine content than in fluorine rich apatite grains (Gleadow and Duddy, 1981; Green *et al.*, 1985; 1986; Burtner *et al.*, 1994; O'Sullivan and Parrish, 1995; Carlson, 1990; Crowley *et al.*, 1991; Crowley, 1993; Carlson *et al.*, 1999; Donelick *et al.*, 1999; Ketcham *et al.*, 1999; Barbarand *et al.*, 2003a; b). Normally, the chemical composition is determined by electron microprobe work (Glasmacher *et al.* 1998, Barbarand *et al.* 2003a, b). Donelick (1993; 1995) first described the linear relation between the etch pit size parallel to the c-axis ($D_{par}^{®}$) and the fluorine and chlorine content of the apatite.

Further research by Barbarand *et al.* (2003a; b) confirmed this relation. D_{par}® can be used in the HeFTy©-modelling program (Ketcham, 2005; Ketcham *et al.*, 2007a; b; Ketcham *et al.*, 2009) as a kinetic parameter.

2) Green and Durrani (1977) first described the influence of the crystallographic orientation of spontaneous fission-tracks on the annealing of those tracks. Tracks orthogonal to the c-axis anneal more rapid than tracks parallel to the c-axis (Green, 1988). This anisotropy increases with annealing (Green, 1981; Laslett *et al.*, 1984; Donelick *et al.*, 1990; 1999; Galbraith *et al.*, 1990; Donelick, 1991). Donelick *et al.* (1990; 1999) and Donelick (1991) further extended the database on crystallographic effects of annealing in apatite and integrated the results in the recent annealing model of Ketcham *et al.* (1999; 2007a; b) and Ketcham (2003). Barbarand *et al.* (2003b) confirmed the strong influence of the crystallographic orientation by presenting a large annealing dataset of apatites with different chemical composition. The measured confined track lengths were corrected for their crystallographic orientation by applying the computer code HeFTy© to the data set.

4.3 Processing and data acquisition

Apatite grain mounts were obtained by applying standard sample processing techniques (Grist and Ravenhurst, 1992a; b). Apatite was etched in 5.5 N HNO_3 for 20 (1) s at 20 (1) °C and detection mica in 48 % HF for 20 (1) min at 20 (1) °C. Samples were irradiated at the research reactor FRM II, Munich, in the presence of three glass neutron dosimeter (CN5) of known uranium content at top, middle and bottom of the sample batch and two Durango apatite age standards.

Area densities (tracks/cm2) of spontaneous and induced tracks, distribution of horizontal confined track lengths and c-axis oriented etch pit diameters (D_{par}®; Donelick 1993; 1995) were determined at the Heidelberg FT-1 system. The Heidelberg FT-1 system consists of an Olympus® 'BX50' optical microscope with an Autoscan® 'AS3000i' 3-axis microscope stage, a high-resolution Peltier-cooled color CCD camera 'ColorView III' (5 megapixel) of Olympus® and a high performing Windows® based computer system with two Samsung 244T flat screens. To increase the precision of stage movement each axis is equipped with the external laser scale sensor 'BL 55 RE' of Sony®. These sensors guarantee a deviation of less than 500 nm along 4-5 cm of movement. The entire setup is operated through the Autoscan® software Trakscan®. Applying the largest possible resolution, each pixel is equivalent to less than 250 nm in size. Area densities were counted by using a 50x dry objective. Horizontal confined track lengths and etch pit size were measured by a 100x dry objective using the Autoscan® computer code 'EasyLength®'.

Apatite fission-track ages were calculated applying the ζ-method (external detector method) described by Hurford and Green (1982; 1983). The ζ-values of 356.21 (11.24) and 337.91 (± 10.31) were obtained by counting several Durango apatite age standards. All ages and 1σ errors were determined by using the computer code 'Trackkey' (Dunkl, 2002). All data are presented in Table 1 according to the recommendation of Hurford (1990).

4.4 Thermal modelling

Determination of the low-temperature thermal history can be achieved by a modelling procedure that combines the annealing kinetics of fission tracks in apatite, the real fission-track data set (single grain ages, confined fission-track length distribution, chemical composition, D_{par}®) and the time-temperature coordinates obtained from the known geological evolution of the area. Therefore, the modelling process tests the thermochronological data against the known tectonic evolution to determine a best fit t-T evolution by using the computer code HeFTy©. The primary goal of the program is to define envelopes in t-T space (goodness of fit > 0.05 (5%) and > 0.5 (50%)) that contain all paths passing baseline statistical criteria and being conformed to the user-entered geological constraints. Using the timescales of Haq and van Eysinga (1998), the geologically constrained time-temperature coordinates are implanted in the program by time-temperature boxes that consider the possible errors of the t-T coordinates. This is the starting procedure of the modelling technique. The computer code

attempts to find more than 10,000 single t-T paths, displaying only those that best approximate the measured data.

5 Results

5.1 Apatite fission-track ages

The 21 apatite fission-track central ages determined range between 78.1 (3.7) and 246.7 (26.9) Ma (Tab. 1). All ages are younger than the corresponding sedimentation, metamorphic or intrusive age of the sampled rocks. All single grain age distributions fulfilled the requirement of the χ^2-test indicating a homogenous distribution within the 1σ error of the single grain ages. Because of the very different nature of the topography from west to east in the sampling area (Fig. 4), we divide the data into two groups; the Galicia area with its, relatively flat topography at lower elevations and the Asturias area with its rugged topography at higher elevations.

5.1.1 The Galicia area

In the Galicia area, 10 samples record central fission-track ages that range from 174.5 (7.7) to 78.1 (3.7) Ma (Tab. 1). The oldest age was obtained from a sample (ESP-16) of a post-Variscan granite with a U-Pb age of 286 (2) Ma (Fernández-Suárez *et al.*, 2000) at 0 m elevation. The rest of the samples were collected from elevations of between 382 m and 645 m yielding an average age of 118 Ma (σ_{std} = 27 Ma). There is little apparent relationship between elevation and central fission-track ages, given that most samples are from similar elevations around the flat area of Lugo (Fig. 5). However, if sample ESP-16 is taken into account, then there is a weak negative trend. The area is cut by two main post-Variscan fault systems with NW-SE and NE-SW trends (González-Lodeiro *et al.*, 1982; Bastida *et al.*, 1984). The As Pontes fault in the north and the Lugo fault in the south are the major faults belonging to those fault systems (Fig. 3). The As Pontes fault has a significant fault scarp with a change in elevation of c. 300 m across it. In the higher topography of its hangingwall samples ESP-27a and b yielded ages of 78.1 (3.7) Ma and 91.8 (4.6) Ma, respectively. To the south, in the lower topography of its footwall, samples ESP-25, 26 and 28 yielded ages of 146.2 (7.6) Ma, 126.0 (6.8) Ma and 104.3 (5.6) Ma, respectively. The Lugo fault has no significant change in topography across it. However, sample ESP-17 to the east yielded an age of 160.5 (9.6) Ma, whereas samples ESP-15 and 30, to the west yielded ages of 116.4 (7.4) and 96.2 (4.8) Ma, respectively. The change in ages across both these faults may reflect differential uplift and erosion related to activity along them.

5.1.2 The Asturias area

In the Asturias area, 11 samples yielded apatite fission-track ages that range from 96.2 (9.4) Ma to 246.7 (26.9) Ma with all ages being younger than the protolith age (Tab. 1). However, there is an apparent relationship between fission-track age and protolith age, with the oldest Neoproterozoic rocks yielding older average fission-track ages than younger rocks. Three samples from Neoproterozoic within the Narcea antiform yielded ages of 202.2 (9.9) Ma (ESP-35), 246.2 (26.9) Ma (ESP-18) and 202.8 (25.2) Ma (ESP-13), with no apparent relationship between age and elevation (Fig. 5). One sample (ESP-33) from the Neoproterozoic rocks of the Narcea antiform yielded an age of 134.0 (9.3) Ma. Furthermore, one sample (ESP-31) from Lower Cambrian rocks within the Mondoñedo antiform yielded an age of 215.7 (21.3) Ma. Carboniferous and Permian syn- and post-kinematic granites yielded ages between 96.2 (9.4) and 162.5 (7.2) Ma. The youngest age 96.2 (9.4) was obtained from a granite sample taken at 1256 m (ESP-10), the highest elevation of all samples. Three samples from small post-Variscan granitic bodies along the central Boal-Ancares dome (ESP-21, 22, 32) yielded an average age of 149 Ma (σ_{std} = 12 Ma), somewhat older than similar rocks in the Galicia area. One sample (ESP-23) from within the sediments near granite samples ESP-21 and 22 yielded an age of 161.3 (8.7), similar to the samples from the granitic rocks. A sample within the Oscos plateau area (ESP-12) at 780 m elevation yielded an age of 143.4 (10.9) that

could be correlated with some samples in the Lugo plain.

The age-elevation relationship (AER) plot for the Austurias area samples shows a large degree of scatter (Fig. 5). However, if the three significantly old ages (ESP-13, 18, 31) which also show significantly high errors obtained from the Neoproterozoic rocks are not taken into account, then there is an overall negative slope that is better defined and steeper than that for the samples in the Galicia area.

5.2 Etch pit size and track length distribution

A total of 4392 D_{par}® values were determined for all apatite grains used in this study (Tab. 2). The mean D_{par}® values shows a very narrow range between 1.3 (0.1) µm and 1.8 (0.2) µm. With the exception of sample ESP-23 (-0.18) all samples exhibit a positive skewness between 0.05 and 1.16. The large skewness values indicate a larger variation in etch pit size. The largest etch pit size of 2.9 (0.1) µm was measured in apatites from sample ESP-35. This sample also shows the largest spread in etch pit size between 0.9 (0.1) µm and 2.9 (0.1) µm. No positive correlation between single grain ages and D_{par}® values has been detected. In addition, D_{par}® values are not dependent on the lithology of the samples.

A total of 1368 track lengths of confined spontaneous fission-tracks were measured (Tab. 2). The obtained mean track lengths range between 10.4 (1.8) µm and 12.4 (1.4) µm. All samples show a unimodal, narrow track length distribution. The track length distributions of the samples show no significant, mostly negative skewness, indicating a simple cooling history with no significant re-heating events. No relation exists between track length distribution and elevation or variation of fission-track ages. After applying the computer code HeFTy© to the data set to correct for their crystallographic orientation, the mean confined fission-track lengths changed to a distribution between 12.4 (1.1) µm and 13.9 (1.0) µm. The c-axis correction had no significant effect of the skewness of track length distribution. Even with this correction, no relation exists between track length distribution and elevation or variation of fission-track ages. No difference in corrected mean confined length distribution exists between the samples from the plain around Lugo and the rest of samples from Galicia and Asturias.

5.3 Time-temperature models

Twelve samples with more than 50 measured confined fission-tracks were used for time-Temperature (t-T) modelling. Since we start with little t-T information, the forward modelling procedure of the program was used to establish those segments of the t-T path where the degree of monotonic cooling or monotonic heating changes. For most of the samples, the boxes that contain t-T constraints were left wide open. The uncertainty is presented in the diagrams in grey shades depending on the reliability level (see Figs. 6 and 7).

The t-T paths show that all twelve samples underwent continuous cooling histories, with no apparent reheating. They show an overall similar pattern with relatively rapid initial cooling, followed by slower cooling and again relatively rapid cooling through the final part of their history. They have been grouped according to the times at which they passed through the partial annealing zone (PAZ). Six samples entered into the PAZ between c. 200 Ma and 170 Ma (Fig. 6), with three of them (ESP-16, 22, 25) undergoing rapid cooling through the PAZ before 150 Ma, whereas three others (ESP-17, 29, 32) had a longer residence time in the upper part of the PAZ. Six other samples entered into the PAZ between 160 Ma and c. 110 Ma and were at temperatures below 80 ºC by 100 Ma (Fig. 7). Three of them passed the upper boundary of the PAZ before 90 Ma (ESP-15, 26, 33), whereas three others passed later (ESP 27a, 27b, 30). The t-T modelling indicates that a total of nine samples had passed the upper boundary of the PAZ before 90 Ma and all twelve samples, including the sample with youngest AFT age (ESP 27a) were at temperatures below 65 ºC by 50 Ma.

6 Discussion

The AFT central ages determined from the western Cantabrian Mountains range from the Middle Triassic to the Late Cretaceous, older

than the Cenozoic shortening that raised the present mountain range. Also, the age distribution shows no simple correlation with elevation, being particularly heterogeneous in the highest areas, furthermore, suggesting that the ages obtained have a complex relationship to the current topography. The complex AFT age distribution and exhumation histories determined from the western Cantabrian Mountains may be related to a number of factors, including: (1) the superposition of thermal histories (varied geothermal gradients) during the various tectonothermal events that affected the area, (2) a complex geothermal profile in the upper crust (Dempster and Persano, 2006) and (3) a spatially heterogeneous, continuous exhumation history. There is no evidence in the track length distributions of the twelve samples used for t-T modelling to suggest that they underwent a significant multiphase heating history. All samples show clearly defined track length peaks with only minor skewness. We, therefore, discard thermal overprinting as a cause of the variation in AFT ages and cooling histories with the available data. Likewise, there is insufficient data to allow a 3D interpretation of the thermal nature of the uppermost crust over the cooling history of the samples. We, therefore, interpret the AFT data to suggest that the rocks exposed in the western Cantabrian Mountains have undergone spatially heterogeneous, continuous cooling and exhumation at varied rates since the end of the Variscan Orogeny. In the following section, we calculate cooling and exhumation rates by assuming a constant geothermal gradient of 27 ºC/km. This value corresponds to the geothermal gradient determined from the present day heat flow density of 65 (5) mWm^2 in the area (Fernández *et al.*, 1998).

6.1 Interpretation of cooling history and exhumation rates

The AFT age distributions along longitudinal and transverse elevation profiles are presented in Figure 8. The age distribution and corresponding t-T paths in the longitudinal profile (A-A') indicate that the rocks were exhumed above the upper boundary of the PAZ through events older than 100 Ma and that samples in the west cooled later than samples in the east, regardless of elevation. This E-W distribution of cooling ages may correlate with the final distribution of rocks within the Variscan section (Fig. 3b). The upper crustal, cooler rocks that underwent shallower deformation conditions are to the east and the deeper, hotter crustal rocks that underwent high-grade metamorphism are to the west (Martínez-Catalán *et al.*, 1990). Furthermore, when combined in three groups (Lugo plain-, Oscos plateau- and Allande- groups; Fig. 8) the age distribution seems to pick a signal that correlates with preservation at different elevations of low relief surfaces in Lugo, Oscos and Allande (Alvarez-Marrón *et al.*, 2003). Along the N-S profiles, only the four samples that are younger than 100 Ma (ESP-10, 27a, 27b, 30) seem to register a local cooling effect possibly due to advection and uplift near fault scarps in Galicia and in areas next to the drainage divide that occurred before 50 Ma (see below).

The detailed cooling and exhumation history of the rocks in the western Cantabrian Mountains is illustrated in Figure 9, by comparing the modelled t-T paths and major tectonic events. An initial, rapid episode of cooling which lasted from the Triassic to the Late Jurassic occurred predominantly before initiation of widespread Mesozoic rifting that led to the opening of the Atlantic and the Bay of Biscay oceans (Le Pichon *et al.*, 1971; Srivastava *et al.*, 1990). It is registered by samples with AFT ages older than 135 Ma (Fig. 9). The modelled t-T paths indicate a rapid cooling to temperatures below 70 °C (Fig. 9b). The three samples that passed the upper boundary of the PAZ before 150 Ma are from the Oscos plateau group (ESP-16, 22, 25). Two other samples, a sample from the Lugo plain (ESP-29) and a sample from a granite near Bierzo basin (ESP-32) that have slightly younger AFT ages, also register this rapid cooling, although they cooled slowly through the upper part of the PAZ since 150 Ma until 100 Ma.

The amount of exhumation that took place during this earliest episode of cooling was larger than 2.5 km, with rates of 0.036 km/Ma. A plausible explanation for this earliest cooling may be that it is related to erosional exhumation

during post Variscan unroofing, that was initiated subsequently to cooling at shallow depths of post orogenic granitoid intrusions by Early Permian times (Fernández-Suárez *et al.*, 2000). A similar unroofing process has been proposed for the cooling during Late Permian to Early Jurassic of the Appalachians in Pennsylvania (Blackmer *et al.*, 1994) that had been part of the orogenic belt that had amalgamated Pangea during Carboniferous and Early Permian times (Ziegler, 1989). Also, similar exhumation rates have been obtained for the cooling during topographic decay of the Dabie Shan orogen in China (Reiners *et al.*, 2003). We found no evidences in our data that indicate possible effects associated to thermal expansion during the Permo-Triassic Pangea continental break-up. However, during this intracontinental rifting episode, the Oviedo and Basque-Cantabrian basins developed to the east of our area (Martínez-García *et al.*, 2004; Espina *et al.*, 2004). These basins contain shallow marine Early Jurassic carbonates, explained as a widespread transgression during post-rifting thermal relaxation that is present across large parts of Europe (Quesada *et al.*, 2005). There is no evidence in the area of interest to this current study to suggest that any marine incursion took place during Early Mesozoic times. Instead, it seems to have been an exposed continental landmass, as previously suggested by Ziegler and Roure (1999), further indicating that erosion during topographic decay may have been the dominant process for the exhumation of rocks in the western Cantabrian Mountains before the Late Jurassic.

A group of younger samples from the Galicia area underwent rapid exhumation through the PAZ after 160 Ma (Fig. 7). However, three samples in this group cooled below 65 ºC by 120 Ma and two of them were below 80 ºC before 150 Ma (ESP-15, 26, 33). They may be also recording latest stages of cooling during post Variscan unroofing. It is possible that the hotter rocks placed at deeper crustal levels in the west needed longer time to be exhumed to shallow levels than the rocks in the foreland areas of Asturias to the east that belonged to shallower crustal levels. The rapid cooling before 100 Ma in samples younger than 140 Ma may also register, however, the effects of the Atlantic and Bay of Biscay main phase of rifting during Late Jurassic to Early Cretaceous times (Le Pichon *et al.*, 1971; Srivastava *et al.*, 1990). Three samples that experienced rapid cooling after 140 Ma and were at temperatures below 80 ºC by 100 Ma are indicating average cooling rates of 0.75 ºC/Ma (ESP-27a, 27b, 30). They are near the NE-SW and NW-SE trending strike-slip fault systems in western Galicia indicating that these fault systems may have been active during the main Mesozoic rifting episode. In particular, this is plausible for the Lugo fault that connects southwards with bounding faults of the Lusitanian basin containing significant thickness of Early Cretaceous sediments (Rasmussen *et al.*, 1998; Alves *et al.*, 2003).

Since 100 Ma, most t-T paths from samples in Asturias and Galicia indicate that cooling occurred above the PAZ. By about 100 Ma most samples had reached temperatures below 60 °C (depths shallower than 3 km) and since about 80 Ma about 1.7 km of denudation took place. The initiation of sea floor spreading in the Atlantic margin of Galicia and in the Bay of Biscay is marked by chron M0 (118 Ma; Verhoef and Srivastava, 1989) and the Aptian-Albian age break-up unconformity in the Cantabrian platform (c. 115 – 110 Ma; Montadert *et al.*, 1979; García-Mondejar *et al.*, 2005). A lack of significant variations of topography in the region since Late Cretaceous and before formation of the present topography may correspond to a time of quiescence during the post-rift stage. In this situation, planation may occur at the surface if the denudational system reached a state of sufficiently low energy due to stabilization of base levels (Gunnell *et al.*, 2009). This process may explain the development of a peneplain across the region since Late Cretaceous times, being the lowlands around Lugo and the elevated surfaces of low relief found in Oscos, the remains of it. This inherited paleolandscape appears now dissected by faulting and fluvial erosion due to Cenozoic tectonism (Alvarez-Marrón *et al.*, 2003). Extensive planation surfaces and common weathering mantles developed by Late Cretaceous times across Variscan terrains in central Europe (Migón and Lidmar-Bergstroem, 2001; Thiry *et al.*, 2006).

Only four samples provided ages younger than 100 Ma. Three of them record cooling

through the upper boundary of the PAZ between 100 and 50 Ma (Fig. 9b), indicating about 1 km of denudation (cooling of 20 ºC) at a rate of 0.05 km/Ma. This exhumation relative to localized enhanced erosion or advection along the As Pontes and Lugo fault escarpments indicate fault activity associated to the transform plate boundary phase along Iberia and Eurasia from 59 Ma (chron 25) to 46 Ma (chron 21) (Srivastava *et al.*, 1990; Roest and Srivastava, 1991).

6.2 Implications for the evolution of the Cantabrian Mountains

The fact that AFT central ages determined from the western Cantabrian Mountains are older than the Cenozoic, indicates that the uplift process responsible for the present mountainous topography was associated with insufficient exhumation to reset the AFT clock. These AFT ages from the Cantabrian Mountains are in contrast with the younger ages obtained from Variscan-age rocks in other ranges of Iberia that underwent compression during Cenozoic. For example, AFT data from Variscan rocks in the central Pyrenees yielded Eocene-Oligocene exhumation ages (Fitzgerald *et al.*, 1999) and in the Iberian Central System ages ranging from the Middle Eocene to recent were obtained (De Bruijne and Andriessen, 2002). These younger ages are in agreement with exhumation related to Alpine compression in the Pyrenees and in the Betics, respectively.

The N-S compression that raised the Cantabrian Mountains was associated to convergence along the North Iberian Margin. The North Atlantic and Bay of Biscay magnetic anomalies indicate that limited southward subduction along this margin started at 49 Ma (chron 21) and went on until 20 Ma (chron 6) (Srivastava *et al.*, 1990; Roest and Srivastava, 1991). Shortening and uplift along the Cantabrian Mountains occurred since Middle Eocene when erosion started to provide sediments to the Duero foreland basin to the south (Alonso *et al.*, 1996; Gallastegui, 2000). However, the amount of N-S shortening that accumulated until the Neogene has been small, only 25 km along a section near 4º W longitude (Espina *et al.*, 1996) and was progressively smaller westwards to the area of our study (Santanach, 1994; Alvarez-Marrón et al, 1997). The reduced shortening is correlative with the relatively small amounts of sediments accumulated within the Paleogene to Neogene Bierzo basin to the south of the drainage divide (Andeweg, 2002) and within the Oligocene to Early Miocene As Pontes basin in Galicia (Huerta *et al.*, 1996). The correlation of AFT ages along the E-W profile with preservation of low relief surfaces in Lugo, Oscos and Allande suggest that those surfaces correspond to relicts of a pre-Alpine paleotopography, and that denudation since then has been insufficient to be registered by the AFT method.

Considering all the data, the recent rough topography in Northern Galicia and Asturias studied here must have formed since the middle Eocene with average estimated cooling rates of ca. 1 ºC/Ma, since 50-40 Ma. The uplift responsible for formation of the incipient mountainous topography seems to have been associated to possibly less than 1.7 km of denudation. Because the AFT method is unable to resolve a detailed cooling history for such a low value of denudation, ongoing research with a lower temperature thermochronometer is being applied. It is intended to provide the detailed cooling history at temperatures below 70 ºC, that may differentiate variation of denudation rates during the 40 to 20 Ma period of faster convergence and the last 20 Ma of very slow convergence (Rosenbaum *et al.*, 2002).

7 Conclusions

The 250 Ma AFT cooling history of rocks exposed in the western Cantabrian Mountains reveals that the faster cooling and main exhumation process occurred during unroofing of the Variscan orogenic topography and Pangea break-up. During the Triassic up to the Late Jurassic rocks in the east (Asturias) reached upper crustal levels with exhumation rates of about 0.036 km/Ma. Rocks in the west (flat areas of Lugo) experienced rapid cooling over the Late Jurassic and Early Cretaceous period of Atlantic and Bay of Biscay rifting. Since 100 Ma they experienced exhumation rates of about 0.02 km/Ma. The rocks in Asturias underwent very little, slow cooling and exhumation during the same rifting episode,

with very slow exhumation rates of 0.014 km/Ma since the Upper Jurassic that lasted during more than 100 Ma. Three samples at fault escarpments in Galicia, record c. 0.7 km of denudation during Late Cretaceous and Eocene. Since Eocene to present, all samples cooled above the PAZ indicating about 1.7 km of denudation during uplift of the Cantabrian Mountains. Surfaces of low relief at mountain summits across the northern slope of the range may have developed from Late Cretaceous to Eocene and are preserved as remnants within the present fluvial network.

Apatite fission-track central ages measured in Variscan Basement rocks across the western termination of the Cantabrian Mountains are older than the end of the Mesozoic, indicating that Cenozoic uplift associated to minor Alpine compression during convergence along the North Iberian Margin caused insufficient exhumation to reset the pre-established apatite fission-track thermal distribution in the upper crust.

Acknowledgements

This study was funded through the National Plan of Research projects BTE2002-00330 and CGL2007-60230/BTE of the Spanish Ministry of Education and Science. It is included in the framework of Consolider-Ingenio 2010 no. CSD2006-00041 (TOPO-Iberia project) and partially funded by the LGFG (Landesgraduiertenförderung des Landes Baden-Württemberg). We thank D. Brown and A. Pérez-Estaún for their comments on the early version of the manuscript. Also we like to thank H. Gerstenberg from the Forschungsneutronenquelle Heinz Maier-Leibnitz, Garching (FRM II) for his support. We are especially grateful to two anonymous reviewers.

References

Allen, P.A., 2008. Time scales of tectonic landscapes and their sediment routing systems, In: Gallagher, K., Jones, S.J., Wainwright, J. (Eds.), Landscape Evolution: Denudation, Climate and Tectonics over Different Time and Space Scales, Special Publications 296, 7-28, Geological Society London.

Alonso, J.L., Pulgar, J.A., García-Ramos, J.C., Barba, P., 1996. Tertiary basins and Alpine tectonics in the Cantabrian Mountains (NW Spain), In: Friend, P.F., Dabrio, C.J. (Eds.), Tertiary Basins of Spain: The Stratigraphic Record of Crustal Kinematics, 214-227, Cambridge Univ. Press, New York.

Alvarez-Marrón, J., Rubio, E., Torne, M., 1997. Alpine age subduction structures in the North Iberian Margin. Journal of Geophysical Research 102, 22,495–22,511.

Alvarez-Marrón, J., Menéndez, R., Marquínez, J., 2003. Intramontane landscape evolution in the initial stages of coastal mountain growth (Cantabrian Mountains, Spain). Geophysical Research Abstracts 5, #3650. European Geophysical Society 2003.

Alvarez-Marrón, J., Hetzel, R., Niedermann, S., Menéndez, R., Marquínez, J., 2008. Origin, structure and exposure history of a wave-cut platform more than 1 Ma in age at the coast of northern Spain: a multiple cosmogenic nuclide approach. Geomorphology 93, 316-334.

Alves, T.M., Gawthorpe, R.L., Hunt, D.W., Monteiro, J.H., 2003. Post-Jurassic tectono-sedimentary evolution of the Northern Lusitanian Basin (Western Iberian Margin). Basin Research 15, 227-249.

Andeweg, B., 2002. Cenozoic tectonic evolution of the Iberian Peninsula causes and effects of changing stress fields. Ph.D. Thesis, Vrije Universiteit Amsterdam, ISBN 90-9015593-7. Netherlands Research School of Sedimentary Geology, publication no. 20020101.

Barbarand, J., Carter, A., Wood, I., Hurford, T., 2003a. Compositional and structural control of fission-track annealing in apatite. Chemical Geology 198, 107-137.

Barbarand, J., Hurford, T., Carter, A., 2003b. Variation in apatite fission-track length measurement: implications for thermal history modelling. Chemical Geology 198, 77-106.

Bastida, F., Marcos, A., Marquínez, J., Martínez-Catalán, J.R., Pérez-Estaún, A., Pulgar, J.A., 1984. Mapa Geológico de España, (Escala 1:200000), Hoja de La Coruña. Instituto Geológico y Minero de España, Servicio de publicaciones del Ministerio de Industria.

Bishop, P., 2007. Long-term landscape evolution: linking tectonics and surface processes. Earth Surface Processes and Landforms 32, 329-365.

Blackmer, G.C., Omar, G.I., Gold, D.P., 1994. Post-Alleghanian unroofing history of the Appalachian Basin, Pennsylvania, from apatite fission track analysis and thermal models. Tectonics 13 (5), 1259-1276.

Boillot, G., Auxietre, J.-L., Dunand, J.-P., Dupeuble, P.-A., Mauffret, A., 1979. The northwestern Iberian margin: a Cretaceous passive margin deformed during Eocene. In: Talwani, M., Hay, W., Ryan, W.B.F. (Eds.), Deep Drilling Results in the Atlantic Ocean: Continental Margins and Paleoenvironment: Am. Geophys. Union, Maurice Ewing Ser., 3, 138-153.

Burtner, R.L., Nigrini, A., Donelick, R. A., 1994. Thermochronology of Lower Cretaceaous source rocks in the Idaho-Wyoming Thrust Belt. AAPG Bull. 78: 1613-1636.

Cabral, J., 1989. An example of intraplate neotectonic activity, Vilarica basin, northeast Portugal. Tectonics 8 (2), 285-303.

Carlson, W. D., 1990. Mechanisms and kinetics of apatite fission-track annealing. Am. Mineral. 75, 1120-1139.

Carlson, W. D., Donelick, R. A., Ketcham, R. A., 1999. Variability of apatite fission-track annealing kinetics: I. Experimental results. Am. Mineral. 84, 1213-1223.

Cocherie, A., 1978. Géochemie des terres rares dans le granitoides. Tesis Doctoral, Univ. Rennes. 207 p.

Crowley, K.D., 1993. Mechanisms and kinetics of apatite fission-track annealing–Discussion. Am. Min. 78, 210-212.

Crowley, K.D., Cameron, M., Schaffer, L.R., 1991. Experimental studies of annealing of etched fission tracks in fluorapatite. Geochim. Cosmochim Acta 55, 1449-1465.

De Bruijne, C.H., Andriessen, P.A.M., 2002. Far field effects of Alpine plate tectonism in the Iberian microplate recorded by fault-related denudation in the Spanish central system. Tectonophysics 349, 161–184.

Dempster, T.J., Persano, C., 2006. Low-temperature thermochronology: Resolving geotherm shapes or denudation histories? Geology, 34 (2), 73-76.

Díaz, J., Gallart J., Gaspà O., Ruiz M., Córdoba D., 2008. Seismicity analysis at the Prestige oil-tanker wreck area (Galicia Margin, NW of Iberia), Marine Geology 249, 150-165.

Donelick, R.A., 1991. Crystallographic orientation dependence of mean etchable fission-track length in apatite: An empirical model and experimental observations. Am. Mineral. 76, 83-91.

Donelick, R.A., 1993. A method of fission track analysis utilizing bulk chemical etching of apatite. U.S. Patent #5,267,274.

Donelick, R.A., 1995. A method of fission track analysis utilizing bulk chemical etching of apatite. Australia Patent #658,800.

Donelick, R.A., Roden, M.K., Mooers, J.D., Carpenter, B.S., Miller, D.S., 1990. Etchable length reduction of induced fission tracks in apatite at room temperature, c. 23 °C. crystallographic orientation effects and "initial" mean lengths. Nucl. Tracks. Radiat. Meas. 17, 261-265.

Donelick, R.A., Ketcham, R.A., Carlson, W.D., 1999. Variability of apatite fission-track annealing kinetics: II. Crystallographic orientation effects. Am. Min. 84, 1224-1234.

Dunkl, I., 2002. Trackkey: a Windows program for calculation and graphical presentation of fission track data. Computer & Geosciences 28, 3-12.

Espina, R.G., Alonso, J.L., Pulgar, J.A., 1996. Growth and propagation of buckle folds determined from syntectonic sediments (the Ubierna Fold Belt, Cantabrian Mountains, N Spain), Journal of Structural Geology 18 (4), 431–441.

Espina, R.G., Alonso, J.L., Pulgar, J.A, 2004. Extensión Triásica en la Cuenca Vasco-Cantábrica. In: Vera, J.A. (Ed.), Geología de España, 338-339, SGE-IGME, Madrid (in Spanish).

Fernández, M., Marzán, I., Correia, A., Ramalho, E., 1998. Heat flow, heat production, and lithospheric thermal regime in the Iberian Peninsula. Tectonophysic 291, 29-53.

Fernández-Suárez, J. Dunning, G.R., Jenner, G.A., Gutiérrez-Alfonso, 2000. Variscan collisional magmatism and deformation in NW Iberia: Constraints from U-Pb geochronology of granitoids. Journal of the Geological Society 157 (3), 565-576.

Fernández-Viejo, G., Gallart, J., Pulgar, J.A., Cordoba, D., Danobeitia, J.J., 2000. Seismic signature of Variscan and Alpine tectonics in NW Iberia: Crustal structure of the Cantabrian Mountains and Duero basin. Journal of Geophysical Research B: Solid Earth 105 (2) ,3001-3018.

Fitzgerald, P.G., Munoz, J.A., Coney, P.J., Baldwin, S.L., 1999. Asymmetric exhumation across the Pyrenean orogen: Implications for the tectonic evolution of a collisional orogen. Earth and Planetary Science Letters. 173 (3), 157-170.

Galbraith, R.F., 1981. On statistical models for fission track counts. Mathematical Geology, 13, 471-478.

Galbraith, R.F., Laslett, G.M., Green, P.F., Duddy, I.R., 1990. Apatite fission track analysis: geological thermal history analysis based on a three-dimensional random process of linear radiation damage. Philos. Trans. R. Soc. Lond., A 332, 419-438.

Gallastegui, J., 2000. Estructura Cortical de la Cordillera y Margen Continental Cantábricos: Perfiles ESCIN-N. Trabajos Geol.Univ. Oviedo, 22, 9-234 (in Spanish).

García-Mondejar, J., Lopez-Horgue, M.A., Aranburu, A., Fernández-Mendiola, P.A., 2005. Pulsating subsidence during a rift episode: Stratigraphic and tectonic consequences (Aptian-Albian, northern Spain). Terra Nova 17 (6), 517-525.

Glasmacher, U.A., Zentilli, M., Grist, A.M., 1998. Apatite fission-track thermochronology of Palaeozoic sandstones and the Hill-Intrusion, Northern Linksrheinisches Schiefergebirge, Germany. In: van den Haute, P., de Corte, F. (Eds.), Advances in Fission-Track Geochronology, Solid Earth Sciences Library 10, 151-172, Kluwer Academic Publishers, London.

Gleadow, A.J.W., Duddy, I.R., 1981. A natural long term track annealing experiment for apatite. Nucl. Tracks 5, 169-174.

González-Lodeiro, F., Hernández-Urroz, J., Klein, E., Martínez-Catalán, J.R., Pablo-Maciá, J.G., 1982. Mapa Geológico de España, (Escala 1:200000) Hoja de Lugo. Instituto Geológico y Minero de España, Servicio de publicaciones del Ministerio de Industria.

Green, P.F., 1981. "Track-in track" length measurements in annealed apatites. Nucl. Tracks 5, 121-128.

Green, P.F., 1988. The relationship between track shortening and fission track age reduction in apatite: combined influences of inherent instabitlity, annealing anisotropy, length bias and systems calibration. EPSL 89, 335-352.

Green, P.F., Durrani, S.A., 1977. Annealing studies of tracks in crystals. Nucl. Track. Det. 1, 33-39.

Green, P.F., Duddy, I.R., Gleadow, A.J.W., Tingate, P.R., Laslett, G.M., 1985. Fission track annealing: track length measurements and the form of the Arrhenius plot. Nucl. Tracks 10: 323-328.

Green, P.F., Duddy, I.R., Gleadow, A.J.W., Tingate, P.R., Laslett, G.M., 1986. Thermal annealing of fission tracks in apatite. 1. A quantitative description. Chem. Geol. 59, 237-253.

Grimaud, S., Boillot, G., Collete, B.J., Mauffret, A., Miles, P.R., Roberts, D.B., 1982. Western extension of the Iberian-European plate boundary during Early Cenozoic (Pyrenean) convergence: a new model, Marine Geology 45, 63-77.

Grist, A.M., Ravenhurst, C.E., 1992a. Mineral Separation Techniques used in Dalhousie University. In: Zentilli, M., Reynolds, P.H. (Eds.), Short Course on low temperature thermochronology, Min. Ass.Can. Short Course V 20, Appendix 2, 203-209.

Grist, A.M., Ravenhurst, C.E., 1992b. A Step-by-Step Laboratory guide to fission-track thermochronology at Dalhousie University. In: Zentilli, M., Reynolds, P.H. (Eds.), Short Course on low temperature thermochronology, Min. Ass.Can. Short Course V 20, Appendix 1, 190-201.

Gunnell, Y., 2000. Apatite fission track thermochronology: an overview of its potential and limitations in geomorphology. Basin Research 12, 115-132.

Gunnell, Y., Calvet, M., Brichau, S., Carter, A., Aguilar, J.-P., Zeyen, H., 2009. Low long-term erosion rates in high-energy mountain belts: Insights from thermo- and biochronology in the Eastern Pyrenees. Earth and Planetary Science Letters 278, 208-218.

Haq, B.U., van Eysinga, F.W.B., 1998. Geological Time Table, 5th ed. Elsevier, Amsterdam

Huerta, A., Parés, J.M ., Cabrera, L., Ferrús, B., Sáez, A., 1996. Datación magnetoestratigráfica de la cuenca terciaria de As Pontes (Galicia, NW España), Geogaceta 20, 1021-1024 (in Galician).

Hurford, A.J., 1990. Standardization of fission track dating calibration: recommendations by the Fission Track Working Group ofthe IUGS. Subcommission on Geochronology. Chemical Geology 80, 171-178.

Hurford, A.J., Green, P.F., 1982. A user's guide to fission track dating calibration. EPSL 59, 343-354.

Hurford, A.J., Green, P.F., 1983. The zeta age calibration of fission track dating. Isotope Geosci. 1, 285-317.

Ketcham, R.A., 2003. Observations on the relationship between crystallographic orientation and biasing in apatite fission-track measurements. Am. Min. 88, 817-829.

Ketcham, R.A., 2005. Forward and inverse modeling of low-temperature thermochronometry data. Reviews in Mineralogy and Geochemistry, 58, 275-314.

Ketcham, R.A., Donelick, R.A., Carlson, W.D., 1999. Variability of apatite fission-track annealing kinetics: III Extrapolation to geological time scales. Am. Min. 84, 1235-1255.

Ketcham, R.A., Carter, A., Donelick, R.A., Barbarand, J., Hurford, A.J., 2007a. Improved measurement of fission-track annealing in apatite using c-axis projection. Am. Min. 92, 789-798.

Ketcham, R.A., Carter, A., Donelick, R.A., Barbarand, J., Hurford, A.J., 2007b. Improved modelling of fission-track annealing in apatite. Am. Min. 92, 799-810.

Ketcham, R.A., Donelick, R.A., Balestrieri, M.L., Zattin, M., 2009. Reproducibility of apatite

fission-track length data and thermal history reconstruction. Earth and Planetary Science

Letters 248, 504–515.

Laslett, G.M., Gleadow, A.J.W., Duddy, I.R., 1984. The relationship between fission track length and track density distributions. Nucl. Tracks 9, 29-38.

Le Pichon, X., Bonnin, J.C. Francheteau, J., Sibuet J.C., 1971. Une hypothese d'evolution tectonique du Golfe de Gascogne. In: Debysier, J., Le Pichon, X., Montadert, M. (Eds.), Histoire structurale du Golfe de Gascogne, VI.11.1-VI.11.44, Technip, Paris (in French).
Lisker, F., Ventura, B., Glasmacher, U.A., 2009. Apatite thermochronology in modern geology. Geol. Soc. London Spec. Publ. 324, 1-23.

López-Fernández, C., Pulgar, J.A., Gallart, J., Glez-Cortina, J.M., Díaz, J., Ruiz, M., 2004. Sismicidad y tectónica en el área de Becerreá–Triacastela (Lugo, NO España). Geogaceta 36, 51–54 (in Galician).

Martínez-Catalán, J.R., Pérez-Estaún, A., Bastida, F., Pulgar, J.A., Marcos, A., 1990. West Asturian-Leonese Zone: Structure. In: Dallmeyer, R.D., Martínez-García, E. (Eds.), Pre-Mesozoic Geology of Iberia, 103–114, Springer-Verlag.

Martínez-Catalán, J.R., Arenas, R., Díaz-García, F., González-Cuadra, P., Gómez-Barreiro, J., Abati, J., Castiñeiras, P., Fernández-Suárez, J., Sánchez Martínez, S., Andonaegui, P., González Clavijo, E., Díez Montes, A., Rubio Pascual, F.J., and Valle Aguado, B., 2007. Space and time in the tectonic evolution of the northwestern Iberian Massif: Implications for the Variscan belt. Hatcher, R.D., Jr., Carlson, M.P., McBride, J.H., Martínez-Catalán, J.R. (Eds.), 4-D Framework of Continental Crust: Geological Society of America Memoir 200, 403–423.

Martínez-García, E., Antona, J.F., García-Sanchez, A., Quiroga de la Vega, J.L., 2004. Tectonics and metallogenic significance of sedimentary manganese deposits in the eastern Cantabrian Domain, Asturias, northwestern Spain. International Geology Review 46 (3), 273-288.

Migón, P., Lidmar-Bergstroem, K., 2001. Weathering mantles and their significance for geomorphological evolution of central and northern Europe since the Mesozoic. Earth-Science Reviews 56, 285-324.

Montadert, L., Roberts, D.G., De Charpal, O., Guennoc, P., 1979. Rifting and subsidence of the northern continental margin of the Bay of Biscay. Initial reports of the Deep Sea Drilling Project, Leg 48, 1025-1060.

O'Sullivan, P.B., Parrish, R.R., 1995. The importance of apatite composition and single-grain ages when interpreting fission track data from plutonic rocks: a case study from the Coast Ranges, British Columbia. EPSL 132, 213-224.

Pedreira D., Pulgar J.A., Gallart J., Díaz J., 2003. Seismic evidence of Alpine crustal thickening and wedging from

the western Pyrenees to the Cantabrian Mountains (north Iberia). Journal of Geophysical Research B: Solid Earth, 108 (4), ETG 10-1 – ETG 10-21.

Pérez-Estaún, A., Bastida, F., Alonso, J.L., Marquínez, J., Aller, J., Alvarez-Marrón, J., Marcos, A., Pulgar, J.A., 1988. A thin-skinned tectonic model for an arcuate fold and thrust belt: Cantabrian Zone. Tectonics 7 (3), 517-537.

Pérez-Estaún, A., Bastida, F., Martínez-Catalán, J.R., Gutiérrez-Marco, J.C., Marcos, A., and Pulgar, J.A., 1990. West Asturian–Leonese Zone: stratigraphy. In: R.D. Dallmeyer and E. Martínez-García (Eds.), Pre-Mesozoic Geology of Iberia, 92-102, Springer-Verlag.

Pérez-Estaún, A., Martínez-Catalán, J.R., Bastida, F., 1991. Crustal thickening and deformation sequence in the footwall to the suture of the Variscan belt of northwest Spain. In: Pérez-Estaún A., Coward, M.P. (Eds.), Deformation and Plate Tectonics, Tectonophysics 191, 243-253.

Pulgar, J., Gallart, J., Fernández-Viejo, G., Pérez-Estaún, A., Alvarez-Marrón, J., and ESCIN Group, 1996. Seismic image of the Cantabrian Mountains uplift in the western extension of the Pyrenean Belt from integrated ESCIN reflection and refraction data. Tectonophysics 264, 1-20.

Quesada, S., Robles, S., Rosales, I., 2005. Depositional architecture and transgressive-regressive cycles within Liassic backstepping carbonate ramps in the Basque-Cantabrian basin, northern Spain. Journal of the Geological Society 162 (3), 531-548.

Rasmussen, E.S., Lomholt, S., Andersen, C., Vejbaek, O.V., 1998. Aspects of the structural evolution of the Lusitanian Basin in Portugal and the shelf and slope area offshore Portugal. Tectonophysics 3000, 199-225.

Reiners, P.W., Zhou, Z., Ehlers T. A., Xu, C., Brandon, M. T., Donelick, R. A., Nicolescu, S., 2003. Post-orogenic evolution of the Dabie Shan, eastern China, from (U-Th)/he and fission-track thermochronology. American Journal of Science 303, 489-518.

Reiners P.W., Brandon, M.T., 2006. Using Thermochronology to Understand Orogenic Erosion. Annu. Rev. Earth Planet. Sci. 34, 419–66.

Reiners, P.W., Ehlers, T.A. (Eds). 2005. Low-temperature thermochronology: techniques, interpretations, and applications. Reviews in Mineralogy and Geochemistry 58, v-ix, 1-622.

Rodríguez-Fernández, L.R., 2004. Mapa Geológico de España (Escala 1:200.000), In: Vera, J.A. (Ed.), Geología de España, SGE-IGME, Madrid

Rodríguez-García, A., Quintana, L., González-Menéndez, L., Suárez-Rodríguez, A., 2006. Neotectónica en el norte de Galicia: Fallas inversas de actividad cuarternica en la cuenca fluvial del alveolo de Alfoz, Lugo. Geogaceta 40, 23-26 (in Galician).

Rosenbaum, G., Lister, G.S., Duboz, C., 2002. Relative motions of Africa, Iberia and Europe during Alpine orogeny, Tectonophysics 359, 117-129.

Roest, W.R., Srivastava, S.P., 1991. Kinematics of the plate boundaries between Eurasia, Iberia, and Africa in the North Atlantic from the Late Cretaceous to the present. Geology 19 (6), 613-616.

Santanach, P., 1994. The Tertiary basins of Galicia in the western termination of the Pyrenean reliefs. Cuadernos Laboratorio Xeoloxico de Laxe. 1957-71.

Sibuet, J.C., Le Pichon, X., 1971. Structure gravimétrique du Golfe de Gascogne a partir des profils de sismique. In: Debysier, J., Le Pichon, X., Montadert, M. (Eds.), Histoire structurale du Golfe de Gascogne, VI.9.11–VI.9.18, Technip, Paris.

Srivastava, S.P., Roest, W.R., Kovacs, L.C., Oakey, G., Lévesque, S., Verhoef, J., Macnab, R., 1990. Motion of Iberia since the Late Jurassic: Results from detailed aeromagnetic measurements in the Newfoundland Basin; Tectonophysics 184, Issues 3-4, 229-260.

Thiry, M., Quesnel, F., Yans, J., Wyns, R., Vergari, A., Theveniaut, H., Simon-Coincon, R., Ricordel, C., Moreau, M.-G., Giot, D., Dupuis, C., Bruxelles, L., Barbarand, J., Baele, J.-M., 2006. Continental France and Belgium during the early cretaceous: Paleoweatherings and paleolandforms. Journal of the Geological Society 163 (4), 723-736

Verhoef, J., Srivastava, S.P., 1989. Correlation of sedimentary basins across the North Atlantic as obtained from gravity and magnetic data, and its relation to the early evolution of the North Atlantic. In: Tankard, A.J., Balkwill, H.R. (Eds.), Extensional tectonics and stratigraphy of the North Atlantic margins, AAPG Memoir 46, 131-147.

Wagner, G.A., 1972. Spaltspurenalter von Mineralen und natürlichen Gläsern: eine Übersicht. Fortschr. Miner. 49, 114-145 (in German).

Wagner, G.A., van den Haute, P., 1992. Fission-Track Dating. In: Enke Verlag - Kluwer Academic Publishers, p. 285.

Ziegler, P.A., 1989. Evlution of the North Atlantic-Overiview. In: Tankard, A.j., Balkwill, H.R. (Eds.), Extensional Tectonics and Stratigraphy of the North Atlantic Margins: AAPG Memoir 46, 11-130

Ziegler, P.A., Roure, F., 1999. Petroleum systems of Alpine-Mediterranean foldbelts and basins. Geological Society Special Publication 156, 517-540.

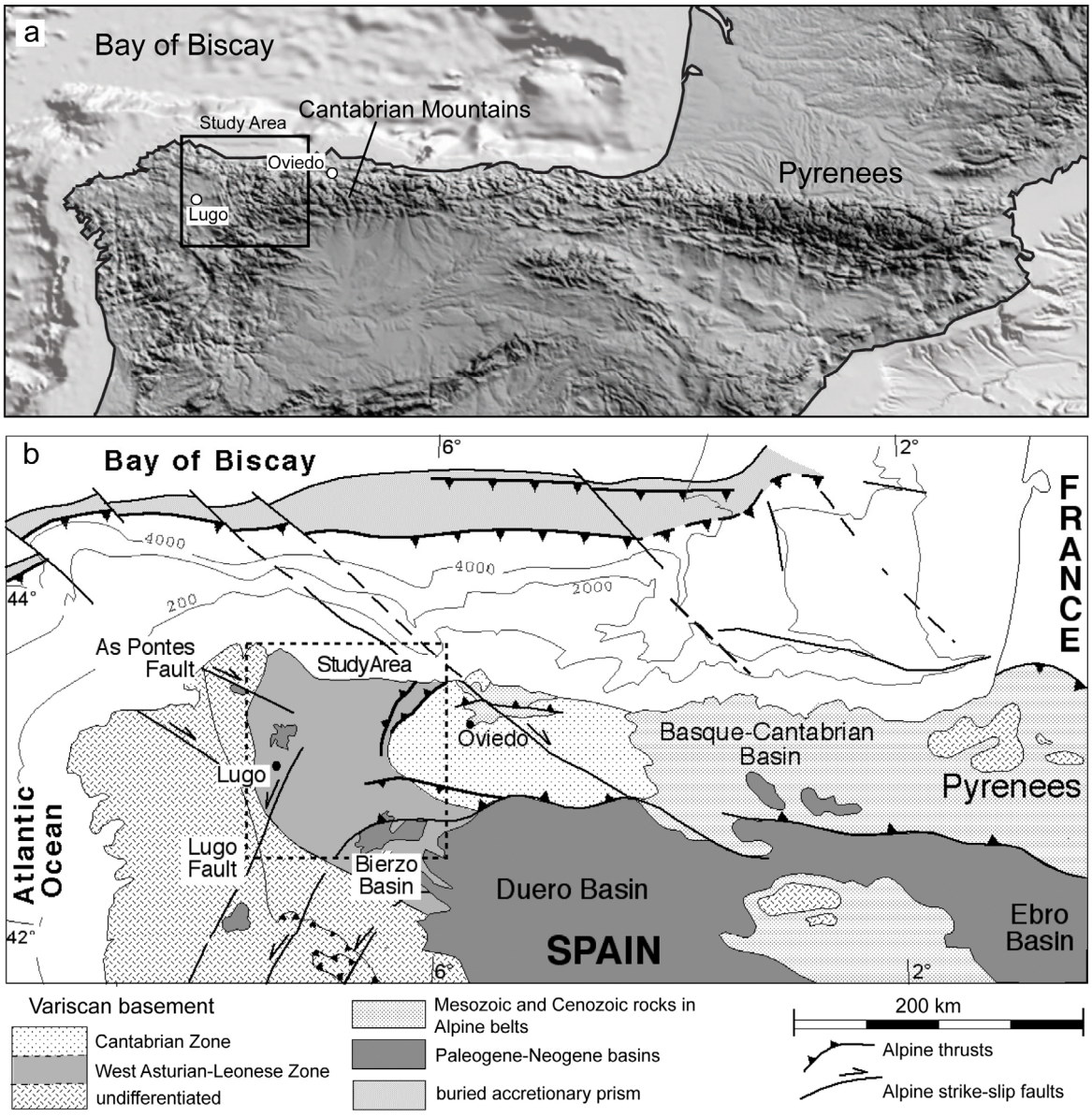

Figure 1: (a) Location of the Cantabrian Mountains along the northern coast of Spain, to the west of the Pyrenees. (b) Geological map showing the location of the study area (dashed square) within the West Asturian-Leonese Zone of the Variscan section in northwestern Spain. Major Alpine structures over that zone are highlighted. The location of the buried accretionary prism developed during Cenozoic convergence at the foot of the continental slope is also shown.

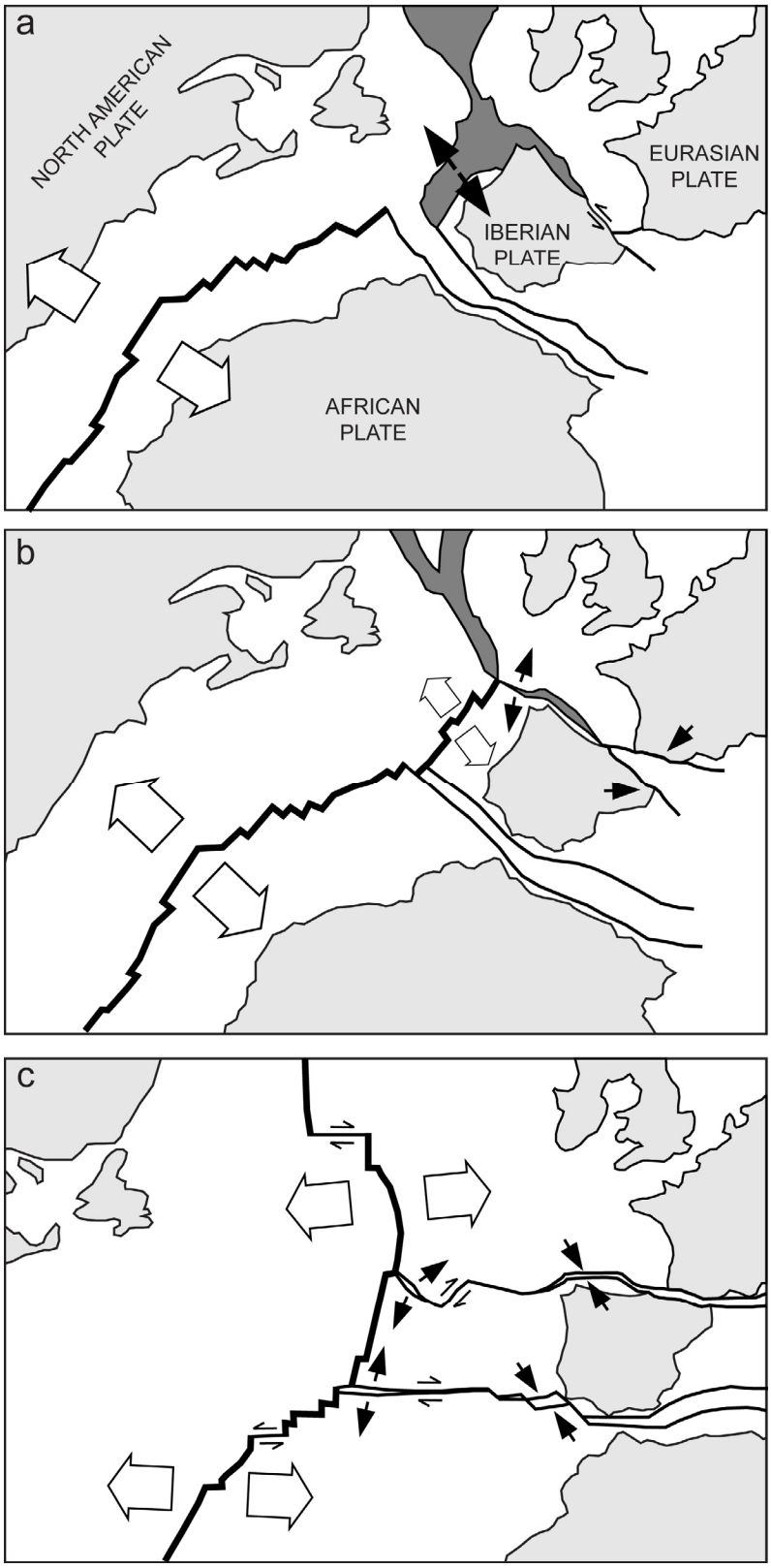

Figure 2: Three time stages with North American and Iberian Plate motions relative to a fixed Eurasian Plate, redrafted from Srivastava *et al.* (1990); (a) shaded areas north and west of Iberia are areas undergoing stretching after 156.5 Ma, (b) indicates seafloor spreading starting by 118 Ma, and (c) oblique convergence was going on along the North Spanish margin by 35.5 Ma.

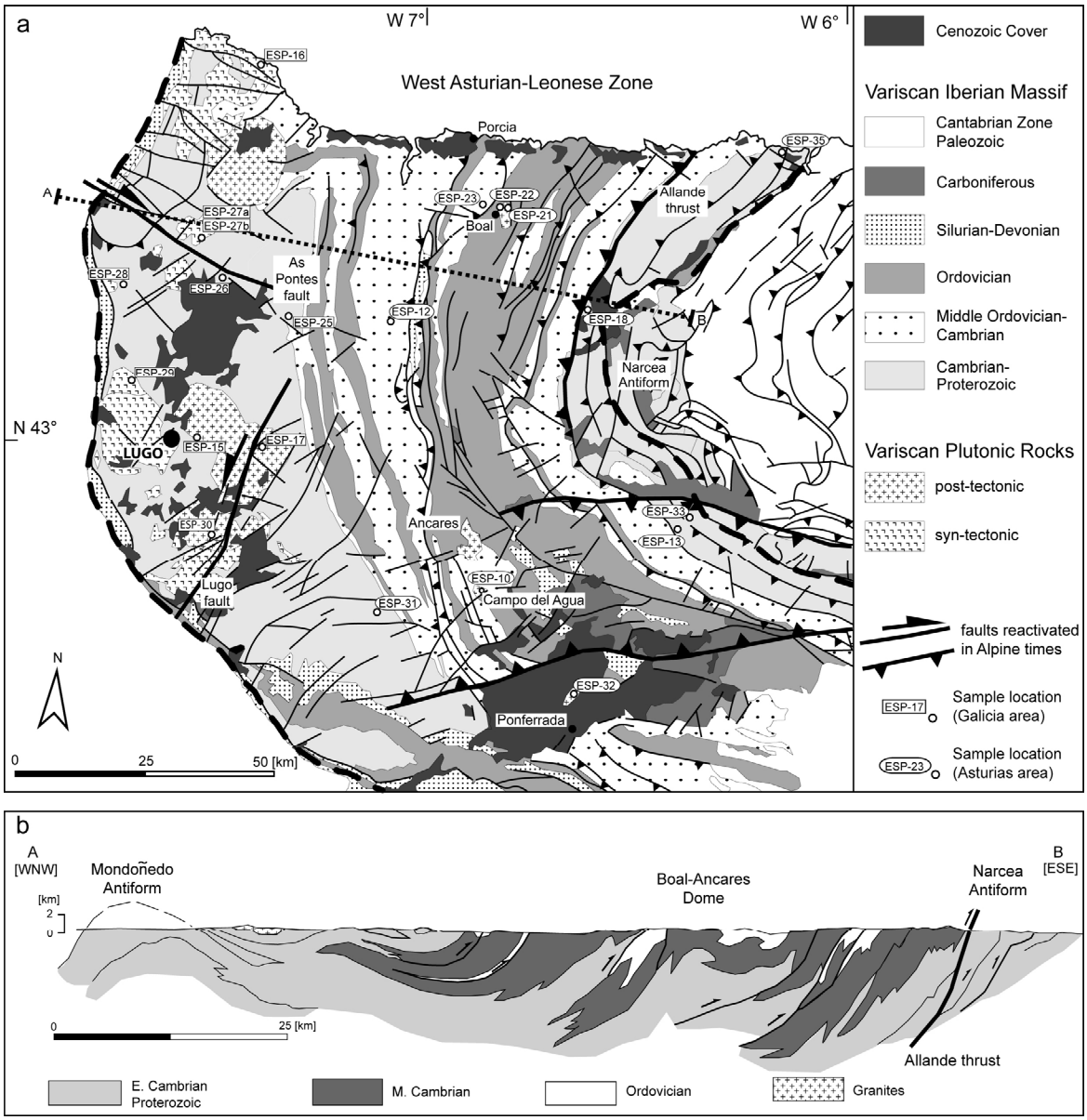

Figure 3: (a) Geological map of the West Asturian-Leonese Zone with sample locations, thick dash lines mark the boundaries with the Cantabrian Zone to the east and the Variscan hinterland to the west, in Galicia (map redrafted from Rodríguez-Fernández, 2004). (b) Geological cross-section through the study area (redrafted from Martínez-Catalán *et al.*, 1990).

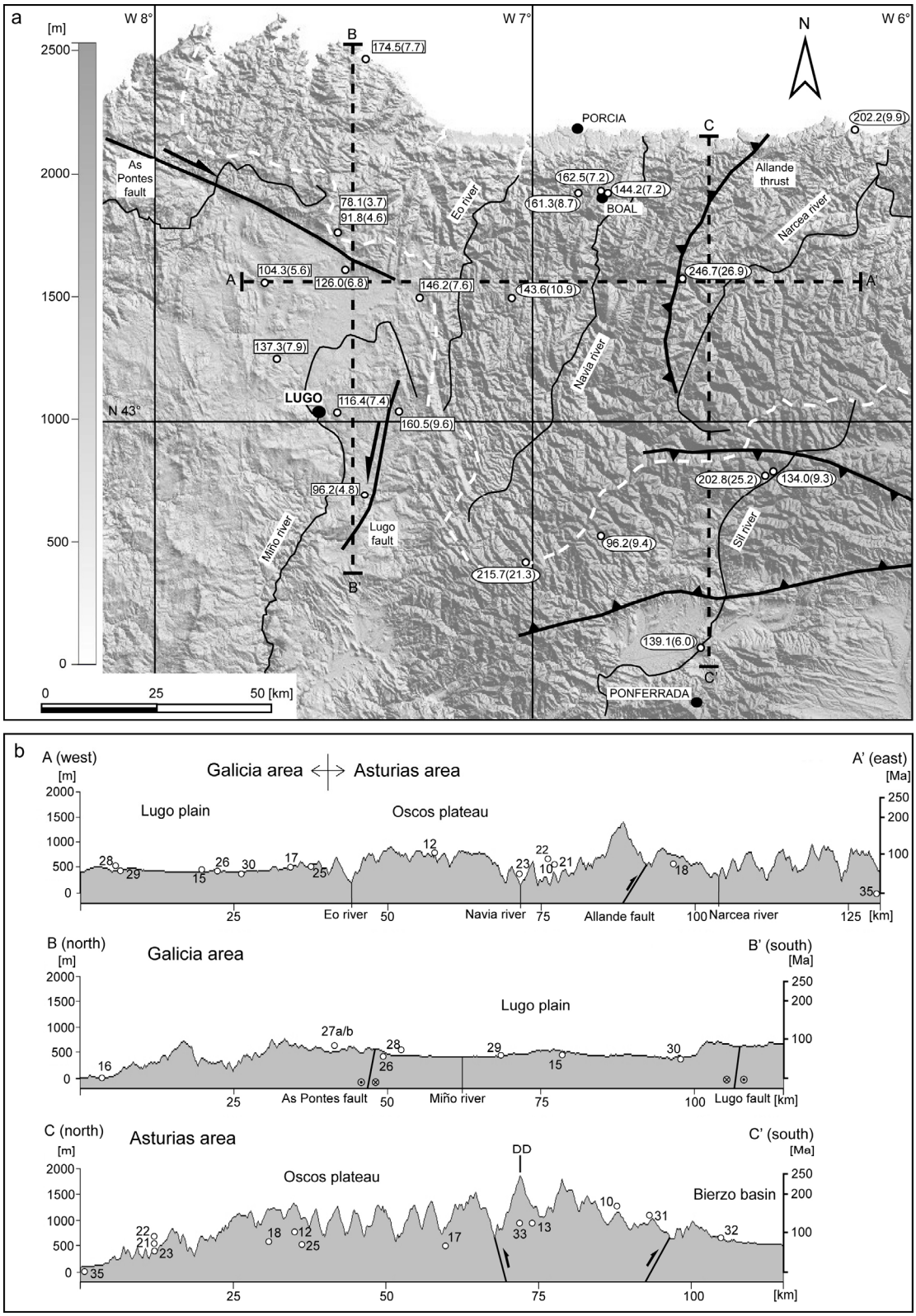

Figure 4: (a) Digital elevation model (90 m resolution from CGIAR-CSI) with sample locations with AFT age and 1σ error (rectangles: Galicia area; rounded rectangles: Asturias area). Major Alpine faults mentioned in the text are in thick black lines. Thin black lines are rivers and dashed white line marks the drainage divide. Dashed thick lines mark location of topographic transects. (b) Topographic transects. (A-A') is an W-E profile through Galicia and Asturias areas, (B-B') is a N-S profile through the Galicia area and (C-C') is a N-S profile through the Asturias area. Topographic profiles show in white circles the projected location of samples to show elevation. DD shows location of drainage divide.

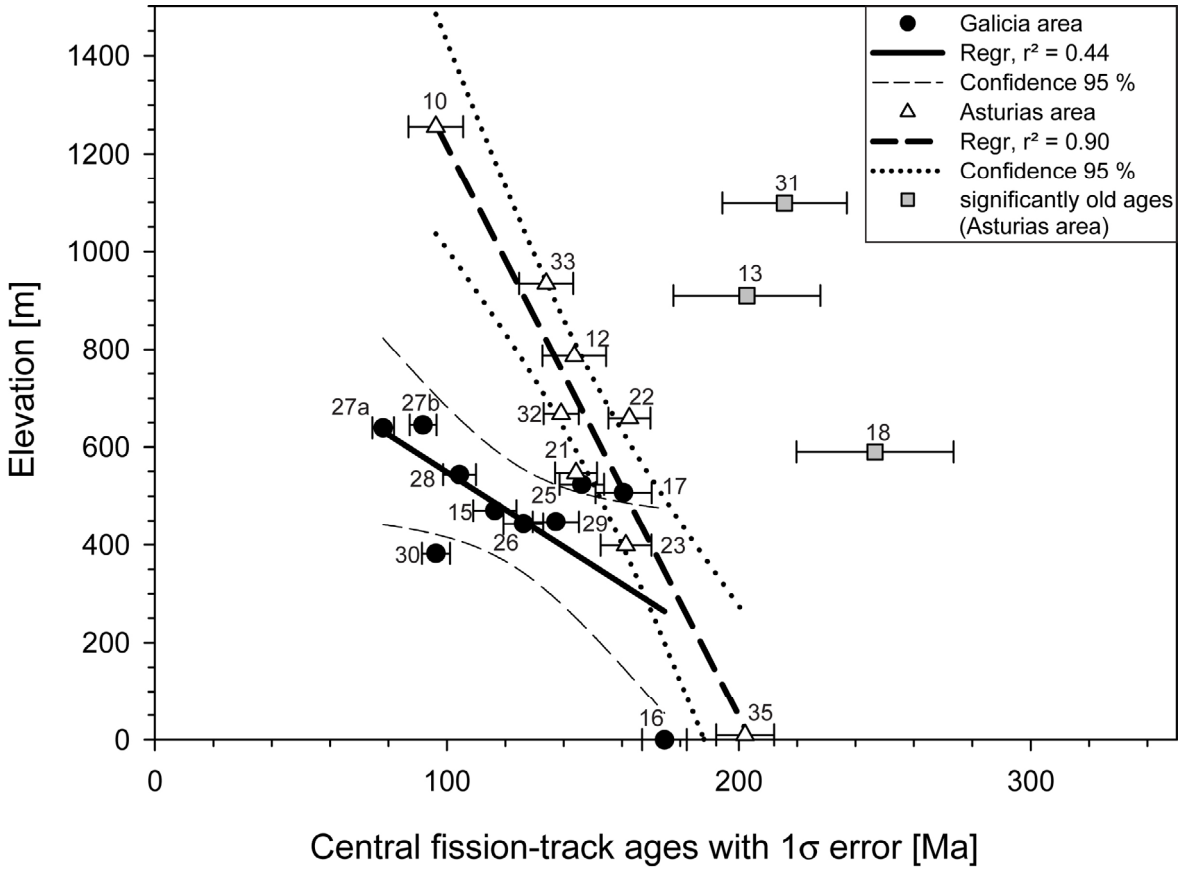

Figure 5: Elevation dependent apatite fission-track age distribution (1σ error) with statistical data. Black dots corresponding to samples from Galicia area and triangles and squares corresponding to the Asturias area. Best fit regression lines excluding squares indicate a reverse age-elevation relationship in both areas. When all samples are considered together, no defined age-elevation relationship is obtained.

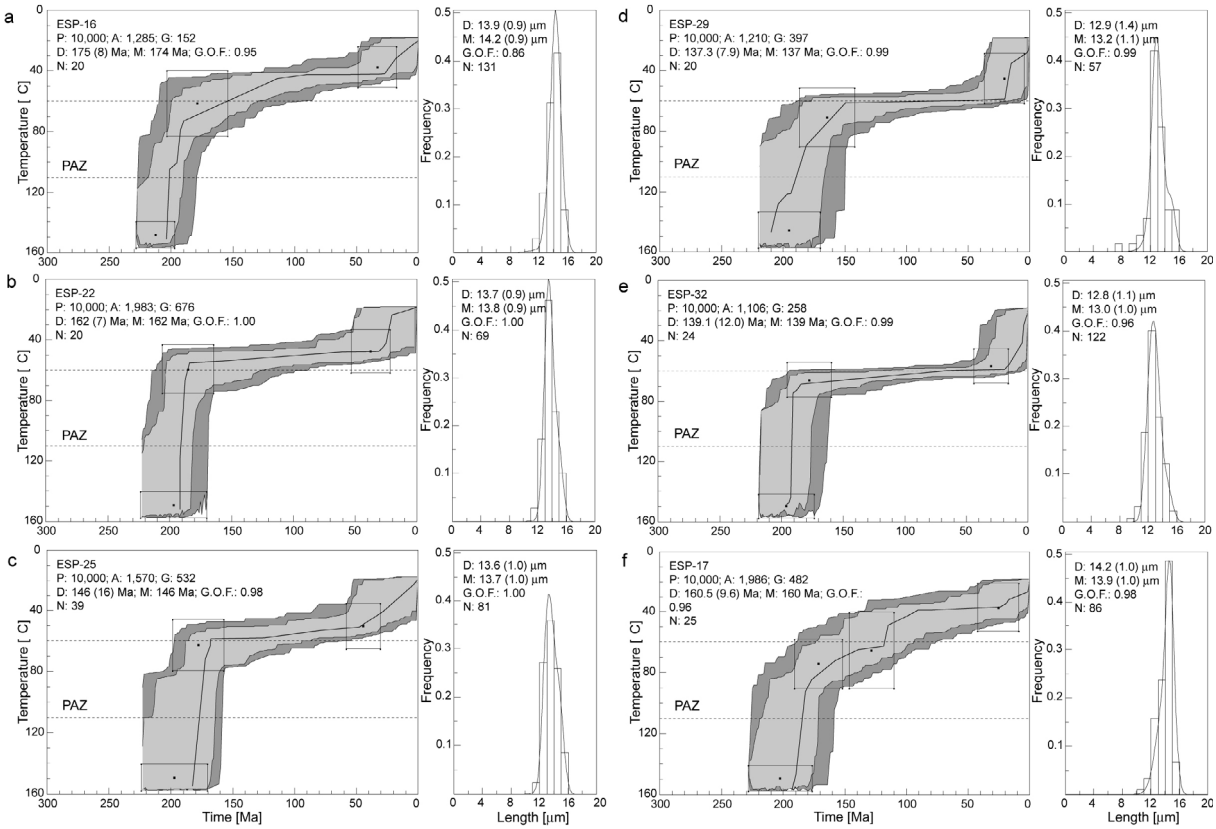

Figure 6: Results of the numerical modelling for samples that passed the PAZ before 150 Ma. Modelling is done using the computer code HeFTy© (Ketcham, 2005; Ketcham *et al.*, 2007a; b; Ketcham *et al.*, 2009). Displayed are the t-T paths (left) and the c-axis corrected confined fission-track length (cC-FT-L) distribution (right) overlain by a calculated probability density function (best fit). The modelling tests possible t-T curves that fit independent geological constraints (squares) against the apatite fission-track data set. The results in the t-T curve show three different reliability levels (dark grey envelope: acceptable fit = all t-T paths with a goodness of fit (G.O.F.) of > 0.05 (5%), light grey envelope: good fit = all t-T paths with a G.O.F. of > 0.5 (50%), black line: best fit). P: number of tested inverse models, A: acceptable fit models, G: good fit models, D: determined FT-age (1σ error) and cC-FT-L, M: modelled FT-age and cC-FT-L, G.O.F.: goodness of fit of best fit model, N: number of single grains and measured confined fission-track lengths.

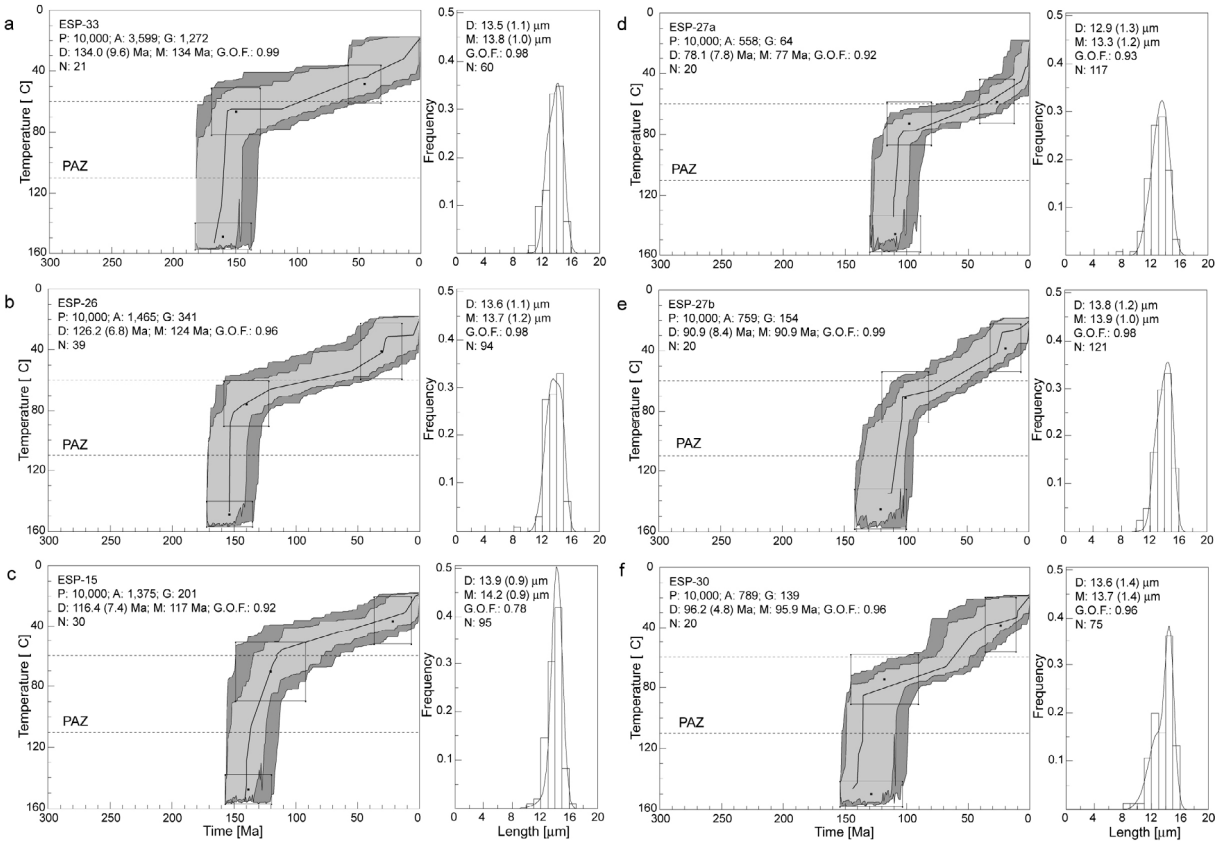

Figure 7: Results of the numerical modelling from six samples that passed the PAZ before 90 Ma. Displayed are the t-T paths (left) and the c-axis corrected confined fission-track length (cC-FT-L) distribution (right) overlain by a calculated probability density function (best fit). For explanation and legend see Figure 6.

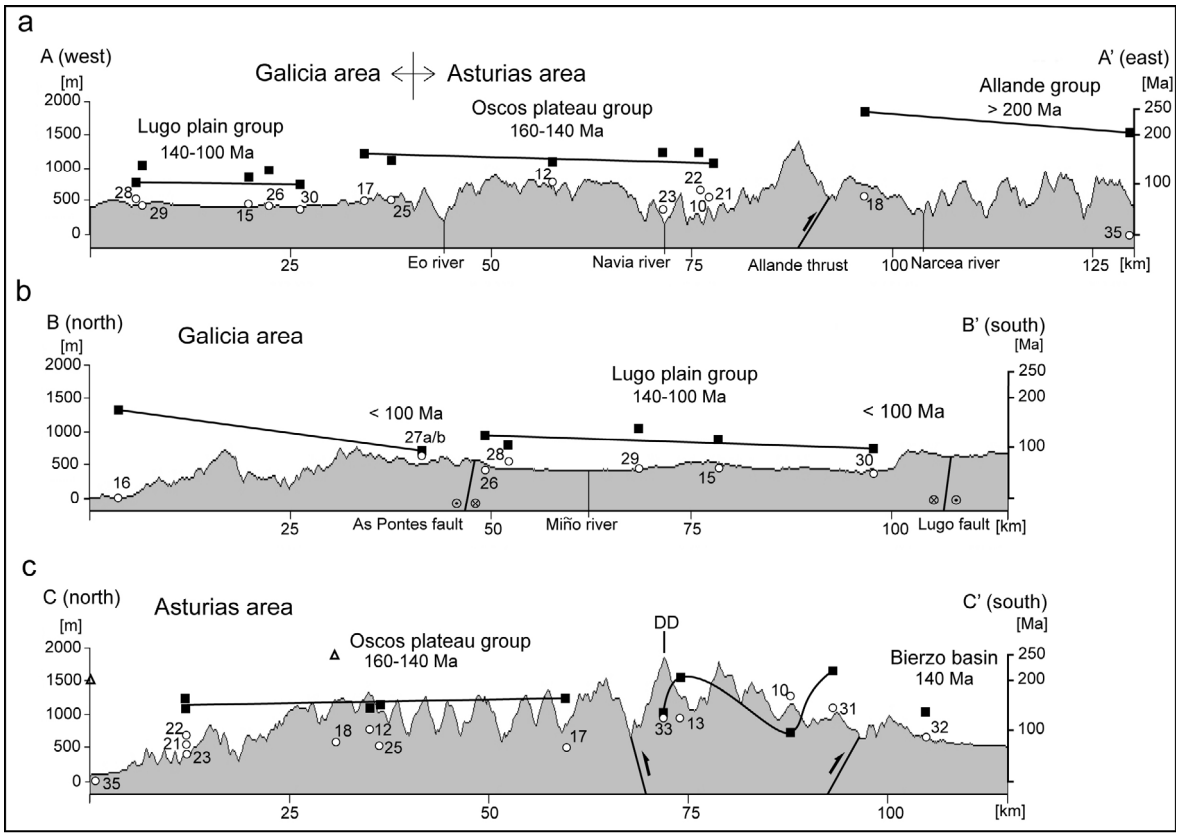

Figure 8: (a) W-E profile with inherited thermal distribution with three regions of AFT ages. The older ages of > 200 Ma are from the east of the Allande fault, ages between 160 and 140 Ma are in the middle (Oscos plateau region) and younger ages between 140 and 100 Ma are in the Lugo plain of Galicia in the west. (b) N-S profile in Galicia with thermal distribution modified since 100 Ma. Youngest age samples next to the faults signal exhumation above 80 ºC between 100 and 40 Ma. (c) N-S profile in Asturias with samples projected over a wide area. A dominant 160-140 Ma age and a complex age distribution within the Alpine thrusts in the southern slope of the range. White circles: projected sample location to show elevation; black squares: central AFT age; white triangles: central AFT age from samples projected from east of the Allande thrust. DD: drainage divide.

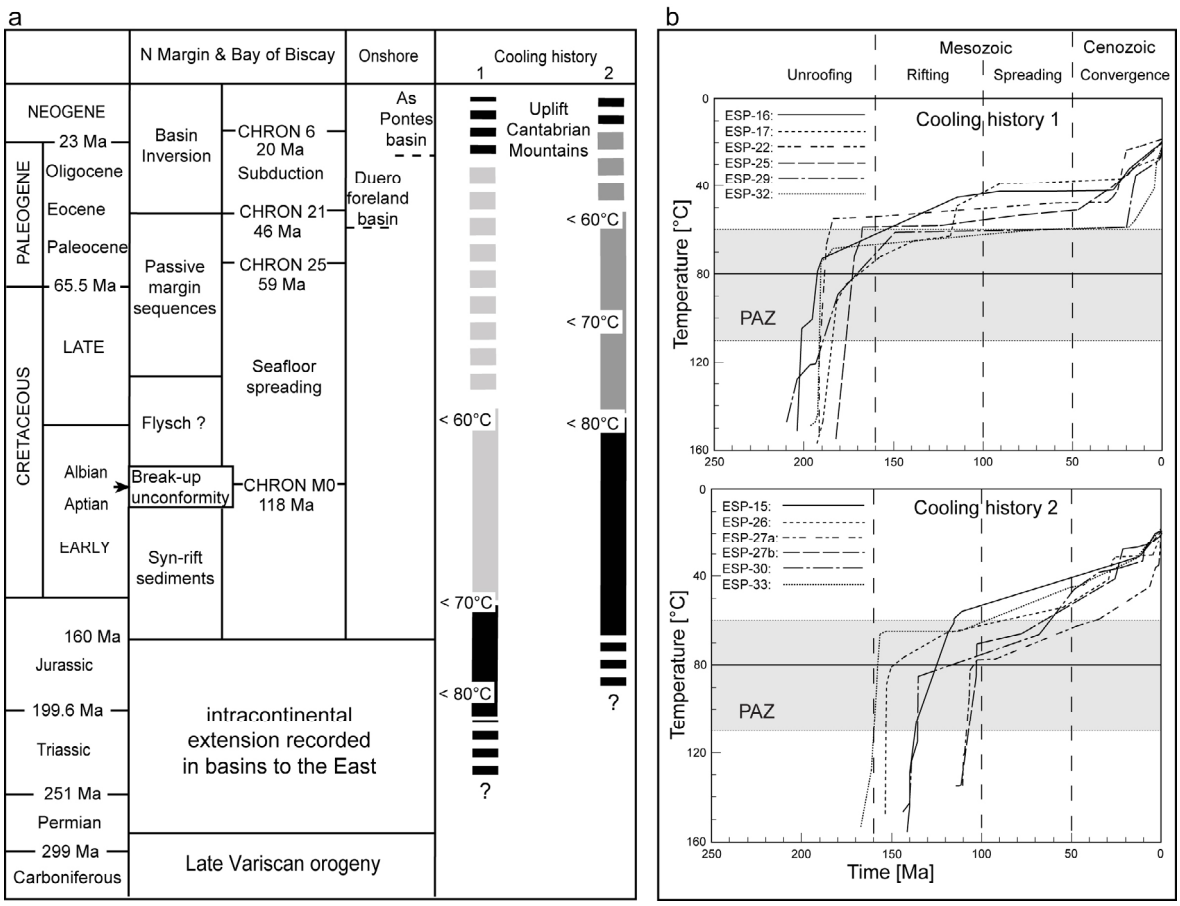

Figure 9: (a) Tectonic events (see text for references on event ages; time-scales of Haq and van Eysinga (1998)) and cooling histories from time-temperature paths. Cooling histories are grouped in (1) t-T paths from samples that where above 70 °C before Mesozoic rifting and show a flat middle part of very slow cooling (lighter grey line) and (2) t-T paths from samples that entered the PAZ during Mesozoic rifting and show a gently dipping middle part of slow cooling (grey part of line). (b) Combined best fit t-T paths of cooling history 1 and 2. Solid black parts of the lines indicate fastest cooling and dashed black parts represent periods of fast cooling less well constrained with our AFT data.

Table 1
Apatite fission-track results.

Sample	Elevation	N Latitude	W Longitude	Lith.	Forming age	U (std)	n	Sp. Tracks		Ind. Tracks		$P(\chi^2)$	Central age	Error
	[m a.s.l.]	DD°MM'SS.S"	D°MM'SS.S"		[Ma]	[µg/g]		ρ_s [10^5 tr/cm^2]	N_s	ρ_i [10^5 tr/cm^2]	N_i	[%]	[Ma]	± 1σ [Ma]
Galicia Area														
ESP-15	470	43°01'02.6"	7°30'55.5"	gr	pok-va	12.6 (5.0)	30	6.941	510	14.141	1039	99.1	116.4	7.4
ESP-16	0	43°41'49.7"	7°26'25.2"	gr	286(2)	49.0 (15.7)	20	39.607	1990	54.136	2720	80.2	174.5	7.7
ESP-17	507	43°01'10.9"	7°21'12.3"	gr	287	6.2 (2.7)	25	4.461	675	6.702	1014	100.0	160.5	9.6
ESP-25*	524	43°14'22.9"	7°17'57.7"	msd	Prot-C	20.2 (12.9)	39	13.028	1010	20.045	1554	81.0	146.2	7.6
ESP-26*	443	43°17'33.1"	7°29'40.7"	msd	Prot	22.0 (15.6)	39	10.732	1206	19.249	2163	13.3	126.0	6.8
ESP-27a*	639	43°21'57.8"	7°30'55.0"	fr-gr	synk-va	40.6 (10.1)	20	15.104	1067	43.132	3047	71.4	78.1	3.7
ESP-27b*	645	43°22'00.2"	7°30'57.8"	gr	synk-va	31.7 (9.2)	20	14.035	1470	34.304	3593	45.0	91.8	4.6
ESP-28*	544	43°16'05.2"	7°42'29.5"	fo-gr	Prot	17.0 (6.6)	21	8.695	910	18.412	1927	21.1	104.3	5.6
ESP-29*	447	43°07'14.2"	7°40'32.8"	gr	synk-va	25.4 (14.0)	20	14.759	715	23.655	1146	49.3	137.3	7.9
ESP-30*	382	42°53'42.9"	6°23'02.8"	gr	pok-va	28.5 (11.7)	20	12.698	955	28.96	2178	82.6	96.2	4.8
Asturias Area														
ESP-10	1256	42°46'25.8"	6°49'13.8"	gr	synk-va	11.9 (10.3)	18	4.788	160	13.047	436	99.3	96.2	9.4
ESP-12	787	43°14'19.7"	7°03'15.3"	sd	C-O	18.2 (12.7)	28	11.877	327	21.611	595	99.9	143.6	10.9
ESP-13	910	43°01'22.6"	6°14'51.5"	sd	Prot-C	7.3 (4.1)	21	6.087	124	7.804	159	100	202.8	25.2
ESP-18*	590	43°16'35.0"	6°36'10.3"	mgrd	Prot	12.5 (2.2)	7	13.604	192	12.541	177	75.9	246.7	26.9
ESP-21*	547	43°26'23.4"	6°48'46.7"	gr	292(3)	42.6 (16.9)	20	27.688	1119	43.622	1763	98.9	144.2	7.2
ESP-22*	659	43°26'34.5"	6°49'04.6"	gr	292(3)	50.0 (19.0)	20	35.66	1872	49.661	2607	94.7	162.5	7.2
ESP-23*	399	43°26'24.3"	6°52'46.0"	sd	C-O	30.2 (16.6)	18	17.782	900	24.875	1259	76.1	161.3	8.7
ESP-31*	1099	42°43'29.5"	7°01'05.6"	msd	Prot-C	11.1 (5.8)	20	11.425	229	11.475	230	91.2	215.7	21.3
ESP-32*	668	42°33'30.3"	6°33' 22.6"	gr	synk-va	37.9 (5.3)	24	25.971	2041	40.553	3187	92.6	139.1	6.0
ESP-33*	935	42°54'12.2"	6°21'59.8"	msd	Prot	19.6 (10.4)	21	11.737	421	18.986	681	94.6	134.0	9.3
ESP-35*	10	43°33'52.7"	6°08'48.3"	msd	Prot	10.8 (6.5)	30	10.555	1724	11.302	1846	56.1	202.2	9.9

Lith.: lithology, U: Uranium concentration, std: standard deviation, n: number of apatite grains, ρ_s: density of spontaneous tracks, N_s: number of spontaneous tracks, ρ_i: density of induced tracks, N_i: number of induced tracks, $P(\chi 2)$: probability that single grain ages are consistent and belong to the same population. Test is passed if $P(\chi 2) > 5\%$ (Galbraith, 1981), Nd = 13802 tracks counted on CN5 dosimeter glass. Ages are calculated using a ζ-value of 356.21 (11.24). Samples marked with "*": Nd = 10474, ζ-value of 337.91 (10.31). gr: granite, fr-gr: fractured granite, fo-gr: foliated granite, mgrd: metagranodiorite, sd: sandstone, msd: metasandstone, synk-va: syn-kinematic Variscan granite, pok-va: post-kinematic Variscan granite, Prot: Proterozoic, Prot-C: Proterozoic-Cambrian, C-O: Cambrian-Ordovician, reference for granitic rock ages: U-Pb geochronology (Fernández-Suárez et al., 2000) except sample ESP-17: Rb-Sr geochronology (Cocherie, 1978), n.a.: not analyzed.

Table 2
Detailed apatite fission-track length data.

Sample	n CT	M.-l. (std)	CT	L_c (std)	L_c	n D_{par}	D_{par} (std)	D_{par}
		[µm]	skew.	[µm]	skew.		[µm]	skew.
Galicia Area								
ESP-15	95	12.4 (1.2)	-0.37	13.9 (0.9)	-0.63	366	1.5 (0.2)	0.41
ESP-16	131	12.4 (1.3)	-0.43	13.9 (0.9)	-0.53	191	1.8 (0.2)	0.78
ESP-17	88	12.4 (1.3)	-0.86	13.9 (1.0)	-1.03	261	1.8 (0.2)	0.26
ESP-25*	81	12.0 (1.5)	-0.05	13.6 (1.0)	0.35	465	1.4 (0.2)	0.15
ESP-26*	94	11.8 (1.6)	-0.56	13.5 (1.1)	-0.97	392	1.4 (0.2)	1.16
ESP-27a*	117	11.8 (1.4)	-0.59	12.9 (1.3)	-0.72	299	1.4 (0.1)	0.17
ESP-27b*	121	12.3 (1.6)	-0.34	13.8 (1.1)	-0.61	331	1.4 (0.1)	0.18
ESP-28*	43	10.6 (1.7)	-0.91	12.8 (1.3)	-0.73	225	1.5 (0.2)	0.05
ESP-29*	57	11.3 (1.6)	-0.08	12.9 (1.4)	-1.03	225	1.5 (0.2)	0.05
ESP-30*	75	12.1 (1.9)	-0.93	13.6 (1.4)	-1.16	229	1.3 (0.1)	0.35
Asturias Area								
ESP-10	13	11.2 (2.6)	0.13	n.a.	n.a.	n.a.	n.a.	n.a.
ESP-12	15	11.4 (1.9)	-1.51	n.a.	n.a.	n.a.	n.a.	n.a.
ESP-13	11	12.4 (1.2)	-1.09	n.a.	n.a.	n.a.	n.a.	n.a.
ESP-18*	24	12.0 (1.4)	-0.88	13.6 (0.9)	-0.51	105	1.6 (0.3)	0.65
ESP-21*	34	10.4 (1.2)	0.7	12.4 (1.1)	-0.11	146	1.5 (0.2)	0.91
ESP-22*	69	12.0 (1.4)	0.39	13.7 (0.9)	0.08	100	1.4 (0.1)	0.34
ESP-23*	50	12.1 (1.2)	0.22	13.6 (0.9)	-0.32	186	1.6 (0.2)	-0.18
ESP-31*	19	11.7 (2.6)	-1.67	13.7 (1.2)	-0.54	146	1.4 (0.2)	0.32
ESP-32*	122	10.4 (1.8)	-0.11	12.8 (1.0)	-0.05	226	1.5 (0.1)	0.36
ESP-33*	60	11.7 (1.8)	-1.12	13.5 (1.1)	-0.66	262	1.4 (0.2)	0.42
ESP-35*	49	12.1 (1.5)	-0.19	13.6 (1.2)	-0.47	237	1.6 (0.3)	1.15

n CT: number of confined tracks measured, M.-l.: mean track length, std: standard deviation, skew.: skewness of distribution relative to the mean value (measure of asymmetry of the distribution), L_c: mean track length after c-axis correction, n D_{par}: number of etch pit diameters measured, Dpar: mean eatch pit diameter.

B. Publication 2

Post-Paleozoic exhumation of the NW Iberian Massif and the remains of a pre-Alpine paleolandscape from apatite fission-track and (U-Th-Sm)/He data.

René W. Grobe[1], Joaquina Alvarez-Marrón[2], Ulrich A. Glasmacher[1], Finlay M. Stuart[3] (2010)

[1]Institute of Earth Sciences, University of Heidelberg, Germany

[2]Institute of Earth Sciences "Jaume Almera", CSIC, Barcelona, Spain

[3]Isotope Geosciences Unit, SUERC, Scottish Enterprise Technology Park, East Kilbride, United Kingdom

Submitted to 'Tectonics' (04th December, 2010)

Abstract

New apatite fission-track (AFT) and (U-Th-Sm)/He (AHe) data combined with time-temperature path modelling constrain the Mesozoic-Cenozoic cooling and exhumation history of the Iberian Massif (Galicia, NW Spain). Two major tectonic episodes affected the region since the end of the Variscan orogeny, 1) Mesozoic rifting that lead to continental break-up by 115 Ma and opening of the Atlantic and Bay of Biscay oceans, and 2) limited convergence along the Bay of Biscay margin since middle Eocene. AFT ages obtained range from 68.1 (5.0)-174.5 (7.7) Ma and AHe ages range from 73.6 (5.4)-147.1 (16.6) Ma. Age-elevation-relationship plots and t-T path modelling together with previous AFT data suggest a thermal and structural evolution with one order of magnitude faster exhumation rates during the Mesozoic tectonic episode of active rifting than those since initiation of seafloor spreading. Cooling patterns in Central Galicia are consistent with Jurassic to Early Cretaceous activity along NNE-SSW trending system of post-Variscan faults. AHe data indicate that less than 1.5km of overburden has been eroded since 100-80 Ma at slow denudation rates of 0.015 km/Ma. These data indicate that the low relief upland at ~500m elevation in Central Galicia corresponds to remains of a pre-Alpine low relief paleolandscape which developed during the postrift quiescence period. Along the coastline in North Galicia a ridge with a 1,000m high peak was uplifted since middle Eocene, associated to activity along the As Pontes fault. This surface uplift is associated with insufficient exhumation to reset AFT ages during activation of the North Iberian Margin.

1 Introduction

Along NW Spain in Galicia, the landscape consists of continental basement rocks of the Iberian Massif corresponding to the westernmost exposures of the Variscan Belt in Europe (Fig. 1.1.). This crystaline basement with a well-known geological history in pre-Mesozoic times (Martínez-Catalán *et al.*, 2007) lacks any representation of Mesozoic sedimentary cover and is only locally unconformably covered by sparse Neogene deposits (Barrón and Santos, 1998, Santanch *et al.*, 2005). This insufficiency of suitable stratigraphic controls has hampered a detailed understanding of the response of this continental basement to tectonic processes that affected the region during the Mesozoic and Cenozoic. For example, little is known about the possible linkage of widespread post-Variscan fractures in Central Galicia with the rifting process that opened the surrounding Atlantic and Bay of Biscay Oceans in the Mesozoic. Available paleogeographic reconstructions interpret the massif as an emergent and passive continental landmass during that process (Ziegler and Roure, 1999; Stampfli and Borel, 2002). However, new thermochronological data indicate that significant upper crustal cooling occurred in the region during the Mesozoic (Grobe *et al.*, 2010). In addition, a large area of low relief landscape around the city of Lugo differs significantly from the adjacent area with high elevations along the Cantabrian Mountains (Fig. 1). While these mountains rose during compression along the Bay of Biscay Margin in the Cenozoic (Pulgar *et al.*, 1996), the Lugo low relief area seems to have remained unaffected by significant Cenozoic tectonism. Thus suggesting that the low relief landscape may have evolved from an inherited pre-Alpine low topography paleolandscape.

This study combines apatite fission-track (AFT) and apatite (U-Th-Sm)/He (AHe) thermochronological data in order to constrain the timing and thermal effects of upper crustal tectonic and geomorphologic processes in the northern Iberian Massif. The AFT system allow to obtain cooling data over a temperature range of 110 °C to 60 °C (Green *et al.*, 1986; Crowley *et al.*, 1991; Carlson *et al.*, 1999), and the AHe chronometer over a temperature range of 70 ºC to 40 °C, approximately (Wolf *et al.*, 1996; Wolf *et al.*, 1998; Farley, 2000). Considering a geothermal gradient of 27 ºC/km (Fernández *et al.*, 1998), the AFT system will be sensitive to the passage of rocks being exhumed between 3.5 and 1.7 km depth, and the AHe system between 2.0 and 0.9 km depth. Thus, this methodology should be well suited to study the northern Iberian Massif with two main

objectives: 1) to obtain a better understanding of its structural and thermal response to the surrounding extensional processes that occurred in the Mesozoic and 2) to quantify fundamental land-forming processes, such as exhumation/erosion across the Lugo low relief area and discuss its landscape evolution during the Cenozoic.

2 Geological background

The Iberian Massif in NW Spain includes a well-known section of the continental margin of Gondwana involved in the Variscan collision (Pérez-Estaún *et al.*, 1991; Martínez-Catalán *et al.*, 2007) (Fig. 1). Along this section, the West Asturian-Leonese Zone (WALZ) outcropping in Galicia includes an extensive sequence of Upper Proterozoic rocks overlain by a thick siliciclastic Paleozoic sequence (Martínez-Catalán *et al.*, 1990; Pérez-Estaún *et al.*, 1990; Martínez-Catalán *et al.*, 2003). Rocks in this zone underwent greenshist and low-grade amphibolite metamorphism and a great deal of strain during Variscan collision in the Carboniferous and Early Permian (Martínez-Catalán *et al.*, 2007). During two main magmatic episodes relative to the Variscan deformation, the area was intruded by abundant granitic magma (Fig. 2). A syn-tectonic association that includes tonalite-granodiorite-monzogranite plutons and leucogranite intrusions with ages ranging between 325 and 310 Ma, and a post-tectonic association that includes abundant tonalite-granodiorite-monzogranite plutons with ages of c. 295-290 Ma and scarce leucogranites with ages of c. 290-285 Ma (Dallmeyer *et al.*, 1997; Cocherie, 1978; Fernández-Suárez *et al.* 2000b). The names and published age data for the plutons that have been sampled in this study within the WALZ are summarized in Table 1.

The Variscan collision contributed to the assembly of the large supercontinent of Pangea that started to break-up during Late Permian and Triassic times (Ziegler and Roure, 1999; Stampfli and Borel, 2002). During this process a separated continental piece known as the Iberian Massif initiated its individualization (Ziegler, 1989). The area of the NW Iberian Massif studied here lacks any representation of an unconformable cover with Permian-Triassic sediments, and the nearest onland sediments of this age appear in the Oviedo basin, more than 100 km to the east (Martínez-García, 2004). A sedimentary cover of this age is well represented further west in the Basque-Cantabrian basin (Espina *et al.*, 2004). The subsequent widespread rifting events that lead to the opening of the Atlantic Ocean to the west and oblique separation of Iberia from Eurasia to open the Bay of Biscay Ocean to the north occurred during Late Jurassic-Early Cretaceous (Le Pichon *et al.*, 1971; Srivastava *et al.*, 1990). Seafloor spreading initiated in both oceanic basins by 118 Ma and stopped in the Bay of Biscay by the Late Cretaceous (Srivastava *et al.*, 1990).

During the Cenozoic, convergence between Iberia and Eurasia caused the activation of the northern margin of Iberia and was responsible for the uplift of the Variscan Basement to form the Cantabrian Mountains (Fig. 1). This convergence caused the oceanic crust to underthrust the continental margin and the development of a small accretionary prism active from Lutetian to Burdigalian times at the foot of the continental slope (Srivastava *et al.*, 1990; Alvarez-Marrón *et al.*, 1997). Foreland basin sedimentation in the Duero basin to the south of the Cantabrian Mountains started by middle Eocene times (Gallastegui, 2000). Convergence along the northern margin of Iberia slowed significantly since the early Miocene (Rosenbaum *et al.*, 2002), although younger brittle faulting has been documented in nearby on land areas (Cabral, 1989; Andeweg, 2002; Rodriguez-García *et al.*, 2006; Alvarez-Marrón *et al.*, 2008). The NW of Spain and surrounding continental margins continue to be weakly seismically active today (López-Fernández *et al.*, 2004; Díaz *et al.*, 2008). Patches of a few hundred meters thick Neogene continental deposits, covering the Iberian Massif rocks unconformably, are common in Galicia (Barrón and Santos, 1998).

The main post-Variscan structures recognized in the WALZ are the westward prolongation of the thrusts to the south of the Cantabrian Mountains and two main fault systems with NW-SE and NE-SW trend (Fig. 1 and 2). The thrusts caused uplift of the Cantabrian Mountains during the evolution of the Bierzo basin since the Early Oligocene

(Freudenthal *et al.*, 2010). Further west, the As Pontes strike-slip fault that trends WNW-ESE and extends for more than 50 km is the largest Alpine fault in Galicia. This fault underwent up to 1 km horizontal right-lateral slip and a maximum of 455 m vertical displacement during formation of the As Pontes basin from 30 to 22 Ma (Huerta *et al.*, 1996; Santanach *et al.*, 2005). A significant south-facing topographic escarpment that reaches locally more than 300 m is associated to the As Pontes fault. The age of other faults trending NW-SE and NE-SW in Central Galicia is not well documented. Some of them are associated to patches of Tertiary sediments and have been found to cut them in a few localities (González-Lodeiro *et al.*, 1982). These faults however, trend parallel to the fault systems that stem from the deformation front of the Cantabrian Mountains and extend for hundreds of km southward into Portugal (Fig. 1). Holocene activity has been reported for faults of this set in Portugal (Cabral, 1989).

The relief pattern in Galicia is characterised by an extensive, relatively flat area around the city of Lugo that averages between 450 to 500 m elevation above sea level and a higher, more rugged topography to the north (Fig. 2). The abrupt transition north of Lugo that is bounded by the As Pontes fault reaches elevations of over 1000 m. A recent regional thermochronological study across the western termination of the Cantabrian Mountains (Grobe *et al.*, 2010) provided initial regional data regarding the timing and magnitude of cooling and exhumation in Galicia. These authors concluded that the area experienced rapid cooling over the Late Jurassic and Early Cretaceous period of Atlantic and Bay of Biscay rifting. Ten samples from the WALZ that were previously discussed by Grobe *et al.* (2010) are incorporated to the present study (Tab. 2).

3 Methods and techniques

3.1 Sampling strategy

The area shows a topographic variation from North to South. A rough topography reaching elevations of up to 1,000 m is represented in the North, while to the South around the city of Lugo a low relief area with elevations ranging between 400 to 500 m can be observed. Considering this topographic variation and major structural features fourteen new samples with a sufficient amount of apatite to perform apatite fission-track analysis were obtained along two transects (Fig. 2). A northern transect (A-A'-A'') was intended for crossing the escarpment of As Pontes fault, since previous AFT results indicated possible advection along this escarpment after 100 Ma and before 50 Ma (Grobe *et al.*, 2010). This transect includes 8 samples, three of them to the north of the escarpment in the La Tojiza pluton (# JU-40, 41, 42), covering elevations between 350 and 835 m, four samples from the Monseibán pluton taken along a linear nearly vertical transect with an elevation range between 606 and 915 m along the escarpment (# JU-27, 28, 29, 30), and one sample from the Roman pluton south of the As Pontes fault (# JU-38).

The southern transect (B-B') includes 6 samples across the low relief area of Lugo at elevations between 410 and 618 m that were taken with the intention to cross the Lugo fault (Fig. 2). The samples east of the Lugo fault are from the Castroverde pluton (# JU-22) and from Lower Cambrian meta-sediments (# JU-21). Sample ESP-17 from Grobe *et al.* (2010), east of the Lugo fault is also incorporated to this transect. The samples west of the Lugo fault are from the Castroverde pluton (# JU-23, 24), the Lugo pluton east of Lugo (# JU-25), and from the Hombreiro pluton west of Lugo (# JU-26). Samples ESP-15 and ESP-30 from Grobe *et al.* (2010) to the west of the fault are also included in this transect. Since previous AFT results by Grobe *et al.* (2010), found that most samples in Galicia cooled to temperatures below 110 °C since 100 Ma (depths shallower than 3.5 km), six samples along or nearby the southern transect that contained crystals of sufficient quality were used to perform (U-Th-Sm)/He thermochronology in order to constrain the exhumation history after 100 Ma. Three of them, samples ESP-15, ESP-17 and ESP-30 correspond to the previous AFT study by Grobe *et al.* (2010), and the other three are new samples (# JU-22, 24, 25).

3.2 Apatite fission-track (AFT) analysis

The concept of AFT dating is based on the analysis of chemically etchable linear defects (fission-tracks) that are caused in apatite by heavy fragments during spontaneous fissioning of ^{238}U (Wagner, 1972). The fission-tracks are metastable in relation to time and temperature. Considering a residence time of 10 Ma, fission-tracks fully anneal at temperatures above c. 110 °C where the chronometer is reset, and the annealing is virtually zero at temperatures below c. 60 °C. Thus, AFT thermochronology is sensitive to the temperature range between c. 110 to 60 °C. This temperature range is called the partial annealing zone (PAZ). The information on the thermal history of apatite is stored in two archives, the etch pit areal density of tracks that provide the cooling age, and the length distribution of horizontal confined fission-tracks that record the cooling path (e.g. Wagner and Van den haute, 1992; Lisker *et al.*, 2009 and literature cited therein).

The annealing behaviour of spontaneous fission-tracks is influenced by two other factors that need to be taken into account in the AFT analysis. One is the chemical composition of apatite, because the annealing speed at a given temperature is slower in apatite grains with high chlorine content than in fluorine rich apatite grains (Gleadow and Duddy, 1981; Green *et al.*, 1985; 1986; Burtner *et al.*, 1994; O'Sullivan and Parrish, 1995; Carlson, 1990; Crowley *et al.*, 1991; Crowley, 1993; Carlson *et al.*, 1999; Donelick *et al.*, 1999; Ketcham *et al.*, 1999; Barbarand *et al.*, 2003a; b). There is a linear relation between the etch pit size parallel to the c-axis ($D_{par}^{®}$) and the fluorine/chlorine content of the apatite (Donelick, 1993; 1995). The other factor is the crystallographic orientation of the spontaneous tracks in the crystal (Green and Durrani, 1977). Tracks orthogonal to the c-axis anneal more rapid than tracks parallel to the c-axis, and this anisotropy increases with annealing (Green, 1981; Laslett *et al.*, 1984; Donelick *et al.*, 1990; 1999; Galbraith *et al.*, 1990; Donelick, 1991; 1993; 1995; Barbarand *et al.*, 2003b).

3.2.1 Sample preparation, processing and data acquisition

Apatite grain mounts were obtained by applying standard sample processing techniques (Grist and Ravenhurst 1992a; b). Sobel and Seward (2010) examined the influence of etching conditions on $D_{par}^{®}$ (Donelick, 1993; 1995). They pointed out the importance of controlled etching conditions for further use of $D_{par}^{®}$ as a kinetic parameter in thermal models like HeFTy©. Apatites were etched in 5.5 M HNO_3 for 20 (1) s at 21 (1) °C and detection mica in 48 % HF for 20 (1) min at 20 (1) °C. Samples were irradiated at the research reactor FRM II, Munich, in the presence of three glass neutron dosimeter (CN5) of known uranium content at top, middle and bottom of the sample batch as well as two Durango apatite age standards. To avoid false lengths measurements due to water release into the horizontal confined tracks as a result of irradiation, sample mounts have been cleaned with 99.9 % ethanol in ultrasonic bath and dried for 10 min at 90 °C.

Area densities (tracks/cm^2) of spontaneous and induced tracks, distribution of horizontal confined track lengths and c-axis oriented etch pit diameters ($D_{par}^{®}$) were determined at the Heidelberg FT-1 system. A detailed description of the system is given in Grobe *et al.* (2010).

Apatite fission-track ages were calculated applying the ζ-method (external detector method) described by Hurford and Green (1982; 1983). The ζ-values of 341.41 (15.48) and 340.59 (14.68) were obtained by counting several Durango apatite age standards. All ages, 1σ errors, and radial plots were determined by using the computer code 'Trackkey' (Dunkl, 2002). The results are shown in Table 3, with AFT ages reported as central ages (Hurford, 1990; Galbraith and Laslett, 1993).

3.3 Apatite (U-Th-Sm)/He (AHe) analysis

The AHe method is based on the accumulation of ^4He as decay products of ^{238}U, ^{235}U, ^{232}Th, their daughter products, and ^{147}Sm in the apatite grain until the closure temperature is reached (Reiners and Ehlers, 2005). In general, the apatite closure temperature is in the range of 70 °C for a simple monotonic cooling

rate of 1 °C/Ma and a subgrain domain size > 60 μm, while at a temperature of less than c. 40 °C/1 Ma the total ^{4}He is retained in the mineral (Farley *et al.*, 1996; Farley, 2000; Stöckli *et al.*, 2000; Wolf *et al.*, 1996; 1998). Therefore, the AHe system is sensitive to the temperature range between c. 40-70 °C/1 Ma, referred to as the He partial retention zone (PRZ). The measured concentrations are corrected to account for the loss/gain of radiogenic ^{4}He, the α-ejection correction (Wolf *et al.*, 1996; Farley *et al.*, 1996; Farley, 2000), and for radiation damage to the crystal structure due to radioactive decay (Shuster *et al.*, 2006; Shuster and Farley, 2009; Flowers *et al.*, 2006; Flowers *et al.*, 2009).

3.3.1 Sample preparation, processing and data acquisition

AHe analytical work needs well defined apatite crystals with a minimum size of 50 μm in diameter that should be free of any mineral or fluid inclusions and free of cracks. Therefore, accurate selection and preparation of apatite crystals appropriate for AHe dating is crucial. At least two grains were processed from each sample, reaching up to five grains analysed whenever the quality of the apatite grains allowed. The AHe analysis was performed at the Isotope Geosciences Unit, SUERC, Scottish Enterprise and Technology Park, East Kilbride, UK, following the procedures in Foeken *et al.* (2006). U, Th and Sm extraction and analysis followed the procedures of Dobson *et al.* (2005). The analytical procedures involved the following steps: i) Measurement of grain dimensions for determination and correction of α-ejection; ii) Measurement of He content: He degassing of single apatite crystals was performed using a diode laser (Foeken *et al.*, 2006), followed by purification and quantification by noble gas spectrometry done with a Hiden quadrupole mass spectrometer (QMS); iii) Measurement of U-Th-Sm content of the degassed crystals: Apatites are removed from vacuum system and dissolved within HNO_3 to analyze U, Th and Sm on an ICP-MS. All quantities were measured on a single crystal, to eliminate uncertainties that arise from grain to grain heterogeneities (Farley and Stöckli, 2002; Ehlers and Farley, 2003).

Raw ages were calculated following procedures by Meesters and Dunai (2005) (Tab. 2). An α-ejection correction was applied to the raw ages using HeFTy© and the recommendations of Ketcham *et al.* (2009). Because models of diffusion kinetics are based on a spherical diffusion domain (Meesters and Dunai, 2002), the equivalent sphere radius was calculated for each grain:

$$radius = \frac{3}{(S/V)} \quad (1)$$

on which the further α-ejection correction was based (Ketcham, 2009).

In some cases, considerable intra-sample single grain age variation can be observed. Several factors, such as U-/Th-rich (micro-) inclusions, fluid inclusions, variation in grain size, radiation damage (high effective Uranium (eU) concentration) , α-ejection correction, zonation, and cooling rate, among others may contribute to age dispersion that mostly cause AHe ages to be "too old" (i.e.: Reiners and Farley, 2001). In order to overcome these common limitations, Fitzgerald *et al.* (2006), proposed to determine a weighted mean age and suggested that the most representative age for the sample lies between the minimum AHe age and the weighted mean age. The approach is most reliable in cases were the full age variability of the sample is covered, and they propose to determine 20-25 single grain ages to robustly constrain the full age variability.

3.4 Thermal modelling – t-T paths

Determination of the low-temperature thermal history can be achieved by a modelling procedure (HeFTy© v1.7 beta 2) that considers known annealing kinetics of fission-tracks in apatite, as well as He-diffusion behaviour of apatite (Ketcham, 2005; Ketcham *et al.*, 2007a; b; Ketcham *et al.*, 2009). The technique combines the real fission-track data set (i.e. single grain ages, length distribution, fluorine and chlorine content with D_{par}® as a proxy) with the determined (U-Th-Sm)/He age (if available), and the time-temperature

coordinates obtained from the known geological evolution of the area. Therefore, the modelling process tests the geological evolution against the thermochronological data set to determine a best fit t-T evolution. The primary goal of the program is to define envelopes in t-T space that contain all paths passing baseline statistical criteria and being conform to the user-entered geological constraints. A good fit corresponds to a merit value of 0.5 or higher (goodness of fit (G.O.F) ≥ 50 %). An acceptable fit corresponds to a merit value of 0.05 or higher (G.O.F ≥ 5 %), indicating that the model has not failed the null hypothesis test of the applied statistics (Ketcham, 2009; Ketcham *et al.*, 2009).

In a first step, the data was modelled in a forward approach, considering information from geological evolution of the study area. The best forward model is taken as the basis for the inverse modelling process. Along the t-T path several constraint boxes can be set, acting as starting fields for the inverse model that follows a Monte Carlo approach. In our tests, 10,000 to 100,000 model runs are sufficient to find the best AFT modelling solution. However, if AHe data is added, in some cases we decided to increase that number up to 1,000,000 runs to ensure to find the best possible fit. A procedure of testing each He-diffusion model available in HeFTy© (Wolf *et al.*, 1996; Farley, 2000; Shuster *et al.*, 2006; Flowers *et al.*, 2009) provided acceptable good fits for those samples with AHe results.

The first constraint box was always chosen at a temperature around 160 °C and with the younger age limit such that the AFT age of the sample is included in the box. The upper age limit was set at about 50-70 Ma older. In this way, the modelling algorithm tests a wide range of cooling paths at which the samples have entered the PAZ. First the samples with the most horizontal confined tracks available (i.e. the most reliable samples for modelling) were modelled and further constraint boxes were introduced to increase the amount of good fits. In the next step samples of the same blocks were modelled with equal constraint boxes to test a similar cooling history on samples of the same block.

4 Results

4.1 Apatite fission-track ages

The AFT ages obtained range from 154.4 (11.6) Ma to 68.1 (5.0) Ma (Tab. 3). All ages are younger than the corresponding sedimentation, metamorphic, or intrusive age of the sampled rocks. Single grain age distributions of each sample fulfilled the $\chi 2$ test, indicating a homogenous distribution within the 1σ error of the single grain ages (Galbraith, 1981). The $\chi 2$ test is passed when $\chi 2 > 5$ %. If we consider the central ages obtained in samples from the previous study (Grobe *et al.*, 2010) the variation of available central ages across Galicia ranges from 68.1 (5.0) Ma to 174.5 (7.7) Ma.

Along the northern transect (A-A'-A''), the seven new samples from north of As Pontes fault, record AFT central ages that range from 68.1 (5.0) Ma to 116.8 (6.3) Ma (Tab. 3). Three samples in the La Tojiza pluton, yielded AFT ages that range between 68.1 (5.0) to 115.7 (5.9) Ma, being sample JU-40 at 350 m elevation the youngest AFT age of 68.1 (5.0) Ma determined so far in Galicia. The four samples along the near vertical transect coinciding with the As Pontes fault escarpment yielded AFT ages that range from 100.4 (5.4) to 116.8 (6.3) Ma.

The age-elevation relationship (AER) indicates a positive trend with a sharp break in slope at c. 115 Ma (Fig. 3a). Samples ESP-27a from a fractured granite, sample JU-41 that had only 5 datable grains and sample ESP-16 from the coast is too far away to be included in the comparison of age and elevation. Only one sample along this transect is located south of the As Pontes fault (# JU-38). It provided a AFT cooling age of 110.5 (6.4) Ma similar to samples north of the fault (Tab. 3). The exhumation rates derived from regression lines are around 0.25 km/Ma for the fast exhumation at 115 Ma and around 0.01 km/Ma after this event.

The samples along the southern transect (B-B') in Central Galicia record AFT central ages that range from 109.4 (6.4) Ma to 154.4 (11.6) Ma. Along the southern transect the Lugo fault separates the Eastern block from the Lugo block and a no-named fault separates the Lugo

block from the Western block. Both faults are trending NNE-SSW (Fig. 2). A sharp change in AFT age occurs across the Lugo fault. Samples to the east of the fault (# JU-21, JU-22 and ESP-17) with ages ranging from 160.5 (9.6) Ma to 142.9 (7.6) Ma are much older than samples to the west. The samples to the west (# JU-23, 24, 25 and ESP-15) range in ages between 109.4 (6.4) and 116.4 (7.4) Ma. This difference is observed also between samples taken across the fault, in the same pluton and at similar elevations. This difference is interpreted to indicate movement along the fault at ~116 Ma. The westernmost sample along the transect (# JU-26) bears an AFT cooling age of 135.3 (6.9) Ma, this is significantly older than the samples from the Lugo block west of the Lugo fault mentioned above. Given that this age is similar to that of 137.3 (7.9) Ma from sample ESP-29 we interpret the age difference as caused by faulting at ~116 Ma. This time of fault activity is similar to that of the Lugo fault, and several faults with the same trend as the Lugo fault are mapped in the area between samples ESP-15 and JU-26 (González-Lodeiro *et al.*, 1982). Our results indicate that this NNE-SSW trending set of faults within the low relief areas of Lugo where active during the main episode of rifting in the Early Cretaceous thus causing significant variation in AFT age (in the order of several tens of Ma) across them.

The resulting age-elevation relationship (AER) plot including all data on or close to the southern transect (Fig. 3b). The plot provides a similar trend for samples from the Lugo block as of those from the northern transect. The AER shows a fast exhumation at a rate around 0.25 km/Ma with a significant break in slope at 115 Ma and a subsequent moderate exhumation at a rate of around 0.01 km/Ma. The trend of the samples from the Eastern and Western block is not very significant due to scarce data.

4.2 Etch pit size and track length distribution

A total of 3283 single D_{par}® values were determined for all apatite grains used in this study (Tab. 4). The mean D_{par}® values determined for each sample show a very narrow range between 1.3 (0.1) to 1.6 (0.1) µm indicating a very homogenous chemical composition with respect to the fluorine and chlorine content of the apatites. The skewness of all single D_{par}® values determined for each sample lies between -0.7 and 5.8. With the exception of samples JU-24, 28 and 42, all other samples exhibit a positive skewness. The positive skewness indicate a tailing towards larger values while negative skewness indicate a tailing towards smaller values. The largest etch pit size of 2.3 (0.1) µm was measured in sample JU-29. This sample shows also the largest spread in etch pit size between 1.0 (0.1) and 2.3 (0.1) µm. No positive correlation between single grain ages and D_{par}® values has been detected.

A total of 1091 lengths of horizontal confined spontaneous fission-tracks were measured. The obtained mean track lengths range from 10.7 (2.6) to 12.6 (1.8) µm. With the exception of sample JU-24 all samples show a negative skewness between -0.17 and -1.56 indicating a tailing towards shorter track lengths. The skewness is not very significant and a simple, continuous cooling history may be assumed. There is no relation between track lengths distribution and elevation or apatite fission-track ages. The measured confined track lengths were corrected for their orientation to the crystallographic c-axis by applying the computer code HeFTy© to the data set. The mean c-axis projected lengths changed to a distribution between 13.0 (1.5) and 14.1 (1.1) µm. With the exception of samples JU-21 and 23 all samples show a negative skewness between -0.15 and -2.59. Again there is no correlation between track lengths and apatite fission-track ages or elevation.

4.3 (U-Th-Sm)/He ages in Central Galicia

AHe ages with 2-5 single grain ages in each were determined for 6 samples from Central Galicia (Tab. 5; Fig 5b). Raw AHe ages range from 42.6 (3.2) to 118.8 (6.3) Ma and change to values between 70.6 (5.2) and 171.8 (16.5) Ma after applying α-ejection correction. Sample ESP-15 shows good intra-aliquot age replication within 10% error, while only the two youngest AHe ages replicate within 10% error in sample ESP-17, and with 15% error in samples JU-22 and 24. The intra-aliquot age

replication in samples ESP-30 and JU-25 is poor. There is no correlation between equivalent grain radius (grain size) and AHe age distribution within the samples. Therefore, the poor reproducibility is most likely caused by undetected mineral/fluid inclusions, as in two samples (# ESP-17; JU-22) with slight positive correlation between single grain AHe age and eU concentration a slow cooling through the PRZ may not be discarded. In one sample (# ESP-30), all AHe single grain ages obtained were older than the corresponding AFT age. The calculated weighted mean AHe ages and 'most representative AHe ages' do not differ significantly from the youngest AHe ages (Tab. 5). Thus, the youngest α-ejection corrected AHe ages ranging from 70.6 (5.2) to 114.4 (14.2) were used for the interpretations.

4.4 Time-temperature models

Fourteen samples that revealed more than 50 measured horizontal confined fission-tracks were used for testing geological constraints against the thermochronological data set to reveal time-temperature (t-T) paths. Out of those, it was possible to perform AFT+AHe based HeFTy modelling in three samples (# ESP-17, ESP-15 and JU-22), being the rest AFT based HeFTy models. Three other samples that yielded AHe ages did not bring AFT and AHe data in concordance during modelling (# JU-24, 25, ESP-30). All fourteen samples show the best fit t-T paths consistent with a continuous cooling history, indicating no apparent reheating.

The t-T paths of samples from the northern transect (Fig. 4a; 5a, 6) show a very similar cooling history, including that of sample JU-38 from south of the As Pontes fault. The models are consistent with one order of magnitude reduction of cooling rate from values that average 4.7 °C/Ma before 120 Ma to values that average 0.5 °C/Ma after that time (Tab. 6). The paths show a relatively fast cooling below temperatures of 80 °C between ~160 and 120 Ma with a mean exhumation rate of ~0.25 km/Ma (Tab. 6) assuming a constant geothermal gradient of 27 ºC/km. This value corresponds to the geothermal gradient determined from the present day heat flow density of 65 (5) mWm^{-2} in the area (Fernández *et al.*, 1998).The subsequent slower cooling after ~120 Ma yielded a reduction in exhumation rates to 0-02 km/Ma. However, two paths (# JU-28, 29) revealed a slightly different 3-phases cooling history with a increased exhumation rate of ~0.07 km/Ma around 20 Ma.

The t-T paths of samples from the southern transect display a larger dispersion in cooling history (Fig. 4b, 5b, 6). However, if grouped into the three different blocks a similar trend as seen in the AER plots can be observed. Samples from the Lugo block cooled below temperatures of 80 °C between 160 and 130 Ma with an average exhumation rate of about 0.25 km/Ma. The subsequent decrease in exhumation rate to ~0.02 km/Ma after 130 Ma can also be monitored. Time-temperature paths from the Eastern and Western block show a significantly different cooling history. Samples cooled below ~80 °C already at times between 210 and 180 Ma at an average rate of 0.25 km/Ma. After 180 Ma the average exhumation rate decreased to 0.01 km/Ma. As observed in the northern transect, the southern transect also reveals samples (# JU22, 23, 24, 26) that tend to show a 3-phased cooling history with an increase of exhumation rates to ~0.04-0.05 km/Ma between 30 an 40 Ma.

5 Discussion

The AFT and AHe age distribution considering all samples available in the NW Iberian Massif ranges from Middle Jurassic to Late Cretaceous. There are no evidences in the track length distributions of the samples to suggest multiphase heating histories. Track lengths distributions show clearly defined peaks with only minor skewness. For these reasons we discard thermal overprinting as a cause of the variation in AFT ages and cooling histories. Modelled time-temperature histories based on AFT lengths distribution further suggest spatially heterogeneous, continuous cooling and exhumation at varied rates since the end of the Variscan orogeny by Late Paleozoic times (Fig. 6).

5.1 Mesozoic structure and exhumation history of the Northern Iberian Massif

The first tectonothermal events to affect the Northern Iberian Massif since the end of the Variscan orogeny by Late Paleozoic times (Martínez-Catalán *et al.*, 2007) are related to intracontinental rifting that developed between the Iberian and the Armorican Massifs in the Triassic (Ziegler, 1989). This author also considers that this Triassic intracontinetal rift is the precursor of the northern Iberian plate margin that developed subsequently during rifting in the North Atlantic. The thermochronological data in Galicia indicate that cooling through shallow crustal levels of 3.5 km depths started by Late Triassic times (Fig. 6). A few samples from across the low relief areas of Central Galicia record cooling rates between ~6.5 °C/Ma and ~2.0 ºC/Ma from ~200 Ma to ~165 Ma. Thus, indicating exhumation across inland areas of the Iberian Massif possibly due to incremental erosion/unroofing of material in the southern shoulder of the Triassic intracontinental rift. However, the main episode of cooling below 80 °C that caused the exhumation of most samples through shallow crustal levels in the NW Iberian Massif occurred between ~160 to ~120 Ma (Fig. 6). This exhumation was coeval with the widespread rifting episode that generated the continental margins to the North and West of Galicia from Late Jurassic to Early Cretaceous times (Le Pichon *et al.*, 1971; Srivastava *et al.*, 1990). The largest average exhumation rates of ~0.5 km/Ma during this event are registered across the Northern transect, possibly indicating largest erosion/unroofing of uplifted material near the rift shoulder. Fast cooling during Late Jurassic – Early Cretaceous was also detected in Variscan basement granites from the SW England coast and interpreted as rift-related surface uplift (Chen *et al.*, 1996). Paleogeographical reconstructions represent this area of SW England as the North Galicia conjugate flank of the Bay of Biscay rift (Ziegler, 1989). In contrast to the fast exhumation across the northern transect, the more inland areas of the southern transect register lower exhumation rates of 0.08-0.2 km/Ma during the same period (Tab. 6). In this Central area of Galicia however, the AFT age distribution with differential exhumation between fault blocks indicates activity ~116 Ma along the NNE-SSW trending system of post-Variscan faults (Fig. 6). The activity of these fault systems during the main Mesozoic rifting episode is plausible considering that the Lugo fault connects southwards with bounding faults of the Lusitanian basin that contains significant thickness of Early Cretaceous sediments (Rasmussen *et al.*, 1998; Alves *et al.*, 2003).

The data from seafloor magnetic anomalies established the continental break-up and initiation of seafloor spreading at chron M0 that corresponds to 118 Ma (Verhoef and Srivastava, 1989). This correlates with the initiation of the Mesozoic post-rift stage and initiation of the passive evolution of the continental margin that is marked by the Aptian-Albian age break-up unconformity in the Cantabrian platform (Montadert *et al.*, 1979; García-Mondejar *et al.*, 2005). In the North Galicia area reduced rates of ~0.02 km/Ma are calculated for the time span between 110 to 60 Ma, during the Early Cretaceous to Early Paleocene period of post-rift evolution of the northern continental margin. This interpretation also coincides with values of 0.01 km/Ma between ~115 Ma and ~70 Ma indicated by the AER in the higher topographic areas of Northern Galicia. However, the t-T path models indicate a significant reduction of exhumation rate since ~120 Ma years ago, reaching exhumation rates of less than 0.02 km/Ma since that time (Tab. 6). These low rates are indicative of stable thermal conditions in the upper crust from the Late Cretaceous to the Eocene across the NW Iberian Massif. A weak indication of a possible short episode of fast cooling at around 115 Ma across the northern transect would be indicative of a rapid and short-lived thermal contraction of the continental crust at the onset of the post-rift stage. A process of fast cooling during continental break-up is explained as due to escarpment retreat in the southern Australian passive margin (Persano *et al.*, 2002). This interpretation would be plausible considering this northern region is closest to the coastline. In order to confirm this interpretation further

ongoing thermochronological studies with a lower temperature thermochronometer are being performed.

5.2 Landscape evolution during the Cenozoic

It is evident from the available thermochronological data that rocks in the NW Iberian Massif where exhumed through the upper kilometres of the crust in relation to processes older than the initiation of convergence along the North Iberian Margin by Middle Eocene times (Srivastava *et al.*, 1990; Alvarez-Marrón *et al.*, 1997; Gallastegui, 2000). In the low relief areas of Central Galicia slow exhumation rates persisted since ~120 Ma (Tab. 6, Fig.6). The apatite (U-Th-Sm)/He data indicate that less than 1.5 km of overburden has been eroded since then at slow average denudation rates of 0.02 km/Ma across Central Galicia.

A continuous slow reduction of topography or insignificant variations of it in the region since Late Cretaceous may correspond to a time of tectonic quiescence initiated since post-rift stage. In this situation, if the denudational system reached a state of sufficiently low energy due to stabilization of base levels planation may occur at the surface (Gunnell *et al.*, 2009). This process could explain the development of a peneplain across the region since Late Cretaceous times, being the lowlands around Lugo the remains of it (Fig. 5b).

The low exhumation rates that persisted in Central Galicia have not been significantly modified during the Oligocene active faulting that caused uplift along the higher topographic areas in Northern Galicia. The modelling suggests that most samples from this northern transect cooled below 60 °C since 80 Ma ago (Fig. 6). Vertical movement along the As Pontes fault of a maximum of 455 m vertical displacement has been calculated during formation of the As Pontes basin from 30 to 22 Ma (Huerta *et al.*, 1996; Santanach *et al.*, 2005). The data indicates that this faulting episode did not modify sufficiently the previously established thermal structure possibly due to minor exhumation during that time. The preservation of the thermal structure in the upper crust during the Lutetian to Burdigalian times also indicates that the upper crust remained unaffected by any significant thermal effects in relation to incipient subduction and development of the small accretionary prism at the foot of the North Iberian Margin (Alvarez-Marrón *et al.*, 1997).

6 Conclusions

The effects of active rifting and subsequent thermal relaxation during the Mesozoic may explain the geographical pattern of cooling ages across the outcropping Iberian Massif in Galicia, NW Spain. The data and the modelling indicate that the region underwent various rates of continuous cooling in post-Variscan times, with the largest coeval with the period of Late Jurassic to Early Cretaceous rifting activity. The post-Variscan faults in the interior areas of Central Galicia were active and caused differential exhumation across fault blocks during the Early Cretaceous. The results indicate that there has not been significant exhumation or sedimentary burial across the area since 115-80 Ma. The Cenozoic convergence associated to limited southward subduction along the North Iberian Margin that caused activation of faults and uplift in North Galicia caused minor effects in the previously attained thermal structure of the upper crust. In the low relief areas of Lugo the total amount of exhumation since 80 Ma ago can be estimated to 1.5 km at an averaged rate of ~0.02 km/Ma. These low topographic areas of Lugo are considered remains of a low relief paleotopography predating the Alpine tectonism along the North Iberian Plate.

Acknowledgements

The position of R.W. Grobe was financed by the LGFG (Landesgraduiertenförderung des Landes Baden-Württemberg). This study was funded through National Plan of Research projects BTE2002-00330 and CGL2007-60230/BTE of the Spanish Ministry of Education and Science. It is included in the framework of Consolider-Ingenio 2010 nº CSD2006-00041 (TOPO-Iberia project). We thank Rosana Menéndez-Duarte, Susana Fernández- Menéndez for their kind support in planning and realization of the field work and Adolfo Castañeda-Zarauz for his assistance during data acquisition. Also we would like to thank H. Gerstenberg from the Forschungsneutronenquelle Heinz Maier-Leibnitz, Garching (FRM II) for his support. The used ASTER GDEM data is a product of METI and NASA.

References

Alvarez-Marrón, J., Hetzel, R., Niedermann, S., Menéndez, R., Marquínez, J., 2008. Origin, structure and exposure history of a wave-cut platform more than 1 Ma in age at the coast of northern Spain: a multiple cosmogenic nuclide approach. Geomorphology 93, 316-334.

Alves, T.M., Gawthorpe, R.L., Hunt, D.W., Monteiro, J.H., 2003. Post-Jurassic tectono-sedimentary evolution of the Northern Lusitanian Basin (Western Iberian Margin). Basin Research 15, 227-249.

Andeweg, B., 2002. Cenozoic tectonic evolution of the Iberian Peninsula causes and effects of changing stress fields. Ph.D. Thesis, Vrije Universiteit Amsterdam, ISBN 90-9015593-7. Netherlands Research School of Sedimentary Geology, publication no. 20020101.

Barbarand, J., Carter, A., Wood, I., Hurford, T., 2003a. Compositional and structural control of fission-track annealing in apatite. Chemical Geology 198, 107-137.

Barbarand, J., Hurford, T., Carter, A., 2003b. Variation in apatite fission-track length measurement: implications for thermal history modelling. Chemical Geology 198, 77-106.

Barrón, E., Santos, L., 1998.Critical paleobotanical synthesis of Galicia Tertiary Basins (Spain). Cuadernos de Paleontología 49, 41-53.

Burtner, R.L., Nigrini, A., Donelick, R. A., 1994. Thermochronology of Lower Cretaceaous source rocks in the Idaho-Wyoming Thrust Belt. AAPG Bull. 78: 1613-1636.

Cabral, J., 1989. An example of intraplate neotectonic activity, Vilarica basin, northeast Portugal. Tectonics 8 (2), 285-303.

Carlson, W. D., 1990. Mechanisms and kinetics of apatite fission-track annealing. Am. Mineral. 75, 1120-1139.

Carlson, W. D., Donelick, R. A., Ketcham, R. A., 1999. Variability of apatite fission-track annealing kinetics: I. Experimental results. Am. Mineral. 84, 1213-1223.

Chen, Y., Zentilli, M.A., Clark, A.H., Farrar, E., Grist, A.M., Willis-Richards, J., 1996. Geochronological evidence for post-Variscan cooling and uplift of the Carnmenellis granite, SW England. Journal of the Geological Society 153, 191-195.

Cocherie, A., 1978. Géochemie des terres rares dans le granitoides. Tesis Doctoral, Univ. Rennes. 207 p.

Crowley, K.D., 1993. Mechanisms and kinetics of apatite fission-track annealing – Discussion. Am. Min. 78, 210-212.

Crowley, K.D., Cameron, M., Schaffer, L.R., 1991. Experimental studies of annealing of etched fission tracks in fluorapatite. Geochim. Cosmochim Acta 55, 1449-1465.

Dallmeyer, R.D., Martínez-Catalán, J.R., Arenas, R., Gil Ibarguchi, J. I., Gutiérrez-Alonso, G., Farias, P., Bastida, F., Aller, J., 1997. Diachronous Variscan tectonothermal activity in the NW Iberian Massif: Evidence from 40Ar/39Ar dating of regional fabrics. Tectonophysics 277, 307-337.

Díaz, J., Gallart J., Gaspà O., Ruiz M., Córdoba D., 2008. Seismicity analysis at the Prestige oil-tanker wreck area (Galicia Margin, NW of Iberia), Marine Geology 249, 150-165.

Dobson, K.J., Olive, V., Persano, C., Stuart, F.M., 2005. A new procedure for the routine zircon (U-Th)/He age measurement. Geophys. Res. Abstr. 7, Abstract EGU05-A-06696.

Donelick, R.A., 1991. Crystallographic orientation dependence of mean etchable fission-track length in apatite: An empirical model and experimental observations. Am. Mineral. 76, 83-91.

Donelick, R.A., 1993. A method of fission track analysis utilizing bulk chemical etching of apatite. U.S. Patent #5,267,274.

Donelick, R.A., 1995. A method of fission track analysis utilizing bulk chemical etching of apatite. Australia Patent #658,800.

Donelick, R.A., Roden, M.K., Mooers, J.D., Carpenter, B.S., Miller, D.S., 1990. Etchable length reduction of induced fission tracks in apatite at room temperature, c. 23 °C. crystallographic orientation effects and "initial" mean lengths. Nucl. Tracks. Radiat. Meas. 17, 261-265.

Donelick, R.A., Ketcham, R.A., Carlson, W.D., 1999. Variability of apatite fission-track annealing kinetics: II. Crystallographic orientation effects. Am. Min. 84, 1224-1234.

Dunkl, I., 2002. Trackkey: a Windows program for calculation and graphical presentation of fission track data. Computer & Geosciences 28, 3-12.

Ehlers, T.A., Farley, K.A., 2003. (Invited), Apatite (U-Th)/He Thermochronology: methods and applications to problems in tectonics and surface processes, EPSL-Frontiers 206, 1-14.

Espina, R.G., Alonso, J.L., Pulgar, J.A, 2004. Extensión Triásica en la Cuenca Vasco-Cantábrica. In: Vera, J.A. (Ed.), Geología de España, 338-339, SGE-IGME, Madrid.

Farley, K.A., 2000. Helium diffusion from apatite: general behaviour as illustrated by Durango fluorapatite. J. Geophys. Res., 105, 2903–2914.

Farley, K.A:, Stöckli, D.F., 2002. (U-Th)/He Dating of Phosphates: Apatite, Monazite, and Xenotime. Reviews of Mineralogy and Geochemisty 48, 559-577, doi:10.2138/rmg.2002.48.15.

Farley, K.A., Wolf, R.A., Silver, L.T., 1996. The effects of long alpha-stopping distances on (U-Th)/He ages. Geochimica et Cosmochimica Acta 60 (21), 4223-4229.

Fernández, M., Marzán, I., Correia, A., Ramalho, E., 1998. Heat flow, heat production, and lithospheric thermal regime in the Iberian Peninsula. Tectonophysic 291, 29-53.

Fernández-Suárez, J. Dunning, G.R., Jenner, G.A., Gutiérrez-Alfonso, 2000b. Variscan collisional magmatism and deformation in NW Iberia: Constraints from U-Pb geochronology of granitoids. Journal of the Geological Society 157 (3), 565-576.

Fitzgerald, P.G., Baldwin, S.L., Webb, L.E. and O'Sullivan, P.P., 2006. Interpretation of (U-Th)/He single grain ages from slowly cooled crustal

terranes: a case study from the transantarctic Mountains of southern Victoria Land. Chem. Geol., 225, 91–120.

Flowers, R. M., Bowring, S. A., and Williams, M. L., 2006, Timescales and significance of high-pressure, high-temperature metamorphism and mafic dike anatexis, Snowbird tectonic zone, Canada: Contributions to Mineralogy and Petrology 151(5), 558-581.

Flowers, R.M., Ketcham, R.A., Shuster, D.L., Farley, K.A., 2009. Apatite (U–Th)/He thermochronometry using a radiation damage accumulation and annealing modelGeochimica et Cosmochimica Acta 73, 2347–2365.

Foeken, J.P.T., Stuart, F.M., Dobson, K.J., Persano, C., Vilbert, D., 2006. A diode laser system for heating minerals for (U-Th)/He chronometry. Geochemistry, Geophysics, Geosystems 7 (4), Q04015, doi:10.1029/2005GC001190.

Freudenthal, M., Martín-Suarez, E., Carballo, N., Rodriguez-Fernández, L.R., Martín-González, F., 2010. Rodents from the Lower Oligocence of the Bierzo Basin (Leon, Spain). Neues Jahrbuch für Geologie und Paläontologie-Abhandlungen 257 (3), 317-340.

Galbraith, R.F., 1981. On statistical models for fission track counts. Mathematical Geology, 13, 471-478.

Galbraith, R.F., Laslett, G.M., 1993. Statistical models for mixed fission track ages. Nucl. Tracks Radiat. Meas. 21 (4), 459-470.

Galbraith, R.F., Laslett, G.M., Green, P.F., Duddy, I.R., 1990. Apatite fission track analysis: geological thermal history analysis based on a three-dimensional random process of linear radiation damage. Philos. Trans. R. Soc. Lond., A 332, 419-438.

Gallastegui, J., 2000. Estructura Cortical de la Cordillera y Margen Continental Cantábricos: Perfiles ESCIN-N. Trabajos Geol.Univ. Oviedo, 22, 9-234.

García-Mondejar, J., Lopez-Horgue, M.A., Aranburu, A., Fernández-Mendiola, P.A., 2005. Pulsating subsidence during a rift episode: Stratigraphic and tectonic consequences (Aptian-Albian, northern Spain). Terra Nova 17 (6), 517-525.

Gleadow, A.J.W., Duddy, I.R., 1981. A natural long term track annealing experiment for apatite. Nucl. Tracks 5, 169-174.

González-Lodeiro, F., Hernández-Urroz, J., Klein, E., Martínez-Catalán, J.R., Pablo-Maciá, J.G., 1982. Mapa Geológico de España, (Escala 1:200000) Hoja de Lugo. Instituto Geológico y Minero de España, Servicio de publicaciones del Ministerio de Industria.

Green, P.F., 1981. "Track-in track" length measurements in annealed apatites. Nucl. Tracks 5, 121-128.

Green, P.F., Durrani, S.A., 1977. Annealing studies of tracks in crystals. Nucl. Track. Det. 1, 33-39.

Green, P.F., Duddy, I.R., Gleadow, A.J.W., Tingate, P.R., Laslett, G.M., 1985. Fission track annealing: track length measurements and the form of the Arrhenius plot. Nucl. Tracks 10: 323-328.

Green, P.F., Duddy, I.R., Gleadow, A.J.W., Tingate, P.R., Laslett, G.M., 1986. Thermal annealing of fission tracks in apatite, 1. A quantitative description. Chem. Geol. 59, 237-253.

Grist, A.M., Ravenhurst, C.E., 1992a. Mineral Separation Techniques used in Dalhousie University. In: Zentilli, M., Reynolds, P.H. (Eds.), Short Course on low temperature thermochronology, Min. Ass.Can. Short Course V 20, Appendix 2, 203-209.

Grist, A.M., Ravenhurst, C.E., 1992b. A Step-by-Step Laboratory guide to fission-track thermochronology at Dalhousie University. In: Zentilli, M., Reynolds, P.H. (Eds.), Short Course on low temperature thermochronology, Min. Ass.Can. Short Course V 20, Appendix 1, 190-201.

Grobe, R.W., Alavrez-Marrón, J., Glasmacher, U.A., Menéndez-Duarte, R., 2010. Low temperature exhumation history of Variscan-age rocks in the western Cantabrian Mountains (NW Spain) recorded by apatite fission-track data. Tectonophysics 489, 76-90.

Gunnell, Y., Calvet, M., Brichau, S., Carter, A., Aguilar, J.-P., Zeyen, H., 2009. Low long-term erosion rates in high-ernergy mountain belts: Insights from thermo- and biochronology in the Eastern Pyrenees. Earth and Planetary Science Letters 278, 208-218.

Haq, B.U., van Eysinga, F.W.B., 1998. Geological Time Table, 5th ed. Elsevier, Amsterdam

Huerta, A., Parés, J.M., Cabrera, L., Ferrús, B., Sáez, A., 1996. Datación magnetoestratigráfica de la cuenca terciaria de As Pontes (Galicia, NW España), Geogaceta 20, 1021-1024.

Hurford, A.J., 1990. Standardization of fission track dating calibration: recommendations by the Fission Track Working Group ofthe IUGS. Subcommission on Geochronology. Chemical Geology 80, 171-178.

Hurford, A.J., Green, P.F., 1982. A user's guide to fission track dating calibration. EPSL 59, 343-354.

Hurford, A.J., Green, P.F., 1983. The zeta age calibration of fission track dating. Isotope Geosci. 1, 285-317.

Ketcham, R.A., 2005. Forward and inverse modeling of low-temperature thermochronometry data. Reviews in Mineralogy and Geochemistry, 58, 275-314.

Ketcham, R.A., 2009. HeFTy Version 1.6.7, Manual.

Ketcham, R.A., Donelick, R.A., Carlson, W.D., 1999. Variability of apatite fission-track annealing kinetics: III Extrapolation to geological time scales. Am. Min. 84, 1235-1255.

Ketcham, R.A., Carter, A., Donelick, R.A., Barbarand, J., Hurford, A.J., 2007a. Improved measurement of fission-track annealing in apatite using c-axis projection. Am. Min. 92, 789-798.

Ketcham, R.A., Carter, A., Donelick, R.A., Barbarand, J., Hurford, A.J., 2007b. Improved modelling of fission-track annealing in apatite. Am. Min. 92, 799-810.

Ketcham, R.A., Donelick, R.A., Balestrieri, M.L., Zattin, M., 2009. Reproducibility of apatite fission-track length data and thermal history reconstruction. Earth and Planetary Science Letters 284, 504-515.

Laslett, G.M., Gleadow, A.J.W., Duddy, I.R., 1984. The relationship between fission track length and track density distributions. Nucl. Tracks 9, 29-38.

Le Pichon, X., Bonnin, J.C. Francheteau, J., Sibuet J.C., 1971. Une hypothese d'evolution tectonique du Golfe de Gascogne. In: Debysier, J., Le Pichon, X., Montadert, M. (Eds.), Histoire structurale du Golfe de Gascogne, VI.11.1-VI.11.44, Technip, Paris.

Lisker, F., Ventura, B., Glasmacher, U.A., 2009. Apatite thermochronology in modern geology. Geol. Soc. London Spec. Publ. 324, 1-23.

López-Fernández, C., Pulgar, J.A., Gallart, J., Glez-Cortina, J.M., Díaz, J., Ruiz, M., 2004. Sismicidad y tectónica en el área de Becerreá–Triacastela (Lugo, NO España). Geogaceta 36, 51–54.

Martínez-Catalán, J.R., Pérez-Estaún, A., Bastida, F., Pulgar, J.A., Marcos, A., 1990. West Asturian-Leonese Zone: Structure. In: Dallmeyer, R.D., Martínez-García, E. (Eds.), Pre-Mesozoic Geology of Iberia, 103–114, Springer-Verlag.

Martínez-Catalán, J.R., Arenas, R., Díez Balda, M.A., 2003. Large extensional structure developed during emplacement of a crystalline thust sheet: the Mondoñedo nappe (NW Spain). Journal of Structural Geology 25, 1815-1839.

Martínez-Catalán, J.R., Arenas, R., Díaz-García, F., González-Cuadra, P., Gómez-Barreiro, J., Abati, J., Castiñeiras, P., Fernández-Suárez, J., Sánchez Martínez, S., Andonaegui, P., González Clavijo, E., Díez Montes, A., Rubio Pascual, F.J., and Valle Aguado, B., 2007. Space and time in the tectonic evolution of the northwestern Iberian Massif: Implications for the Variscan belt. Hatcher, R.D., Jr., Carlson, M.P., McBride, J.H., Martínez-Catalán, J.R. (Eds.), 4-D Framework of Continental Crust: Geological Society of America Memoir 200, 403–423.

Martínez-García, E., Antona, J.F., García-Sanchez, A., Quiroga de la Vega, J.L., 2004. Tectonics and metallogenic significance of sedimentary manganese deposits in the eastern Cantabrian Domain, Asturias, northwestern Spain. International Geology Review 46 (3), 273-288.

Meesters, A.G.C.A., Dunai, T.J., 2005. A noniterative solution of the (U-Th)/He equation. Geochemistry, Geophysics, Geosystems 6, Q04002.

Montadert, L., Roberts, D.G., De Charpal, O., Guennoc, P., 1979. Rifting and subsidence of the northern continental margin of the Bay of Biscay. Initial reports of the Deep Sea Drilling Project, Leg 48, 1025-1060.

O'Sullivan, P.B., Parrish, R.R., 1995. The importance of apatite composition and single-grain ages when interpreting fission track data from plutonic rocks: a case study from the Coast Ranges, British Columbia. EPSL 132, 213-224.

Pérez-Estaún, A., Bastida, F., Alonso, J.L., Marquínez, J., Aller, J., Alvarez-Marrón, J., Marcos, A., Pulgar, J.A., 1988. A thin-skinned tectonic model for an arcuate fold and thrust belt: Cantabrian Zone. Tectonics 7 (3), 517-537.

Pérez-Estaún, A., Bastida, F., Martínez-Catalán, J.R., Gutiérrez-Marco, J.C., Marcos, A., and Pulgar, J.A., 1990. West Asturian–Leonese Zone: stratigraphy. In: R.D. Dallmeyer and E. Martínez-García (Eds.), Pre-Mesozoic Geology of Iberia, 92-102, Springer-Verlag.

Pérez-Estaún, A., Martínez-Catalán, J.R., Bastida, F., 1991. Crustal thickening and deformation sequence in the footwall to the suture of the Variscan belt of northwest Spain. In: Pérez-Estaún A., Coward, M.P. (Eds.), Deformation and Plate Tectonics, Tectonophysics 191, 243-253.

Persano, C., Stuart, F.M., Bishop, P., Barfod, D.N., 2002. Apatite (U-Th)/He age constraints on the development of the Great Escarpment on the southeastern Australian passive margin. EPSL 200, 79-90.

Pulgar, J., Gallart, J., Fernández-Viejo, G., Pérez-Estaún, A., Alvarez-Marrón, J., and ESCIN Group, 1996. Seismic image of the Cantabrian Mountains uplift in the western extension of the Pyrenean Belt from integrated ESCIN reflection and refraction data. Tectonophysics 264, 1-20.

Rasmussen, E.S., Lomholt, S., Andersen, C., Vejbaek, O.V., 1998. Aspects of the structural evolution of the Lusitanian Basin in Portugal and the shelf and slope area offshore Portugal. Tectonophysics 3000, 199-225.

Reiners, P.W., Ehlers, T.A. (Eds). 2005. Low-temperature thermochronology: techniques, interpretations, and applications. Reviews in Mineralogy and Geochemistry 58, v-ix, 1-622.

Reiners, P.W., Farley, K.A., 2001. Infuence of crystal size on apatite (U-Th)/He thermochronology: an example from the Bighorn Mountains, Wyoming. Earth and Planetary Science Letters 188, 413-420.

Rodríguez-Fernández, L.R., 2004. Mapa Geológico de España (Escala 1:200.000), In: Vera, J.A. (Ed.), Geología de España, SGE-IGME, Madrid

Rodríguez-García, A., Quintana, L., González-Menéndez, L., Suárez-Rodríguez, A., 2006. Neotectónica en el norte de Galicia: Fallas inversas de actividad cuarternica en la cuenca fluvial del alveolo de Alfoz, Lugo. Geogaceta 40, 23-26.

Rosenbaum, G., Lister, G.S., Duboz, C., 2002. Relative motions of Africa, Iberia and Europe during Alpine orogeny, Tectonophysics 359, 117-129.

Santanach, P., Ferrús, B., Cabrera, L., Sáez, A., 2005. Origin of a restraining bend in an evolving strike-slip system: The Cenozoic As Pontes basin (NW Spain). Geologica Acta 3 (3), 225-239.

Shuster, D.L., Farley, K.A., 2009. The influence of artificial radiation damage and thermal annealing on helium diffusion kinetics in apatite. Geochimica et Cosmochimica Acta 73, 183–196.

Shuster, D.L., Flowers, R.M., Farley, K.A., 2006. The influence of natural radiation damage on helium diffusion kinetics in apatite. EPSL 249, 148-161.

Sobel, E.R., Seward, D., 2010. Influence of etching conditions on apatite fission-track etch pit diameter. Chemical Geology 271, 59-69.

Srivastava, S.P., Roest, W.R., Kovacs, L.C., Oakey, G., Lévesque, S., Verhoef, J., Macnab, R., 1990. Motion of Iberia since the Late Jurassic: Results from detailed aeromagnetic measurements in the Newfoundland Basin; Tectonophysics 184, Issues 3-4, 229-260.

Stampfli, G.M., Borel, G.D., 2002. A plate tectonic model for Paleozoic and Mesozoic constrained by dynamic

plate boundaries and restored synthetic oceanic isochrones. EPSL 196 (1-2), 17-33.

Stöckli, D.F., Farley, R.A., Dumitru, T.A., 2000. Calibration of the apatite (U-Th)/He thermochronometer on an exhumed fault block, White Mountains, California. Geology 28 (11), 983-986.

Verhoef, J., Srivastava, S.P., 1989. Correlation of sedimentary basins across the North Atlantic as obtained from gravity and magnetic data, and its relation to the early evolution of the North Atlantic. In: Tankard, A.J., Balkwill, H.R. (Eds.), Extensional tectonics and stratigraphy of the North Atlantic margins, AAPG Memoir 46, 131-147.

Wagner, G.A., 1972. Spaltspurenalter von Mineralen und natürlichen Gläsern: eine Übersicht. Fortschr. Miner. 49, 114-145.

Wagner, G.A., van den Haute, P., 1992. Fission-Track Dating. In: Enke Verlag - Kluwer Academic Publishers, p. 285.

Wolf, R.A., Farley, K.A. and Silver, L.T. 1996. Helium diffusion and low-temperature thermochronometry of apatite. Geochimica et Cosmochimica Acta 60, 4231-4240.

Wolf, R.A., Farley, K.A. and Kass, D.M. 1998. Modeling of the temperature sensitivity of the apatite (U-Th)/He thermochronometer. Chemical Geology 148, 105-114.

Ziegler, P.A., 1989. Evlution of the North Atlantic-Overiview. In: Tankard, A.j., Balkwill, H.R. (Eds.), Extensional Tectonics and Stratigraphy of the North Atlantic Margins: AAPG Memoir 46, 11-130.

Ziegler, P.A., Roure, F., 1999. Petroleum systems of Alpine-Mediterranean foldbelts and basins. Geological Society Special Publication 156, 517-540.

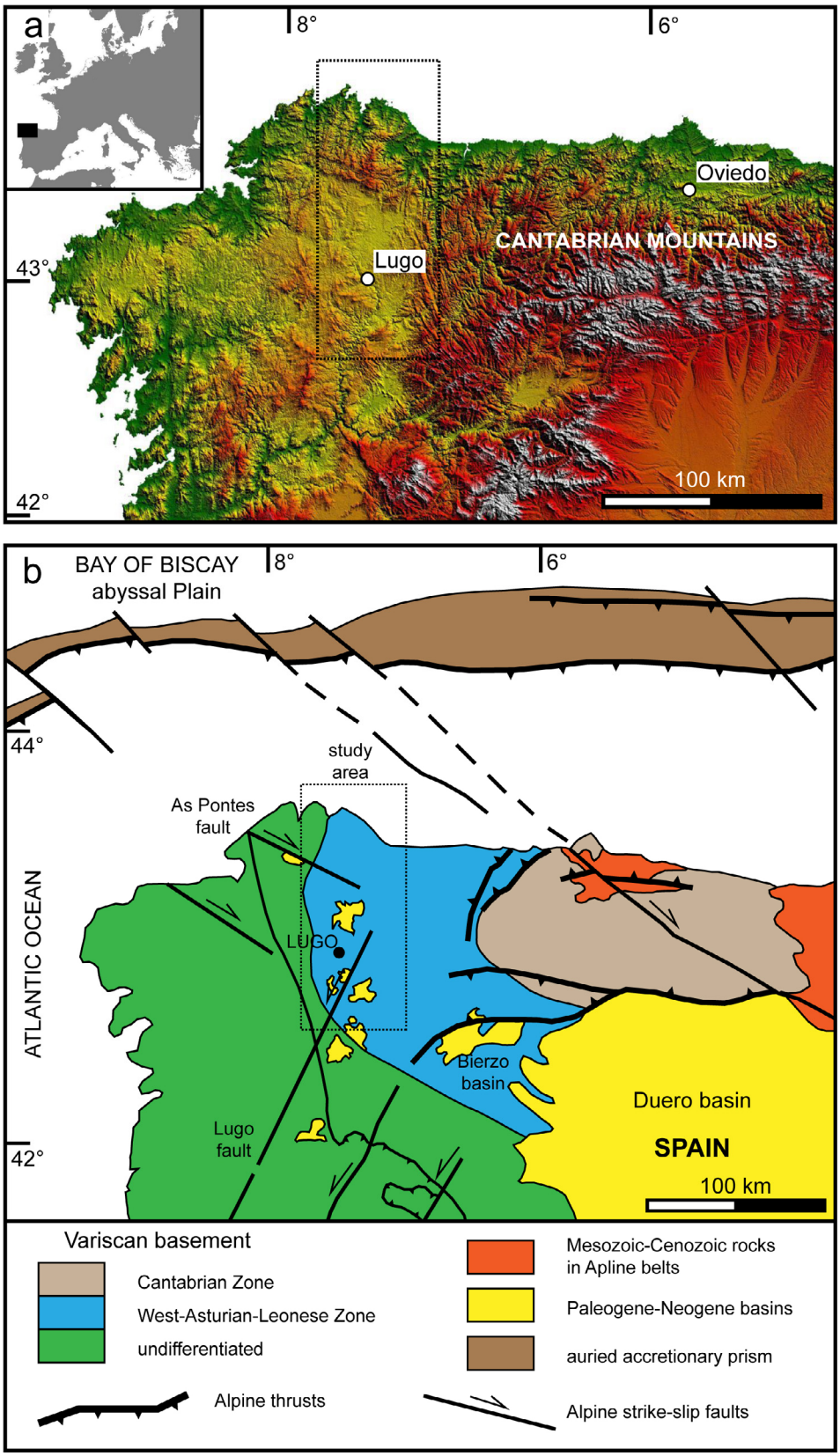

Figure 1: (a) Overview digital elevation model (ASTER GDEM) with the location of the study area at the western termination of the Cantabrian Mountains along the northern coast of Spain. (b) Geological overview map of the northwestern Iberian coast. Dashed rectangle shows the location of the study area in the West-Asturian-Leonese Zone. Major Alpine structures as well buried accretionary prism developed during Cenozoic convergence are highlighted.

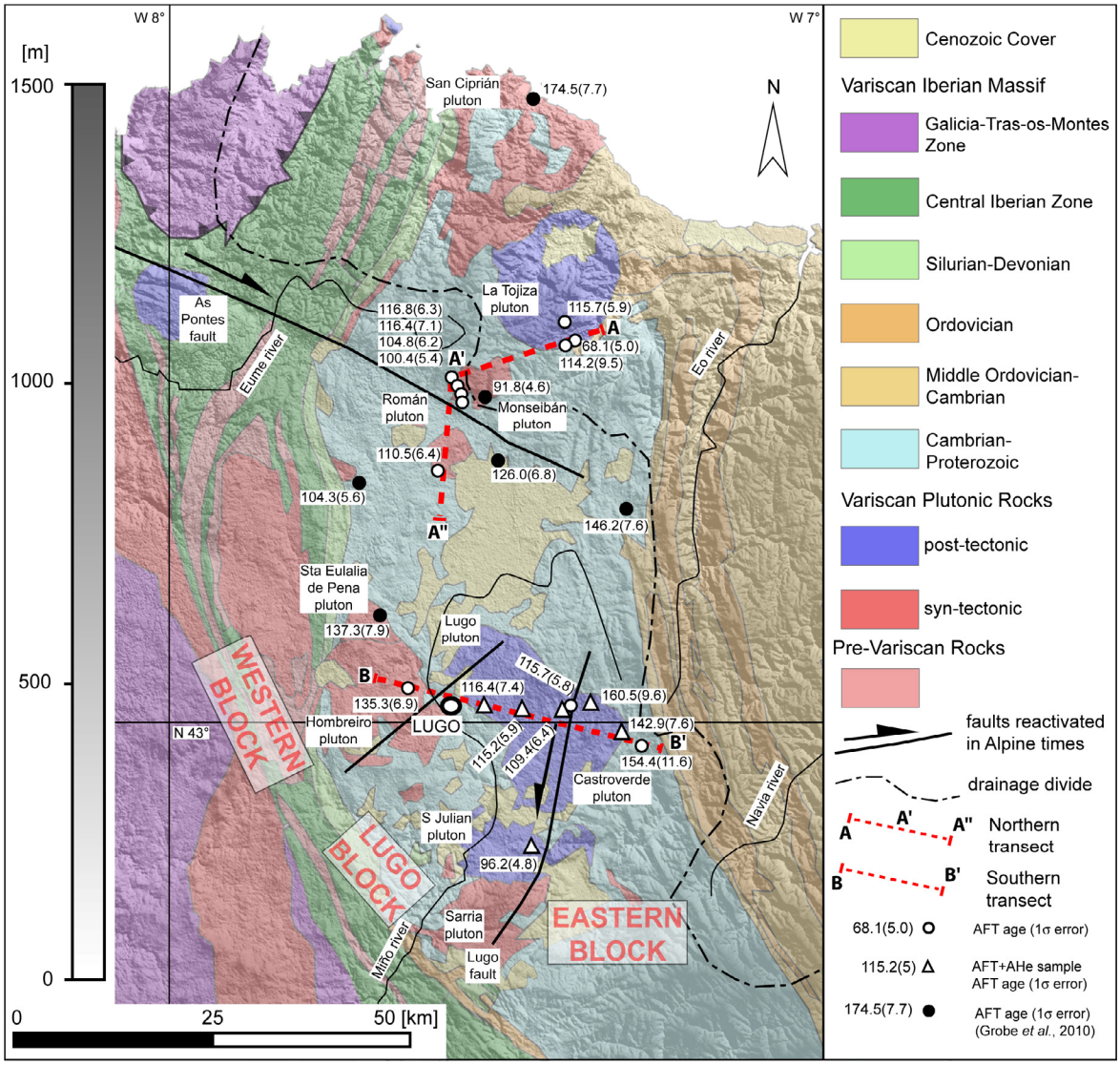

Figure 2: DEM showing the topography of the study area with a transparent colored overlay of the geology together with sample locations, names of Varsican plutons and major Alpine structures. Thin black lines are rivers and wide dashed line marks the drainage divide. Red dashed lines mark the location of topographic transects (geological map redrafted from Rodríguez-Fernández, 2004).

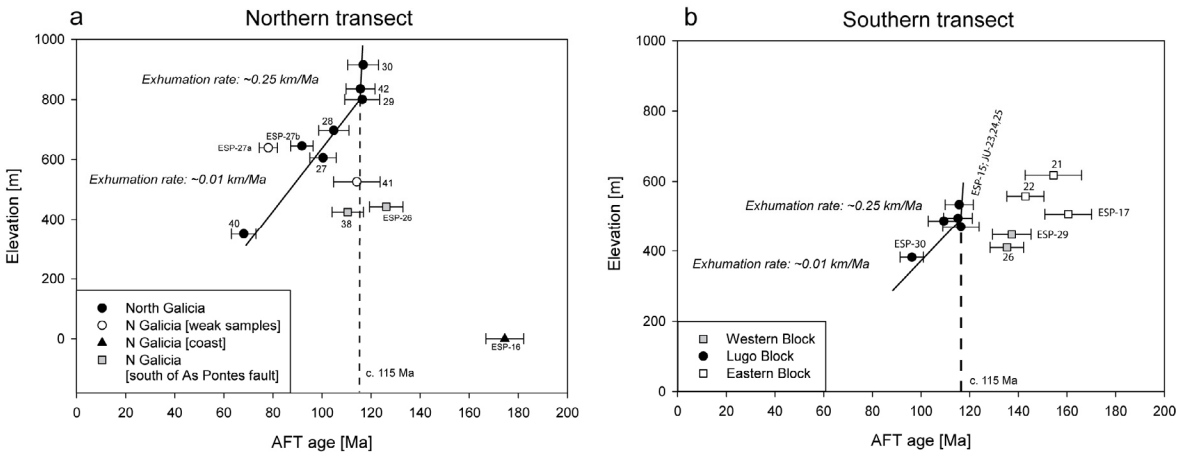

Figure 3: (a) Age-elevation relationship plot (error bars: 1σ error) including all samples from northern transect. Includes samples ESP-16, 26, 27a, b from Grobe *et al.* (2010). (b) Age-elevation relationship plot (error bars: 1σ error) with the samples from the southern transect. Includes samples ESP-15, 17, 29, 30 from Grobe *et al.*, (2010). Black line: regression lines drawn by eye through selected samples. Dashed line marks 115 Ma considering the age of continental break-up and initiation of seafloor spreading in the Atlantic and Bay of Biscay margins (Srivastava *et al.*, 1990).

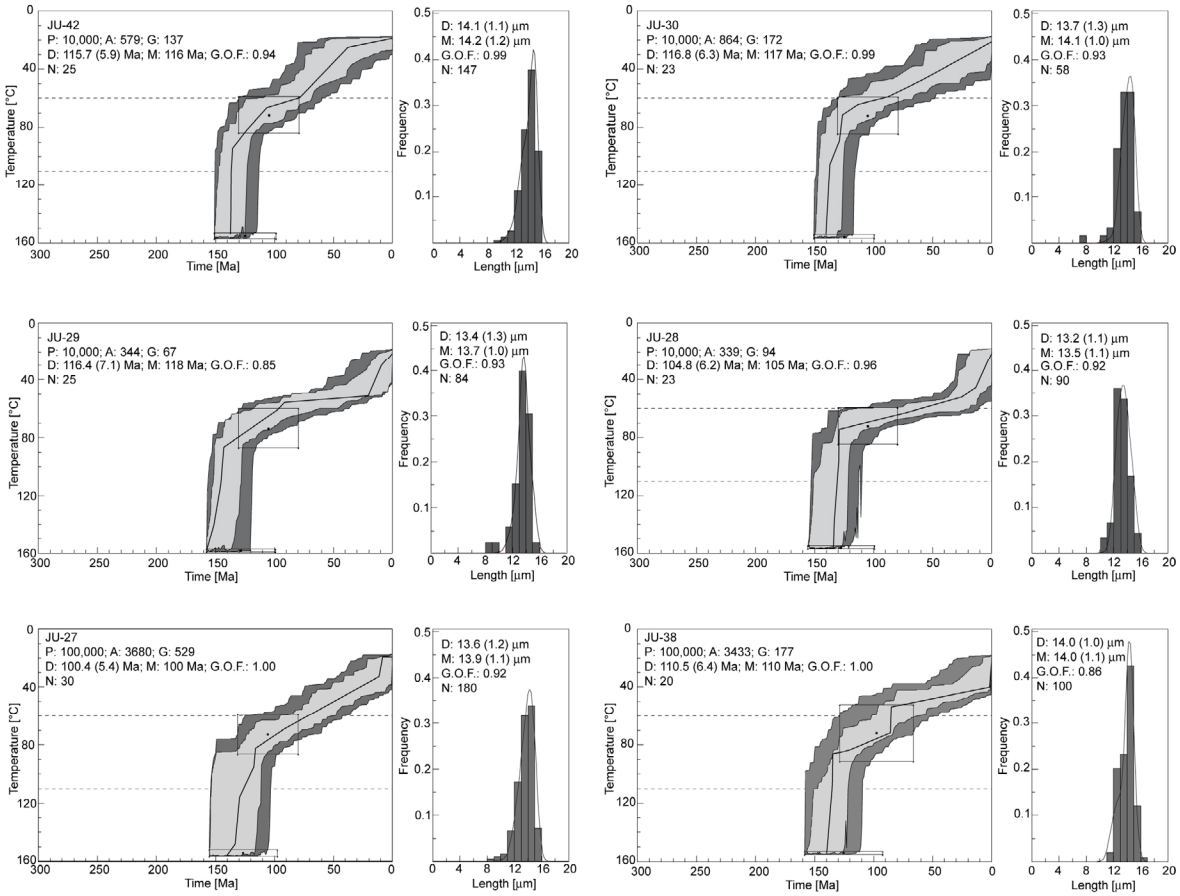

Figure 4: (a) Results of the numerical modelling of samples from the northern transect. Order according to appearance of samples from N to S. Modelling is done using the computer code HeFTy© (Ketcham, 2005; Ketcham *et al.*, 2007a; b; Ketcham *et al.*, 2009). Displayed are the t-T paths (left) and the c-axis corrected confined fission-track length (cC-FT-L) distribution (right) overlain by a calculated probability density function (best fit). The results in the t-T curve show three different reliability levels (dark grey envelope: acceptable fit = all t-T paths with a goodness of fit (G.O.F.) of > 0.05 (5%), light grey envelope: good fit = all t-T paths with a G.O.F. of > 0.5 (50%), black line: best fit. P: number of tested inverse models, A: acceptable fit models, G: good fit models, D: determined FT-age (1σ error) and cC-FT-L, M: modelled FT-age and cC-FT-L, G.O.F.: goodness of fit of best fit model, N: number of single grains and measured confined fission-track lengths.

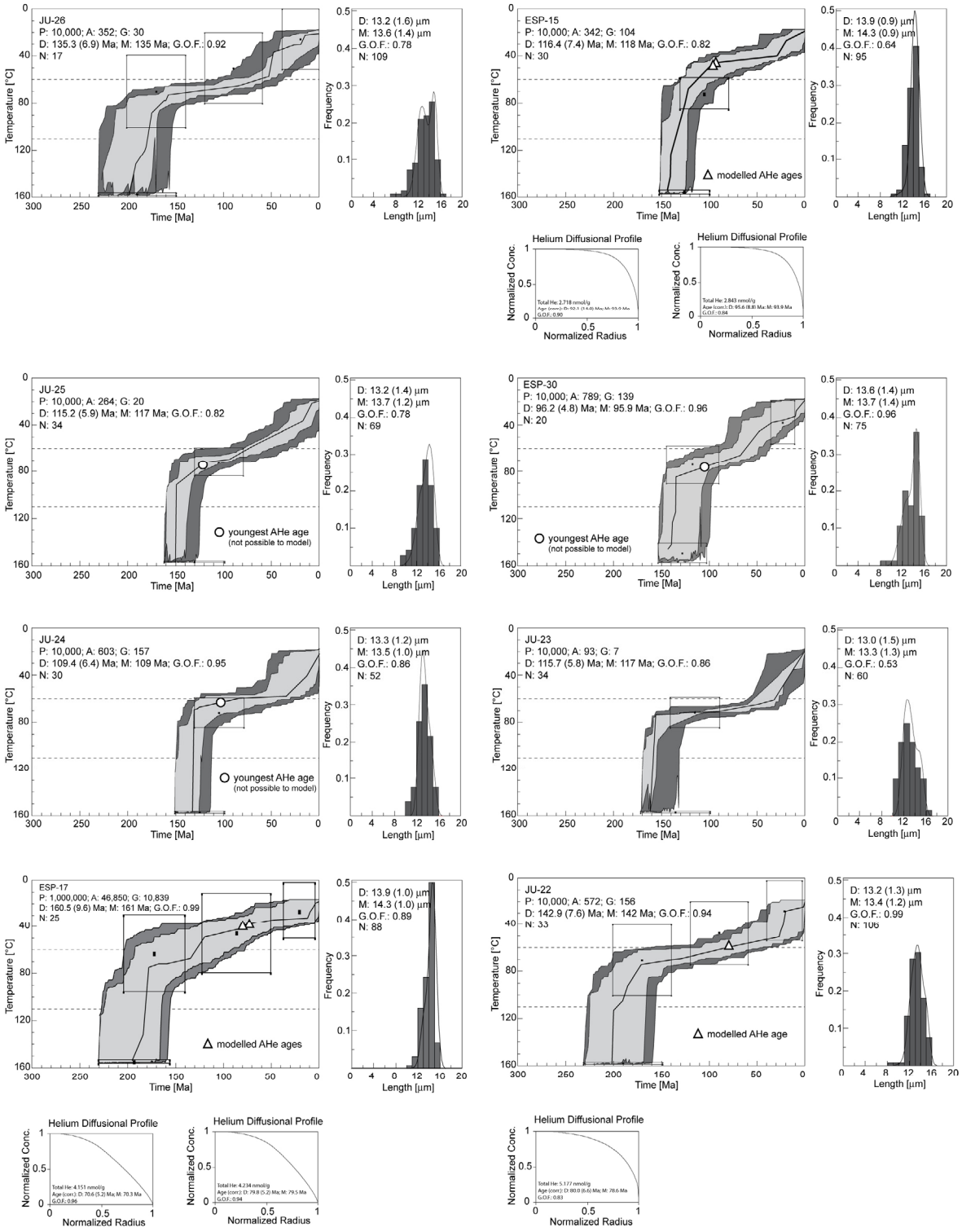

Figure 4: (b) Results for the thermal modelling of samples from the southern transect. Order according to appearance of samples from W to E. For samples where AHe ages could be modelled the Helium diffusion profile is given for each modelled grain. (see (a) for further details of the models).

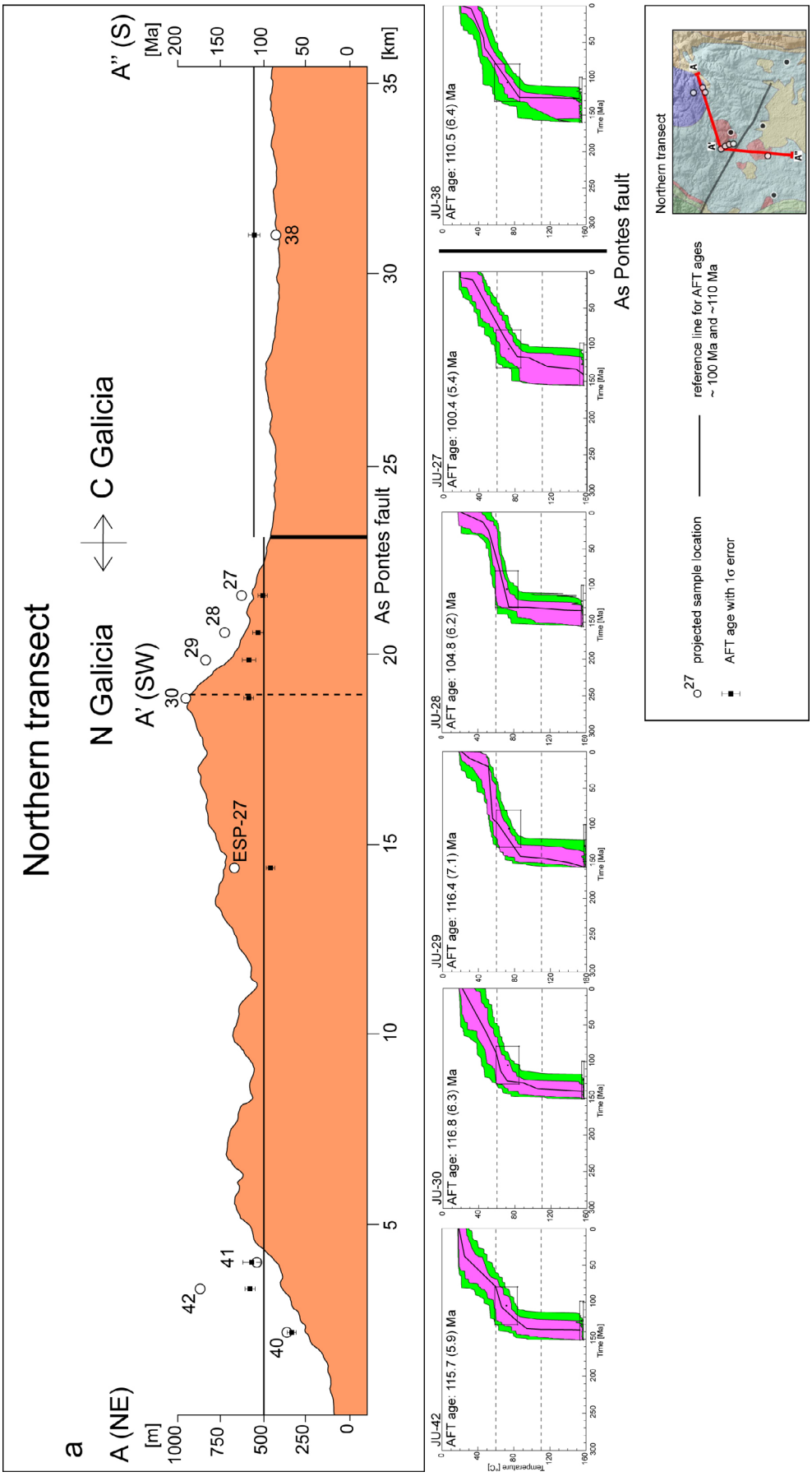

Figure 5: a) NE-SW/N-S topographic transect (A-A'-A'') across North Galicia with indication of projected sample location and AFT ages. A reference line at 100 Ma and 110 Ma intenc the variation in AFT ages across the As Pontes fault. t-T path models beneath the transect.

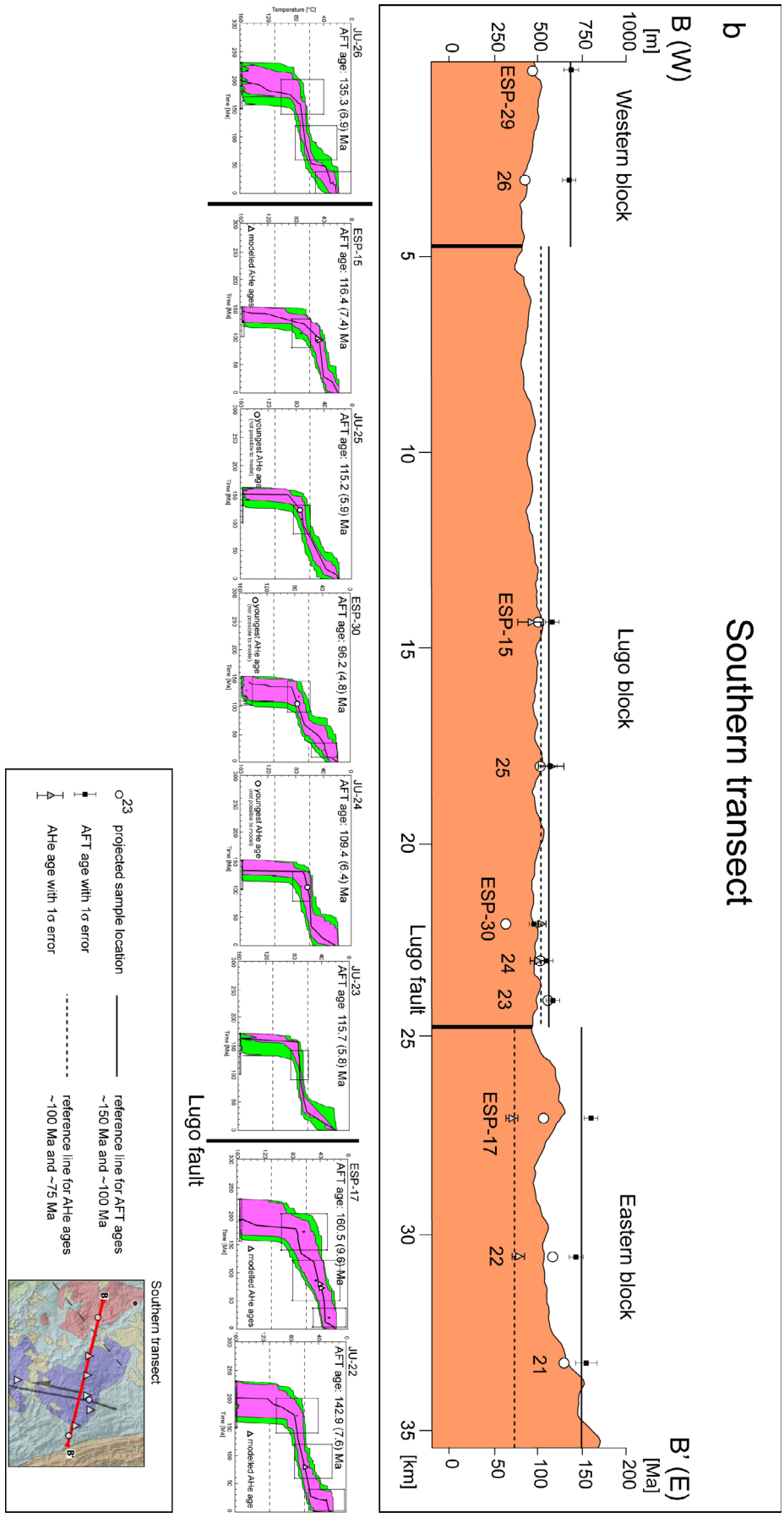

Figure 5: b) W-E topographic transect in Central Galicia (B-B') with indication of projected sample location as well as AFT and AHe ages. Reference solid lines indicate AFT ages near 150 Ma in the Eastern fault block, near 100 Ma in the Lugo block and slightly younger than 150 Ma in the western block. The dashed line indicates younger AHe ages across the Eastern block than in the Lugo block.

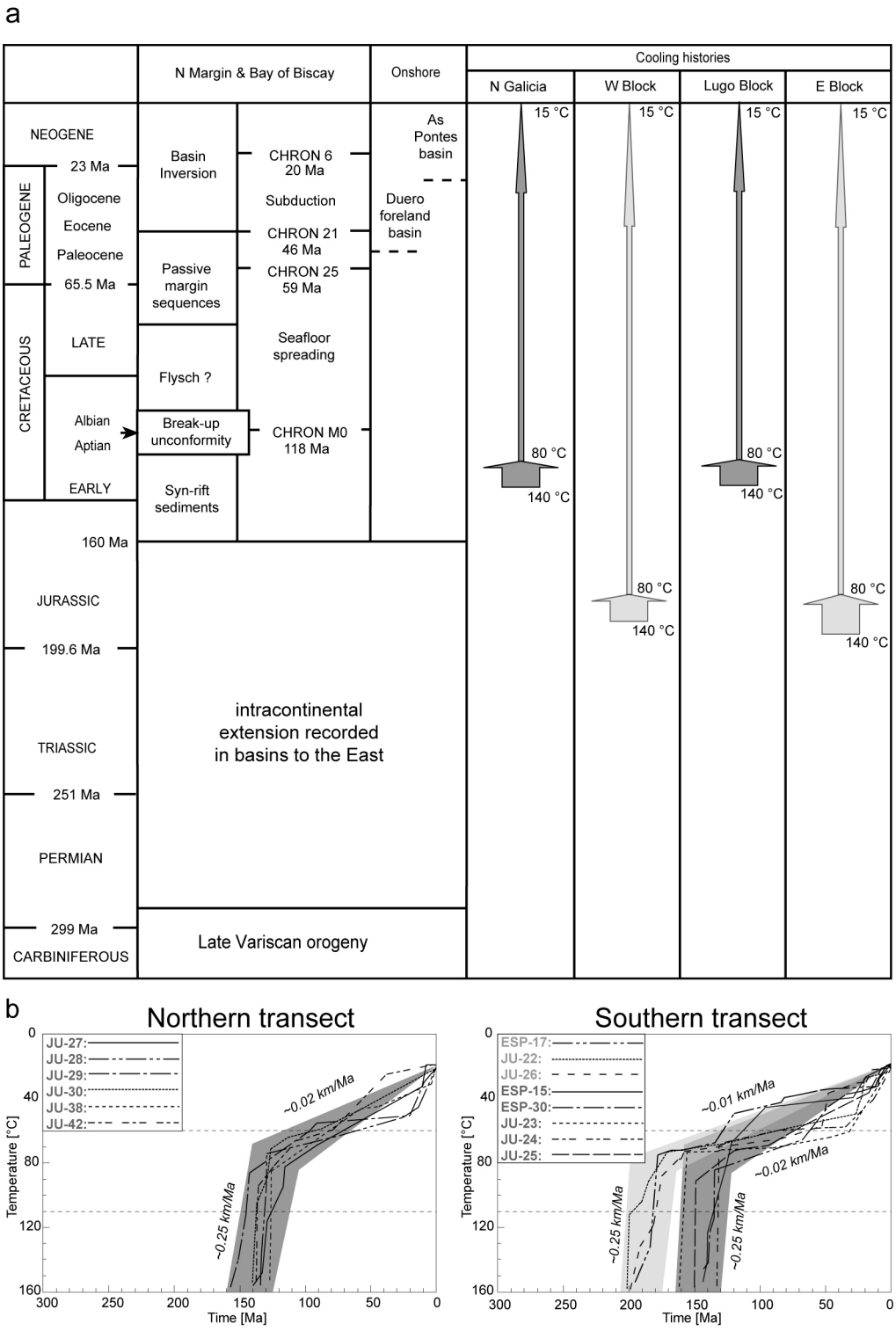

Figure 6: (a) Cooling histories combined with tectonic events (text for references on event ages; time-scales of Haq and van Eysinga (1998)) Cooling histories are grouped in 1) North Galicia; 2) Western block; 3) Lugo block; 4) Eastern block. Arrows: cooling histories of blocks compared to tectonic events. (b) Compilations of best fit cooling paths for the northern and southern transect. Grey envelopes highlight the common cooling history with calculated average exhumation rates (Tab. 6) for different segments.

Table 1
Published geochronological data of several granitoids and rocks from the WALZ

Pluton Name (Sample Name)	Lithology	Age [Ma]	Dating Method	Reference
Vivero (VGI-20)	synk. calc-alkaline	323 +9/-5	U-Pb (zircon-monazite)	Fernández-Suárez et al., 2000b
Vivero (VGI-20)	synk. calc-alkaline	323	Pb-Pb (monazite)	Fernández-Suárez et al., 2000b
Vivero (VGI-20)	synk. calc-alkaline	295 ± 2	U-Pb (monazite)	Fernández-Suárez et al., 2000b
San Ciprián (VIV-7)	synk. leucogranite	286 ± 2	U-Pb (monazite)	Fernández-Suárez et al., 2000b
San Ciprián (VIV-7)	synk. leucogranite	318	Pb-Pb (zircon)	Fernández-Suárez et al., 2000b
San Ciprián (WALZ-4)	synk. leucogranite	274.1 ± 0.7	$^{40}Ar/^{39}Ar$ (muscovite)	Dallmeyer et al., 1997
La Tojiza (TOJ-5)	postk. calc-alkaline	295 ± 2	U-Pb (zircon-monazite)	Fernández-Suárez et al., 2000b
La Tojiza (WALZ-6)	postk. calc-alkaline	283.8 ± 0.7	$^{40}Ar/^{39}Ar$ (muscovite)	Dallmeyer et al., 1997
Castroverde	postk. calc-alkaline	287	Rb-Sr (whole rock)	Cocherie, 1978
Sarria (SA-4)	synk. leucogranite	313 ± 2	U-Pb (monazite)	Fernández-Suárez et al., 2000b
Sarria (WALZ-1)	synk. leucogranite	282.2 ± 0.8	$^{40}Ar/^{39}Ar$ (muscovite)	Dallmeyer et al., 1997
WALZ-2 near ESP-26	Precambrian shist	298.2 ± 0.6	$^{40}Ar/^{39}Ar$ (muscovite)	Dallmeyer et al., 1997

synk.: syn-kinematic, postk.: post-kinematic.

Table 2
Published apatite fission-track ages from the WALZ

Sample	Elevation [m a.s.l.]	N Latitude	W Longitude	Lith.	Pluton	Central age [Ma]	Error ± 1σ [Ma]	Reference
North Galicia								
ESP-16	0	43°41'49.7"	7°26'25.2"	synk-gr	San Ciprián	174.5	7.7	Grobe et al., 2010
ESP-27a	639	43°21'57.8"	7°30'55.0"	synk-fr-gr	Monseibán	78.1	3.7	Grobe et al., 2010
ESP-27b	645	43°22'00.2"	7°30'57.8"	synk-gr	Monseibán	91.8	4.6	Grobe et al., 2010
Central Galicia								
ESP-15	470	43°01'02.6"	7°30'55.5"	postk-gr	Lugo	116.4	7.4	Grobe et al., 2010
ESP-17	507	43°01'10.9"	7°21'12.3"	postk-gr	Castroverde	160.5	9.6	Grobe et al., 2010
ESP-25	524	43°14'22.9"	7°17'57.7"	LC-msd		146.2	7.6	Grobe et al., 2010
ESP-26	443	43°17'33.1"	7°29'40.7"	PC-msd		126.0	6.8	Grobe et al., 2010
ESP-28	544	43°16'05.2"	7°42'29.5"	fo-gr		104.3	5.6	Grobe et al., 2010
ESP-29	447	43°07'14.2"	7°40'32.8"	synk-gr	Sta. Eulalia de Pena	137.3	7.9	Grobe et al., 2010
ESP-30	382	42°53'42.9"	6°23'02.8"	postk-gr	S. Julian	96.2	4.8	Grobe et al., 2010
FG-1	470	-	-	postk-gr	Lugo	131.4	6.7	Martín-González et al., 2008

synk.: syn-kinematic, postk.: post-kinematic, gr.: granite, msd.; meta-sandstone, fo-gr.: foliated granite, LC: Lower-Cambrian, PC: Proterozoic-Cambrian.

Table 3
Apatite fission-track results.

Sample	Elev. [m a.s.l.]	N Latitude	W Longitude	Lith.	Pluton	Form. age [Ma]	U (std) [μg/g]	n	Sp. Tracks ρ_s [10^5 tr/cm^2]	Sp. Tracks N_s	Ind. Tracks ρ_i [10^5 tr/cm^2]	Ind. Tracks N_i	$P(\chi^2)$ [%]	Central age [Ma]	Error ± 1σ [Ma]
North Galicia															
JU-27	606	43°21'51"	7°33'48"	gr	Monseibán	synk-va	29.9 (13.4)	21	14.3	2362	32.2	5312	26.5	100.4	5.4
JU-28	697	43°22'29"	7°33'54"	gr	Monseibán	synk-va	34.3 (9.3)	23	17.3	1364	37.3	2938	13.1	104.8	6.2
JU-29	800	43°22'51"	7°34'04"	gr	Monseibán	synk-va	18.8 (6.8)	25	10.6	976	20.4	1885	86.1	116.4	7.1
JU-30	915	43°23'19"	7°34'26"	gr	Monseibán	synk-va	24.7 (7.4)	23	13.4	2077	25.6	3986	41.2	116.8	6.3
JU-38	425	43°17'02"	7°36'00"	gr	Román	synk-va	24.2 (11.6)	20	11.5	1631	25.6	3618	13.1	110.5	6.4
JU-40	350	43°25'57"	7°23'08"	gr	La Tojiza	pok-va	6.4 (3.4)	17	2.1	399	7.6	1426	79.4	68.1	5.0
JU-41	526	43°25'39"	7°24'18"	gr	La Tojiza	pok-va	18.5 (14.4)	5	8.0	305	17.0	642	81.1	114.2	9.5
JU-42	835	43°27'09"	7°24'18"	gr	La Tojiza	pok-va	21.5 (6.9)	25	11.8	3630	24.3	7501	46.8	115.7	5.9
Central Galicia															
JU-21*	618	42°58'37"	7°17'23"	sl	-	LC	11.9 (8.0)	14	9.3	444	14.5	688	99.2	154.4	11.6
JU-22*	558	42°59'22"	7°19'10"	gr	Castroverde	pok-va	11.6 (4.2)	33	8.2	1823	13.8	3061	99.8	142.9	7.6
JU-23*	534	43°01'18"	7°23'31"	gr	Castroverde	pok-va	17.1 (8.2)	34	9.6	2649	19.9	5516	97.9	115.7	5.8
JU-24	487	43°00'52"	7°24'21"	gr	Castroverde	pok-va	15.6 (4.2)	30	8.1	1298	16.8	2687	23.6	109.4	6.4
JU-25*	495	43°01'00"	7°28'09"	grd	Lugo	pok-va	16.1 (4.5)	34	9.5	2084	19.9	4368	95.9	115.2	5.9
JU-26*	410	43°02'36"	7°38'47"	gr	Hombreiro	synk-va	44.5 (19.6)	17	29.9	3065	53.3	5458	17.5	135.3	6.9

Geodetic reference system of coordinates: WGS 84, Lith.: lithology, U: Uranium concentration, std: standard deviation, n: number of apatite grains, ρs: density of spontaneous tracks, Ns: number of spontaneous tracks, ρi: density of induced tracks, Ni: number of induced tracks, $P(\chi^2)$: probability that single grain ages are consistent and belong to the same population. Test is passed if $P(\chi^2) > 5\%$ (Galbraith, 1981), Nd = 15555 tracks counted on CN5 dosimeter glass. Ages are calculated using a ζ -value of 341.41 (15.48). Samples marked with "*": Nd = 15386, ζ-value of 340.59 (14.68). gr: granite, sl: slate, grd: granodiorite, synk-va: syn-kinematic Variscan granite, pok-va: post-kinematic Variscan granite, LC: Lower-Cambrian.

Table 4
Detailed apatite fission-track length data.

Sample	n CT	M.-l. (std) [µm]	Stdev [µm]	CT skew factor	Lc (std) [µm]	Stdev [µm]	Lc skew factor	n D_{par}	D_{par} [µm]	Stdev [µm]	D_{par} skew factor
North Galicia											
JU-27	180	11.8	1.9	-1.14	13.6	1.2	-1.11	346	1.3	0.1	1.40
JU-28	90	11.0	1.7	-0.35	13.2	1.1	-0.15	260	1.3	0.1	-0.30
JU-29	84	11.6	1.9	-1.36	13.4	1.3	-1.59	305	1.3	0.1	4.30
JU-30	58	12.2	1.7	-1.54	13.7	1.3	-2.59	175	1.3	0.1	0.60
JU-38	100	12.4	1.5	-0.44	14.0	1.0	-0.30	294	1.4	0.1	5.80
JU-40	n.a.	n.a.	n.a.	n.a.	11.7	1.9	n.a.	84	1.4	0.1	0.30
JU-41	n.a	n.a.	n.a.	n.a.	n.a.	n.a.	n.a.	25	1.4	0.1	0.00
JU-42	147	12.6	1.8	-1.14	14.1	1.1	-0.98	135	1.5	0.1	-0.40
Central Galicia											
JU-21	36	11.4	2.0	-1.56	13.3	1.2	0.24	150	1.6	0.1	1.50
JU-22	106	11.4	1.9	-0.30	13.2	1.3	-0.64	396	1.5	0.1	0.49
JU-23	60	10.7	2.6	-0.17	13.0	1.5	0.19	362	1.4	0.1	4.87
JU-24	52	11.6	1.5	0.07	13.3	1.2	-0.25	269	1.2	0.1	-0.70
JU-25	69	11.4	2.0	-0.57	13.2	1.4	-0.46	382	1.3	0.1	0.60
JU-26	109	11.6	2.2	-0.41	13.2	1.6	-0.79	100	1.5	0.1	0.80

n CT: number of confined tracks measured, M.-l.: mean track length, std: standard deviation, skew.: skewness of distribution relative to the mean value (measure of asymmetry of the distribution), Lc: mean track length after c-axis correction, n Dpar: number of etch pit diameters measured, Dpar: mean eatch pit diameter.

Table 5
Apatite (U-Th-Sm)/He data

Sample	m	Eq. SV Sphere Radius	F_t	U	U Error	Th	Th Error	Sm	$_4$He	$_4$He Error	TAE	Th/U	eU	Raw age	Error	Corr. Age	Error
	[µg]	[µm]		[µg/g]	[%]	[µg/g]	[%]	[µg/g]	[nmol/g]	[%]	[%]		[µg/g]	[Ma]	± 1σ [Ma]	[Ma]	± 1σ [Ma]
ESP-15a	3.0	49.57	0.70	5.6	6.6	9.9	6.2	b.d.l.	2.90	1.3	9.1	1.8	7.9	67.43	6.14	95.6	8.7
b	4.0	57.56	0.74	12.9	4.0	18.0	3.7	b.d.l.	6.92	1.3	5.6	1.4	17.1	74.04	4.15	99.0	5.6
c	2.7	51.63	0.71	9.0	4.6	13.3	5.1	b.d.l.	4.85	1.3	7.0	1.5	12.1	73.45	5.11	102.2	7.1
d	3.0	51.92	0.71	6.2	5.9	11.1	6.0	b.d.l.	3.45	1.3	8.5	1.8	8.8	71.97	6.12	100.2	8.5
e	0.9	34.85	0.57	7.9	6.4	4.5	13.7	b.d.l.	2.69	1.3	15.2	0.6	9.0	55.02	8.35	***92.1***	***14.0***
															Mean	**97.8**	**4.0**
															Wt mean	**99.0**	**3.5**
															most represantative age	**95.6**	**8.7**
ESP-17a	1.3	35.65	0.58	15.4	4.4	11.5	5.8	b.d.l.	4.21	1.3	7.4	0.7	18.1	42.61	3.16	***70.6***	***5.2***
b	0.6	29.69	0.50	18.3	7.7	26.1	10.0	b.d.l.	8.24	1.3	12.7	1.4	24.4	61.94	7.86	118.6	15.0
c	0.8	32.94	0.54	14.4	7.8	24.0	9.4	b.d.l.	7.57	1.3	12.3	1.7	20.0	69.22	8.50	122.6	15.1
d	1.1	36.56	0.59	14.3	5.4	20.5	7.4	b.d.l.	6.37	1.3	9.2	1.4	19.1	61.05	5.62	100.6	9.3
e	2.0	43.54	0.66	10.3	4.6	19.2	4.3	b.d.l.	4.27	1.3	6.5	1.9	14.8	53.07	3.43	79.8	5.2
															Mean	**98.4**	**23.0**
															Wt mean	**82.6**	**3.3**
															most represantative age	**76.6**	**4.2**
ESP-30a	1.3	45.00	0.67	31.6	2.9	6.6	5.4	b.d.l.	17.88	1.3	6.2	0.2	33.2	98.35	6.12	142.5	8.9
b	0.6	43.75	0.66	37.4	3.1	78.1	2.3	b.d.l.	21.00	1.3	4.1	2.1	55.7	69.00	2.80	***103.7***	***4.2***
c	0.8	45.00	0.67	40.3	3.4	11.5	8.9	b.d.l.	27.99	1.3	9.6	0.3	43.0	118.55	11.38	171.8	16.5
d	1.1	71.21	0.79	22.2	3.0	6.4	4.2	b.d.l.	15.43	1.3	5.3	0.3	23.7	118.80	6.31	148.0	7.9
															Mean	**141.5**	**28.2**
															Wt mean	**120.0**	**3.4**
															most represantative age	**111.8**	**3.8**
JU-22b	5.6	59.34	0.75	18.0	3.6	23.9	2.9	b.d.l.	14.30	1.3	4.8	1.3	23.6	110.52	5.28	146.1	5.7
c	1.8	43.98	0.66	14.6	5.7	14.8	5.7	b.d.l.	5.31	1.3	8.2	1.0	18.0	53.94	4.42	***80.0***	***6.6***
d	2.2	46.67	0.68	15.3	3.6	20.4	3.2	b.d.l.	7.13	1.3	5.0	1.3	20.1	65.08	3.24	94.3	4.7
e	1.0	35.69	0.58	16.9	5.4	29.6	6.3	b.d.l.	9.06	1.3	8.3	1.8	23.9	69.47	5.80	116.6	9.7
f	2.4	47.21	0.68	16.3	3.9	22.1	4.2	b.d.l.	11.82	1.3	5.8	1.4	21.5	100.38	5.84	144.6	8.4
															Mean	**116.3**	**29.5**
															Wt mean	**112.2**	**2.8**
															most represantative age	**96.1**	**4.7**
JU-24d	2.8	49.09	0.69	12.4	5.2	16.9	5.9	b.d.l.	6.26	1.3	8.0	1.4	16.3	70.11	5.61	***99.4***	***8.0***
g	1.4	37.70	0.60	20.8	4.9	26.8	7.0	b.d.l.	10.11	1.3	8.7	1.3	27.1	68.29	5.91	110.2	9.5
															Mean	**104.8**	**7.6**
															Wt mean	**103.9**	**6.1**
															most represantative age	**101.6**	**7.1**
JU-25a	1.1	36.56	0.59	10.6	6.6	13.9	9.1	b.d.l.	6.58	1.3	11.3	1.3	13.9	86.73	9.81	142.4	16.1
b	0.6	30.00	0.50	13.1	7.6	3.4	9.7	b.d.l.	4.71	1.3	12.4	0.3	13.9	61.91	7.68	***114.4***	***14.2***
e	0.7	31.03	0.52	18.4	2.8	14.7	3.6	b.d.l.	9.00	1.3	4.7	0.8	21.8	75.43	3.57	137.5	6.5
															Mean	**131.4**	**15.0**
															Wt mean	**134.6**	**5.6**
															most represantative age	**124.5**	**9.9**

Av. Radius: average radius of crystal; Eq. Sphere Radius: equivalent sphere radius of crystal; F_t: alpha recoil correction factor after Farley *et al.* (1996); U: Uranium concentration; Th: Thorium concentration; Sm: Samarium concentration; ^{4}He: ^{4}He concentration; TAE: total analytical error; eU: effective Uranium concentration; Corr. Age: corrected age; b.d.l.: below detection limit; Wt Mean: weighted mean age; youngest AHe age is highlighted in bold italics.

Table 6
Cooling and exhumation rates derived from modelled t-T paths

Sample	Elevation [m a.s.l.]	t-t segment [Ma]		T-T segment [°C]		Cooling rate [°C/Ma]	Geothermal gradient [°C/km]	Exhumation rate [km/Ma]
Northern transect								
JU-27	606	135	115	140	80	3.00	27	0.111
		115	0	80	15	0.57	27	0.021
JU-28	697	135	130	140	75	13.00	27	0.481
		130	15	75	45	0.26	27	0.010
		15	0	45	15	2.00	27	0.074
JU-29	800	150	140	140	85	5.50	27	0.204
		140	20	85	50	0.29	27	0.011
		20	0	50	15	1.75	27	0.065
JU-30	915	140	125	140	70	4.67	27	0.173
		125	0	70	15	0.44	27	0.016
JU-38	425	130	125	140	85	11.00	27	0.407
		125	0	85	15	0.56	27	0.021
JU-42	835	150	140	140	90	5.00	27	0.185
		140	0	90	15	0.54	27	0.020
Southern transect								
ESP-15	470	140	120	140	60	4.00	27	0.148
		120	0	60	15	0.38	27	0.014
ESP-17	507	190	180	140	75	6.50	27	0.241
		180	0	75	15	0.33	27	0.012
ESP-30	507	140	135	140	85	11.00	27	0.407
		135	0	85	15	0.52	27	0.019
JU-22	558	200	170	140	75	2.17	27	0.080
		170	30	75	50	0.18	27	0.007
		30	0	50	15	1.17	27	0.043
JU-23	534	160	155	140	75	13.00	27	0.481
		155	30	75	60	0.12	27	0.004
		30	0	60	15	1.50	27	0.056
JU-24	487	135	130	140	70	14.00	27	0.519
		130	35	70	60	0.11	27	0.004
		35	0	60	15	1.29	27	0.048
JU-25	495	150	140	140	85	5.50	27	0.204
		140	0	85	15	0.50	27	0.019
JU-26	410	195	160	140	80	1.71	27	0.063
		160	50	80	60	0.18	27	0.007
		50	0	60	15	0.90	27	0.033
Mean Northern transect								
2-segmented paths		139	126	140	81	4.70	27	0.174
		126	0	81	15	0.52	27	0.019
3-segmented paths		143	135	140	80	8.00	27	0.296
		135	18	80	48	0.28	27	0.010
		18	0	48	15	1.86	27	0.069
Mean Southern transect								
2-segmented paths Lugo block		143	132	140	77	5.43	27	0.201
		132	0	77	15	0.47	27	0.017
3-segmented paths Lugo block		148	143	140	73	13.50	27	0.500
		143	33	73	60	0.11	27	0.004
		33	0	60	15	1.38	27	0.051
2-segmented paths E and W block		190	180	140	75	6.50	27	0.241
		180	0	75	15	0.33	27	0.012
3-segmented paths E and W block		198	165	140	78	1.92	27	0.071
		165	40	78	55	0.18	27	0.007
		40	0	55	15	1.00	27	0.037

C. Publication 3

3D thermokinematic modelling of long-term landscape evolution of Variscan basement in Galicia, NW Spain.

René W. Grobe[1], Joaquina Alvarez-Marrón[2], Ulrich A. Glasmacher[3], Jean Braun[3], Francisco J. Cueto-Berciano[1]
(2010)

[1]Institute of Earth Sciences, University of Heidelberg, Germany
[2]Instituto de Ciencias de la Tierra Jaume Almera, CSIC, Barcelona, Spain
[3]Université Joseph Fourier de Grenoble, France

Submitted to 'International Journal of Earth Sciences' (07th December, 2010)

Abstract

The present study sets out to analyse and interpret thermochronological data (apatite fission-track, (U-Th-Sm)/He) by means of 3D thermokinematic modelling to better resolve the possible coupling of tectonic events, climate and landscape evolution. The Cantabrian Mountains in NW Spain are a well-studied area, providing a well-suited area to examine the impact of tectonic events on the topography. Reasonable estimates on the initial maximum mean elevation of the area after the end of the Variscan orogeny are determined between 2,400 and 3,400m. The subsequent decay in relief at rates between 0.002 to 0.03 km/Ma has been constrained. The modelling provides the largest decay in relief during the time period of 115 to 85Ma. This coincides with seafloor spreading that was active in the Bay of Biscay. In North Galicia the Alpine convergence caused shortening and surface uplift at a rate of 0.015 km/Ma between 35Ma and present. Long-term exhumation rates in North Galicia between 295-85 Ma appear homogenous between 0.03 and 0.04 km/Ma. This period reflects the widespread rifting between Iberia and Eurasia and subsequent seafloor spreading. The interval between 85-35Ma is characterized by relative quiescence with slow exhumation rates of 0.012 km/Ma. The onset of Alpine convergence and activation of the As Pontes fault caused an increase of exhumation rates between ~0.04-0.07 km/Ma, whereat the exhumation rate in the Northern block north of the As Pontes fault is significantly larger than in the Southern block. In Central Galicia between 290-165Ma the blocks are exhumed with a large exhumation rate of 0.138 km/Ma. This period coincides with the break-up of Pangea. The subsequent history is characterized by a different evolution of the two blocks. The exhumation rate pattern in the Lugo block is characterized by ongoing high rates between 0.256 and 0.113 km/Ma until 85Ma during the period of seafloor spreading and coincides with the assumed movement of the Lugo fault between 115-100Ma. The following period from 85Ma to present shows a decrease to 0.002 km/Ma. The Eastern block shows significant decrease in exhumation rate to 0.009 km/Ma and subsequent moderate increase to 0.33 and 0.019 km/Ma, respectively, between 115Ma and present. The strong coincidence between timing of major tectonic events and changes in topography and exhumation rates suggest that the major controlling factor in this area is tectonic forcing while climate effects have probably only a second order impact.

1 Introduction

Due to their mere extend mountain ranges are one decisive factor that controls basic features of the Earth's system, such as climate, ecology and hydrology for example. Nevertheless, orogens themselves are no static features representing fixed geographic boundary conditions but evolve dynamically over space and time within geological timescales (Reiners and Shuster, 2009). This evolution is supposed to be controlled mainly by the complex coupling between solid earth and atmospheric processes (i.e. tectonic and erosion) (e.g. England and Molnar, 1990; Willett *et al.*, 1993; Roe *et al.*, 2008). Therefore, the understanding of the effect of the coupling between tectonic and erosion on mountain ranges and landscape evolution is a matter of intense research efforts (e.g. Bishop, 2007; Reiners, 2007; Reiners and Ehlers, 2005; Whipple *et al.*, 1999; Beaumont *et al.*, 1999; Kooi and Beaumont, 1996). Temperature isotherms within the Earth's crust are perturbed by the (evolving) topography as well as by the rock uplift and exhumation rate. Because this perturbation decreases exponentially with depth (Braun, 2002b), low-temperature thermochronology is a well-suited tool to unravel rates of exhumation in a variety of tectonic scenarios, such as active orogens (Reiners and Ehlers, 2005; Reiners and Brandon, 2006; Bishop, 2007), rifting and passive margins (i.e. Gunnell *et al.*, 2009) and post-orogenic topographic decay in areas of tectonic quiescence (Reiners *et al.*, 2003), among others. However, the rates of exhumation of upper crustal rocks and, therefore, the behaviour of the tectonic-erosion system are not well documented in natural examples of early stages of rock uplift along juvenile coastal orogens. The Cantabrian Mountains, thus, are a well suited natural laboratory to understand this coupling, not least

as the tectonic evolution and geology of the area is well-documented.

Grobe *et al.* (2010) and Grobe *et al.* (in review) provided an extensive thermochronological history of the Variscan basement in Galicia (NW Spain) at the western termination of the Cantabrian Mountains by using conventional thermochronological interpretation tools like cooling age distributions at the surface, age-elevation-relationship plots and single sample cooling path modelling with HeFTy© (Ketcham, 2005; Ketcham *et al.*, 2007a; b; Ketcham *et al.*, 2009). However, an integrated 3D thermokinematic model of the complete dataset taking additional parameters (e.g. surface evolution, rock uplift rate etc.) into account to get closer to a realistic geological scenario is missing. As shown e.g. by Braun and Van der Beek (2004), Herman *et al.* (2007; 2009), Valla *et al.* (2010) and van der Beek *et al.* (2010), an integrated 3D thermokinematic model is essential for getting a better idea of the coupling between tectonic and climate forcing (interaction between solid Earth and overlying atmosphere) and, therefore, the long-term landscape evolution. Recent developments in computer technologies allow to provide large computing power routinely and, therefore, to perform state-of-the-art numerical modelling of sophisticated integrated 3D models closer to reality. Braun (2003a) provided such 3D thermokinematic model with the software code PECUBE. The present study aims to test the previously quantified cooling paths (Grobe *et al.*, 2010 and Grobe *et al.*, in review) and resulting exhumation rates against reasonable geologic scenarios and provide a better understanding of the long-term landscape evolution and exhumation history of the area.

2 Geological background

The area of Galicia is situated at the western termination of the Cantabrian Mountains, a juvenile evolving mountain range at an incipient active margin that represents the westernmost prolongation of the Pyrenees at the northern coast of Spain (Fig. 1).

In terms of their tectonic evolution and the geology the Cantabrian Mountains are a well examined example for a juvenile coastal orogen. Therefore, and because of its structural complexity and the abundance of granitic rocks well suitable for low-temperature thermochronology, the area of Galicia was chosen to quantify the timing and rate of exhumation and furthermore the coupling of internal and external processes driving landscape evolution.

The tectonic history of the Northern Iberian Peninsula may be summarized into three large-scale events: (1) the Variscan orogeny, (2) the rifting during Pangea break-up and subsequent opening of the Atlantic Ocean and Bay of Biscay, and (3) limited convergence between Iberia and Eurasia since Middle Eocene times. The end of the Variscan orogeny caused by the collision between Gondwana and Laurussia in Paleozoic times in the study area is commonly assumed at around 290 Ma (Pérez-Estaún *et al.*, 1990; 1991; Martínez-Catalán *et al.*; 2007). Subsequent extensional tectonics began in Late Permian and Triassic times during the initiation of the break-up of Pangea. The main widespread rifting phase occurred during Late Jurassic to Early Cretaceous times characterized by oblique separation of Iberia from Eurasia which caused formation of the Atlantic and Bay of Biscay margins (Le Pichon *et al.*, 1971; Srivastava *et al.*, 1990). The onset of this rifting period was set to 165 Ma in the following models. The end of this extensional phase is marked by chron M0 (118 Ma; Verhoef and Srivastava, 1989) and the Aptian-Albian break-up unconformity in the Cantabrian platform (c.115 Ma; Montadert *et al.*, 1979; García-Mondejar *et al.*, 2005) when subsequent sea floor spreading was active in the Bay of Biscay since Early Cretaceous until Late Cretaceous (Srivastava *et al.*, 1990). Limited convergence between Eurasia and Iberia during the Cenozoic started at 49 Ma and went on until 20 Ma (Srivastava *et al.*, 1990). Since then the convergence slowed significantly (Rosenbaum *et al.*, 2002) but the area is still weakly seismically active (López-Fernández *et al.*, 2004; Díaz *et al.*, 2008). Galicia is characterized by abundant intrusions of post- to syn-Variscan plutonic rocks. The occurrence of these plutonic rocks increases from the foreland in the east towards the suture in the west.

The study area is dominated by two major post-Variscan fault systems. The As Pontes fault belongs to a NW-SE strike-slip system

related to the opening of the Atlantic and the relative motion of the European and African plates (Mauffret *et al.*, 1978; Boillot and Malod, 1988). The total slip of the fault is assumed to be 1 km (Huerta *et al.,* 1996). The As Pontes fault has a significant fault scarp with a change in elevation of c. 300 m across it. Sedimentation in the As Pontes basin lasted at least until 22.5 Ma (Huerta *et al*, 1996). The main tectonic thrust movements, normal faults and NW-SE dextral strike-slip fault systems began in the Stampian (33.9 (0.1)-28.4 (0.1)) and finished in the upper Aquitanian-Burdigalian (~20 Ma). The end of the movement of the onshore and offshore strike-slip fault systems in NW Iberia coincides with the end of the seafloor spreading in the NW Iberian Plate boundary during upper Aquitanian-Burdigalian (~20 Ma). The Lugo fault in Central Galicia belongs to the NNE-SSW strike-slip fault system that extends for hundreds of km into Portugal. In particular, the faults trending NNE-SSW near Lugo are linked to the Mesozoic Lisbon basin. Holocene activity along these strike-slip fault systems in Portugal has been documented (Cabral, 1989). The Lugo fault has no significant change in topography across it.

The Morphology of the study area is characterized by a significant change in topographic relief shape. A plateau-like topography with long-wavelength relief and moderate amplitude in the central part of Galicia in the area around Lugo is bound to the North and East by rugged topography with short-wavelength relief of abrupt amplitude (Fig. 2). The elevation in the Lugo plateau ranges between 450-500 m and is separated from the rough northern topography by a c. 400 m high escarpment, related to the WNW-ESE trending As Pontes fault. To the east the area is bound by the Lugo fault as well as by a transition in relief shape to elevations up to 1000 m with a shorter wavelength and higher amplitude of topography due to abundant deeply incised river valleys.

2.1 Implications on thermal and structural history from previous studies

Several studies have been carried out to decipher the thermal and structural evolution of the Cantabrian Mountains by means of low-temperature thermochronology (Grobe *et al.*, 2010, Martín-González *et al.*, 2006; Schärer *et al.*, 1995; Ancochea *et al.*, 1992). As shown by Grobe *et al.*, (2010) and Grobe *et al.* (in review) the thermal and structural evolution of the Cantabrian Mountains in general and the area of Galicia in particular have been affected by various tectonic events resulting in a diverse and complex cooling and exhumation history of rocks presently exposed at the surface. The apatite fission-track (AFT) age distribution (Grobe *et al.*, 2010; Grobe *et al.*, in review; Fig. 3a; Tab. 1) in the area is rather heterogeneous. While cooling ages in the high elevation topography area in North Galicia north of the As Pontes fault, except for one sample at the coast, show ages not older than Lower Cretaceous (Aptian; ~120 Ma), the age distribution in Central Galicia is more complex. Here the ages range from Middle Jurassic (Callovian-Oxfordian; ~160 Ma) to Lower Cretaceous (Albian; ~110 Ma). Apatite (U-Th-Sm)/He (AHe) cooling ages are only available for Central Galicia (Grobe *et al.*, in review; Fig. 3b; Tab. 1) covering a transect crossing the Lugo fault. It seems that AHe ages east of the fault are consistently younger than those from the western flank of the fault. Moreover, the AFT-AHe age relationship is significantly different with old AFT (~160-140 Ma) and young AHe ages (~80-70 Ma) in the eastern flank and more or less similar AFT (~115-100 Ma) and AHe (~115-90 Ma) ages in the Lugo block. This indicates a distinct thermal and structural evolution of the eastern and western flank and suggests a fault movement around 115-100 Ma.

Time-temperature path modelling of the thermochronological data performed by Grobe *et al.* (2010) and Grobe *et al.* (in review) indicates that continuous cooling at different rates took place during the three main tectonic events that affected the area. A rapid cooling event that ended by the Late Jurassic corresponds to topographic decay during

unroofing of the Variscan orogeny and the break-up of Pangea, and is responsible for the largest amount of exhumation.

Figure 4 shows the condensed cooling history (i.e. temperature history) of all samples derived from the modelled cooling paths at different time steps. It illustrates the complex cooling history and its relationship to the major fault systems, the As Pontes and the Lugo fault, respectively. These fault systems separate areas with fast exhumation around 115 Ma from areas with a fast exhumation around 200-150 Ma and overall slow exhumation since then. Central Galicia was, therefore, divided into three blocks (Western block, Lugo block and Eastern block). Western and Eastern block show a similar history with incipient exhumation around 200 Ma. The Lugo block seems to have been exhumed later with a fast exhumation around 115 Ma. However, these exhumation rates provide only a first order assumption on exhumation rates as they are calculated on the basis of cooling rates and the assumption of a fixed geothermal gradient of 27 °C/km (Fernández *et al.*, 1998). As stated above, the isotherms and, therewith, the geothermal gradient are influenced by an evolving topography as well as changing rock uplift rates and the resulting exhumation rates. It is therefore recommendable to take these effects into account to calculate and interpret exhumation rates. The present study sets out to provide 3D thermokinematic models of these complex cooling histories together with reasonable assumptions on long-term landscape evolution since the end of Variscan orogeny.

3 Methods and techniques

In order to predict thermal histories and thermochronological ages at the Earth's surface from a given thermal and structural scenario the transient heat transport equation has to be solved in three dimensions, including conductive and convective terms as well as the effect of an evolving surface topography and changing rock uplift rates on the temperature field in the underlying crust. Three-dimensional heat transfer in the crust is governed by the following equation (Carslaw and Jaeger, 1959):

$$\rho_c c\left(\frac{\partial T}{\partial t}+\dot{R}\frac{\partial T}{\partial z}\right)=\left[\kappa\frac{\partial^2 T}{\partial x^2}+\kappa\frac{\partial^2 T}{\partial y^2}+\kappa\frac{\partial^2 T}{\partial z^2}\right]+\rho_c H \quad (1)$$

Where T is temperature, t is time, x, y and z are spatial coordinates, ($\dot{R}$) is the vertical rock uplift rate (i.e. the velocity of rocks with respect to the fixed base at z = -L) (see paragraph "*Rock uplift, surface uplift, rock exhumation"*), κ is the thermal diffusivity, H is the rate of radiogenic heat production per unit mass, ρ_c is crustal density, and c is heat capacity.

This equation has to be solved for a given initial temperature distribution:

$$T_0 = T_0(x, y, z, t = 0) \quad (2)$$

and a set of boundary conditions:

$$T(x, y, z = -L, t) = T_L \quad (3)$$

$$T(x, y, z = S(x, y, t), t) = T_{MSL} + \beta S \quad (4)$$

$$\frac{\partial T}{\partial n} = 0 \text{ along the side boundaries} \quad (5)$$

where $S(x,y,t)$ is the assumed, time-varying surface topography. T_L is the assumed temperature at the base of the model (e.g. Moho or the base of the lithosphere), T_{MSL} is the assumed temperature at mean sea level, and β is the atmospheric lapse rate (i.e. the rate of change of temperature with elevation in the atmosphere), n is the outward normal to the side boundaries.

3.1 PECUBE

The software code PECUBE (Fig. 5a) developed by Braun (2003a) is a 3D thermokinematic model based on a finite element method (FEM) code solving the transient heat transport equation in three dimensions. It has been designed to accurately predict the effect of a finite-amplitude, time-varying surface topography on the underlying structure. From the solution of the transient heat transport equation it determines the temperature history of rock particles that will end up at the

surface of the model at the end of the computations. From the thermal histories (*t-T* paths) it computes AFT ages, using the annealing models of Laslett *et al.* (1987) and Crowley *et al.* (1991), as well as AHe ages using a finite difference scheme to solve the time-dependent, thermally activated solid-state diffusion equation for helium in apatite (Wolf *et al.*, 1998) for all points at the surface of the model. It enables, therefore, predictions of thermal histories and thermochronological ages from input rock uplift rates and relief development histories (i.e. long-term landscape evolution). PECUBE is combined with an inversion method (Fig. 5b) based on the Neighbourhood Algorithm (NA) of Sambridge *et al.* (1999a; b). This allows to 'invert' the forward approach to search through a predefined parameter space for an optimal set of parameter values that result in age predictions that best agree with the observed ages (within uncertainties). The agreement of predicted and observed ages is calculated by a misfit function, which is defined as the L^2-norm of the weighted difference between the observation vector (O) and the prediction vector (P):

$$\text{misfit} = \frac{1}{n}\sqrt{\sum_{i}^{n}\left(\frac{O_i - P_i}{\Delta O_i}\right)^2} \qquad (6)$$

where n is the number of measured ages and ΔO_i are the observational errors. Misfit values of ≤ 1 imply that the observed ages could be reproduced within uncertainty. The higher the misfit value the worse is the replication of observed data.

To perform this inversion the NA method navigates through parameter space to find, in an optimum manner, the minimum of the misfit function, i.e. the best agreement of predicted and observed ages, by using the natural neighbour interpolation and Voronoi diagram concepts.

3.2 Rock uplift, surface uplift, rock exhumation/denudation

To avoid misconception while describing rock movements, we followed the recommendations of England and Molnar (1990) (see also Ring *et al.*, 1999a; Lisker *et al.*, 2009) defining the terms rock uplift, surface uplift and rock exhumation. Rock uplift and surface uplift describe the displacement of rocks or the Earth's surface, respectively, with respect to the geoid (or another frame of reference), while rock exhumation specifies the movement of rocks with respect to the Earth's surface.

The relationship of the three displacements is given by the equation:

surface uplift = rock uplift – rock exhumation (7)

The rate of rock exhumation equals the rate of denudation, i.e. the rate of removal of overburden by tectonic or erosional processes from a region or point. While exhumation describes the unroofing of a point, denudation applies to an area (Ahnert, 2003, Summerfield and Brown, 1998). As described above PECUBE is able to model the parameters rock uplift and surface uplift. These two parameters, therefore, govern directly the exhumation. Figure 6 shows a sketch illustrating the impact of the amplification factor of topography on the surface and the relationships between the various displacements (rock uplift, rock exhumation, surface uplift).

4 Model setup and parameterization

In the models all parameters except for the rock uplift rate and the surface uplift rate (defined by the amplification factor of the topography) and, therewith, the resulting exhumation rate, are spatially uniform and constant through time over the whole model (i.e. the boundary conditions of the model). The surface uplift rate can vary through time, controlled by the time steps, but is spatially uniform, whereas the rock uplift rate can vary through space and time controlled by the fault movement. We, therefore, have to differentiate between parameters that are: (1) uniform through space and constant through time, (2) uniform through space and variable through time and (3) variable through space and time. Furthermore, it is differentiated between 'fixed'

parameters (representing the boundary conditions of the model) and the 'free' parameters which are inverted for.

4.1 Boundary conditions – 'fixed' parameters

The model spatial resolution (see Fig. 6) depends on the wavelength of the topography that will affect the isotherm corresponding to the closure temperature of the thermochronological system(s) being used. This wavelength is thus given by the following relationship (Braun, 2002a):

$$\omega_c = \frac{T_c}{G_0} \quad (7)$$

where T_c is the closure temperature of the thermochronometer used and G_0 is the local geothermal gradient. In our case the 'critical wavelength' for the AFT thermochronometer is equal to 4 km for a closure temperature of 110 (10) °C (Gleadow and Duddy, 1981) and a geothermal gradient of 27 °C (Fernández *et al.*, 1998). Accordingly, the 'critical wavelength' for the AHe thermochronometer is equal to 2.6 km for a T_c of 70 (5) °C (Farley *et al.*, 1996; Farley, 2000; Stöckli *et al.*, 2000; Wolf *et al.*, 1996; 1998). Therefore, the initial horizontal spacing between the nodes (i.e. the horizontal resolution of the model) was originally set to 480 m. However, a test run to determine the sensitivity of the model revealed that a decreased resolution of 640 m yielded indistinguishable results at much lower computing costs.

Two key areas have been selected for modelling (Fig. 2) and were modelled separately: (1) North Galicia area, (2) Central Galicia area. The intention was to model across the major structural features to catch the difference in timing and rate of exhumation of different fault blocks. The modelled area in North Galicia has been defined as a rectangle with about 40 x 24 km edge length in E-W and N-S extension, respectively, with 63 x 38 nodes. In Central Galicia an area of about 40 x 28 km has been defined with 64 x 44 nodes. The gridding between each node is 0.008 arc degrees. As discussed above this corresponds to a spacing of 640 m between the nodes. The model (crustal) thickness has been set to 30 km with a resolution of 1 km, i.e. 30 nodes in z-direction. The temperature at the surface has been set to 15 °C while the temperature at the base of the model is specified to 825 °C. This gives an initial geothermal gradient of 27 °C/km. Thermal diffusivity has been set to 25 km^2/Ma, a value most likely for rocks of the Earth's crust.

4.1.1 Thermochronological data

A total of 12 observed AFT cooling ages in the North Galicia area as well as 8 AFT and 6 AHe cooling ages (Fig. 2; Tab. 1) in the Central Galicia area published by Grobe *et al.*, (2010) and Grobe *et al.* (in review.) have been integrated in the 3D thermokinematic model for comparison with predicted cooling ages.

4.1.2 Fault geometry

In the North Galicia area a NW-SE striking fault (Fig. 2; 9a), representing the As Pontes fault, has been defined, dividing the crustal block in the Northern and the Southern block. In Central Galicia a NW-SE striking fault (Fig. 2, 9b) representing the Lugo fault has been defined, dividing the area in the Lugo and the Eastern block. The vertical dipping of the faults is unknown, therefore, the dipping of the faults is set to 90°. This enables to model vertical rock movements at each side of the fault and neglect lateral mass movements.

4.1.3 Time steps

Subsequently, the time steps to characterize the tectonomorphic scenario have to be defined (Tab. 2). The starting point (Ma in the past) of each model has been set to 290 Ma, marking the end of the Variscan orogeny (Pérez-Estaún *et al.*, 1990; 1991; Martínez-Catalán *et al.*; 2007). The ending point is set at present. Intermediate time steps describe (assumed) important breaks in the tectonothermal evolution, i.e. a change in rock uplift rate or relief evolution (surface uplift rate), according to geological constraints. They are set to:165 Ma which coincides with the onset of active rifting in the continental margin (Le Pichon *et*

al., 1971; Srivastava *et al.*, 1990); 115 Ma marks the starting of the post-rift phase in the continental margin (García-Mondejar *et al.*, 2005; Verhoef and Srivastava, 1989; Montadert *et al.*, 1979). The time step at 85 Ma was chosen to better resolve the post-rift phase that culminated with a low relief surface whose remains are preserved in Central Galicia today. Only in the North Galicia area an additional time step at 35 Ma was set to simulate a flat surface until 35 Ma and the onset of activity along the As Pontes fault through Late Paleogene times (Huerta *et al.*, 1996; Santanach *et. al.*, 2005).

4.2 Inverse modelling – 'free' parameters

As the major task of this study is to determine the timing and quantify the rate of exhumation governed by the evolving topography and the rock uplift, these two parameters (surface uplift and rock uplift) have been inverted for. The parameter space of the inversions as well as the resulting ranges for exhumation rates are summarized in Table 2.

4.2.1 Landscape evolution (surface uplift rate)

At each time step an amplification factor of the topography is imposed to change the amplitude of the topography, i.e. to model changes in surface relief. It has to be considered that the topography only varies in amplitude but not in shape. This necessary simplification is likely to be correct during the post-orogenic phase of a mountain belt, where the potential for stream capture and reorganization of the fluvial network is assumed to be small and, therefore, valleys and interfluves are regarded as static features (Braun and Robert, 2005). In the Central Galicia area the intention was to simulate a continuous decay in relief since the end of Variscan orogeny until present. A similar continuous decay in relief was simulated for the North Galicia area with the exception that the decay occurred faster and ended already at 85 Ma with a flat surface. From 35 Ma this flat relief was intended to grow to present elevation as a result of Alpine fault activity (Boillot *et al.*, 1979; Alonso *et al.*, 1996; Pulgar *et al.*, 1996; Alvarez-Marrón *et al.*, 1997).

North Galicia

The maximum height of a mountain range is controlled and, therefore, limited by several factors (i.e. climate, glaciation, isostatic effects) (Thomson *et al.*, 2010, Whipple and Meade, 2004; Montgomery and Brandon, 2002; Dahlen and Suppe, 1988). In North Galicia the range for the initial mean elevation was set between 4080-1530 m (Tab. 2) as a reasonable range for the maximum mean elevation of Variscan orogen topography. Subsequently a nearly linear decrease of topography with an elevation range between 1530-1020 m at 165 Ma and 1020-510 m at 115 Ma to a flat surface at 85 Ma was simulated. The flat surface was simulated to last until 35 Ma, when the increase of surface relief to mean present elevation was initiated. The flat surface at time steps 85 and 35 Ma takes the constraints of Huerta *et al.* (1996) and Santanach *et al.* (2005) taking the evolution of the As Pontes basin into account. These dated continental deposits in the basin are cut by the As Pontes fault between 30-22 Ma.

Central Galicia

A similar decrease of topography was simulated for the Central Galicia area. The range for initial mean elevation was set between 4320-2700 m (Tab. 2). The subsequent decay of relief over the time steps 165, 115, 85 Ma until present was simulated to be nearly linear with mean elevations between 2700-1620 m at 165 Ma, 1620-1080 m at 115 Ma, and 1080-540 m at 85 Ma.

4.3 Rock uplift rate

The range for the rock uplift rates within each time interval between the various time steps was set between 0-0.3 km/Ma for each model and each block.

North Galicia

The rock uplift rates during all intervals except the last interval between 35 Ma until present where coupled. This means, the fault

activity was allowed to start not until 35 Ma taking the constraints from Huerta *et al.* (1996) and Santanach *et al.* (2005) into account.

Central Galicia

The rock uplift rate during the first interval was coupled and decoupled not until the second time step. This means, the fault activity was allowed to start not until 165 Ma.

The output after all computations consists of the complete 3D temperature field at any pre-defined time step, as well as the exhumation rates and the temperature experienced through time by rocks that end up at the surface at the end of the computations. These t-T paths are then used to predict AFT and AHe cooling ages which are compared to the observed ages (Fig. 5a).

5 Results

5.1 North Galicia

5.1.1 All inverse models

A total of 2408 model runs was performed to find a best fit model in the final modelling step. Figure 7a (Northern block) and b (Southern block) show the results of all 2,408 models plotting the two parameters which have been inverted for, i.e. the amplification factor of topography and the rock uplift rate, at each time interval against each other. The different time intervals between the time steps (290-165 Ma; 165-115 Ma; 115-85(35) Ma; 85(35)-0 Ma) are marked by different greyscales to discriminate against each other. The 35 Ma time step is set in brackets as the topographic evolution is decoupled from the fault movement. While the surface was set to be flat already between 85-35 Ma the fault movement started not until 35 Ma. The grey fields of each time interval also illustrate the parameter space (range) of the inverted parameters. Each point of the plots represents one model run at the accordant time interval (i.e. 2,048 points for 2,048 models at each interval). The color of the points visualizes the resulting misfit. There is a large range of misfit values between c. 41.1 and 0.5. The large range indicates that the chosen parameter space was wide enough to give enough freedom not forcing the model in advance to a good fit. In contrast, the good fits cluster in narrow areas, indicating that the model calculations migrated fast towards the lowest misfits. In the first three time intervals from 290 to 35 Ma, the rock uplift rates of the two blocks were coupled, therefore, the plots show the same results in this time span. From 290-165 Ma the plot shows two clusters very close to each other. The amplification factor of the topography ranges from ~6 to 4.5 while the rock uplift rate plots between 0 and 0.025 km/Ma with a trend towards larger rock uplift rates at lower amplification of topography. During the second interval from 165-115 Ma the topography decays as predefined by the model to factors between 2.3 and 2.6 while the rock uplift rate varies between 0.01 and 0.05 km/Ma. This time there is no correlation between rock uplift and topography as the topography is very stable around 2.5. During the next interval the topography again is sharply determined at ~1.6 while the range for the rock uplift rate decreases slightly from 0.01-0.05 km/Ma with a trend towards lower values (see best fit). At the last time steps the topography was predefined as flat surface from 85-35 Ma (indicated by the flat line at 0 elevation in Fig. 7a, b). Also the fault has been activated allowing each block a different movement. The rock uplift rate from 35 Ma to present in the Northern block increases significantly in comparison to the former interval. It now ranges from 0.025 to 0.090 km/Ma. In the Southern block the change is more undifferentiated. The best fit model also points to an increase in rock uplift rate but with a total range between 0 to 0.070 km/Ma.

5.1.2 Exhumation rates (best fit model)

The results for the best fit model are given in Table 3. Northern and Southern block movement was coupled until 35 Ma. Therefore, between 290-35 Ma N and S block yielded similar rates. Values for surface uplift and rock uplift rates resulted in exhumation rates for both blocks of 0.029 km/Ma between 290-165 Ma, 0.031 km/Ma between 165-115 Ma and 0.040 km/Ma between 115-35 Ma. From 35 Ma until present fault movement was active and the blocks have been decoupled. The exhumation

rate of the Northern block was determined to 0.066 km/Ma between 35 Ma until present, while the exhumation rate in the Southern block was 0.043 km/Ma during this time span.

The modelled AFT ages are in good agreement with the correspondent ages observed at each side of the fault (Fig. 8a; 9a, b, c).

5.2 Central Galicia

5.2.1 All inverse models

Again 2,408 model runs have been performed in order to find a combination of surface subsidence rate and rock uplift rate that best reproduces the observed ages. The results are given in Figure 7c (Lugo block) and d (Eastern block). In comparison to the previous model in North Galicia, here a much larger spread of low misfits can be observed as well as a much smaller range in misfit values from ~3.88 to 0.35. This can be indicative for two things either 1) the model is not well constrained by the data or 2) the parameter space has been defined more narrow with respect to the possible solutions (therefore, the difference in appearance of the plots of each area is a problem of scale, or in other words: for the Galicia area there is a wider range of reasonable rock uplift rates to reproduce the observed data). We prefer the second explanation because the very low misfit values do not support the first assumption. During the first time interval from 290 to 165 Ma the Lugo and the Eastern block were coupled allowing no fault movement. The models with the lowest misfit cluster around an amplification factor of topography between 6 and 6.9 and rock uplift rates between 0.08 and 0.10 km/Ma. From 165 Ma onward both blocks have been decoupled allowing different rock uplift rates at each side of the fault. While in the western flank of the fault in the Lugo block the rock uplift rate increased significantly to a large range of values between 0.15 and 0.27 km/Ma. However, most of the low misfit models as well as the best fit cluster between 0.23 and 0.26 km/Ma. On the contrary the models suggest a considerable decrease in rock uplift rates in the Eastern block ranging from 0 to 0.03 km/Ma. The amplification factor of the topography plots between 3 and 4. While the rock uplift rate in the Eastern block during the subsequent time step from 115 to 85 Ma show no change suggesting still relative quiescence with respect to rock uplift rates the rates in the Lugo block decrease slightly to a range from 0.04 to 0.10 km/Ma and are, therefore, still notably higher than in the Eastern block. Models with the lowest misfit suggest an amplification factor of topography between 2.5 and 3 at this time step. During the last time step from 85 Ma to present the rock uplift rates of each block again adapt ranging from 0 to 0.02 km/Ma. However, in contrast to the previous time steps now the rates in the Eastern block seem to be slightly higher. The amplification factor of topography settles around 1.3.

5.2.2 Exhumation rates (best fit model)

The results for the best fit model are given in Table 3. The values for surface uplift and rock uplift rates resulted in exhumation rates for the Eastern block of 0.138 km/Ma between 290-165 Ma, 0.009 km/Ma between 165-115 Ma, 0.033 km/Ma between 115-85 Ma and 0.019 km/Ma from 85 Ma until present. The exhumation rates of the Lugo block were determined to 0.138 km/Ma between 290-165 Ma (same like in the Eastern block because of coupling), an acceleration of exhumation rate to 0.256 km/Ma between 165-115 Ma, 0.113 km/Ma between 115-85 Ma and very slow exhumation at a rate of 0.002 km/Ma from 85 Ma until present.

The modelled AFT and AHe ages are in good agreement with the correspondent ages observed at each side of the fault (Fig. 8b; 9d, e, f, g).

6 Discussion

6.1 North Galicia

In North Galicia, we simulated a scenario with constant decrease in topography since Variscan orogeny from 290 Ma to 85 Ma. From 85-35 Ma we pre-determined a flat surface according to afore mentioned geological constraints. Subsequently, we simulated the surface uplift from 0 elevation (flat surface) at 35 Ma to present elevation until recent times.

The best fit model suggested a mean elevation of the area of ~2,400 m after Variscan orogeny and a subsequent decay of relief to ~1,200 m at 165 Ma, 830 m at 115 Ma and 0 m at 85 Ma. This corresponds to surface subsidence rates in orders of magnitude between ~0.01 to ~0.03 km/Ma. The surface uplift from 0 at 35 Ma to 510 m present mean elevation corresponds to a rate of 0.015 km/Ma. The exhumation rates of both blocks (Northern and Southern block) were coupled until 35 Ma to allow fault activity not to start until then. For the Northern block the exhumation rates are in an order of 0.03 to 0.04 km/Ma from 290 to 85 Ma. This is in good agreement with HeFTy© derived exhumation rates for the Northern block from previous studies (Tab. 3; Grobe *et al.*, 2010; Grobe *et al.*, in review) which derived exhumation rates of 0.111 km/Ma from 165-115 Ma and 0.029 km/Ma from 115-85 Ma for a fixed geothermal gradient of 27 °C/km and a surface temperature of 15 °C. In the Southern block HeFTy© derived exhumation rates were slightly slower with 0.090 km/Ma from 165-115 Ma and 0.010 km/Ma from 115-85 Ma. Also we see in both modelling approaches, HeFTy© and PECUBE, a subsequent decrease in exhumation rate to 0.012 km/Ma (PECUBE; both blocks) compared with 0.014 km/Ma (Northern block) and 0.011 km/Ma (Southern block). The important observation is the significant increase during the last time step when also the both blocks were decoupled in the PECUBE models to allow fault activity. The increase led to exhumation rates of 0.066 km/Ma (PECUBE; Northern block) and 0.043 km/Ma (PECUBE; Southern block) compared to 0.029 and 0.031 km/Ma, respectively (HeFTy©). Both approaches, therefore, record a significant increase in exhumation rate around 35 Ma, which is also in good agreement with the incipient Alpine convergence in this area. However, comparing the exhumation rates derived from the two models and evaluating the results, different model features which complicate the direct comparison have to be taken into consideration. HeFTy© calculates cooling rates by taking the cooling age as well as the valuable track lengths distribution of a sample into account. This cooling rate is then translated into an exhumation rate by assuming a fixed geothermal gradient. HeFTy© models, therefore, do not account for changes in surface elevation or rock uplift rate nor do they integrate several samples into one single model. At high exhumation rates the relationship between cooling rate and exhumation rate becomes highly non-linear. Due to the large convection of heat the geothermal gradient becomes exponential resulting in compressed isotherms towards the surface. In this case of high exhumation rates the cooling age of a sample is twice influenced by (1) a shorter travel time to the surface due to the increased travel speed as well as (2) a shorter travel distance from the closure isotherm to the surface due to the compressed isotherms. The fact that the comparison of both modelling approaches can be considered as in good accordance can, therefore, be related to the overall slow exhumation rates in the area. This would result in a weak influence of the exhumation rate on the geothermal gradient and in turn minimize the difference to model approaches with a fixed geothermal gradient.

6.2 Central Galicia

In Central Galicia we simulated a scenario with constant decay in relief from 290 Ma until present. Fault movement of the Lugo fault was allowed to be active between 165 Ma until present. The best fit model suggests an elevation of topography of ~3400 m at 290 Ma and subsequent decay to ~2000 m at 165 Ma, ~1500 m at 115 Ma and 680 m at 85 Ma unless recent mean elevation with 540 m is reached. The resulting rate of surface subsidence ranges from 0.012 km/Ma over 0.008 km/Ma, 0.028 km/Ma to 0.002 km/Ma during the last time step. Comparing the exhumation rates with the HeFTy© derived exhumation rates the picture is not as concordant like in North Galicia. The PECUBE derived exhumation rates in the Lugo block show fast rates with 0.138 km/Ma between 290-165 Ma, even an increase to 0.256 km/Ma between 165-115 Ma, subsequent decrease to 0.113 km/Ma between 115-85 Ma and very slow exhumation with 0.002 km/Ma between 85 Ma until present. In the first time step the exhumation rate in the Eastern block is coupled to that of the Lugo block and, therefore, equals 0.138 km/Ma. During the next time interval between 165-115 Ma the rate

decreases dramatically to 0.009 km/Ma. While in the subsequent interval between 115-85 Ma it increases to 0.033 km/Ma. In the last time interval between 85 Ma to present the exhumation rate again decreases moderately to 0.019 km/Ma. These values differ significantly from those derived from HeFTy© modelled cooling paths. As stated above, this is reasonable because the difference can be explained by the more complex cooling history in Central Galicia, which has in turn a much larger effect on the complicating factors that impede to compare the two approaches. In areas with such complex cooling histories either a detailed discussion of each single sample cooling path is mandatory to find a synthesis like provided by Grobe *et al.* (in review) or integrated 3D thermokinematic modelling has to be applied. In fact, the overall picture that the PECUBE model draws is a fast exhumation of the Lugo block between 165-85 Ma and very slow exhumation thereafter while in the Eastern block the fastest exhumation occurred between 290-165 Ma with subsequent quiescence and a moderate reactivation between 115-85 Ma. This is in good agreement with the thermal history based on AFT, AHe and HeFTy© modelling results discussed in Grobe *et al.* (in review).

7 Conclusions

The Northern and Central Galicia areas provide good fit with the applied thermochronological data by modelling an evolution of continuous surface decay. The PECUBE models show the largest decay in topographic relief at the time interval between 115-85 Ma with a rate of 0.028 km/Ma. This decay coincides with the onset of seafloor spreading and the postrift stage in the continental margin. Surface uplift rates of 0.015 km/Ma from 35 Ma until present may explain the higher topography observed across in North Galicia area. This surface uplift is associated to the shortening and inversion along the continental margin during Alpine convergence. The exhumation rates in North Galicia with larger exhumation rates between 290-85 Ma reflect the widespread rifting caused by the oblique separation of Iberia from Eurasia and the subsequent seafloor spreading. The period of quiescence between 85-35 Ma was followed by an increase in exhumation from 35 Ma until present attributed to the re-activation of the As Pontes fault as well as the onset of Alpine convergence. Also the exhumation in the Northern block is, as expected, significantly larger as in the Southern block. In contrast to the North Galicia area, the exhumation history in Central Galicia is more differentiated. Both blocks across the Lugo fault were being exhumed equally with a rather large exhumation rate between 290-165 Ma. This is attributed to the rifting period that caused the break-up of Pangea. After 165 Ma the two blocks evolve differently. In the Lugo block the exhumation rate increases and holds a high level of exhumation between 165-85 Ma. This high exhumation rate in the Lugo block reflects the sea-floor spreading active in the Bay of Biscay as well as the assumed movement of the Lugo fault between 115-100 Ma. The subsequent period is characterized by relative tectonic quiescence (i.e. no significant exhumation) and seems, therefore, not to be influenced by the Alpine convergence. In the Eastern block the exhumation rate decreases dramatically after 165 Ma showing no coincidence with the rifting period. The subsequent increase from 115 Ma is relatively moderate showing only mild correlation to the Alpine convergence which is reasonable due to the large distance to the margin. The lack of profound and detailed data of paleoclimate impede a final conclusion whether the changes in surface evolution and rock uplift rates are climatically or tectonically controlled. The strong coincidence between timing of major tectonic events and the derived changes in topography and rock uplift rates, however, strongly suggest that the major driving factor in this area is the tectonic forcing rather than changes in climate. The comparatively good agreement between PECUBE and HeFTy© derived exhumation rates despite their different approaches can be related to the overall slow exhumation rates in the area which results in a weak influence of the exhumation rate on the geothermal gradient. The present study could show that it is possible to simulate geologically reasonable scenarios of long-term landscape evolution, which produce as well reasonable results that are in good agreement with the observed data. Moreover, the results of single

sample cooling history modelling from previous studies could be approved by the provided 3D integrated thermokinematic models. Where this is not the case it could be demonstrated why. In the present slowly evolving scenario with small differences in elevations the surface uplift/subsidence rate does not have large influence on the overall exhumation rates and the data is, therefore, not very sensitive to a change in surface evolution over a timescale of 290 Ma. That is why 3D thermokinematic modelling is a powerful tool to better resolve the long-term landscape evolution.

Acknowledgements

This study was funded through National Plan of Research projects BTE2002-00330 and CGL2007-60230/BTE of the Spanish Ministry of Education and Science. It is included in the framework of Consolider-Ingenio 2010 nº CSD2006-00041 (TOPO-Iberia project). The position of R.W. Grobe was funded by the LGFG (Landesgraduiertenförderung des Landes Baden-Württemberg). We thank Friederike Bauer for her comments on the early version of the manuscript. ASTER GDEM is a product of METI and NASA.

References

Ahnert, F., 2003. Einführung in die Geomorphologie. UTB/Ulmer, Stuttgart, 440 p.

Alonso, J.L., Pulgar, J.A., García-Ramos, J.C., Barba, P., 1996. Tertiary basins and Alpine tectonics in the Cantabrian Mountains (NW Spain), In: Friend, P.F., Dabrio, C.J. (Eds.), Tertiary Basins of Spain: The Stratigraphic Record of Crustal Kinematics, 214-227, Cambridge Univ. Press, New York.

Alvarez-Marrón, J., Rubio, E., Torne, M., 1997. Alpine age subduction structures in the North Iberian Margin. Journal of Geophysical Research 102, 22495–22511.

Ancochea, E., Huertas, M.J., Ibarrola, E., Snelling, E., 1992. Diques basálticos en lasproximidades de Orense. Evidencia de actividad magmática Cretácica en el Noroeste de la Península Ibérica. Rev. Soc. Geol. Esp. 5, 65–71.

Beaumont, C., Kooi, H. and Willett, S., 1999. Coupled tectonic-surface process models with applications to rifted margins and collisional orogens. In: Summerfield, M.A. (ed.), Geomorphology and Global Tectonics: John Wiley and Sons Ltd., 29-55.

Bishop, P., 2007. Long-term landscape evolution: linking tectonics and surface processes. Earth Surface Processes and Landforms 32, 329-365.

Boillot, G., Malod, J., 1988. The north and north-west Spanish continental margin: a review, Rev. Soc. Geol. Esp. 1 (3–4), 295–316.

Boillot, G., Auxietre, J.-L., Dunand, J.-P., Dupeuble, P.-A., Mauffret, A., 1979. The northwestern Iberian margin: a Cretaceous passive margin deformed during Eocene. In: Talwani, M., Hay, W., Ryan, W.B.F. (Eds.), Deep Drilling Results in the Atlantic Ocean: Continental Margins and Paleoenvironment: Am. Geophys. Union, Maurice Ewing Ser., 3, 138-153.

Braun, J., 2002a. Estimating exhumation rate and relief evolution by spectral analysis of age-elevation datasets. Terra Nova 14, 210-214.

Braun, J., 2002b. Quantifying the effect of recent relief changes on age-elevation relationships. EPSL 200, 331-343.

Braun, J., 2003a. Pecube: a new finite-element code to solve the 3D heat transport equation including the effects of a time-varying, finite-amplitude surface topography. Computers & Geosciences 29, 787-794.

Braun, J., van der Beek, P., 2004. Evolution of passive margin escarpments: What can we learn from low-temperature thermochronology? Journal of Geophysical Research 109, F04009, doi:10.29/2004JF000147.

Braun, J., Robert, X., 2005. Constraints on the rate of post-orogenic erosional decay from low-temperature thermochronological data: application to the Dabie Shan, China. Earth Surf. Process. Landforms 30, 1203-1225.

Cabral, J., 1989. An example of intraplate neotectonic activity, Vilarica basin, northeast Portugal. Tectonics 8 (2), 285-303.

Carslaw, H.S., Jaeger, C.J., 1959. Conduction of Heat in Solids, 3rd Edition. Clarendon Press, Oxford, 510pp.

Crowley, K.D., Cameron, M. and Schaffer, L.R., 1991. Experimental studies of annealing of etched fission tracks in fluorapatite. Geochim. Cosmochim Acta 55: 1449-1465.

Dahlen FA, Suppe J. 1988. Mechanics, growth, and erosion of mountain belts. In: Clark, S.P.J., Burchfiel, B.C., Suppe, J., (Eds.), Processes in Continental Lithospheric Deformation, pp. 161–78. Denver, CO: Geol. Soc. Am.

Díaz, J., Gallart J., Gaspà O., Ruiz M., Córdoba D., 2008. Seismicity analysis at the Prestige oil-tanker wreck area (Galicia Margin, NW of Iberia), Marine Geology 249, 150-165.

England, P., Molnar, P., 1990. Surface uplift, uplift of rocks, and exhumation of rocks. Geology 18, 1173-1177.

Farley, K.A., Wolf, R.A., Silver, L.T., 1996. The effects of long alpha-stopping distances on (U-Th)/He ages. Geochimica et Cosmochimica Acta 60 (21), 4223-4229.

Farley, K.A., 2000. Helium diffusion from apatite: general behaviour as illustrated by Durango fluorapatite. J. Geophys. Res., 105, 2903–2914.

Fernández, M., Marzán, I., Correia, A., Ramalho, E., 1998. Heat flow, heat production, and lithospheric thermal regime in the Iberian Peninsula. Tectonophysic 291, 29-53.

García-Mondejar, J., Lopez-Horgue, M.A., Aranburu, A., Fernández-Mendiola, P.A., 2005. Pulsating subsidence during a rift episode: Stratigraphic and tectonic consequences (Aptian-Albian, northern Spain). Terra Nova 17 (6), 517-525.

Gleadow, A.J.W., Duddy, I.R., 1981. A natural long term track annealing experiment for apatite. Nucl. Tracks 5, 169-174.

Grobe, R.W., Alavrez-Marrón, J., Glasmacher, U.A., Menéndez-Duarte, R., 2010. Low temperature exhumation history of Variscan-age rocks in the western Cantabrian Mountains (NW Spain) recorded by apatite fission-track data. Tectonophysics 489, 76-90.

Grobe, R.W., Alvarez-Marrón, J., Glasmacher, U.A., Menéndez-Duarte, R., (in review). Post-Paleozoic exhumation of the NW Iberian Massif and the remains of a pre-Alpine paleolandscape from apatite fission-track and (U-Th-Sm)/He data. Submitted to Tectonics.

Gunnell, Y., Calvet, M., Brichau, S., Carter, A., Aguilar, J.-P., Zeyen, H., 2009. Low long-term erosion rates in high-ernergy mountain belts: Insights from thermo- and biochronology in the Eastern Pyrenees. Earth and Planetary Science Letters 278, 208-218.

Herman, F., Braun, J., Dunlap, W.J., 2007. Tectonomorphic scenarios in the Southern Alps of New Zealand. Journal of Geophysical Research 112. B04201, doi:10.1029/2004JB003472.

Herman, F., Cox, S.C., Kamp, P.J.J., 2009. Low-temperature thermochronology and thermokinematic modeling of deformation, exhumation, and development of topography in the central Southern Alps, New Zealand. Tectonics 28, TC5011, doi: 10.1029/2008TC002367

Huerta, A., Parés, J.M., Cabrera, L., Ferrús, B., Sáez, A., 1996. Datación magnetoestratigráfica de la cuenca terciaria de As Pontes (Galicia, NW España), Geogaceta 20, 1021-1024.

Ketcham, R.A., 2005. Forward and inverse modeling of low-temperature thermochronometry data. Reviews in Mineralogy and Geochemistry, 58, 275-314.

Ketcham, R.A., Carter, A., Donelick, R.A., Barbarand, J., Hurford, A.J., 2007a. Improved measurement of fission-track annealing in apatite using c-axis projection. Am. Min. 92, 789-798.

Ketcham, R.A., Carter, A., Donelick, R.A., Barbarand, J., Hurford, A.J., 2007b. Improved modelling of fission-track annealing in apatite. Am. Min. 92, 799-810.

Ketcham, R.A., Donelick, R.A., Balestrieri, M.L., Zattin, M., 2009. Reproducibility of apatite fission-track length data and thermal history reconstruction. Earth and Planetary Science Letters 284, 504-515.

Kooi, H., Beaumont, C., 1996. Large-scale geomorphology: classical concepts reconciled and integrated with contemporary ideas via a surface processes model. Journal of Geophysical Research 101, 3361–3386.

Laslett, GM., Green, P.F., Duddy, LR., and Gleadow, A.JW., 1987. Thermal annealing of fission tracks in apatite. II. A quantitative analysis. Chemical Geology, 65, 1-13.

Le Pichon, X., Bonnin, J.C. Francheteau, J., Sibuet J.C., 1971. Une hypothese d'evolution tectonique du Golfe de Gascogne. In: Debysier, J., Le Pichon, X., Montadert, M. (Eds.), Histoire structurale du Golfe de Gascogne, VI.11.1-VI.11.44, Technip, Paris.

Lisker, F., Ventura, B., Glasmacher, U.A., 2009. Apatite thermochronology in modern geology. Geol. Soc. London Spec. Publ. 324, 1-23.Sambridge, M., 1999a. Geophysical inversion with a neighbourhood algorithm-I. Searching a parameter space. Geophys. J. Int. 138, 727-746.

López-Fernández, C., Pulgar, J.A., Gallart, J., Glez-Cortina, J.M., Díaz, J., Ruiz, M., 2004. Sismicidad y tectónica en el área de Becerreá–Triacastela (Lugo, NO España). Geogaceta 36, 51–54.

Martínez-Catalán, J.R., Arenas, R., Díaz-García, F., González-Cuadra, P., Gómez-Barreiro, J., Abati, J., Castiñeiras, P., Fernández-Suárez, J., Sánchez Martínez, S., Andonaegui, P., González Clavijo, E., Díez Montes, A., Rubio Pascual, F.J., and Valle Aguado, B., 2007. Space and time in the tectonic evolution of the northwestern Iberian Massif: Implications for the Variscan belt. In: Hatcher, R.D., Jr., Carlson, M.P., McBride, J.H., Martínez-Catalán, J.R. (Eds.), 4-D Framework of Continental Crust: Geological Society of America Memoir 200, 403–423.

Martín-González, F., Capote, R., Barbero, L., Insua, J.M., Martínez-Díaz, J.J., 2006. Primeros resultados de huellas de fisión en apatito en el sector Lugo-Ancares (Noroeste de la Península Ibérica). Geogaceta 40, 79–82.

Mauffret, A., Boillot, G., Auxietre, J.L., Dunand, J.P., 1978. Evolution structurale de la marge continentale au Nord-Ouest de la péninsule ibérique. Bull. Soc. Géol. Fr. XX (4), 375–388.

Montadert, L., Roberts, D.G., De Charpal, O., Guennoc, P., 1979. Rifting and subsidence of the northern continental margin of the Bay of Biscay. Initial reports of the Deep Sea Drilling Project, Leg 48, 1025-1060.

Montgomery, D.R, Brandon, M.T, 2002. Topographic controls on erosion rates in tectonically active mountain ranges. EPSL 201, 481-489.

Pérez-Estaún, A., Bastida, F., Martínez-Catalán, J.R., Gutiérrez-Marco, J.C., Marcos, A., and Pulgar, J.A., 1990. West Asturian–Leonese Zone: stratigraphy. In: R.D. Dallmeyer and E. Martínez-García (Eds.), Pre-Mesozoic Geology of Iberia, 92-102, Springer-Verlag.

Pérez-Estaún, A., Martínez-Catalán, J.R., Bastida, F., 1991. Crustal thickening and deformation sequence in the footwall to the suture of the Variscan belt of northwest Spain. In: Pérez-Estaún A., Coward, M.P. (Eds.), Deformation and Plate Tectonics, Tectonophysics 191, 243-253.

Pulgar, J., Gallart, J., Fernández-Viejo, G., Pérez-Estaún, A., Alvarez-Marrón, J., and ESCIN Group, 1996. Seismic image of the Cantabrian Mountains uplift in the western extension of the Pyrenean Belt from integrated

ESCIN reflection and refraction data. Tectonophysics 264, 1-20.

Reiners, P.W., 2007, Thermochronologic Approaches to Paleotopography, In: Kohn, M.J. (Ed.), Paleoaltimetry: Geochemical and Thermodynamic Approaches, Reviews in Mineralogy and Geochemistry 66, 243-267.

Reiners P.W., Brandon, M.T., 2006. Using Thermochronology to Understand Orogenic Erosion. Annu. Rev. Earth Planet. Sci. 34, 419–66.

Reiners, P.W., Ehlers, T.A. (Eds). 2005. Low-temperature thermochronology: techniques, interpretations, and applications. Reviews in Mineralogy and Geochemistry 58, v-ix, 1-622.

Reiners, P.W., Zhou, Z., Ehlers T. A., Xu, C., Brandon, M. T., Donelick, R. A., Nicolescu, S., 2003. Post-orogenic evolution of the Dabie Shan, eastern China, from (U-Th)/he and fission-track thermochronology. American Journal of Science 303, 489-518.

Ring, U., Brandon, M.T., Willett, S.D, Lister, G.S., 1999. Exhumation processes. In: Ring, U., Brandon, M.T., Lister, G.S., Willett, S.D. (eds.), Exhumation Processes: Normal Faulting, Ductile Flow, and Erosion, Special Publications 154, 1-27, Geological Society London.

Roe, G.H., Whipple, K.X., Fletcher, J.K., 2008. Feedbacks among climate, erosion, and tectonics in a critical wedge orogen. American Journal of Science 308, 815-842, doi:10.2475/07.2008.01.

Rosenbaum, G., Lister, G.S., Duboz, C., 2002. Relative motions of Africa, Iberia and Europe during Alpine orogeny, Tectonophysics 359, 117-129.

Sambridge, M., 1999a. Geophysical inversion with a neighbourhood algorithm-I. Searching a parameter space. Geophys. J. Int. 138, 479-494.

Sambridge, M., 1999b. Geophysical inversion with a neighbourhood algorithm-II. Appraising the ensemble. Geophys. J. Int. 138, 727-746.

Santanach, P., Ferrús, B., Cabrera, L., Sáez, A., 2005. Origin of a restraining bend in an evolving strike-slip system: The Cenozoic As Pontes basin (NW Spain). Geologica Acta 3 (3), 225-239.

Schärer, U., Kornprobst, J., Beslier, M.O., Boillot, G., Girardeau, J., 1995. Gabbro and related rock emplacement beneath rifting continental crust: U–Pb geochronological and geochemical constraints for the Galicia passive margin (Spain). Earth Planet. Sci. Lett. 130, 187–200.

Srivastava, S.P., Roest, W.R., Kovacs, L.C., Oakey, G., Lévesque, S., Verhoef, J., Macnab, R., 1990. Motion of Iberia since the Late Jurassic: Results from detailed aeromagnetic measurements in the Newfoundland Basin; Tectonophysics 184, Issues 3-4, 229-260.

Stöckli, D.F., Farley, R.A., Dumitru, T.A., 2000. Calibration of the apatite (U-Th)/He thermochronometer on an exhumed fault block, White Mountains, California. Geology 28 (11), 983-986.

Summerfield, M.A., Brown, R.W. (1998) Geomorphic factors in the interpretation of fission-track data. In Advances in Fission-Track Geochronology, 269-284.

Thomson, S.N., Brandon, M.T., Tomkin, J.H., Reiners, P.W., Vásquez, C., Wilson, N.J., 2010. Glaciation as a destructive and constructive control on mountain building. Nature 467, 313-317.

Valla, P.G., Herman, F., Van der Beek, P.A., Braun, J., 2010. Inversion of thermochronological age-elevation profiles to extract independent estimates of denudation and relief history – I: Theory and conceptual model. EPSL 295, 511-522.

Van der Beek, P.A., Valla, P.G., Herman, F., Braun, J., Persano, C., Dobson, K.J., Labrin, E., 2010. Inversion of thermochronological age-elevation profiles to extract independent estimates of denudation and relief history – II: Application to the French Western Alps. EPSL 296, 9-22.

Verhoef, J., Srivastava, S.P., 1989. Correlation of sedimentary basins across the North Atlantic as obtained from gravity and magnetic data, and its relation to the early evolution of the North Atlantic. In: Tankard, A.J., Balkwill, H.R. (Eds.), Extensional tectonics and stratigraphy of the North Atlantic margins, AAPG Memoir 46, 131-147.

Whipple, K.X., Kirby, E., Brocklehurst, S.H., 1999. Geomorphic limits to climate-induced increases in topographic relief. Nature 401, 39-43.

Whipple, K.X., Meade, B.J., 2004. Controls on the strength of coupling among climate, erosion, and deformation in two-sided, frictional orogenic wedges at steady state. Journal of Geophysical Research 109, 1-24.

Willett, S., Beaumont, C., Fullsack, P., 1993. Mechanical model for the tectonics of doubly vergent compressional orogens. Geology 21 (4) 371-374.

Wolf, R.A., Farley, K.A., Silver, L.T., 1996. Helium diffusion and low-temperature thermochronometry of apatite. Geochimica et Cosmochimica Acta 60, 4231-4240.

Wolf, R.A., Farley, K.A., Kass, D.M., 1998. Modeling of the temperature sensitivity of the apatite (U–Th)/He thermochronometer. ChemicalGeology 148, 105–114.

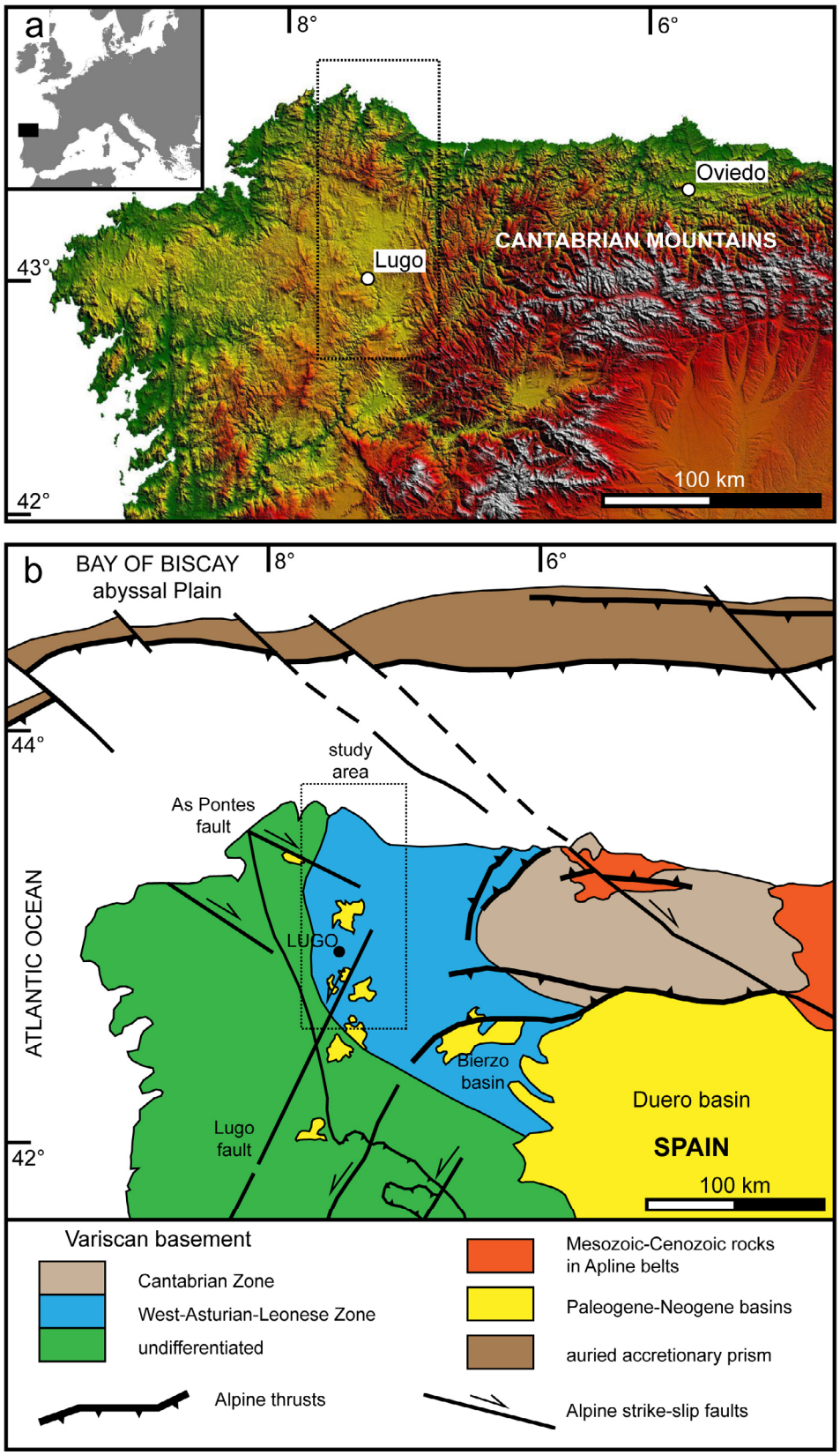

Figure 1: (a) Overview 30m DEM (digital elevation model; ASTER GDEM) with the location of the study area at the western termination of the Cantabrian Mountains along the northern coast of Spain. (b) Geological overview map of the northwestern Iberian coast. Dashed rectangle shows the location of the study area in the West-Asturian-Leonese Zone. Major structural features are highlighted.

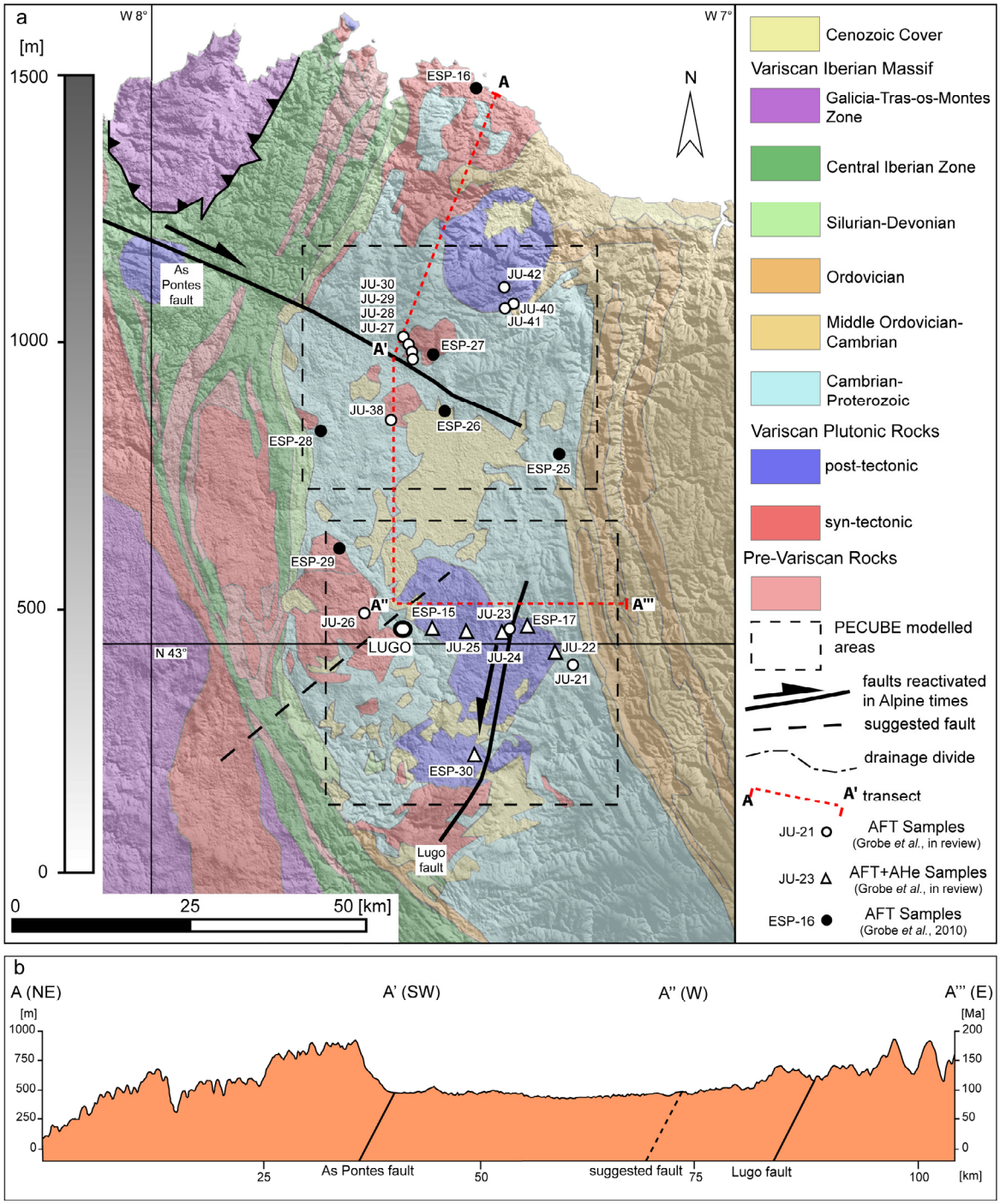

Figure 2: 30m DEM (ASTER GDEM) showing the topography of the study area combined with a transparent colored overlay of the geology together with sample locations, major structural features as well as the course of the of topographic transect: b) Profile of topographic transect.

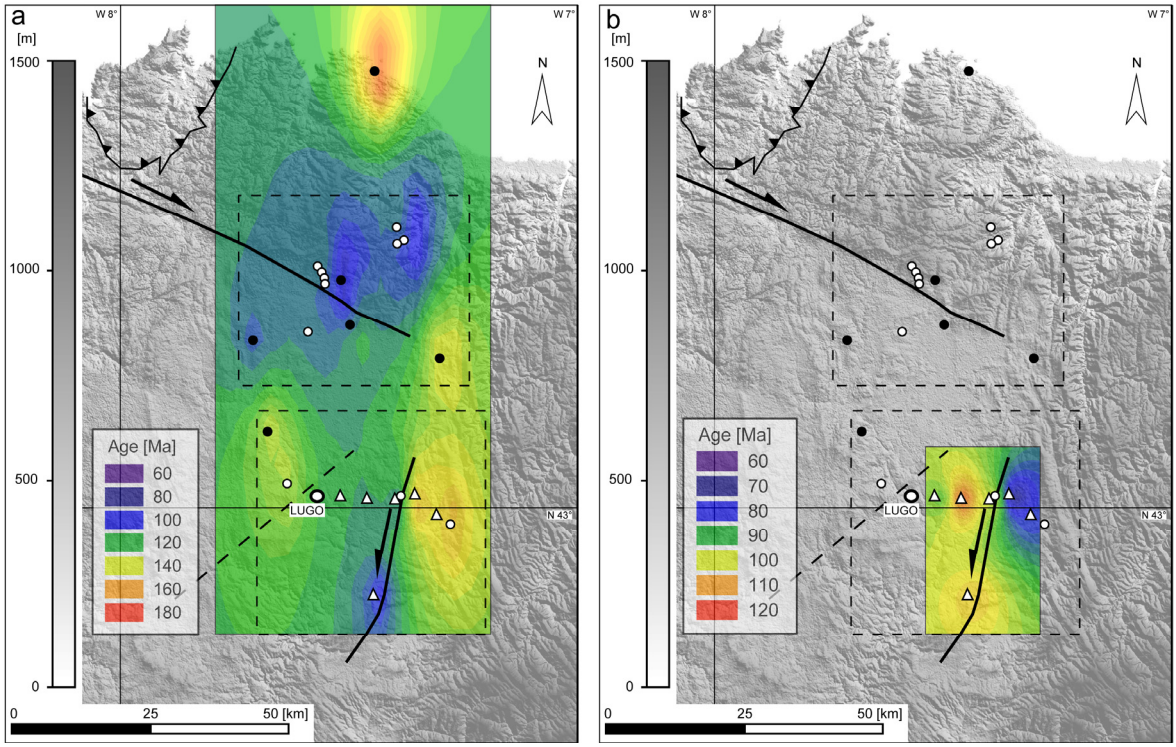

Figure 3: Contour maps illustrating the cooling age distribution over the study area of (a) the AFT central age and (b) the AHe age. Note that the temperature scales between ATF and AHe differ, as the age range of the AHe ages is much smaller and the same scale would have caused problems with differentiability.

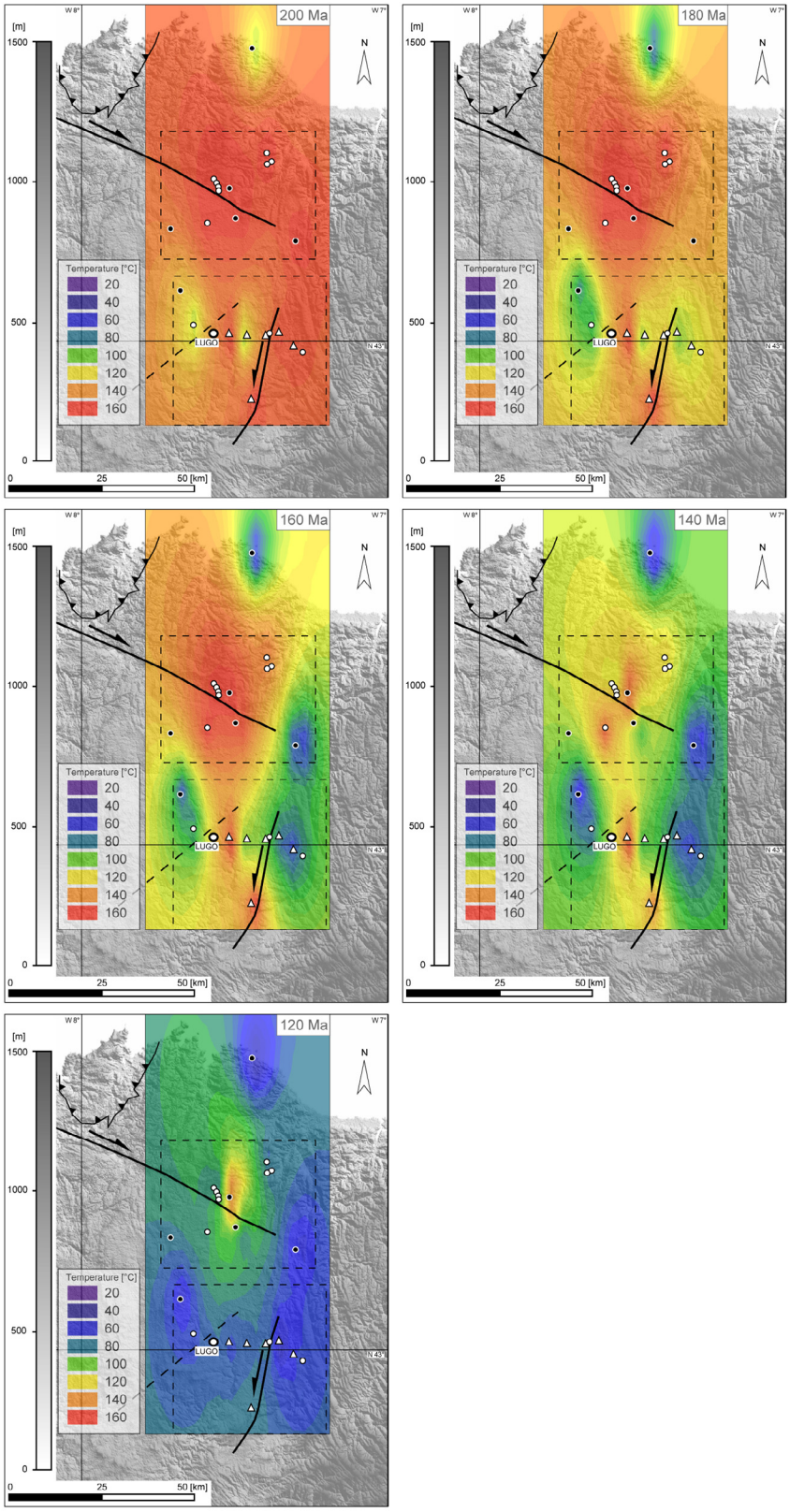

Figure 4: Condensed cooling history derived from the modelled cooling paths at different time steps (a) 200 Ma, (b) 180 Ma, (c) 160 Ma, (d) 140 Ma and (e) 120 Ma.

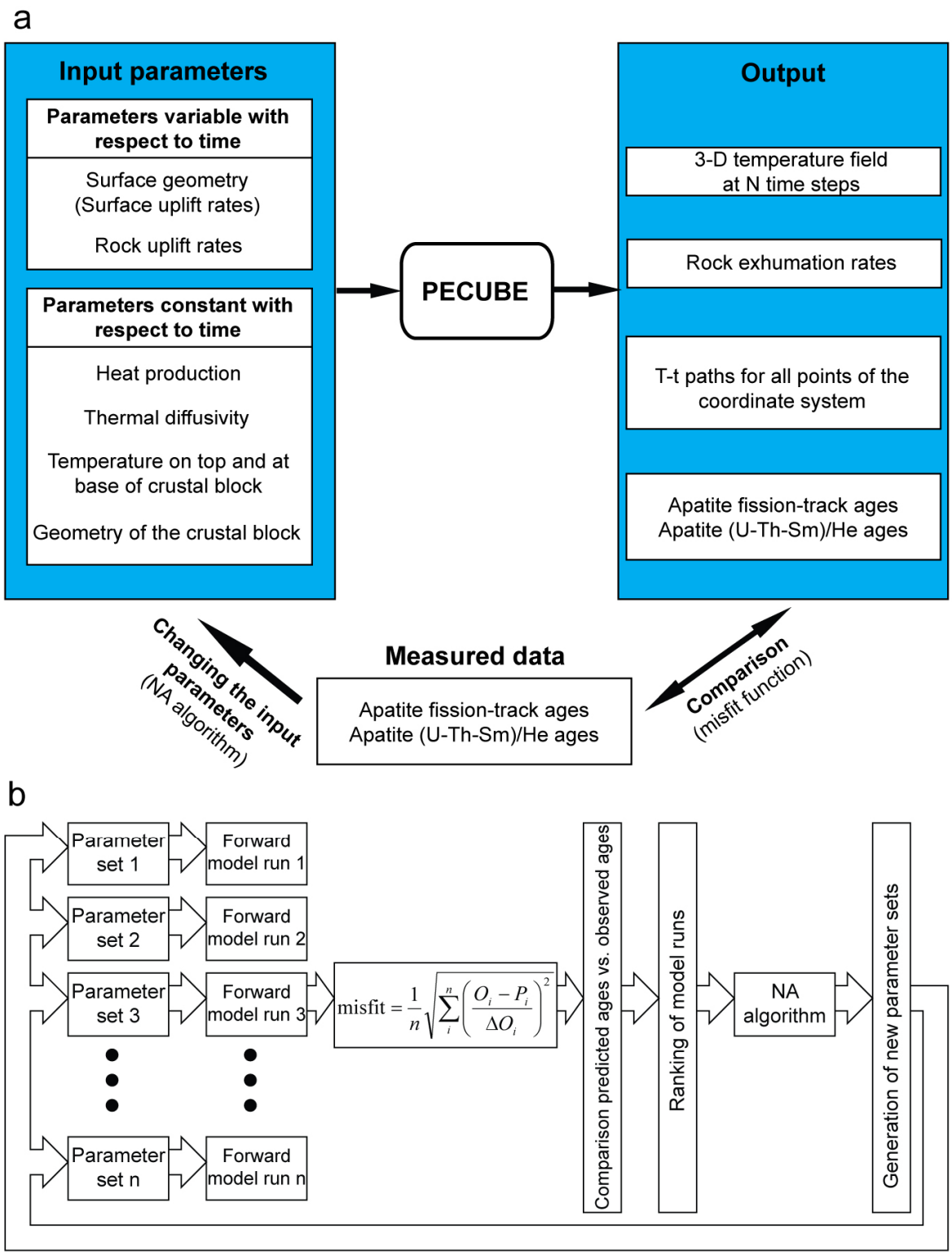

Figure 5: Sketch describing (a) the general operating mode of PECUBE (modified after Braun, 2003a) and (b) a more detailed sketch illustating the operating mode of the inverse approach of PECUBE (modified after Braun, 2003a).

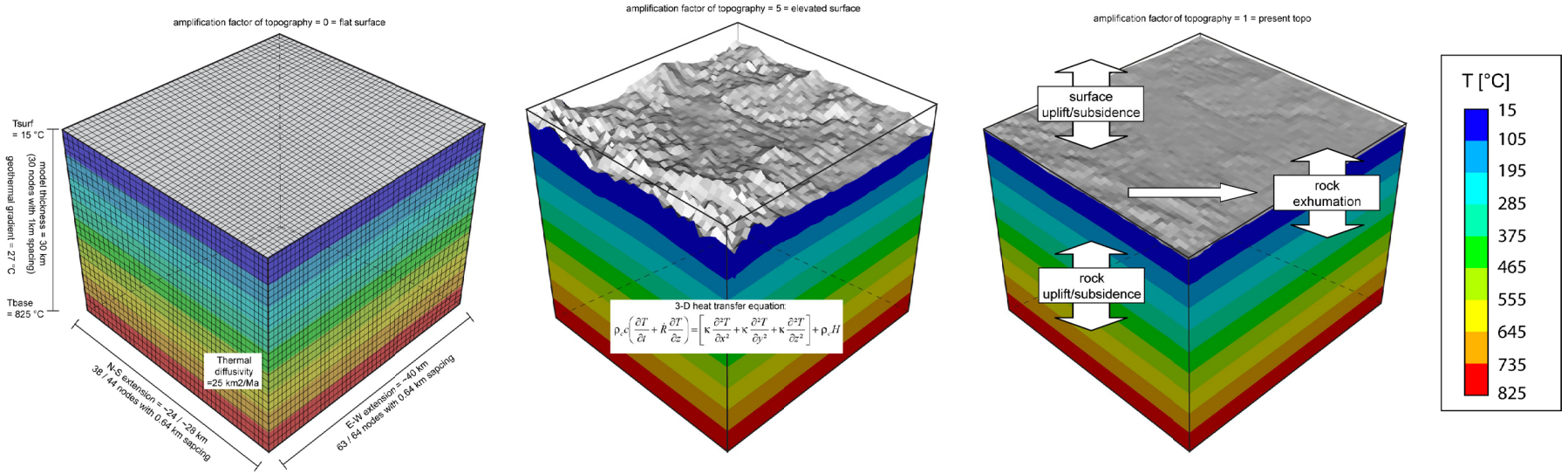

Figure 6: Modelled crustal block with boundary conditions, FEM discretization (model resolution) showing also the basic 3D heat transfer equation to be solved as well as the relationship between rock uplift, surface uplift (amplification factor of topography) and rock exhumation.

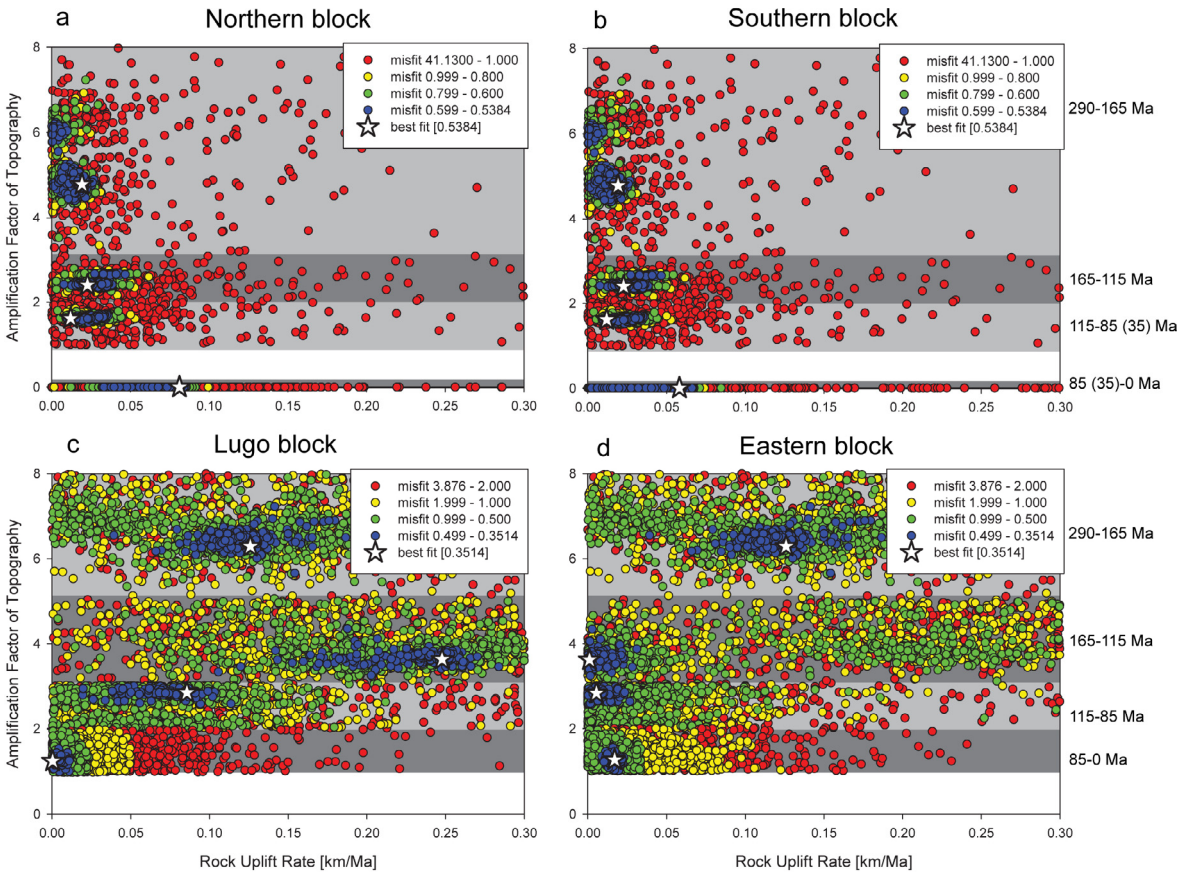

Figure 7: Scatter plots showing summary of all 2408 model runs from each modelled block. Each plot is subdivided into the accordant modelled time intervals marked by different greyish colors. Each point represents one model run at the accordant time step, while the shape and the colors of the points indicate the level of misfit (star: best fit; decreasing misfit in the order blue (low misfit), green, yellow, red (high misfit)). (a) and (b) Northern and Southern block of the North Galicia area with the time intervals 290-165 Ma; 165-115 Ma; 115-85(35) Ma; 85(35) Ma-present. (c) and (d) Lugo and Eastern block of the Central Galicia area with the time intervals 290-165 Ma; 165-115 Ma; 115-85 Ma; 85 Ma-present.

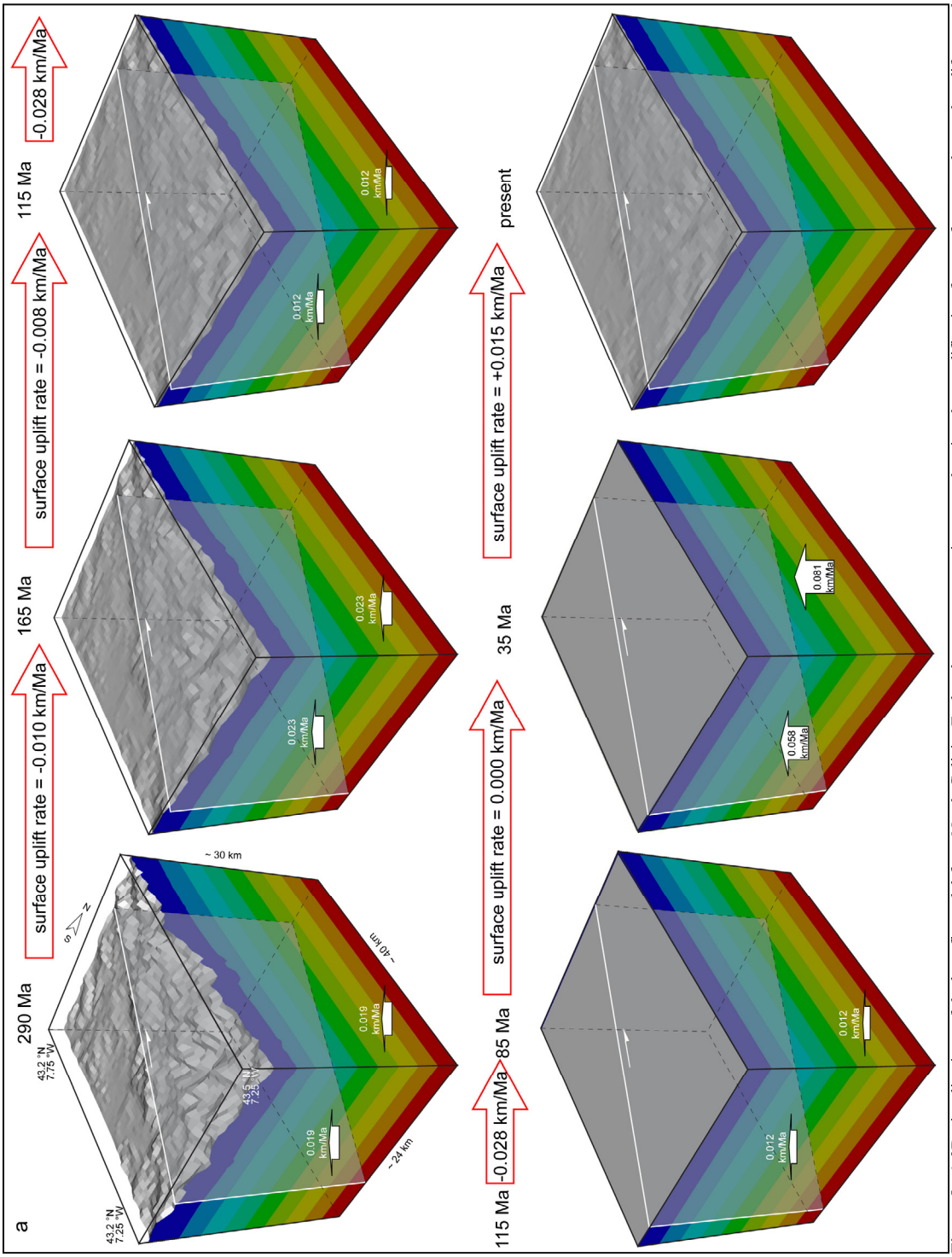

Figure 8: a) 3D visualizations of the best fit model from North Galicia. Each cube represents a time step showing the amplification factor of topography, rock uplift rate of each block from this time step to the next, the surface uplift/subsidence rates as well as the underlying temperature field.

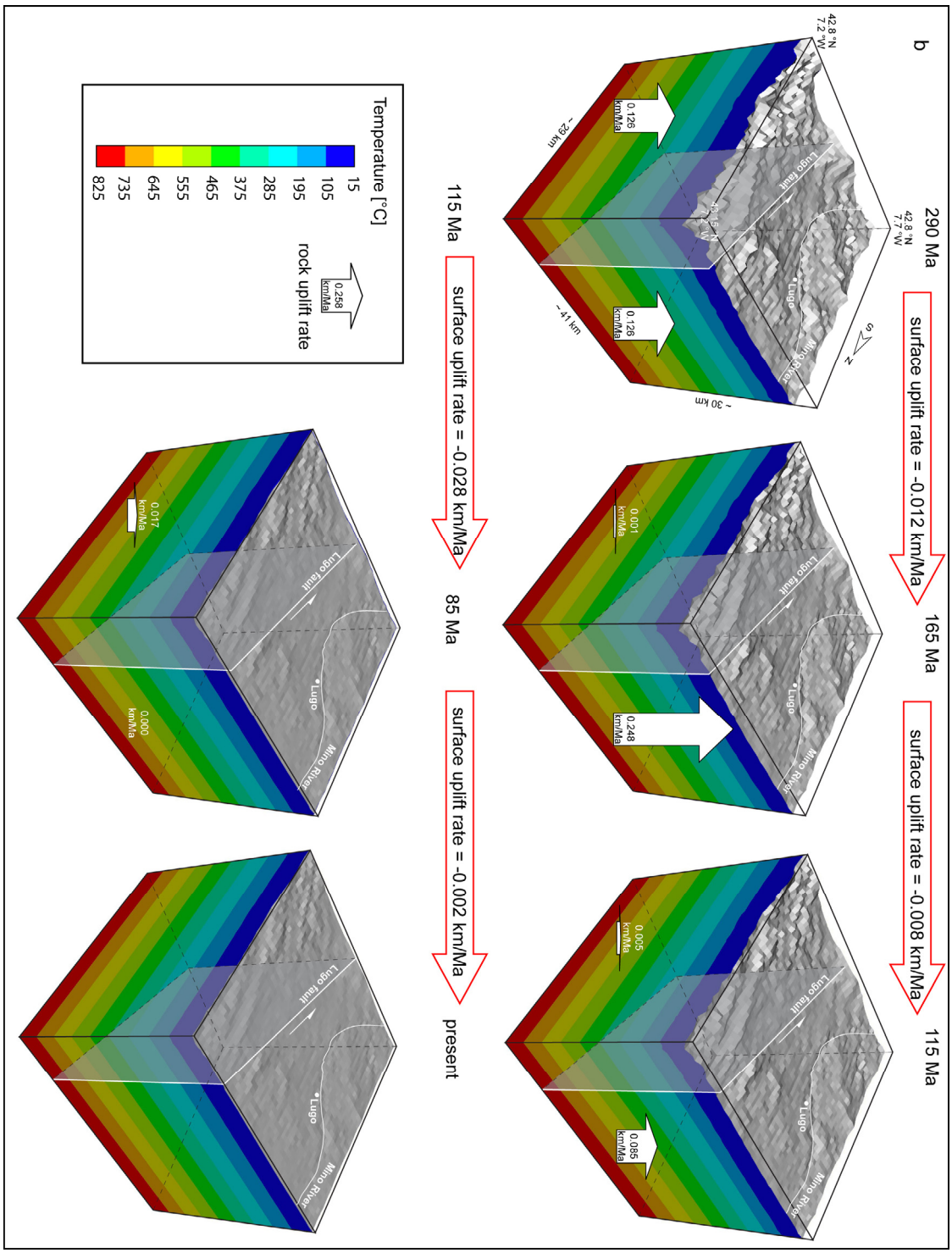

Figure 8: b) 3D visualizations of the best fit model from South Galicia. Each cube represents a time step showing the amplification factor of topography, rock uplift rate of each block from this time step to the next, the surface uplift/subsidence rates as well as the underlying temperature field.

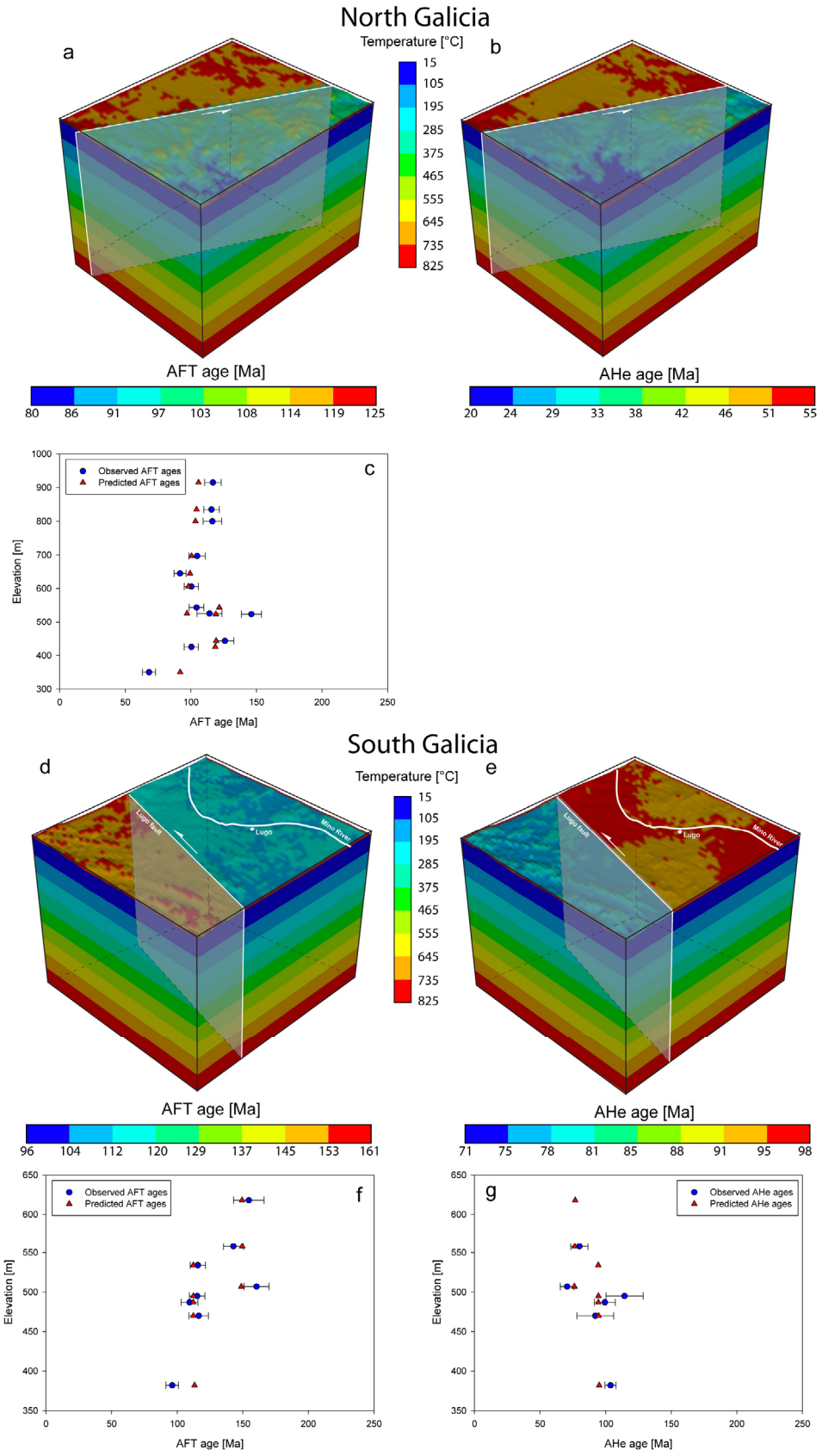

Figure 9: Predicted cooling age distribution at surface from each best fit model as well as AER plots comparing observed and predicted cooling ages. (a) AFT North Galicia, (b) AHe North Galicia, (c) AER-AFT North Galicia, (d) AFT South Galicia, (e) AHe South Galicia, (f) AER-AFT South Galicia, (g) AER-AHe South Galicia.

Table 1
Modelled apatite (U-Th-Sm)/He and apatite fission-track ages

Sample	Elevation [m a.s.l.]	N Latitude	W Longitude	AHe age [Ma]	Error ± 1σ [Ma]	AFT age [Ma]	Error ± 1σ [Ma]	Reference
North Galicia								
ESP-16	0	43°41'49.7"	7°26'25.2"	n.a.	n.a.	174.5	7.7	Grobe et al., 2010
ESP-25	524	43°14'22.9"	7°17'57.7"	n.a.	n.a.	146.2	7.6	Grobe et al., 2010
ESP-26	443	43°17'33.1"	7°29'40.7"	n.a.	n.a.	126.0	6.8	Grobe et al., 2010
ESP-27b	645	43°22'00.2"	7°30'57.8"	n.a.	n.a.	91.8	4.6	Grobe et al., 2010
ESP-28	544	43°16'05.2"	7°42'29.5"	n.a.	n.a.	104.3	5.6	Grobe et al., 2010
JU-27	606	43°21'51"	7°33'48"	n.a.	n.a.	100.4	5.4	Grobe et al., in review
JU-28	697	43°22'29"	7°33'54"	n.a.	n.a.	104.8	6.2	Grobe et al., in review
JU-29	800	43°22'51"	7°34'04"	n.a.	n.a.	116.4	7.1	Grobe et al., in review
JU-30	915	43°23'19"	7°34'26"	n.a.	n.a.	116.8	6.3	Grobe et al., in review
JU-38	425	43°17'02"	7°36'00"	n.a.	n.a.	110.5	6.4	Grobe et al., in review
JU-40	350	43°25'57"	7°23'08"	n.a.	n.a.	68.1	5.0	Grobe et al., in review
JU-41	526	43°25'39"	7°24'18"	n.a.	n.a.	114.2	9.5	Grobe et al., in review
JU-42	835	43°27'09"	7°24'18"	n.a.	n.a.	115.7	5.9	Grobe et al., in review
Central Galicia								
ESP-15	470	43°01'02.6"	7°30'55.5"	92.1	14.0	116.4	7.4	Grobe et al., 2010
ESP-17	507	43°01'10.9"	7°21'12.3"	70.6	5.2	160.5	9.6	Grobe et al., 2010
ESP-30	382	42°53'42.9"	6°23'02.8"	103.7	4.2	96.2	4.8	Grobe et al., 2010
JU-21	618	42°58'37"	7°17'23"	n.a.	n.a.	154.4	11.6	Grobe et al., in review
JU-22	558	42°59'22"	7°19'10"	80.0	6.6	142.9	7.6	Grobe et al., in review
JU-23	534	43°01'18"	7°23'31"	n.a.	n.a.	115.7	5.8	Grobe et al., in review
JU-24	487	43°00'52"	7°24'21"	99.4	8.0	109.4	6.4	Grobe et al., in review
JU-25	495	43°01'00"	7°28'09"	114.4	14.2	115.2	5.9	Grobe et al., in review

Table 2
Model parameterization and parameter space.

	Evolving Topography					**Surface Uplift**				**Rock uplift**				**Rock exhumation**			
Time steps [Ma]	present mean elevation [m]	amplification factor of topography		resulting mean elevation [m]		Time segment [Ma]		surface uplift rate [km/Ma]		Time segment [Ma]		rock uplift rate [km/Ma]		Time segment [Ma]		rock exhumation rate [km/Ma]	
		min	max	min	max	from	to	min	max	from	to	min	max	from	to	min	max
North Galicia																	
290	510	3	8	1530	4080					*Northern Block*				*Northern Block*			
165	510	2	3	1020	1530	290	165	-0.004	-0.024	290	165	0	0.3	290	165	0.024	0.304
115	510	1	2	510	1020	165	115	-0.010	-0.020	165	115	0	0.3	165	115	0.020	0.310
85	510	0	0	0	0	115	85	-0.017	-0.034	115	85	0	0.3	115	85	0.034	0.317
35	510	0	0	0	0	85	35	0.000	0.000	85	35	0	0.3	85	35	0.000	0.300
0	510	1	1	510	510	35	0	0.015	0.015	35	0	0	0.3	35	0	-0.015	0.285
										Southern Block				*Southern Block*			
										290	165	0	0.3	290	165	0.024	0.304
										165	115	0	0.3	165	115	0.020	0.310
										115	85	0	0.3	115	85	0.034	0.317
										85	35	0	0.3	85	35	0.000	0.300
										35	0	0	0.3	35	0	-0.015	0.285
South Galicia																	
290	540	5	8	2700	4320					*Lugo Block*				*Lugo Block*			
165	540	3	5	1620	2700	290	165	-0.009	-0.022	290	165	0	0.3	290	165	0.022	0.309
115	540	2	3	1080	1620	165	115	-0.011	-0.032	165	115	0	0.3	165	115	0.032	0.311
85	540	1	2	540	1080	115	85	-0.018	-0.036	115	85	0	0.3	115	85	0.036	0.318
0	540	1	1	540	540	85	0	0.000	-0.006	85	0	0	0.3	85	0	0.006	0.300
										Eastern Block				*Eastern Block*			
										290	165	0	0.3	290	165	0.022	0.309
										165	115	0	0.3	165	115	0.032	0.311
										115	85	0	0.3	115	85	0.036	0.318
										85	0	0	0.3	85	0	0.006	0.300

Greyish colour marks time steps during which the block movement is coupled

Table 3
Model result from best fit model.

Evolving Topography				Surface Uplift			Rock uplift			Rock exhumation			*HeFTy*
Time steps [Ma]	present mean elevation [m]	amplification factor of topography	resulting mean elevation [m]	Time segment [Ma]		surface uplift rate [km/Ma]	Time segment [Ma]		rock uplift rate [km/Ma]	Time segment [Ma]		rock exhumation rate [km/Ma]	rock exhumation rate [km/Ma]
				from	to		from	to		from	to		
North Galicia													
290	510	4.79	2441						*Northern Block*				
165	510	2.41	1229	290	165	-0.010	290	165	0.019	290	165	0.029	n.a.
115	510	1.63	830	165	115	-0.008	165	115	0.023	165	115	0.031	0.111
85	510	0.00	0	115	85	-0.028	115	85	0.012	115	85	0.040	0.029
35	510	0.00	0	85	35	0.000	85	35	0.012	85	35	0.012	0.014
0	510	1.00	510	35	0	0.015	35	0	0.081	35	0	0.066	0.029
									Southern Block				
							290	165	0.019	290	165	0.029	n.a.
							165	115	0.023	165	115	0.031	0.090
							115	85	0.012	115	85	0.040	0.010
							85	35	0.012	85	35	0.012	0.011
							35	0	0.058	35	0	0.043	0.031
Central Galicia													
290	540	6.29	3397						*Lugo Block*				
165	540	3.61	1951	290	165	-0.012	290	165	0.126	290	165	0.138	n.a.
115	540	2.83	1528	165	115	-0.008	165	115	0.248	165	115	0.256	0.121
85	540	1.26	680	115	85	-0.028	115	85	0.085	115	85	0.113	0.016
0	540	1.00	540	85	0	-0.002	85	0	0.000	85	0	0.002	0.018
									Eastern Block				
							290	165	0.126	290	165	0.138	0.094
							165	115	0.001	165	115	0.009	0.012
							115	85	0.005	115	85	0.033	0.007
							85	0	0.017	85	0	0.019	0.012

Greyish colour marks time steps during which the block movement is coupled

D. Publication 4

Low-temperature exhumation history of Variscan-age rocks in the western Cantabrian Mountains (NW Spain) recorded by AFT-(U-Th-Sm)/He thermochronology and 2D-3D t-T path modelling. (Abstract)

René W. Grobe, Joaquina Alvarez-Marrón, Ulrich A. Glasmacher, Finlay M. Stuart (2010)

12th International Thermochronology Conference, Glasgow 16-20 August, 2010

We present the first regional study of the complex post-orogenic history of cooling, denudation, and long-term landscape evolution of Paleozoic rocks exposed in the western termination of the Cantabrian Mountains (NW Spain). We use apatite fission-track and apatite (U-Th-Sm)/He thermochronological techniques combined with 2D and 3D time-temperature (t-T) path modelling using the software codes HeFTy© (e.g. Ketcham *et al.*, 2009) and PECUBE (Braun, 2003a). The topography presents major differences across the area, with long wavelength and moderate amplitude relief in large areas to the west, and dominant shorter wavelength with higher amplitude in the east.

The area experienced two major tectonic events since the end of the Variscan orogeny in the Late Paleozoic: 1) continental break-up and Mesozoic rifting leading to the opening of the Atlantic Ocean and the Bay of Biscay, and 2) limited convergence between Iberia and Eurasia since Middle Eocene times.

Apatite fission-track ages range from 68.1 (5.0) Ma to 246.7 (26.9 Ma) (e.g. Grobe *et al.*, 2010) and apatite (U-Th-Sm)/He ages range from 56.6 (5.1) Ma to 177.7 (17.1) Ma. Age-elevation plots and t-T path modelling suggest a tectonothermal evolution with continuous cooling at different rates related to the main tectonic events that affected the area. A rapid cooling event that ended by the Late Juarassic corresponds to topographic decay during unroofing of the Variscan orogen and the break-up of Pangea. Another cooling event occurred over the Late Jurassic and Early Cretaceous period of Atlantic and Bay of Biscay rifting. Only samples at Alpine fault escarpments record denudation during Late Cretaceous and Eocene. Less than 1.7 km of denudation occurred during uplift of the Cantabrian Mountains since ~45 Ma ago.

References

Ketcham, R.A., Donelick, R.A., Balestrieri, M.L., Zattin, M. (2009): Reproducibility of apatite fission-track length data and thermal history reconstruction. – Earth and Planteray Science Letters 284, 504-515.

Braun, J. (2003): Pecube: a finite-element code to solve the 3D heat transport equation including the effect of a time-varying, finite amplitude surface topography. – Computers & Geosciences 29, 787-794.

Grobe, R.W., Alvarez-Marrón, J., Glasmacher, U.A., Menéndez-Duarte, R. (2010): Low-temperature exhumation history of Variscan-age rocks in the western Cantabrian Mountains (NW Spain) recorded by apatite fission-track data. – Tectonophysics 489 (1-4), 76-90.

E. Publication 5

Post-orogenic exhumation history of a Variscan mid-crustal basement in Galicia (NW Spain). (Abstract)

René W. Grobe, Joaquina Alvarez-Marrón, Ulrich A. Glasmacher, Finlay M. Stuart, Adolfo Castañeda-Zarauz (2010)

Geophysical Research Abstracts Vol. 12, EGU2010-1214, EGU General Assembly 2010

The present study aims to quantify the complex post-orogenic history of cooling, denudation, and long-term landscape evolution of a mid-crustal section of Variscan basement in Galicia (NW Spain). We use apatite fission-track and apatite (U-Th-Sm)/He thermochronological techniques combined with time-temperature (t-T) path modelling using the software code HeFTy©. The topography is characterized by an extensive, low relief area at ~500 m elevation in central Galicia, and a WNW-ESE ridge that reaches up to 1000 m to the North. The area experienced two major tectonic events since the end of the Variscan orogeny in the Late Paleozoic: 1) continental break-up and Mesozoic rifting leading to the opening of the Atlantic Ocean and the Bay of Biscay, and 2) limited convergence between Iberia and Eurasia since Middle Eocene times. Apatite fission-track ages range from 68.1 (5.0) Ma to 174.5 (7.7) Ma and apatite (U-Th-Sm)/He ages range from 73.6 (5.4) Ma to 147.1 (16.6) Ma. Age-elevation plots and t-T path modelling suggest a tectonothermal evolution with faster exhumation associated to faulting during Mesozoic rifting. In particular, two major fault systems trending WNW-ESE and NNE-SSW, the As Pontes and the Lugo faults respectively separate areas with the fastest exhumation around 115 Ma from areas with overall slow exhumation since 200-150 Ma. A landscape of subdued topography in central Galicia was acquired prior to Eocene convergence. The higher elevation areas along the northern ridge formed since Middle Eocene times due to fault reactivation and minor exhumation occurred along the fault escarpment.

F. Publication 6

Low temperature exhumation history of Variscan-age rocks in the western Cantabrian Mountains (NW Spain) recorded by apatite fission-track data. (Abstract)

René W. Grobe, Joaquina Alvarez-Marrón, Ulrich A. Glasmacher, Rosana Menéndez-Duarte (2009)

5th TOPO-EUROPE Workshop, Villa Bosch, Klaus Tschira Foundation, Heidelberg, 15-17 October, 2009

The western Cantabrian Mountains are comprised of a Variscan crustal section uplifted due to shortening and incipient subduction associated to Cenozoic convergence along the northern Iberian plate. The mountains reach elevations of over 2600 m along the northern coast of Spain. Here, we present the first regional study of apatite fission-track (AFT) cooling ages in an area 150 by 100 km in the western termination of the mountain belt that places constraints on the pattern and history of exhumation of the Paleozoic bedrock over the past ~ 240 Ma (Grobe *et al.*, 2010). Twenty-one apatite fission-track samples range in age from 246.7 (26.9) Ma to 78.1 (3.7) Ma, with mean track lengths between 10.4 (1.8) µm and 12.4 (1.4) µm. Time-temperature path modelling of the data indicates that continuous cooling at different rates took place during the three main tectonic events that affected the area. A rapid cooling event that ended by the Late Jurassic, corresponds with unroofing of the Variscan orogen and is responsible for the largest amount of exhumation. Westernmost samples cooled coinciding with rifting in the North Atlantic and Bay of Biscay during the Late Jurassic to Early Cretaceous. By about 100-80 Ma most samples had reached, or passed through, the upper boundary of the apatite partial annealing zone, which indicate that regional denudation has not exceeded ~ 1.6 km since then, for geothermal gradients ≥ 26 ºC/km. This helps to place time constraints on the preservation and development of large peneplain surfaces in the area. Only three samples next to fault escarpments in the west cooled below 70 ºC since 80 Ma, reaching below 65 ºC before initiation of incipient subduction along the North Iberian Margin by 46 Ma. An average cooling rate of ≤ 1 ºC/Ma reflects latest denudation as the new mountainous relief developed since then.

References

Grobe, R. W., Alvarez-Marrón J., Glasmacher, U. A., Menéndez-Duarte, R., (2010). Low temperature exhumation history of Variscan-age rocks in the western Cantabrian Mountains (NW Spain) recorded by apatite fission-track data. Tectonophysics 489 (1-4), 76-90.

G. Publication 7

Early Mesozoic cooling from low temperature thermochronology in N Spain and N Africa. (Abstract)

René W. Grobe, Joaquina Alvarez-Marrón, Ulrich A. Glasmacher, Rosana Menéndez-Duarte (2009)

Geophysical Research Abstracts Vol. 11, EGU2009-944, EGU General Assembly 2009

In the western prolongation of the Pyrenees, the substratum of the Cantabrian Mountains consists of an E-W crustal section of the Gondwana continental margin involved in the Variscan collision. In Mesozoic times, the region was modified by rifting and the opening of the Atlantic and the Bay of Biscay, while in Paleogene-Neogene times it was affected by the convergence of the Iberian Plate with the Eurasian Plate resulting in the present mountains. Our thermochronological data and modelled time-temperature histories suggest an earlier, relative fast cooling period during Early Triassic to Early Jurassic. This cooling event coincides temporally with the process of rifting that caused Pangea continental break-up and the opening of the North Atlantic. Other authors report similar cooling histories from Early Triassic to Middle Jurassic from other parts of the Iberian Peninsula (Juez-Larré, 2003; Barbero *et al.*, 2005) as well as from the Moroccan Meseta, in N Africa (Ghorbal *et al.*, 2008). Furthermore, the time span of this cooling event includes the period of main activity of the Central Atlantic Magmatic Province (CAMP) magmatism at around 200 Ma (Marzoli *et al.*, 1999).Wilson (1997) postulates a relationship between this magmatic activity and upwelling of a large-scale mantle plume (super-plume) beneath the West African craton. Correlatives of this province have been identified as far as the southern Iberian Peninsula, Newfoundland, and possibly in Brittany, among other European areas (Pe-Piper *et al.*, 1992; Jourdan *et al.*, 2003). The current presentation aims to discuss possible African far-field effects on thermochronological data in the Cantabrian Mountains of NW Spain.

References

Barbero, L.; Glasmacher, U. A.; Villaseca, C.; López García, J. A.; Martín-Romera, C. (2005). Long-term thermo-tectonic evolution of the Montes de Toledo area (Central Hercynian Belt, Spain): constraints from apatite fission-track analysis. International Journal of Earth Sciences, Volume 94, Issue 2, pp.193-203.

Ghorbal, B., Bertotti, G., Foeken, J., Andriessen, P. (2008). Unexpected Jurassic to Neogene vertical movements in 'stable' parts of NW Africa revealed by low temperature geochronology. Terra Nova, Volume 20, Number 5, October 2008 , 355-363(9).

Jourdan, F.; Marzoli, A.; Bertrand, H.; Cosca, M.; Fontignie, D. (2003). The Northernmost CAMP: 40Ar/39Ar Age, petrology and Sr–Nd–Pb isotope geochemistry of the Kerforne Dike, Brittany, France. In: Hames, W.E., McHone, J.G., Renne, P.R., Ruppel, C. (Eds.), The Central Atlantic Magmatic Province: Insights From Fragments of Pangea. AGU, Geophys. Mon., vol. 136, 209-226.

Juez-Larré, J. (2003). Post Late Paleozoic tectonothermal evolution of the northeastern margin of Iberia, assessed by fission-track and (U-T)/He analysis: a case history from the Catalan Coastal Ranges. Ph.D. thesis, Free University of Amsterdam. 200 pp.

Marzoli, A.; Renne, P.R.; Piccirillo, E.M.; Ernesto, M.; Bellieni, G.; De Min, A. (1999). Extensive 200-million-year-old continental food basalts of the Central Atlantic magmatic province. Science 284, 616-618.

Pe-Piper, G.; Jansa, L.F.; Lambert, R.St.-J. (1992). Early Mesozoic magmatism of the Eastern Canadian margin. In: Puffer, J.H., Ragland, P.C. (Eds.), Eastern North American Mesozoic magmatism. Geol. Soc. Am., Spec. Paper, vol. 268, 13-36.

Wilson, M. (1997). Thermal evolution of the Central Atlantic passive margins: continental break-up above a Mesozoic super-plume. J. Geol. Soc. (Lond.) 154, 491-495.

H. Publication 8

Low-temperature thermochronology, exhumation, and long-term landscape evolution in the western Cantabrian Mountains, NW Spain. (Abstract)

René W. Grobe, Joaquina Alvarez-Marrón, Ulrich A. Glasmacher, Rosana Menéndez-Duarte (2008)

Geophysical Research Abstracts Vol. 10, EGU2008-A-01435, EGU General Assembly 2008

The present study aims to quantify the complex post-orogenic history of cooling, denudation, and exhumation of a Variscan crustal segment, exemplified by the Cantabrian Mountains. The substratum of the Cantabrian Mountains, that are located in NW Spain, in the western continuation of the Pyrenees, represents the eroded relict of a mountain range that was built during the Variscan orogeny, and that had been possibly peneplained by Permian-Triassic times. In Mesozoic times, this region was modified by rifting and opening of the Bay of Biscay, while in Paleogene-Neogene times it was affected by the convergence of the Iberian Plate with the Eurasian Plate. The long-term history of formation of the present topography with maximum heights of up to 2,648 m is not well established and is the subject of current research. Low-temperature thermochronology, i.e. apatite fission-track (AFT) dating, and modelling of time-temperature (t-T) paths are used in order to constrain the post-Variscan exhumation history. Furthermore, the thermochronological data will be utilised to determine

The long-term landscape evolution by thermokinematic modelling. The study area is characterized by diverse morphologies. On the one hand there is a sector with long wave length topography and low amplitudes that is used to distinguish the rate of landform evolution, in terms of an increase or a decrease in relief. On the other hand, there is another sector with short wave length topography and abrupt relief, due to deeply incised river valleys, that is used to determine exhumation rates. The study is based on an overview sampling of 21 samples taken within specified intervals over the entire area. AFT ages range from 270 (36) Ma (Permian) to 78 (4) Ma (Upper Cretaceous). The age-elevation relationship shows negative slopes that are indicative of a decrease in relief. Mean horizontal confined track lengths vary between 10.4 (1.8) µm and 12.8 (1.8) µm. C-axis oriented etch pit diameters range from 1.3 (0.2) µm to 1.6 (0.2) µm. The time-temperature (t-T) paths for selected samples were modelled by applying the computer code HeFTy© with independent geological constraints.

I. Publication 9

Evolution of the Albertine Rift in East Africa, evidence from the Western Rift shoulder (DRC). (Abstract)

Friederike U. Bauer, Ulrich. A. Glasmacher, René. W. Grobe, Matthias Starz, Meni Malikwisha, Vikandy S. Mambo, Bin V. Mutete (2010)

12th International Thermochronology Conference, Glasgow 16-20 August, 2010

For a long time large parts of the Eastern Congo have been almost impossible to access for field-work and, therefore, neglected in the ongoing scientific research. Here, along the eastern margin is one gateway to the Congo basin and, even more important, one piece to its evolution.

To understand the geomorphology/geomorphic evolution of an area or landscape, knowledge about phases of (dis)equilibrium between denudation/erosion/exhumation and rock uplift governed by climatic and tectonic processes is essential. Low-temperature thermochronological techniques, like fission-track and (U-Th-Sm)/He dating on apatite and zircon are well established tools to trace rock displacements/exhumation through the upper crust. And, therefore, provide fundamental information helping to decipher the long-term landscape evolution of an area.

Along a N-S transect from Butembo (W of Lake Edward) up to Bunia (Blue Mountains, Lake Albert) a set of samples was taken for apatite fission-track and (U-Th-Sm)/He analyses, providing the first thermochronological data set of this area. Subsequent modelling of the obtained data allows constraining the exhumation history of the eastern margin of the Congo basin.

J. Publication 10

Exhumation history of the eastern border of the Congo basin. (Abstract)

Friederike U. Bauer, Ulrich. A. Glasmacher, René. W. Grobe, Matthias Starz, Meni Malikwisha, Vikandy S. Mambo, Bin V. Mutete (2010)

23rd Colloquium of African Geology, South Africa 8-14 January, 2011

The present study aims to quantify the complex post-orogenic history of cooling, denudation, and exhumation of a Variscan crustal segment, exemplified by the Cantabrian Mountains. The substratum of the Cantabrian Mountains, that are located in NW Spain, in the western continuation of the Pyrenees, represents the eroded relict of a mountain range that was built during the Variscan orogeny, and that had been possibly peneplained by Permian-Triassic times. In Mesozoic times, this region was modified by rifting and opening of the Bay of Biscay, while in Paleogene-Neogene times it was affected by the convergence of the Iberian Plate with the Eurasian Plate. The long-term history of formation of the present topography with maximum heights of up to 2,648 m is not well established and is the subject of current research. Low-temperature thermochronology, i.e. apatite fission-track (AFT) dating, and modelling of time-temperature (t-T) paths are used in order to constrain the post-Variscan exhumation history. Furthermore, the thermochronological data will be utilised to determine

the long-term landscape evolution by thermokinematic modelling. The study area is characterized by diverse morphologies. On the one hand there is a sector with long wave length topography and low amplitudes that is used to distinguish the rate of landform evolution, in terms of an increase or a decrease in relief. On the other hand, there is another sector with short wave length topography and abrupt relief, due to deeply incised river valleys, that is used to determine exhumation rates. The study is based on an overview sampling of 21 samples taken within specified intervals over the entire area. AFT ages range from 270 (36) Ma (Permian) to 78 (4) Ma (Upper Cretaceous). The age-elevation relationship shows negative slopes that are indicative of a decrease in relief. Mean horizontal confined track lengths vary between 10.4 (1.8) µm and 12.8 (1.8) µm. C-axis oriented etch pit diameters range from 1.3 (0.2) µm to 1.6 (0.2) µm. The time-temperature (t-T) paths for selected samples were modelled by applying the computer code HeFTy© with independent geological constraints.

Erklärung

Hiermit erkläre ich, dass ich die vorliegende Dissertation selbst verfasst und mich dabei keiner anderen als der von mir ausdrücklich bezeichneten Quellen und Hilfen bedient habe.

Ich erkläre weiterhin, dass ich an keiner anderen Stelle ein Prüfungsverfahren beantragt bzw. die Dissertation in dieser oder anderer Form bereits anderweitig als Prüfungsarbeit verwendet oder einer anderen Fakultät als Dissertation vorgelegt habe.

Heidelberg, den 31. Dezember 2010

René W. Grobe